

**Development of recombinant antibody
fragments for toxin and microbial
contaminant detection and investigations
of microcystin and azaspiracid toxicity.**

Daniel McPartlin B.Sc. (Hons.)

This thesis is submitted to Dublin City University for the degree of

Ph.D.

August 2019

Based on research carried out at
School of Biotechnology,
Dublin City University,
Dublin 9
Ireland

**Supervisors: Professor Richard O’Kennedy
Professor Fiona Regan
Dr. Caroline Murphy**

Declaration

I hereby certify that this material, which I now submit for assessment on the programme of study leading to the award of Doctor of Philosophy is entirely my own work, that I have exercised reasonable care to ensure that the work is original, and does not to the best of my knowledge breach any law of copyright, and has not been taken from the work of others save and to the extent that such work has been cited and acknowledged within the text of my work.

Signed: _____

ID No.: 14212186

Date: 01/08/19

Acknowledgements

I would firstly like to express my sincere thanks to Professor Richard O’Kennedy for the opportunity to carry out a PhD in his research group and for his expert supervision throughout the ups and (many) downs of the PhD process. His leadership, guidance and enthusiasm were a vital source of inspiration and fuelled my belief and love of science.

Secondly, I would like to thank Professor Fiona Regan, Dr. Caroline Murphy and Dr. Jenny Fitzgerald whose unending support and guidance kept me motivated and on track, and without whom I’d probably be still trying to screen the AZA library (for the sixth time). I’d also like to give huge thanks to all in the Applied Biochemistry Group, Jonny, Ivan (honorary ABG member), Kara, Aoife, Arabelle, Jenny, Caroline, Fay, Ciara, and all of the people who’ve gone through the ROK lab. The morning coffees, nights out to Dicey’s (always) and the laughs had at Aoife’s expense are memories that will stay with me long hereafter.

I’d like to say a huge thank you to everyone in the Biological Research Society that I’ve become close friends with and that I’ve shared amazing experiences with. If I did nothing else during the PhD but meet some of the best people I’ve ever known, then that would be just fine with me.

A special thank you goes out to my parents, Audrey and Peter, my brother and sister, Paul and Sarah, and the doggos, Dexie and Lexie. You always motivated me to achieve my best and your un-ending love and support kept me going back at it even when times got particularly tough.

Finally, I’d like to thank Rach, my best friend and partner in crime. Without your love and support over the last four years, none of this would have been possible. Thank you for the laughs, for your belief in me, for your love and for just being there for me. This work I dedicate to you.

“All we have to decide is what to do with the time that is given to us” – Gandalf

Table of Contents

1	Introduction	1
1.1	Introduction to the thesis	2
1.2	Harmful algal blooms and algal toxins.....	2
1.2.1	Azaspiracid and <i>Azadinium spinosum</i>	5
1.2.2	Occurrences of AZAs and <i>A. spinosum</i>	7
1.2.3	Current monitoring programs for algal toxins and HABs.....	10
1.2.4	<i>Microcystis aeruginosa</i> and microcystins	12
1.2.5	Occurrences of <i>M. aeruginosa</i> in brackish waters	15
1.2.6	Co-exposure to multiple toxins	17
1.2.7	Studies on the toxic effects of AZAs	17
1.2.8	Studies on the toxic effects of <i>M. aeruginosa</i> and MCs	19
1.2.9	Molecular pathways of MC-induced toxicity	21
1.2.10	Principles of High Content Analysis (HCA).....	23
1.3	Development of Biosensors.....	24
1.3.1	Immune system	24
1.3.2	Immunoglobulin structure	25
1.3.3	Antibody gene organisation	27
1.3.4	Recombinant antibodies	28
1.3.5	Bacteriophage.....	31
1.3.6	Phage display	32
1.3.7	Panning.....	33
1.4	<i>Bacillus cereus</i>	35
1.4.1	Types of poisonings	37
1.4.2	Biomarkers for <i>B. cereus</i>	39
1.4.3	Current detection methods	42
1.4.4	Flow cytometry	44

1.4.5	Cell-based panning	47
1.5	Antibody optimisation	49
1.5.1	Protein solubility and stability	50
1.5.2	Hydrophobic to hydrophilic mutations	53
1.6	Thesis aims	58
2	Materials and Methods	60
2.1	Materials	61
2.2	Methods	70
2.2.1	General Methods	70
2.2.2	Generation of murine scFv library for AZA1	71
2.2.3	Elucidating Microcystin-LR-antibody interactions by <i>in silico</i> docking and <i>in vitro</i> mutagenesis.....	98
2.2.4	Optimisation of anti-MC-LR scFv stability and solubility by targeted mutagenesis	104
2.2.5	Generation of an avian scFv library for <i>Bacillus cereus</i>	109
2.2.6	Investigation into the toxic effects of MC-LR, <i>M. aeruginosa</i> and AZA1 on the Hepatocellular Carcinoma cell line, HepG2	128
3	Generation of a murine anti-AZA1 scFv antibody fragment.....	136
3.1	Introduction	137
3.2	Results	138
3.2.1	Determination of AZA1-BSA and AZA1-KLH protein concentration by BCA assay.....	139
3.2.2	Determination of murine immune response to AZA1 by indirect ELISA	139
3.2.3	Spectrophotometric determination of extracted mouse RNA concentration	141
3.2.4	Spectrophotometric determination of synthesised cDNA concentration	141

3.2.5	Amplification of antibody genes; variable light and variable heavy chain genes	141
3.2.6	Generation of scFv-encoding gene by SOE PCR	143
3.2.7	pComb3XSS concentration measurement.....	143
3.2.8	Restriction enzyme digestion and ligation of scFv DNA and pComb3XSS.....	144
3.2.9	Electroporation of SOE-pComb3XSS into XL1 Blue electrocompetent <i>E. coli</i>	146
3.2.10	Screening the anti-AZA1 scFv phage library by panning.....	146
3.2.11	Polyclonal phage ELISA of panning output phage.....	147
3.2.12	Colony pick PCR of panning input and output phage.....	148
3.2.13	Determination of wild type M13 response towards AZA1 by indirect ELISA	148
3.2.14	Generation of a new AZA1-OVA conjugate and construction of a new anti-AZA1 scFv library	149
3.2.15	Screening the re-constructed anti-AZA1 scFv library	151
3.2.16	Polyclonal phage ELISA.....	151
3.2.17	Development of an assay to measure AZA1 using polyclonal mouse antiserum	152
3.3	Discussion	154
3.4	Future work	162
4	Optimisation of anti-MC-LR scFv binding site and stability.....	165
4.1	Introduction	166
4.2	Results – Binding Site Optimisation	169
4.2.1	Identification of the potential 2G1 binding site and associated binding residues	169
4.2.2	<i>In vitro</i> targeted mutagenesis of 2G1	172
4.3	Discussion – Binding Site Optimisation	177

4.3.1	The role of tyrosine	179
4.3.2	L-P55 appears to maintain 2G1 tertiary structure	181
4.3.3	L-S56 and L-D57 appear to sterically hinder the antibody-toxin interaction.....	181
4.3.4	H-L2 appears to engage in a hydrophobic interaction with MC-LR	182
4.3.5	The critical role of glutamic acid	183
4.4	Future work – binding site optimisation.....	185
4.5	Results – stability optimisation	185
4.5.1	Amino acid residues targeted for mutation	186
4.5.2	Determination of mutant binding response by indirect ELISA	188
4.5.3	Determination of mutant binding response by competitive ELISA.....	189
4.5.4	Evaluation of the effect of mutations to surface-exposed hydrophilic residues on protein expression	191
4.5.5	Analysis of the solubility of 2G1 wild type and hydrophobicity mutants	194
4.5.6	Investigation into the temperature stability of the 2G1 wild type and hydrophobicity mutants.....	197
4.6	Discussion – stability optimisation.....	199
4.7	Future work – stability optimisation	208
4.8	Future work – integration of antibodies into a microfluidic detection system.....	209
5	Generation of an avian anti- <i>B. cereus</i> scFv antibody fragment.....	212
5.1	Introduction	213
5.2	Results	214
5.2.1	Development of polyclonal anti- <i>B. cereus</i> IgY.....	214
5.2.2	Development of an anti- <i>B. cereus</i> recombinant scFv library.....	219
5.3	Discussion	229

6	Evaluation of the toxic effects of AZA1, MC-LR and <i>M. aeruginosa</i> on human hepatocellular carcinoma cells	238
6.1	Introduction	239
6.2	Results	241
6.2.1	Determination of the effects of MC-LR, <i>M. aeruginosa</i> cells and AZA1 on HepG2 cell proliferation	241
6.2.2	Analysis of the effects of AZA1 on HepG2 cell health using High Content Analysis (HCA)	244
6.2.3	Investigation of the combined effects of MC-LR with <i>M. aeruginosa</i> and MC-LR with AZA1 on HepG2 proliferation	248
6.2.4	Determination of the combined effects of MC-LR-, AZA1- and <i>M. aeruginosa</i> -exposure on HepG2 using HCA	250
6.2.5	Determination of the effect of MC-LR- and AZA1-exposure on caspase-dependent apoptosis in HepG2 cells.....	256
6.2.6	IL1 β and TNF α ELISAs.....	257
6.3	Discussion	257
6.3.1	The effects of individual exposure to MC-LR, <i>M. aeruginosa</i> cells and AZA1 on HepG2 cell proliferation	258
6.3.2	HCA indicates that AZA1 induces apoptosis.....	262
6.3.3	Investigations into the combined effects of MC-LR with <i>M. aeruginosa</i> and MC-LR with AZA1 on HepG2 proliferation	264
6.3.4	High Content Analysis – Combination of MC-LR and AZA1	266
6.3.5	FAM-FLICA experiments indicated MC-LR induced apoptosis in HepG2	270
6.3.6	Cytokine ELISAs	272
7	Outcomes and Conclusions	273
8	Bibliography.....	278
9	Appendix A	323

List of Figures

- Figure 1.1: (1) Azaspiracid-1 structure. (2) *Azadinium spinosum*. 7
- Figure 1.2: Occurrences of *Azadinium/Heterocapsa* spp. and AZA toxins (in shellfish) off the Cork coast from 2013 to 2014. 9
- Figure 1.3: Occurrences of *Azadinium/Heterocapsa* spp. and AZA toxins (in shellfish) off the Galway coast from 2013 to 2014..... 9
- Figure 1.4: Structure of IgG. Inset: Structure of antigen-binding domain, showing the CDR regions. 27
- Figure 1.5: Recombinant antibody format examples 30
- Figure 1.6: Structure of Ff bacteriophage. 32
- Figure 1.7: pComb3XSS phagemid map. 33
- Figure 1.8: Concept of panning..... 35
- Figure 1.9: Structure of cereulide..... 38
- Figure 3.1: BCA standard curve..... 139
- Figure 3.2: Serum titre of Mouse A Bleed 8..... 140
- Figure 3.3: Serum titre of Mouse B and C, Bleed 10..... 140
- Figure 3.4: V_κ gene amplification. 142
- Figure 3.5: V_λ gene amplification. 142
- Figure 3.6: V_H gene amplification. 142
- Figure 3.7: SOE PCR. 143
- Figure 3.8: Digested SOE product. 144
- Figure 3.9: Digested pComb3XSS product..... 145
- Figure 3.10: Ligated pComb3XSS plasmid with SOE insertion..... 145
- Figure 3.11: Colony pick PCR. 146
- Figure 3.12: Response of polyclonal phage pools towards AZA1-BSA and BSA. 147
- Figure 3.13: Colony pick PCR of panning input and output phage. 148
- Figure 3.14: M13 phage exhibited non-specific binding to AZA1-BSA..... 149
- Figure 3.15: Binding response of (A) mouse B antiserum and (B) wtM13 towards AZA1-OVA..... 150

- Figure 3.16: Colony pick PCR of 10 clones from the re-constructed anti-AZA1 scFv library. 151
- Figure 3.17: Response of polyclonal phage pools towards AZA1-OVA..... 152
- Figure 3.18: Checkerboard ELISA of various AZA1-OVA coating concentrations and Mouse B antiserum dilutions. 153
- Figure 3.19: Competitive ELISA results of Mouse B antiserum for free AZA1. 154
- Figure 3.20: Concept of the enrichment of non-displaying M13 phage during panning. 160
- Figure 4.1: Concept of the approach used in this work..... 167
- Figure 4.2: 2G1 scFv sequence highlighting the CDRs and putative binding residues..... 170
- Figure 4.3: 3D structure of the 2G1 scFv in complex with MC-LR..... 171
- Figure 4.4: Sequence alignment of the 2G1 wild type with mutants. 173
- Figure 4.5: Western blot of 2G1 scFv wild type and mutant lysates. 174
- Figure 4.6: Indirect ELISA comparing the binding profiles of 2G1 wild type and 2G1 alanine mutant lysates (A) and the 2G1 special case mutants (B). 175
- Figure 4.7: Competitive ELISAs of 2G1 wild type and mutants. 176
- Figure 4.8: Illustration of 2G1 scFv model..... 186
- Figure 4.9: Sequence alignment of 2G1 wild type and six stability mutant clones..... 187
- Figure 4.10: Indirect ELISA comparing the binding profiles of 2G1 wild type and stability mutant lysates. 189
- Figure 4.11: Competitive ELISAs of 2G1 wild type and stability mutants. 190
- Figure 4.12: Analysis of 2G1 wild type and mutant clones by (i) SDS-PAGE and (ii) Western blotting..... 193
- Figure 4.13: Protein yields of 2G1 wild type and hydrophobicity mutants. 194
- Figure 4.14: Native solubility of the 2G1 wild type compared to the stability mutants. 195
- Figure 4.15: Non-native solubility of the wild type 2G1 scFv compared to the stability mutants. 196

- Figure 4.16: Functional temperature stability of wild type 2G1 and mutant clones..... 198
- Figure 4.17: Native solubility measurements of antibody mutants reported by Perchiacca *et al.* (2014)..... 204
- Figure 4.18: ToxiSense LOAD design..... 210
- Figure 5.1: Serum titre of *B. cereus*-immunised chicken pre-bleed and bleed 3 antisera..... 215
- Figure 5.2: BCA assay standard curve..... 216
- Figure 5.3: Response of polyclonal IgY from *B. cereus*-immunised (test) and non-immunised (control) chickens..... 217
- Figure 5.4: Protein concentration measurements after affinity preparation of IgY..... 218
- Figure 5.5: Binding response of the affinity preparation samples towards *B. cereus* and *B. subtilis* cells and spores..... 219
- Figure 5.6: Small-scale V_L and V_H amplification..... 220
- Figure 5.7: Large-scale V_L amplification..... 221
- Figure 5.8: V_H PCR optimisation..... 221
- Figure 5.9: Large-scale V_H amplification..... 221
- Figure 5.10: SOE PCR..... 222
- Figure 5.11: Colony pick PCR of transformed anti-*B. cereus* scFv library..... 223
- Figure 5.12: Colony pick PCR of panning input and output titres..... 225
- Figure 5.13: Monoclonal ELISA Plate 1..... 226
- Figure 5.14: Monoclonal ELISA Plate 2..... 226
- Figure 5.15: Monoclonal ELISA Plate 1 Response Ratio..... 227
- Figure 5.16: Monoclonal ELISA Plate 2 Response Ratio..... 228
- Figure 5.17: Colony pick PCR of nine clones from Monoclonal ELISA..... 229
- Figure 5.18: Concept for immunoaffinity-purification of IgY sample..... 232
- Figure 6.1: Proliferation of HepG2 cells after 24 h exposure to (A) MC-LR and (B) MC-LR + 100 ng/mL LPS..... 243
- Figure 6.2: Proliferation of HepG2 cells after 24 h exposure to (A) whole and (B) lysed *M. aeruginosa* cells..... 243
- Figure 6.3: Effect of 24 h exposure to AZA1 on HepG2 cells..... 243

- Figure 6.4: Effects of AZA1 alone and in the presence of 100 ng/mL LPS on HepG2 cell health.....246
- Figure 6.5: Proliferation of HepG2 cells after 24 h exposure to MC-LR and AZA1.249
- Figure 6.6: Proliferation of HepG2 cells after 24 h exposure to MC-LR and *M. aeruginosa*.249
- Figure 6.7: Effects of combined exposure of HepG2 cells to MC-LR and AZA1 for 18 h.....252
- Figure 6.8: Microscopy images of HepG2 cells exposed to combinations of 2.5 µM MC-LR with 0 – 0.05 µM AZA1.....254
- Figure 6.9: Effects of combined exposure of HepG2 cells to MC-LR and *M. aeruginosa* cells for 18 h.255
- Figure 6.10: Effect of 24 h exposure to MC-LR and AZA1, with and without 100 ng/mL LPS, on activation of Caspase 3/7 in HepG2 cells.....257
- Figure 9.1: Response of anti-*B. cereus* chicken polyclonal antibody to *B. cereus* and *B. subtilis* strains.324

List of Tables

• Table 1.1: Summary of the five major shellfish poisoning toxins.	4
• Table 1.2: European Commission regulatory limits for marine biotoxins compared to the EFSA recommended guidelines	5
• Table 1.3: Summary of the main cyanotoxins and their cyanobacterial producers.	15
• Table 2.1: Reagents.	61
• Table 2.2: Bacterial culture media composition.	64
• Table 2.3: Cell Lines.	65
• Table 2.4: General Buffers.	65
• Table 2.5: Chromatography buffers.	66
• Table 2.6: Antibiotic and IPTG stocks.	67
• Table 2.7: SDS-PAGE gel compositions.	67
• Table 2.8: Equipment.	68
• Table 2.9: Molar ratios for AZA1 conjugate syntheses.	72
• Table 2.10: Immunisation schedule of BALB/C mice.	73
• Table 2.11: Superscript™ III mixture 2 composition.	76
• Table 2.12: Murine scFv primer sequences.	77
• Table 2.13: V _κ PCR master mix composition.	81
• Table 2.14: PCR thermal cycler conditions.	81
• Table 2.15: V _λ PCR master mix composition.	82
• Table 2.16: V _H PCR master mix composition.	82
• Table 2.17: SOE PCR reaction composition.	83
• Table 2.18: SOE PCR conditions.	83
• Table 2.19: Large-scale SOE PCR reaction composition.	84
• Table 2.20: SOE digestion reaction mixture composition.	85
• Table 2.21: pComb3XSS digestion reaction mixture composition.	86
• Table 2.22: Ligation reaction composition.	87
• Table 2.23: Colony pick PCR master mix composition.	88
• Table 2.24: Panning conditions used for screening the anti-AZA1 scFv library.	89
• Table 2.25: Colony pick PCR master mix composition.	93

• Table 2.26: Binding site mutagenesis primer sequences.	100
• Table 2.27: QuikChange Mutagenesis reaction composition.	101
• Table 2.28: QuikChange Mutagenesis reaction conditions.....	101
• Table 2.29: Stability mutagenesis primer sequences.	104
• Table 2.30: Composition of Superscript™ reaction Mixtures 1 and 2.	115
• Table 2.31: Avian scFv primer sequences.	116
• Table 2.32: V _L and V _H PCR reaction composition.	117
• Table 2.33: V _L and V _H PCR amplification conditions.....	117
• Table 2.34: Large scale V _L PCR master mix composition.	118
• Table 2.35: V _H PCR optimisation reaction composition.	118
• Table 2.36: Large Scale V _H PCR master mix composition.	119
• Table 2.37: SOE PCR composition.....	119
• Table 2.38: SOE PCR amplification conditions.	120
• Table 2.39: Large-scale SOE PCR composition.....	120
• Table 2.40: SOE DNA digestion reaction mixture composition.....	121
• Table 2.41: pComb3XSS digestion reaction mixture composition.....	121
• Table 2.42: Ligation reaction composition.	122
• Table 2.43: Colony pick PCR master mix composition.....	123
• Table 2.44: Conditions used for the screening of the anti- <i>B. cereus</i> scFv library	125
• Table 2.45: Colony pick PCR master mix composition.....	127
• Table 3.1: Extracted mouse spleen RNA concentrations.....	141
• Table 3.2: DNA concentration measurements of V _L , V _H and SOE PCR products.....	143
• Table 3.3: Input and output phage titres from each round of panning.....	147
• Table 3.4: Input and output phage titres from each round of panning.....	151
• Table 4.1: This table shows the region of each identified residue.....	171
• Table 4.2 Titres of 2G1 wild type and mutant lysates as determined by indirect ELISA.	175
• Table 4.3: Comparison of IC ₅₀ values for the 2G1 wild type and mutants.....	177
• Table 4.4: Theoretical pI values for the 2G1 wild type, single Asp/Arg mutants and triple Asp/Arg mutants	188

- Table 4.5: Titre values of the 2G1 wild type and hydrophobic residue mutant lysates as determined by indirect ELISA..... 189
- Table 4.6: Comparison of IC₅₀ values for the 2G1 wild type and mutants..... 191
- Table 4.7: Image analysis results of 2G1 wild type and mutant SDS-PAGE images. 193
- Table 4.8: ET₅₀ values of hydrophobicity mutants after temperature treatment..... 198
- Table 4.9: Summary of findings in this section. 199
- Table 5.1: Titre values of *B. cereus*-immunised and control IgY samples for *B. cereus* and *B. subtilis* cells or spores. 217
- Table 5.2: Measurement of extracted RNA and synthesized cDNA concentrations 219
- Table 5.3: DNA concentration measurements of purified PCR products as determined by spectroscopic measurement at 260 nm..... 222
- Table 5.4: Input and output phage titres from each round of panning..... 224
- Table 5.5: Clones chosen from Monoclonal ELISA..... 228
- Table 6.1: Summary of the effects of AZA1 alone and with 100 ng/mL LPS on five HepG2 cell health parameters. 247
- Table 6.2: Summary of the effects of combinations of MC-LR and AZA1 on five HepG2 cell health parameters..... 253
- Table 6.3: Summary of the effects of combinations of MC-LR and lysed *M. aeruginosa* cells on five HepG2 cell health parameters..... 255

Abbreviations

AA	Amino acid
APC	Antigen-presenting cell
APS	Ammonium persulfate
ARfD	Acute reference dose
AZA	Azaspiracid
AZP	Azaspiracid Shellfish Poisoning
BCA	Bicinchoninic Acid
BMAA	β -N-methylamino-L-alanine
BSA	Bovine Serum Albumin
CD	Circular dichroism
cDNA	Complementary deoxyribonucleic acid
CDR	Complementarity determining region
C_H	Constant heavy chain
C_L	Constant light chain
CN	Cell number
CyanoHAB	Cyanobacterial harmful algal bloom
dAb	Domain antibody
dH₂O	Deionised water
DMEM	Dulbecco's modified Eagle's medium
DMSO	Dimethyl sulfoxide
DNA	Deoxyribonucleic acid
DSB	DNA double strand break
EC	European Commission
EDC	N-ethyl-N'-(dimethylamiopropyl)-carbodiimide
EDTA	Ethylenediaminetetraacetic acid
EFSA	European Food Safety Authority
ELISA	Enzyme linked immunosorbent assay
EPA	Environmental Protection Agency
EU	European Union
Fab	Fragment antigen binding
FBS	Foetal bovine serum

Fc	Fragment crystallisable
FCM	Flow cytometry
FITC	Fluorescein isothiocyanate
FR	Framework region
Fv	Fragment variable
GST	Glutathione-s-transferase
HA	Hemagglutinin
HAB	Harmful algal bloom
HCA	High content analysis
hERG	Human <i>ether-a-go-go</i> related gene
HPLC	High Performance Liquid Chromatography
HRP	Horse Radish Peroxidase
IC₅₀	50% inhibitory concentration
Ig	Immunoglobulin
IL	Interleukin
IMAC	Immobilised metal affinity chromatography
IP	Intra-peritoneal
IPTG	Isopropyl- β -D-galactopyranoside
KLH	Keyhole limpet hemocyanin
LB	Lysogeny broth
LC-MS	Liquid chromatography-mass spectrometry
LM	Light microscopy
LOD	Limit of detection
LOQ	Limit of quantification
LPS	Lipopolysaccharide
mAb	Monoclonal antibody
MBA	Mouse bioassay
MC	Microcystin
MC-LR	Microcystin-leucine-arginine
MM	Mitochondrial mass
MMP	Mitochondrial membrane potential
MPT	Membrane permeabilisation transition
mRNA	Messenger ribonucleic acid

MTT	3-(4,5-dimethylthiazol-2-yl)-2,5-diphenyltetrazolium bromide
NA	Nuclear Area
ND	Non-displaying
NHS	N-hydroxysuccinimide
NI	Nuclear Intensity
OVA	Ovalbumin
pAb	Polyclonal antibody
PAGE	Polyacrylamide gel electrophoresis
PBS	Phosphate buffered saline
PBS-T	Phosphate buffered saline with 0.05% (v/v) Tween 20
PCR	Polymerase chain reaction
PEG	Polyethylene glycol
PP	Serine/threonine protein phosphatase
rAb	Recombinant antibody
RNA	Ribonucleic acid
RT	Reverse transcription
SB	Super broth
scFv	Single chain fragment variable
SDS	Sodium dodecyl sulfate
SEC	Size exclusion chromatography
SEM	Standard error of the mean
SOE	Splice by overlap extension
ssDNA	Single stranded DNA
TDI	Tolerable daily intake
TEF	Toxic equivalence factor
TMB	3,3',5,5'-tetramethylbenzidine
TNF	Tumour necrosis factor
VBNC	Viable but non-culturable
V_H	Variable heavy chain
V_L	Variable light chain
WHO	World Health Organisation
wt	Wild type

Units

%	Percent
°C	Degrees Celsius
Abs	Absorbance
ANOVA	Analysis of variance
bp	Base pair
cfu	Colony forming unit
Da	Dalton
g	Grams
kDa	Kilodalton
kg	Kilogram
L	Litre
M	Molar
mg	Milligram
mL	Millilitre
mmol	Millimole
mM	Millimolar
MW	Molecular weight
ng	Nanogram
OD	Optical density
rpm	Revolutions per minute
v/v	Volume per volume
w/v	Weight per volume
µg	Microgram
µL	Microlitre

List of Publications

McPartlin, D.A., Lochhead, M.J., Connell, L.B., Doucette, G.J., O’Kennedy, R.J. (2016). Use of biosensors for the detection of marine toxins. *Essays Biochem*, **60**, 49–58.

McPartlin, D.A., Loftus, J.H., Crawley, A.S., Silke, J., Murphy, C.S., O’Kennedy, R.J. (2017). Biosensors for the monitoring of harmful algal blooms. *Current Opinion in Biotechnology*, **45**, 164–169.

McPartlin, D.A., O’Kennedy, R.J. (2014). Point-of-care diagnostics, a major opportunity for change in traditional diagnostic approaches: potential and limitations. *Expert Review of Molecular Diagnostics*, **14**, 979–998.

Moran, K.L.M., Fitzgerald, J., **McPartlin, D.A.**, Loftus, J.H., O’Kennedy, R. (2016). ‘Biosensor-Based Technologies for the Detection of Pathogens and Toxins’, in: *Comprehensive Analytical Chemistry, Biosensors for Sustainable Food - New Opportunities and Technical Challenges*. Elsevier, pp. 93–120.

Murphy, C., Stack, E., Krivelo, S., **McPartlin, D.A.**, Byrne, B., Greef, C., Lochhead, M.J., Husar, G., Devlin, S., Elliott, C.T., O’Kennedy, R.J. (2015). Detection of the cyanobacterial toxin, microcystin-LR, using a novel recombinant antibody-based optical-planar waveguide platform. *Biosensors and Bioelectronics*, **67**, 708–714.

Sanders, M., **McPartlin, D.**, Moran, K., Guo, Y., Eeckhout, M., O’Kennedy, R., De Saeger, S., Maragos, C., Sanders, M., McPartlin, D., Moran, K., Guo, Y., Eeckhout, M., O’Kennedy, R., De Saeger, S., Maragos, C. (2016). Comparison of Enzyme-Linked Immunosorbent Assay, Surface Plasmon Resonance and Biolayer Interferometry for Screening of Deoxynivalenol in Wheat and Wheat Dust. *Toxins*, **8**, 103.

List of Posters

‘Aisling Project Outreach’. Daniel A. McPartlin, Richard J. O’Kennedy. Science Foundation Ireland Review Meeting, Dublin City University (26th Sep., 2018).

‘Development of an autonomous, *in-situ*, point-of-need system for monitoring harmful algae species *Azadinium spinosum* and its toxin azaspiracid’. Daniel A. McPartlin, Caroline Murphy, Rogério Chumbinho, Joe Silke, Richard J. O’Kennedy. Protein and Antibody Engineering Summit (PEGS), Lisbon, Portugal (3rd Nov., 2015).

‘Development of an immunosensor platform to detect *Azadinium spinosum* and associated toxin azaspiracid-1, a shellfish poisoning toxin’. Daniel A. McPartlin, Caroline Murphy, Joe Silke, Rogério Chumbinho, Richard J. O’Kennedy. School of Biotechnology Research Day, Dublin City University (30th Jan., 2015).

List of Presentations

McPartlin, D.A. *Development of marine-deployable biosensor platforms targeting four algal toxins.* 11th International Conference for Molluscan Shellfish Safety (ICMSS), National University of Ireland, Galway (NUIG) (18th Mar., 2017).

McPartlin, D.A. *We need to talk about our toxic waters.* School of Biotechnology Research Day, Dublin City University (27th Jan., 2017).

McPartlin, D.A. *Development of an immunosensor-based platform to detect *Azadinium spinosum* and associated toxin azaspiracid-1.* Amgen Biotech Experience – Education and Outreach, Dublin City University (28th Sep., 2016).

McPartlin, D.A. *News Just In; Algal Bloom Strikes Again.* Dublin City University, Tell It Straight Competition, *First place winner* (28th Apr., 2016).

McPartlin, D.A. *Point-of-care testing – the key to marine toxin monitoring?* School of Biotechnology Research Day, Dublin City University (30th Jan., 2015).

Courses, Scholarships and Awards

DCU President's Award for Engagement – Special Merit, awarded to the Biological Research Society, Dublin City University (April, 2018).

Chair of the Biological Research Society (BRS), School of Biotechnology, Dublin City University (2017 – 2018).

Laboratory Animal Science and Training (LAST) Animal Handling Training Course for Ireland and UK License. Trinity College Dublin (17 – 18 June, 2014).

Irish Research Society Enterprise Partnership Scheme Scholarship recipient. (2014)

Development of recombinant antibody fragments for toxin and microbial contaminant detection and investigations of microcystin and azaspiracid toxicity.

Daniel McPartlin

Abstract

Harmful algal blooms (HABs) have significant detrimental effects on the environment and on food and water quality. Furthermore, toxins produced by some algal species may enter the food web via shellfish, finfish or by consumption of contaminated drinking water causing gastrointestinal disorders, liver damage and tumour promotion. This research focused on the algal toxins azaspiracid-1 (AZA1) and microcystin-LR (MC-LR). In addition, the Gram positive bacterium, *Bacillus cereus*, is a ubiquitous foodborne pathogen with severe health implications. Strict controls are imposed on the levels of these food contaminants and national monitoring programs help to ensure consumer safety.

Biosensor technology affords a viable approach to monitor food contaminants with high sensitivity and low cost. In addition, the ability to fully automate such systems allows the possibility for fully autonomous, *in situ* monitoring systems for algal toxins and for species-level identification of harmful bacterial species. This thesis describes the development and optimisation of recombinant antibody fragments specific to AZA1 and MC-LR for incorporation into such biosensor systems. An anti-AZA1 scFv library was developed but screening programs could not isolate AZA1-specific clones. However, a competitive assay, using polyclonal antibodies, was developed which could detect 1.19 ng/mL of AZA1. A previously developed anti-MC-LR scFv, designated 2G1, was studied by *in silico* computational modelling and targeted mutagenesis, which allowed for improvements in both antigen-binding and protein stability. An anti-*B. cereus* scFv library was developed and screened which allowed for the enrichment of clones generating antibodies with preferential binding to *B. cereus*.

This research also focused on investigating the effects of AZA1, MC-LR, and the cyanobacterium *Microcystis aeruginosa* on the human hepatocellular carcinoma cell line, HepG2. The effects of individual and combined exposure to these contaminants was determined using High Content Analysis. The results demonstrated that AZA1 displayed cytotoxic and apoptotic effects on HepG2 cells, whereas MC-LR exposure resulted in both proliferative and necrotic effects. Co-exposure to MC-LR and AZA1 resulted in antagonistic effect whereas synergistic effects were observed for co-exposure to MC-LR and *M. aeruginosa*.

1 Introduction

1.1 Introduction to the thesis

This chapter introduces the concepts of harmful algal blooms and algal toxins and the hazards that they pose to the environment and in terms of food safety. In particular, the two algal toxins of interest for the research described in this thesis are azaspiracid-1 (AZA1) and microcystin-leucine-arginine (MC-LR). The overall effects of these toxins in terms of human health and environmental and economic impact will be introduced. Emphasis will be placed on the importance of monitoring these toxins in water bodies and in food so as to mitigate their harmful effects. In addition to these two waterborne toxins, another focus of this thesis was on the Gram positive, food poisoning bacterium, *Bacillus cereus*. The routes of exposure to and the effects of *B. cereus* in terms of food poisoning will be discussed. The current monitoring techniques for each these toxins/bacterial species will be analysed and will be compared to use of biosensors, which have shown great promise in ensuring food safety with added benefits of ‘real-time’ monitoring at greatly reduced costs.

In addition, concepts of the immune system will be introduced, with particular focus on antibodies. Recombinant antibody fragments and their development will also be introduced, including the generation of an immune response in a host, the construction of recombinant antibody libraries from the immunised host’s antibody repertoire and the screening of antibody libraries to specific targets. Key concepts of antibody library screening, such as phage display and panning, will be discussed. In addition, concepts of antibody structure optimisation will be discussed to provide a background for the work carried out in Chapter 4.

One of the focuses of this thesis was on the effects of AZA1, MC-LR and the MC-LR-producing species, *Microcystis aeruginosa*, on a human liver cell line. Thus, the specific *in vivo* and *in vitro* effects of these contaminants in numerous animal and cell models will be discussed so as to lay a foundation for the toxicity work described in this thesis.

1.2 Harmful algal blooms and algal toxins

Harmful algal blooms (HABs) are a global phenomenon occurring in oceans in all parts of the world. A myriad of factors play a role in influencing the dynamics of bloom growth. Physical factors include temperature (Nair *et al.*, 2013; Horecka *et al.*, 2014), salinity, current, water level (Cusack *et al.*, 2016), water turbulence, shear forces

(Farrell *et al.*, 2012), occurrence of upwelling or downwelling winds (Nair *et al.*, 2013), light availability (Horecka *et al.*, 2014) and biological factors, such as excystment behaviour (cyst/spore formation) (Ní Rathaille and Raine, 2011), tropism and cell–cell interactions (Jonsson *et al.*, 2009). Nutrient-loading into fresh and marine water bodies, especially from phosphorus- and nitrogen-containing sources, can lead to proliferation of HABs, leading to eutrophication (Mostofa *et al.*, 2013; Watson *et al.*, 2016; Zhou *et al.*, 2017). HABs have led to increasing concerns among international authorities in terms of human and animal health, and environmental preservation. Furthermore, HABs are associated with economic challenges, with the annual losses in the realm of tens of billions of US dollars (Anderson *et al.*, 2001; ASIMUTH, 2014; Sanseverino *et al.*, 2016). These concerns largely stem from the increasing occurrence of a number of toxin-producing algal species within HABs. Phycotoxins and cyanotoxins are secondary metabolites produced by marine algae and blue-green algae (cyanobacteria), respectively. Algae act as primary food sources in the aquatic food web. The concerns around toxins produced by harmful algae stem from the fact that filter-feeding bivalve shellfish, including mussels, oysters and clams, and finfish feed on such toxic algae and bioaccumulate toxins to dangerous levels. Consumption of such contaminated shellfish can lead to acute intoxication syndromes, which vary depending on the toxin group in question and the exposure level. The five major shellfish poisoning-associated marine toxins are summarised in Table 1.1.

Global populations are on the rise and thus the demand for safe food sources is greater than ever. In order to help protect consumer safety, the European Commission (EC) developed regulatory limits for each toxin group (European Commission, 2004). However, due to fears that the EC regulatory limits did not sufficiently protect human health, the European Food Safety Authority (EFSA) made recommendations to impose stricter regulations on marine toxins than the current EC regulations (see Table 1.2). These limits were developed based on the criteria that, if consuming a large portion (400 g) of shellfish, one would not exceed the acute reference dose (ARfD) for the associated toxin. For example, consumption of a 400 g portion of shellfish contaminated with the EU limit of 160 µg okadaic acid (OA) equivalent/kg shellfish would lead to a dietary exposure of approximately three times higher than the ARfD (EFSA, 2008).

Table 1.1: Summary of the five major shellfish poisoning toxins.

Syndrome	Toxin group	Algae/Bacteria Producer	Cellular Target	Symptoms
Amnesic Shellfish Poisoning (ASP)	Domoic Acid (DA)	<i>Pseudo-nitzschia</i> spp., <i>Nitzschia navis-varingica</i> , <i>Chondria armata</i>	Glutamate receptors	Short-term memory loss, confusion, disorientation, vomiting, diarrhoea, death.
Diarrhetic Shellfish Poisoning (DSP)	Okadaic Acid (OA) Dinophysistoxin (DTX)	<i>Dinophysis</i> spp., <i>Prorocentrum</i> spp.	Protein phosphatases	Nausea, vomiting, diarrhoea, stomach cramps.
Azaspiracid Shellfish Poisoning (AZP)	Azaspiracid (AZA)	<i>Azadinium</i> spp., <i>Amphidoma languida</i>	Human <i>ether-à-go-go</i> -related gene potassium channel	Nausea, vomiting, diarrhoea, stomach cramps.
Paralytic Shellfish Poisoning (PSP)	Saxitoxin (STX)	<i>Alexandrium</i> spp., <i>Gymnodinium catenatum</i> , <i>Pyrodinium bahamense</i>	Sodium channels	Gastrointestinal symptoms, numbness/tingling in mouth and extremities, dizziness, headache, fever, ataxia, respiratory distress, death.
Neurotoxic Shellfish Poisoning (NSP)	Brevetoxin (BTX)	<i>Karenia</i> spp.	Sodium channels	Gastrointestinal symptoms, numbness, tingling sensation, hypotension, paralysis, seizures, coma.

Table 1.2: European Commission regulatory limits for marine biotoxins compared to the EFSA recommended guidelines (EFSA, 2008a, 2008b, 2009a, 2009b, 2010).

Toxin and equivalents	EFSA recommended limit	
	EC regulatory limit (μg toxin eq./kg shellfish/fish)	(μg toxin eq./kg shellfish/fish)
DA	20000	4500
OA	160	45
AZA	160	30
STX	800	75
BTX	800*	NA

*No EU limit in place for BTX. Value equals US FDA action limit.

HABs and their associated marine toxins have severe economic implications; one study estimated the annual global economic impact of marine toxins was approximately USD \$4 billion (GESAMP, 2001). These economic implications are associated with the closures of coastal fisheries, loss of valuable shellfish goods, job losses, reduction in tourism and recreational activities and medical treatment for related foodborne- or waterborne-illnesses. HABs and marine toxin levels are also expected to rise, as their occurrence is closely linked to increasing ocean temperatures and to eutrophication (Anderson *et al.*, 2002; Moore *et al.*, 2008). Therefore, there is a pressing need for sufficient monitoring programs to be in place in order to effectively mitigate the potential harmful effects on HABs and algal toxins.

1.2.1 Azaspiracid and *Azadinium spinosum*

One of the focuses of this work is on the phycotoxin AZA1 (see Figure 1.1), which was discovered after a human intoxication event occurred in 1995 in the Netherlands (McMahon and Silke, 1996). Following the consumption of blue mussels (*Mytilus edulis*) originating from Killary Harbour in Ireland, a number of consumers became ill, showing symptoms typical of DSP. However, subsequent analysis found insignificant amounts of DSP toxins present in the suspect shellfish material. In 1997, the toxin was isolated and structurally characterised from Irish mussels (Satake *et al.*, 1998) (and it was later structurally revised) as a novel nitrogen-containing polyether toxin with a structure composed of a cyclic amine (or aza group), a tri-spiro-assembly and a

carboxylic acid group. Since the discovery of AZA1, more than 32 analogues have been discovered, each with varying toxicities (Twiner *et al.*, 2008). It was not until 2008 that *A. spinosum* was discovered as the *de novo* producer of AZA1 and -2 (Tillman *et al.*, 2009).

In vivo mouse toxicological studies have shown that AZAs target the liver, pancreas, lung, spleen, thymus and small intestine. Chronic exposure was also associated with the development of lung tumours in mice (Ito *et al.*, 2000; Ito *et al.*, 2002). It was determined that AZA1-3 exert their toxic effects by binding to the human *ether-a-go-go* related gene (hERG) potassium channel (also called Kv11.1), albeit with moderate/low binding affinity (Twiner *et al.*, 2012; Ferreiro *et al.*, 2014). Using such *in vivo* studies, the relative toxicity of AZA1, -2 and -3 was deduced and allowed the establishment of toxic equivalence factors (TEFs) of 1.0, 1.8 and 1.4, respectively (Alexander *et al.*, 2008). However, *in vitro* studies suggest more drastic potency differences, with TEFs relative to AZA1 of 8.3-fold and 4.5-fold greater for AZA2 and AZA3, respectively. This potency also appeared to be dependent on the cell line tested; for example, AZA2 was more cytotoxic to T lymphocytes while AZA3 was most potent against neocortical neurons (Twiner *et al.*, 2012). Thus far, *in vitro* studies of the cytotoxic potential of AZA1 have shown that all tested cell lines were susceptible, with effects observed down to low nanomolar concentrations (Twiner *et al.* 2012). It was also shown that AZAs are teratogenic to finfish embryos (Colman *et al.*, 2005), suggesting that this toxin group could have severe ecological and economic implications associated with the endangering of fish populations. To date, AZAs and/or *A. spinosum* have been reported in Europe, North Africa, North and South America, and East Asia (Vale *et al.*, 2008; Gu *et al.*, 2013; Trainer *et al.*, 2013; Bacchiocchi *et al.*, 2015). Therefore, the harmful effects of AZAs could be far-reaching, which means that effective monitoring programs are required to mitigate their harmful effects on a global scale.

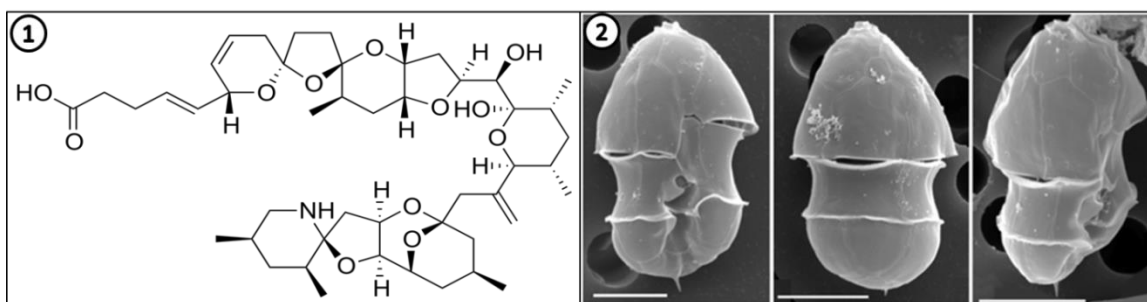


Figure 1.1: (1) Azaspiracid-1 structure. (2) *Azadinium spinosum*. Scale bar = 5 μm . Sourced from Tillman *et al.* (2009).

1.2.2 Occurrences of AZAs and *A. spinosum*

As was discussed earlier, AZAs have been detected in mussels, oysters, scallops, clams, cockles and crabs, and such shellfish/crustaceans serve as the primary vectors for AZAs entering the human food chain. Currently, the only regulated means to monitor AZA levels is the analysis of shellfish tissue that is entering the food chain. This system is effective for helping to ensure consumer safety, but it does not necessarily aid in the prediction of when and where toxic blooms may occur. This is due to the inherent requirements of laboratory-based testing, which may have a turnaround time of up to several days due to transport of samples from the sampling site to the laboratory for subsequent testing.

Examples of the marine monitoring data for the occurrences of AZAs and *Azadinium/Heterocapsa* spp. are presented in Figure 1.2 and 1.3. The data was kindly provided by the Marine Institute, Galway. (Note: These algal genera were grouped together in this manner due to the difficulty of discerning these algae using light microscopy. Therefore, the data shown may at times under- or over-estimate levels of harmful *Azadinium spinosum*). Figure 1.2 displays the occurrences of *Azadinium/Heterocapsa* spp. from water samples and AZA toxins extracted from shellfish from the coast of Co. Cork, Ireland, from 2013 to 2014. It was observed in this data that the levels of AZAs exceeded the regulatory ‘cut-off’ levels during Q3 of 2013, with very high *Azadinium/Heterocapsa* spp. levels observed at a similar time. However, a very different trend was observed for 2014, with AZA toxin levels exceeding the regulatory ‘cut-off’ throughout Q1 and Q2 of the year; in these instances, the levels of *Azadinium/Heterocapsa* spp. did not appear to correlate with the observed high levels of AZAs. Meanwhile, Figure 1.3 displays a similar dataset but represents data from samples acquired off the coast of Co. Galway, Ireland. Despite geographical differences

of only a few hundred kilometres, a very different trend for the occurrences of AZA toxins was observed. In 2013, Q1 experienced levels exceeding the regulatory limit, while Q3 and Q4 displayed levels up to 12-fold greater than the 'cut-off'. In 2014, Q1 experienced AZA levels exceeding the regulatory limit, while the AZA levels for remainder of the year were largely within the acceptable limits. This comes despite the very high cell concentrations of *Azadinium/Heterocapsa* spp. that occurred at this time, with levels exceeding 10^6 cells/L. These data highlight the significant variation of cell numbers and shellfish toxin levels observed annually. One of the possible factors contributing to the observed unpredictable nature of this data is that the toxin levels accumulated in bivalves can remain high for 8 – 12 months after the initial exposure (James *et al.*, 2004). Thus, the high levels of AZAs observed in Cork during Q1 and Q2 of 2014 (Figure 1.2) may have been due to carry-over from Q4 of 2013 when levels were extremely high. The same may also have been the case for the Galway data (Figure 1.3). Furthermore, the grouping of *Azadinium/Heterocapsa* spp. was due to the similar morphological appearance of these genera as determined by light microscopy, which highlights the need for better species-specific methodologies. In particular, these data sets highlight the difficulty in monitoring and predicting when and where toxic algal blooms may occur.

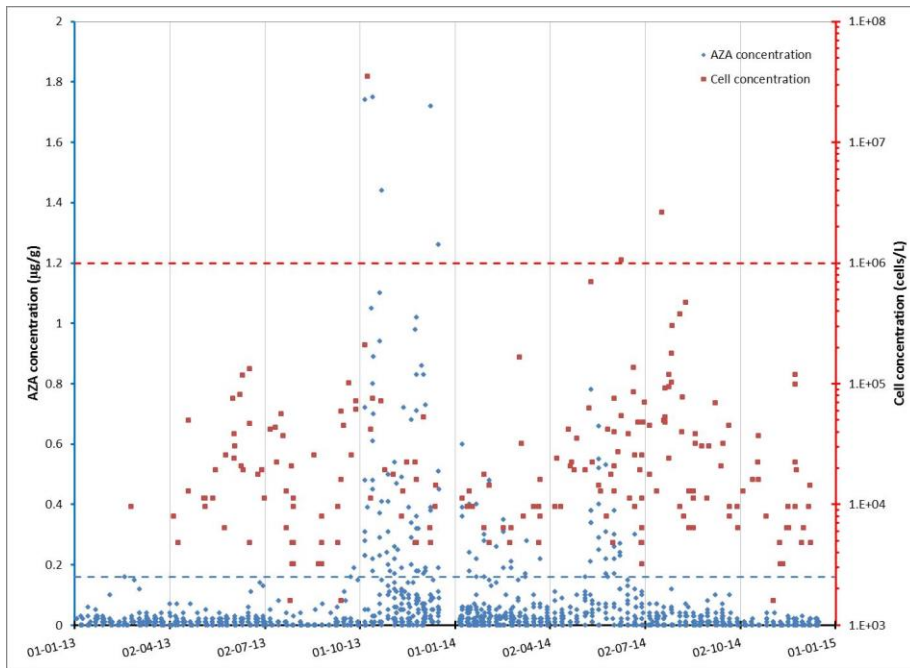


Figure 1.2: Occurrences of *Azadinium/Heterocapsa* spp. and AZA toxins (in shellfish) off the Cork coast from 2013 to 2014. The blue dashed line represents the current regulatory ‘cut-off’ levels of AZA toxins in shellfish (160 µg/kg). The red dashed line represents the level of a high volume algal bloom. Image sourced from McPartlin *et al.* (2017). Data sourced from Silke *et al.* (2016a).

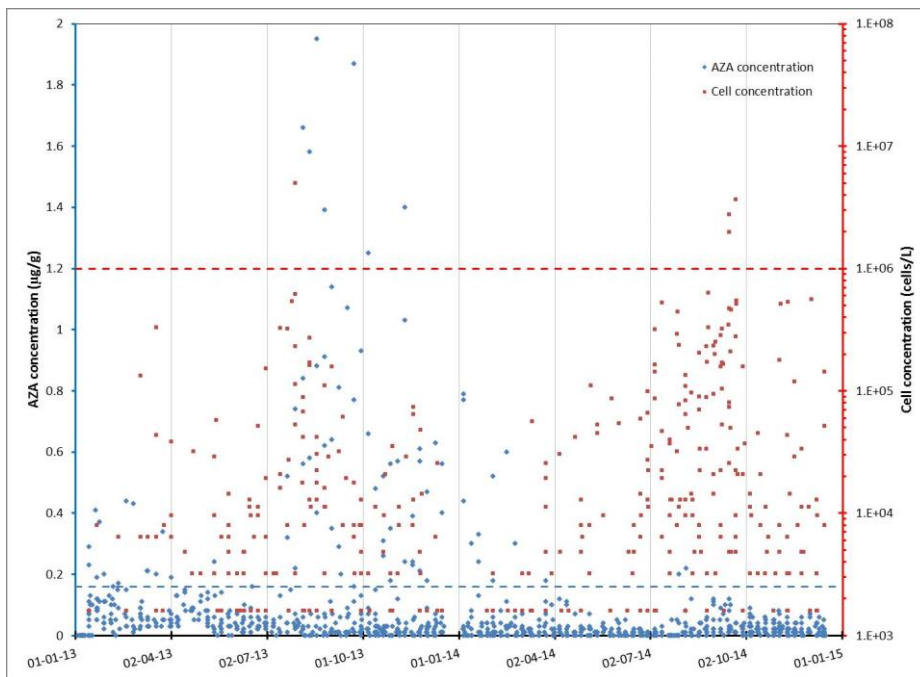


Figure 1.3: Occurrences of *Azadinium/Heterocapsa* spp. and AZA toxins (in shellfish) off the Galway coast from 2013 to 2014. The blue dashed line represents the current regulatory ‘cut-off’ levels of AZA toxins in shellfish (160 µg/kg). The red dashed line represents the level of a high volume algal bloom. Image sourced from McPartlin *et al.* (2017). Data sourced from Silke *et al.* (2016b).

One established means to predict the spatial and temporal occurrences of HABs is through the development of predictive models. However, it is of paramount importance

to have access to up-to-date and high resolution sampling data on the water's physical characteristics and the current algal and toxin levels in order for predictive models to provide a reliable forecast (Anderson *et al.*, 2012; Dale and Murphy, 2014). Thus, the currently employed laboratory-based testing are, unfortunately, not sufficiently rapid enough to provide such up-to-date, or 'near-real-time' data on algal species and their toxins. There are no measures currently in place for monitoring the ongoing levels of toxins and harmful algae, however, recent pioneering work has attempted to address this issue and to strive toward providing 'real-time' monitoring of algae and their associated toxins. In the following section, the current monitoring programs for algal toxins and HABs will be discussed. In addition, notable systems that were recently reported and that could facilitate *in situ* 'real-time' monitoring will also be examined.

1.2.3 Current monitoring programs for algal toxins and HABs

It was mentioned in Section 1.2.2 that the current EC legislation covers only marine toxins present in shellfish; there is an absence of legislation for marine toxins in seawater. Therefore, the approved monitoring programs focus only on detecting marine toxins in seafood. Previously, the most widely employed method for detection of marine toxins in seafood was the mouse bioassay (MBA). This method involved the intra-peritoneal (IP) injection of suspect shellfish tissue extracts into a mouse and the monitoring of symptoms over time until death. This method had obvious ethical issues associated with it and it was also hampered by poor sensitivity. Therefore, as of 1st January 2015, the MBA was prohibited in the EU for marine toxin detection (European Commission, 2011). A number of analytical methods are approved for the marine toxin detection; high-performance liquid chromatography (HPLC) is used for the detection of DA, OA and STX, while liquid chromatography-tandem mass spectrometry (LC-MS/MS) is the approved method for BTX and AZA detection. HPLC methods have superior sensitivity than MBA for marine toxin detection at the current legislative limits; however, this sensitivity may not be sufficient if stricter legislative limits are imposed. This issue may be addressed through the use of LC-MS/MS for detection of all toxin classes, as it possesses excellent sensitivity and the ability to discern different toxin analogues (and therefore overall sample toxicity), and it can also facilitate high-throughput analysis. However, HPLC and LC-MS/MS are both labour-intensive analytical methods, requiring highly trained personnel and expensive equipment.

Monitoring of HABs is currently heavily reliant on traditional methods such as light microscopy (LM), which is highly time-consuming, labour-intensive and requires trained personnel. Additionally, as was exemplified in Section 1.2.2, accurate species-level identification using LM is very difficult, and often requires electron microscopy for confirmation. Frequent sample-acquisition is another requirement of this method, to ensure year-round monitoring of blooms. A more advanced method of HAB-monitoring makes use of satellite imaging to remotely sense ocean colour, which serves as a proxy for ‘in-water’ molecules, such as chlorophyll, that can be used to estimate levels and changes in algal biomass. However, this method is limited by factors including poor sensitivity at low cell concentrations, the detection being restricted to the water surface and interference from clouds. Finally, neither LM or satellite-imaging can identify toxin levels associated with a bloom. Thus, there is a pressing need for an inexpensive, remote, ‘real-time’ monitoring system that can detect toxin-producing algal species and toxin levels in tandem. Such a monitoring system will allow for the early-warning of HAB-development as it commences and will also provide information on the associated toxins levels and if they may present a threat to shellfish farms and consumer safety. A system that can monitor algal and toxin levels in tandem may also provide a greater insight into the seasonality of algae growth and toxin-production, which is a phenomenon that is not fully understood, and this may contribute towards the development of predictive models. A number of notable works have been published in the literature which aimed to address some of the key issues with the monitoring of algal blooms and toxins. For example, a novel microarray system was reported by McCoy *et al.* (2015), which was designed to allow for species-specific identification of harmful algal species using 18S and 28S rDNA probes. This system, called ‘Microarrays for the Detection of Toxic Algae’ (MIDTAL), was designed to specifically alleviate the difficulties associated with LM-based monitoring programs, namely species-identification. Another notable system was reported by Yamahara *et al.* (2015). This system, called the Environmental Sample Processor (ESP) was designed to facilitate fully-automated, species-level identification of harmful algae *in situ*. A number of other recently developed biosensors for monitoring harmful algae and marine toxins were reviewed by McPartlin *et al.* (2016, 2017).

The work in Chapter 3 of this thesis focused on the development of recombinant antibodies specific to AZA1 to be incorporated onto a biosensor platform to detect and

monitor AZA1 levels *in situ*. The principles of biosensors and recombinant antibodies are described in Section 1.3.

1.2.4 *Microcystis aeruginosa* and microcystins

Cyanobacterial HABs (CyanoHABs) are comprised of naturally occurring photosynthetic prokaryotes. Like HABs these occur in a wide variety of aquatic environments and produce toxic secondary metabolites (Preece *et al.*, 2017). It was estimated that ~75% of CyanoHABs are toxic (Chorus *et al.*, 2000). Of all CyanoHAB species, *Microcystis* are the most common (Preece *et al.*, 2017). *Microcystis* is a bloom-forming cyanobacterium of freshwater ecosystems, of which, *M. aeruginosa* is the best-characterised toxin-producing species (Kaneko *et al.*, 2007). The *Microcystis* genus is morphologically characterised by buoyant, unicellular, coccoid-shaped cells with a diameter of 1 – 9 μm (Komárek and Komárková, 2002). CyanoHAB formation and toxin production are influenced by numerous environmental factors such as temperature, salinity, nutrient and light availability, water turbulence, and grazing by higher organisms (Paerl and Huisman, 2009; O’Neil *et al.*, 2012; Visser *et al.*, 2016). Blooms of *Microcystis* tend to occur when the water temperature exceeds 15 °C (Reynolds *et al.*, 1981; Jacoby *et al.*, 2000) and when water bodies become nutrient-enriched (Perovich *et al.*, 2008; Dolman *et al.*, 2012). It is expected that the occurrences and intensity of CyanoHABs will increase, due to increasing global temperatures and increasing nutrient enrichment from activities such as industry and farming (Paerl and Huisman, 2009; Michalak *et al.*, 2013; Preece *et al.*, 2017).

One of the main hazards associated with *Microcystis* blooms is the production of hepatotoxic microcystins (MCs), which are the most common cyanotoxins, with over 100 known variants (Vesterkvist *et al.*, 2012). This inherently poses a significant risk to those using contaminated water resources for drinking water, fishing and recreational activities. *Microcystis* species are among the most common CyanoHABs species, and, in terms of the global distribution, with the exception of Antarctica, *Microcystis* was detected on every continent (Zurawell *et al.*, 2005). A report on global distribution found that *Microcystis* blooms were detected in 108 countries. Of these, the presence of MCs was confirmed in 79 countries (Harke *et al.*, 2016). This indicates a marked increase over time, as a previous analysis suggested the presence of *Microcystis* in less than 30 countries (Zurawell *et al.*, 2005). Exposure to MCs can cause permanent liver

damage and promote tumour development (Grosse *et al.*, 2006; Fujiki and Suganuma, 2009; Li *et al.*, 2011). Numerous MC poisonings have been reported in humans, pets, livestock and wildlife (Merel *et al.*, 2013; Backer *et al.*, 2013; Hilborn *et al.*, 2014).

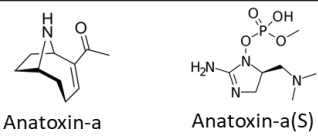
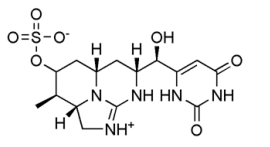
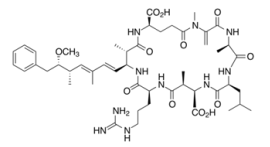
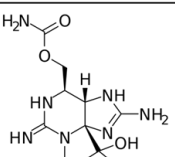
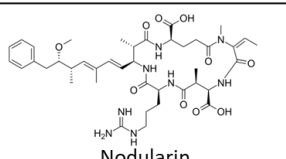
MC is the most well-known of the cyanotoxins. Other cyanotoxins, including anatoxin-a, cylindrospermopsin, saxitoxin and nodularin, can exhibit hepatotoxicity, neurotoxicity, nephrotoxicity and dermatotoxicity. Many of the cyanotoxins and their cyanobacterial producers are summarised in Table 1.3 below. It was also suggested that *Microcystis* can produce β -N-methylamino-L-alanine (BMAA) in addition to microcystins (Cox *et al.*, 2005). BMAA is a non-protein amino acid with links to neurodegenerative diseases such as Parkinson's and Alzheimer's Disease (Bradley and Mash, 2009; Cox and Sacks, 2018). MC was originally designated 'Fast-Death Factor' (Bishop *et al.*, 1959) but was renamed 'microcystin' by Konst *et al.* (1965). MCs are cyclic heptapeptides containing the unique β -amino acid, Adda (3-amino-9-methoxy-2,6,8-trimethyl-10-phenyldeca-4,6-dienoic acid (Tillett *et al.*, 2000). Generally, microcystins contain two standard D-amino acids in positions 1 and 6, a D-erythro- β -methylaspartic acid in position 3, and N-methyldehydroalanine in position 7 (Tillett *et al.*, 2000). The various analogues of microcystin are named according to the single letter codes of the amino acids at positions 2 and 4. For example, Microcystin-Leucine-Arginine (MC-LR) contains leucine and arginine at positions 2 and 4, respectively (Rinehart *et al.*, 1994). The Adda moiety is critical to MC activity (Song *et al.*, 2006).

MCs exert their toxic effects by forming an irreversible covalent bond with serine/threonine protein phosphatases 1 (PP1) and 2A (PP2A) (MacKintosh *et al.*, 1990; Maynes *et al.*, 2006). A number of reports documented the routes of MC-associated illnesses, including consumption of contaminated water, accidental ingestion of water or skin contact during recreational water usage as well as inhalation (Ressom *et al.*, 2004; Wood and Dietrich, 2011). One of the most severe documented cases of MC poisoning was in 1996 in Brazil when microcystin-contaminated water was used in a dialysis treatment clinic. This event resulted in the deaths of 60 people (Azevedo *et al.*, 2002). The main target organ of MCs is the liver, however, it was shown in a number of studies that MCs can also affect other organs such as the intestines, lungs, reproductive system, brain and kidneys (Botha *et al.*, 2004; Ding *et al.*, 2006; Maidana *et al.*, 2006; Soares *et al.*, 2007; Zegura *et al.*, 2008; Li *et al.*, 2009; Lone *et al.*, 2015). Exposure to MCs

manifests in the forms of illnesses such as liver disease, gastroenteritis, and allergic and irritation reactions (Campos and Vasconcelos, 2010).

MC-LR is the most potent and common MC variant, and the World Health Organisation (WHO) set a guideline limit of 1 µg MC-LR per L for water designated for human consumption. MC-LR was also classified as a possible human carcinogen (Group 2B) by the International Agency for Research on Cancer (IARC, 2010). A number of methods have been developed for the measurement of microcystins. These include biological assays such as protein phosphatase inhibition assays (PPIA) and enzyme-linked immunosorbent assay (ELISA) (Almeida *et al.*, 2006; Triantis *et al.*, 2010; Sedda *et al.*, 2016) and numerous analytical chemistry-based methods such as HPLC coupled with photodiode array detection (HPLC-PDA) (Spooft *et al.*, 2003; Tillmanns *et al.*, 2007; Shamsollahi *et al.*, 2015) or coupled with numerous forms of mass spectrometry (MS)-based detection (Ortea *et al.*, 2004; Meriluoto and Codd, 2005; Sangolkar *et al.*, 2006; Allis *et al.*, 2007; Triantis *et al.*, 2010).

Table 1.3: Summary of the main cyanotoxins and their cyanobacterial producers. (Sourced from Neilan *et al.* (2013), Stucken *et al.* (2014), Cirés and Ballot (2016), McAllister *et al.* (2016), Ongley *et al.* (2016), and Cirés *et al.* (2017)).

Toxin	Genera	Toxin structure
Anatoxin-a	<i>Anabaena, Aphanizomenon, Cuspidothrix, Phormidium</i>	 Anatoxin-a Anatoxin-a(S)
Cylindrospermopsin	<i>Aphanizomenon, Chrysochlorum, Cylindrospermopsis, Oscillatoria</i>	 Cylindrospermopsin
Microcystins	<i>Anabaena, Microcystis, Nostoc, Oscillatoria, Phormidium, Planktothrix</i>	 Microcystin-LR
Paralytic Shellfish Toxins	<i>Anabaena, Aphanizomenon, Cuspidothrix, Cylindrospermopsis, Raphidiopsis</i>	 Saxitoxin
Nodularin	<i>Microcystis, Nodularia</i>	 Nodularin

1.2.5 Occurrences of *M. aeruginosa* in brackish waters

A number of studies have shown that marine mussels can become contaminated with MCs to dangerously high levels (Rita *et al.*, 2014; San Francisco Estuary Institute, 2015; Preece *et al.*, 2017). Generally, CyanoHABs tend to occur in freshwater environments, raising the question as to how marine mussels become contaminated with MCs. In this section, the occurrences of *M. aeruginosa* in brackish waters and the exposure of marine mussels to MCs will be discussed.

The tolerable daily intake (TDI) for lifetime exposure to MC-LR is 0.04 $\mu\text{g}/\text{kg}/\text{d}$ (WHO, 2003). From this, the acceptable daily limit of MCs in seafood was established by an Australian Scientific Advisory Board as 40 $\mu\text{g}/\text{kg}/\text{d}$ (Mulvenna *et al.*, 2012). Shellfish consumption poses the greatest risk for toxin exposure, due to the consumption of the entire organism. Furthermore, it was shown that shellfish depurate the toxin slower than finfish (Miller *et al.*, 2010) and some may never completely depurate MCs

(Paldaviciene *et al.*, 2015). On the other hand, finfish primarily accumulate MCs in the liver (Carmichael, 1992), which is not generally consumed. However, fish muscle can also accumulate high levels of MCs (Magalhaes *et al.*, 2001; Poste *et al.*, 2011).

Most freshwater cyanobacteria cannot survive in saline waters for extended periods; however, some genera have high salt tolerance and can grow rapidly in high salinity environments, such as the common MC-producing genera *Anabaena*, *Oscillatoria*, *Microcystis* and *Anabaenopsis* (Robson and Hamilton, 2003; Ross *et al.*, 2006; Tonk *et al.*, 2007). In particular, *M. aeruginosa* has one of the highest salt tolerances and can grow and produce MCs under saline conditions (Otsuka *et al.*, 1999; Orr *et al.*, 2004; Verspagen *et al.*, 2006; Tonk *et al.*, 2007). A number of studies have shown that *Microcystis* spp. can survive for several days at salinities of approximately 50% that of sea water and can survive in sea water for about 2 days (Lehman *et al.*, 2005; Tonk *et al.*, 2007; Miller *et al.*, 2010). This would indicate the *M. aeruginosa* could thrive in estuarine environments where freshwater input reduces the salinity to within the tolerable range of the cyanobacterium (Black *et al.*, 2011; Martín-Luna *et al.*, 2015). Furthermore, it was shown in many studies that salinities of up to 1% (w/v) do not affect MC-production (Tonk *et al.*, 2007; Black *et al.*, 2011; Martín-Luna *et al.*, 2015).

The introduction of freshwater into estuarine waters, via rivers, precipitation and runoff, can enhance vertical stratification in which the lighter freshwater forms a layer over the denser saltwater. This in turn creates favourable conditions for buoyant cyanobacteria such as *Microcystis* (Paerl, 2014). Furthermore, it is expected that heavy rainfall and storm events can mobilise nutrients and cause nutrient enrichment in estuarine waters (Paerl *et al.*, 2006; Paerl and Huisman, 2009). Thus, as global climates change and such storm events become more commonplace, it can be expected that blooms of much higher intensity will occur.

The growing occurrence of *Microcystis* blooms in estuarine waters may also be due to the drifting downstream of CyanoHABs species from upstream lakes and reservoirs (Doi *et al.*, 2008; Preece *et al.*, 2017). This is facilitated by the ability of *M. aeruginosa* to survive over very long distances of travel; for example, it was reported that *M. aeruginosa* survived a 300 km from the bloom source to estuary waters where it was detected (Otten *et al.*, 2015).

1.2.6 Co-exposure to multiple toxins

Together, the evidence here indicates the increasing likelihood of contamination of marine shellfish with MCs. Elsewhere, the appearance of AZAs and OA/DTX2 was recorded in mussels in 2001 in Bantry Bay and the depuration rate of these toxins was similar (Hess *et al.*, 2001). It was subsequently found that the mussels were also contaminated with pectenotoxins (PTXs) (Wilkins *et al.*, 2006). Thus, co-exposure to at least 3 toxins is possible. Furthermore, there is mounting evidence that humans and other organisms are more likely to be exposed to multiple environmental toxins/contaminants than individual toxins (Altenburder *et al.*, 2013; Ma *et al.*, 2017). Previously, the US EPA devised a strategy for risk assessment of the cumulative effects of co-exposure to pesticides (EPA, 2007) but a similar risk assessment has not yet been devised for algal toxins.

Much of the previous research on exposure to toxins has focused on investigating the effects of individual toxins, and few have reported the effects of co-exposure to multiple toxins. Thus, the focus of Chapter 6 of this thesis was on the effects of co-exposure of the hepatocellular carcinoma cell line, HepG2, to combinations of MC-LR with AZA1 and/or *M. aeruginosa*, which have not been investigated to date. In the following sections, previous reports on exposures to MCs, AZAs and *M. aeruginosa* individually will be discussed.

The work in this thesis was carried out on the HepG2 cell line, exposing these cells to AZA1, MC-LR and *M. aeruginosa*. The effects of individual toxins/cyanobacteria on HepG2 were determined using a number of assays; changes in cell proliferation were determined using the MTT assay; changes in the activity of the apoptosis-associated enzymes, caspases-3 and -7, were determined using FAM-FLICA caspase-inhibitor assays; and changes in the overall HepG2 cell health were determined using high content analysis (HCA) (see Section 6.2).

1.2.7 Studies on the toxic effects of AZAs

As was discussed in Section 1.2.1, azaspiracid-1 (AZA1) is a polyether marine toxin produced by *Azadinium spinosum*. AZA1 is associated with severe gastrointestinal problems and the contamination of this toxin in farmed shellfish has major economic implications associated with product losses and recalls. The European Commission's regulatory limit for AZA1 is 160 µg per kg of shellfish product (European Commission,

2004). A number of studies have been conducted to investigate the toxic effects of AZA1 both *in vitro* and *in vivo*, which will be discussed in this section.

Early *in vitro* investigations into the cytotoxic effects of AZA1 on different cell lines identified that the toxin exerts cell-line-dependent effects; AZA1 was shown to exert cytotoxic effects on Jurkat T lymphocytes, Raji B lymphocytes, lung epithelial cells (A549), neuroblasts (Neuro-2A), THP-1 monocytes, human embryonic kidney cells (HEK-293), pituitary epithelial cells (GH₄C₁), and MCF-7 breast cancer cells resulting in a variety of different EC₅₀ values depending on cell line and exposure times (Twiner *et al.*, 2005; Ronzitti *et al.*, 2007). Further investigations into the death pathways activated by AZA1-exposure have also been conducted; for instance, it was shown by Román *et al.* (2002) that AZA1 did not modify mitochondrial activity and did not induce apoptosis in BE(2)-M17 neuroblastoma cells. However, it was subsequently shown by Twiner *et al.* (2012b) that AZA1 can indeed induce apoptosis in BE(2)-M17 cells as well as in Jurkat T lymphocytes and CaCo-2 intestinal cells, activating a number of members of the caspase family. More recently, the genotoxicity of AZA1-3 was investigated in Jurkat T cells, CaCo-2 and HepG2 cells. As was discussed earlier, AZAs are moderate/low blockers of hERG potassium channels (Twiner *et al.*, 2012b, Ferreira *et al.*, 2014a). Ferreira *et al.* (2014b) investigated the effects of AZA2 on hERG channels using CHO cells that were programmed to overexpress hERG channels on their surface. Cells treated with 50 and 200 nM AZA2 for 12 h showed significant increases in hERG channels on their cell surface. It was shown by Annexin-V staining that apoptosis did not yet occur, indicating that AZA2-induced increase of hERG in the plasma membrane occurred before apoptosis. However, it was shown by Xia *et al.* (2016) that increasing the expression of hERG in HepG2 cells allowed for greater influx of potassium ions into the cells and this caused an imbalance of mitochondrial membrane potential that led to the induction of apoptosis. This may be a putative means for AZA-induced apoptosis. In HepG2 cells, AZA1 was tested at 10 – 0.01 nM for 24 and 48 h, and despite showing significant effects on viability at these concentrations, however, the EC₅₀ values were not reported. Furthermore, no apoptotic effect could be observed at the concentrations and duration tested with HepG2 cells (Doerr *et al.*, 2016).

Much of the toxicity work on AZAs reported in the literature has been carried out on *in vivo* models. For example, intra-peritoneal (IP) administration of AZA-containing mussel extracts into mouse models can cause ‘neurotoxin-like’ symptoms, such as respiratory difficulties, sluggishness, spasms, progressive paralysis and death within 20 – 90 min (Satake *et al.*, 1998; McMahon and Silke, 1996, 1998). The IP minimum lethal dose of partially purified AZA reported by Satake *et al.* (1998) was 150 µg/kg. At this concentration, swelling of the stomach and liver was observed and reductions in size and weights of the thymus and spleen were observed. Furthermore, Ito *et al.* (1998) reported that vacuole formation and fatty acid accumulation was observed in hepatocytes after IP administration of AZAs, with dead lymphocyte debris observed in the thymus and spleen, parenchymal cell pyknosis in the pancreas and erosion and bleeding in the stomach were also observed. Also, from such *in vivo* work, the liver has been identified as an organ heavily influenced by AZA1 exposure; *in vivo* exposures to AZA1 can cause swelling of the stomach and liver (Ito *et al.*, 1998). In another study, it was shown that fatty acid droplets formed in the liver as early as 1 h after exposure and the liver was observed to increase in weight after 24 h exposure (Ito *et al.*, 2000). A number of other *in vivo* studies indicate harmful effects of AZAs on the liver (Ito *et al.*, 2002; Twiner *et al.*, 2008). More recent work featuring oral toxicity of AZAs in mouse models showed that after 24 h, the liver was the organ with the third highest accumulation of AZA1, after the stomach and intestinal contents (Pelin *et al.*, 2018). Aside from the report by Doerr *et al.* (2016) mentioned above, who used a AZA1 concentration range of 10 – 0.01 nM, the only other reports of the *in vitro* effects of AZAs on liver cell lines was by Flanagan *et al.* (1999, 2001), who observed significant cytotoxicity in the hepatocellular carcinoma cell line, HepG2. However, in this report, crude mussel extracts were used for which the AZA concentration was not known. Therefore, there is an apparent gap in the knowledge about the effects of higher concentrations of pure AZA1 on liver cells *in vitro*. There is also no report on the EC₅₀ or of the apoptotic effects of AZA1 after 24 h exposure in HepG2 cells. Thus, one of the aims in this study was to address this gap in the knowledge.

1.2.8 Studies on the toxic effects of *M. aeruginosa* and MCs

MCs represent a serious health hazard to animals and human due to their ubiquitous nature in fresh and brackish water bodies around the globe. However, while most environmental monitoring programs are concerned with levels of MC-LR in water

bodies, there is growing evidence that *M. aeruginosa* cells are also a cause for concern. In this section, toxicity work carried out to date on *M. aeruginosa* and MC-LR will be discussed.

Most recent work on *M. aeruginosa*-exposure in the literature has focused on *in vivo* treatments of fish with *M. aeruginosa*-containing water or extracts. For example, it was observed by Rogers *et al.* (2011) that *M. aeruginosa*-exposure in zebrafish caused upregulation of genes associated with exposure to oestrogenic substances, which suggests that *M. aeruginosa* cells may be a natural source of environmental oestrogen, with implications for animal reproduction. In a study by Qian *et al.* (2019), zebrafish were exposed to *M. aeruginosa* cells for 96 h. The results indicated that *M. aeruginosa* exposure enhanced the inflammatory response and caused changes in intestinal microbiota, increasing the proportion of pathogenic bacteria. In another study by Rodrigues Pires Júnior *et al.* (2018), *Lithobates catesbeianus* tadpoles were exposed to *M. aeruginosa* cultures. The results indicated that exposure caused significant damage in multiple organs, characterised by nuclear fragmentation, haemorrhage, loss of adhesion between cells and necrosis. Co-exposure of blunt snout bream to *M. aeruginosa* cells and ammonium had a synergistic effect on immunotoxicity in this fish, in which toxicity was characterised by nuclear shrinkage and mitochondrial dysfunction in lymphocytes (Xia *et al.*, 2018). It was also shown by Abdel-Latif and Khashaba (2017) that *M. aeruginosa* induced toxic effects on Nile tilapia fish via multiple routes of exposure. There are few recent *in vitro* studies examining the effects of pure *M. aeruginosa* cultures on mammalian cell lines. For example, it was observed by Masango *et al.* (2008) that *M. aeruginosa*-containing extracts had a higher potency on primary hepatocytes than pure MC-LR. In baby hamster kidney (BHK-21) cells and mouse embryo fibroblasts (MEF) primary cells, exposure to *M. aeruginosa* cell-free extracts caused significant DNA fragmentation, which is an indicator of necrosis (Lakshmana Rao *et al.*, 1998).

Within the relevant literature, much work has been published on the effects of MC-LR and its analogues on many different cell lines and organisms. *In vivo* studies on MC-LR-exposure have primarily focused on using rodent models. Numerous *in vivo* studies have shown effects of MC-LR leading to direct DNA damage and oxidative DNA damage, as well as the effects of MC-LR on enhancing tumour promotion and tumour

initiation (Ito *et al.*, 1997; Lakshmana Rao *et al.*, 1998, Ding *et al.*, 1999; Sekijima *et al.*, 1999; Gupta *et al.*, 2003; Gaudin *et al.*, 2008).

In terms of *in vitro* work within the published literature, major focus was on the effects of MC-LR on liver cells lines, in particular investigating the effects on primary hepatocytes and the human liver carcinoma cell line, HepG2. A number of different markers of toxicity have been studied, such as the effects of MC-LR on direct DNA damage, oxidative DNA damage and impairment of DNA repair (Zegura *et al.*, 2004; Gehringer *et al.*, 2004; Bouaicha *et al.*, 2005; Lankoff *et al.*, 2006; Gan *et al.*, 2010; Zhang *et al.*, 2013; Ma *et al.*, 2018; Meneely *et al.*, 2018). Other cell lines such as kidney, fibroblast, lymphocytes, Chinese hamster ovary epithelial cells (CHO-K1) and colon adenocarcinoma cell lines have also been used to study MC-LR toxicity (Lankoff *et al.*, 2006; Zegura *et al.*, 2008; Zegura *et al.*, 2011; Wang *et al.*, 2013).

To date, the effects of MC-LR on liver cells is well documented, including the induction of apoptosis at higher concentrations and the induction of cellular proliferation at lower concentrations. Such a bi-phasic response is known as the hormesis effect (Calabrese and Baldwin, 2002). However, there are few reports in the literature on the effects of combinations of MC-LR with other toxins or microbial components on liver cell lines (see below).

1.2.9 Molecular pathways of MC-induced toxicity

The pathways affected by MC-toxicity are diverse and have numerous complex cellular functions. However, two key components that are central to MC toxicity are the inhibition of the PP1 and PP2A enzymes and the induction of free radical-formation.

As mentioned previously, MCs bind to and inhibit the activity of PP1 and PP2A (MacKintosh *et al.*, 1990; Goldberg *et al.*, 1995; Gulledega *et al.*, 2002; Maynes *et al.*, 2006). Inhibition of these enzymes can significantly impact the cell's homeostasis as the critical role of PP1 and PP2A is protein de-phosphorylation. Two pathways that are heavily influenced by the phosphorylation state of cellular proteins are associated with DNA repair; the nucleotide excision repair (NER) and DNA double strand break (DSB) repair by non-homologous end joining (NHEJ) pathways (Douglas *et al.*, 2001; Lankoff *et al.*, 2006). Inhibition of PP1 and PP2A can result in inhibition of these pathways, which in turn increases the chances of DNA damage. The stress caused by DNA

damage activates p53, a nuclear protein that plays a role as a transcriptional trans-activator in DNA repair, apoptosis and tumour suppression pathways (Fu *et al.*, 2005). Furthermore, p53 is regulated by PP2A (Li *et al.*, 2007) and so MC-toxicity also regulates p53. p53 regulates the expression of members of the BCL-2 family, such as Bcl-2, Bax and Bid. Bcl-2 is a protein with an anti-apoptotic role, as it prevents the activation of Bax and Bid (among others). It is also a direct substrate of PP2A. When Bcl-2 is in its phosphorylated form, it is degraded by proteases and thus allow for activation of Bax and Bid (Lin *et al.*, 2006). These proteins play a critical role in the mitochondrial apoptotic pathway, as they form pores in the mitochondrial membrane, a process called membrane permeabilisation transition (MPT) (Weng *et al.*, 2007). This in turn causes the release of cytochrome c into the cytoplasm from the mitochondria (Lemasters *et al.*, 1998). Cytochrome c release triggers apoptosis via activation of cysteine-aspartic proteases (caspases) (Cai *et al.*, 1998; Ott *et al.*, 2002; Morselli *et al.*, 2008).

In addition to the pathways associated with protein phosphatase-inhibition, it was shown in numerous *in vitro* mammalian cell studies and rodent *in vivo* studies that MC-LR-exposure can induce DNA damage. MPT can cause a loss of mitochondrial membrane potential (MMP) and the elevated formation of free radicals such as reactive oxygen species (ROS) and reactive nitrogen species (RNS), further enhancing cell stress. This can negatively affect cellular redox homeostasis and can result in induction of DNA strand breaks (Ding *et al.*, 1998; Zegura *et al.*, 2004; Bouaicha and Maatouk, 2004). Such DNA strand breaks can lead to activation of apoptosis via the mitochondrial pathway described above. Alternatively, the oxidative stress associated with MC-LR-exposure and ROS-formation can cause genome alterations. A number of studies have also indicated that the proliferative effects associated with exposure to low concentrations of MC-LR might be due to the induction of genome alterations, which can lead to cancer development (Yoshizawa *et al.*, 1990; Ohta *et al.*, 1992; Nishikawa-Matsushima *et al.*, 1992; Humpage *et al.*, 2000). Key players involved in this are mitogen-activated protein kinases (MAPKs), which are involved in regulation of proto-oncogenes (Gehring, 2004) and are regulated by PP2A. Thus, MC-inhibition of PP2A may influence MAPK activation, thereby affecting cell proliferation and cancer (Li *et al.*, 2009).

In addition to activation of the mitochondrial apoptotic pathway, the binding to and inhibition of PP1 and PP2A can lead to hyperphosphorylation of cytoskeletal proteins, which can further disrupt a number of cellular processes. Furthermore, this can result in disturbances in cellular homeostasis, cytoskeleton alterations and rearrangements and disruption of liver architecture (Falconer and Yeung, 1992; Toivola and Eriksson, 1999; Ding *et al.*, 2003).

To add further complexity to the toxic effects of MCs, ROS elevation and MMP loss associated with MC-exposure can also lead to depletion of ATP, which can result in necrosis (Zhang *et al.*, 2008; Morselli *et al.*, 2008). Furthermore, the free radical induction and genotoxic effects associated with MC-exposure occur at much lower MC concentrations in hepatic cells versus non-hepatic cells (Zegura, 2016), which may indicate that the liver is more susceptible to MC-damage than other organs.

1.2.10 Principles of High Content Analysis (HCA)

As discussed in Section 1.2.6, the work reported in this thesis featured experiments carried out using High Content Analysis (HCA). HCA (also referred to as High content screening (HCS)) is a cell imaging technique that combines automated fluorescence microscopy and quantitative image analysis. This allows for the acquisition of unbiased multiparametric analysis from the scale of whole cell populations to the sub-cellular scale. The power of HCA is owed to the ability to infer hundreds of biologically relevant quantitative measurements from acquired images of whole cell populations and one of the key strengths of HCA is the ability to screen large sample sizes in high throughput. HCA can be coupled with organelle-specific fluorescent probes (e.g. nuclear and mitochondrial stains, such as those used in this work) allowing for quantitative analysis at the sub-cellular level, which can be used to infer changes in the physiological state of the cell population (such as apoptosis or necrosis). A highly important consideration for HCA experiments is the negating of user-error that can occur from highly-subjective manual scoring of images. Manual scoring is replaced by automated image-processing and data-analysis techniques, which lead to quantitative and highly reproducible results. Indeed, the high sensitivity of HCA comes thanks to the assessment of multiple parameters in-tandem, which allows for identification of subtle phenotypic differences that would not be possible with manual image analysis (Mattiuzzi Usaj *et al.*, 2016; Wilson *et al.*, 2016).

Furthermore, a considerable portion of the toxicology work carried out in this thesis focused on the effects of combinations of toxins/pathogens on HepG2 cells. This was based on much evidence that humans and other organisms are expected to be exposed to complex mixtures of chemical and toxins in the environment, and are less likely to be exposed to one particular compound alone (Altenburder *et al.*, 2013; Ma *et al.*, 2017). Current toxicological risk assessments do not sufficiently estimate the impact of co-exposure to multiple toxins (Maffini and Neltner, 2015). This is due to the complexity of measuring the effects of multiple compounds, which can result in antagonistic and synergistic effects (Seidle and Stephens, 2009). However, the use of HCA facilitates the assessment of such complex mixtures, as exemplified by a number of recent articles (Clarke *et al.*, 2015; Meneely *et al.*, 2018). Given the capability of *A. spinosum* and *M. aeruginosa* to persist in marine and brackish water environments, it is quite possible that during a harmful algal bloom, co-exposure to AZA1, MC-LR and *M. aeruginosa* could occur. Thus, one of the aims of Chapter 6 was to investigate the combined effects of these contaminants on HepG2 cells using HCA.

1.3 Development of Biosensors

Biosensors are devices that combine a biological recognition element, such as an antibody, lectin or enzyme, with a transduction element, i.e. a physical or chemical signalling element that relays the biological signal (Bunde *et al.*, 1998; Healy *et al.*, 2007). The biological recognition element is responsible for the specific interaction with the target ligand and these interactions are converted by the transduction element into digital signals and translated into a readout for user-interpretation (Bunde *et al.*, 1998; Byrne *et al.*, 2009). The quality of the biological recognition element and the specific properties of the transduction element are critical for the overall sensitivity and specificity of the biosensor. The focus of this work is on biosensors that incorporate antibody fragments as their biological recognition element. The immune system and antibody structure and generation are described in detail in the following sections.

1.3.1 Immune system

The immune system is the body's natural defence against pathogens and/or their toxic by-products. It is categorised into two main elements; the innate and adaptive immune systems (Conroy *et al.*, 2009; Yatim and Lakkis, 2015). The innate immune system is a

non-specific defensive barrier against infection, comprising of physical/chemical barriers, such as the skin, mucosal secretions and stomach and intestinal pH, cells such as macrophages, dendritic cells and natural killer cells and other components such as the complement system, which recognise pathogens as foreign and destroy them. Dendritic cells are also important antigen-presenting cells (APCs), displaying foreign antigens to T helper (Th) cells, linking the innate and adaptive immune systems (Paul, 2011). The adaptive immune system has the ability to recognise previously-encountered pathogens and tailor the immune response accordingly. It is mediated by B lymphocytes that are responsible for the secretion of immunoglobulins (antibodies), which are proteins that can bind to virtually any molecule with high affinity and specificity. Antibodies have a number of functions; by binding to the target antigen they form immune complexes which are destroyed by macrophages. The Fc region allows antibodies to interact with the complement cascade and lymphocyte Fc-receptors, mediating complement-dependent cytotoxicity (CDC) and antibody-dependent cell-mediated cytotoxicity (ADCC), respectively (Hansel *et al.*, 2010). Antibodies can also prevent the foreign molecule from interacting with its cellular target in the host, for example, in response to bacterial lipopolysaccharide (LPS) (McCullough and Summerfield, 2005). The adaptive immune system also has the ability to improve its response to known antigens through the development of immunological memory. This allows the immune system to respond to previously encountered antigens with antibodies of a higher affinity in a shorter time after infection (Janeway *et al.*, 2001). The ability of antibodies to bind to virtually any molecule means they are excellent candidates for use as biological recognition elements in biosensors. This work focuses on the development of recombinant antibodies, which are discussed later.

1.3.2 Immunoglobulin structure

Antibodies are heterodimers consisting of two identical heavy (H) chains, with molecular mass of 50-77 kDa, and two identical light (L) chains, with molecular mass of ~25 kDa (Altshuler *et al.*, 2010). The L chain is either a κ or λ chain and consists of a variable region (V_L) joined to a constant region (C_L). The H chain consists of a variable region (V_H) joined to three consecutive constant regions (C_{H1} , C_{H2} and C_{H3}) (IgM and IgE have a fourth C_H region, C_{H4}) (see Figure 1.4). A disulfide bond connects the L and

H chains and two interchain disulfide bonds join the two H chains in C_H2 near the hinge region, while intrachain disulfide bonds stabilise domain folding. There are five isotypes of immunoglobulin, IgG, IgM, IgA, IgD and IgE, which are defined by differences in their H chains. IgG is the predominant Ig isotype in the body, with the longest serum half-life and is the main class of Ig used in the areas of diagnostics and therapeutics (Barbas *et al.*, 2001; Roopenian and Shreeram, 2007). Four IgG subclasses (IgG1-4) were identified, based on structural, antigenic and functional differences in the C_H domains. Generally, IgG1 and -3 are produced in response to protein antigens, while IgG2 and -4 are produced against polysaccharide antigens (Schroeder and Cavacini, 2010). The work in this thesis focused on recombinant antibodies from mice, which were based on IgG, and also on recombinant antibodies from chickens, which were based on IgY. IgY is an immunoglobulin present in avian serum and egg yolk and it is similar in structure to IgG, but includes a fourth C_H domain (Schade *et al.*, 2005).

The C_H2 and C_H3 regions comprise the fragment crystallisable (Fc) domain of the antibody. This domain has a number of functions including interacting with complement and with Fc receptors on the surface of immune cells, such as neutrophils and macrophages, to activate immune pathways (Selvaraj *et al.* 2004). The fragment, antigen binding (Fab) domain of the antibody is comprised of the V_L, C_L, V_H and C_H1 domains. The V_H and V_L domains contain the hypervariable regions of the antibody, called the complementarity determining regions (CDRs). These regions come into close contact with the target antigen to facilitate binding. While the constant domains have highly conserved sequences across different antibody classes, the CDRs exhibit high sequence diversity, which allows antibodies to bind to virtually any antigen (Schroeder and Cavacini, 2010). There are three CDRs in each of the V_L and V_H domains (CDRL1-3 and CDRH1-3). They are located between β -sheets that have high variability in length and amino acid sequence. Typically, CDRH3 is considered to make the main contribution towards antigen-binding, often being at the geometric centre of the antibody-antigen contact (Sundberg, 2009; Diskin *et al.*, 2011). The CDRs are separated by four relatively invariant regions called the framework regions (FRs). The FRs help to maintain the three dimensional structure of the CDRs to allow for the specific interaction with the target antigen. The size and shape of the antigen-binding region can vary significantly, depending on antigen size, Antibodies targeting small molecules such as haptens often have a concave binding surface or cavity, while antibodies targeting

larger molecules such as proteins often have more planar surfaces (Sundberg, 2009; Altshuler *et al.*, 2010). Antibody-antigen interactions occur between the ‘paratope’ on the antibody and the ‘epitope’ on the antigen. These interactions mainly occur through electrostatic interactions, hydrogen bonding and van der Waals interactions (Altshuler *et al.*, 2010).

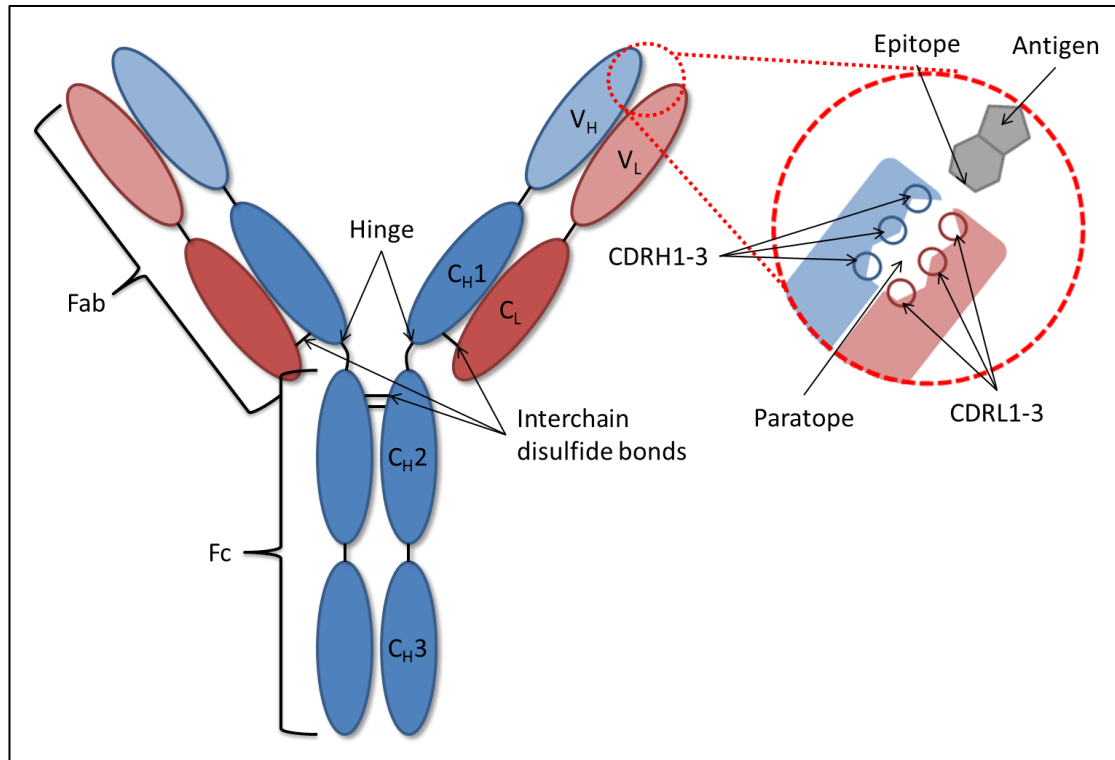


Figure 1.4: Structure of IgG. Inset: Structure of antigen-binding domain, showing the CDR regions.

1.3.3 Antibody gene organisation

Antibody heavy and light chains are separately encoded in different multigene families, and the V domains are encoded by the Variable (V), Diversity (D) and Joining (J) segments (Berg *et al.*, 2002). V_L genes are generally comprised of FR1, -2 and -3, CDRL1, -2 and the amine terminal portion of CDRL3. The joining region of the light chain (J_L) generally contains the carboxy terminus portion of CDRL3 and FR4. V_L diversity is created by rearrangement of the V and J segments. The terminal ends of each gene can also undergo a loss of 1 to 5 nucleotides during rearrangement, which yields ‘junctional diversity’ (Lee *et al.*, 1992). The H chain is considerably more complex than the L chain. The V_H gene is comprised of FR1, -2 and -3, CDRH1, -2 and the amino terminal portion of CDRH3. The heavy chain diversity region (D_H) forms the

middle of CDRH3 and the J_H forms the carboxy end of CDRH3 and FR4. The D and J segments join at the beginning of gene rearrangement to form a DJ intermediate and the V_H region joins to the amino terminal end. V_H gene diversity is generated by the random recombination of one of ~50 V_H elements, one of 27 D_H elements and one of 6 J_H segments, which can produce greater than 10⁴ different VDJ combinations. Additionally, diversity can be expanded by D_H segment inversion or deletion and the D_H segment can be spliced into the three different reading frames. The terminal portions of each of the V_H, D_H and J_H elements can undergo a loss of one or more nucleotides. Nucleotides can also be inserted anywhere between the gene elements in a variable manner by the terminal deoxynucleotide transferase (TdT) enzyme. Overall, V gene recombination events can generate a pre-immune antibody library of greater than 10¹⁶ different antibodies (Berg *et al.*, 2002; Schroeder and Cavacini, 2010).

After antigen presentation by T helper cells, the V genes of germinal centre lymphocytes undergo somatic hypermutation (SHM) (Kim *et al.*, 1981), which induces base pair changes at a rate of 10⁻⁵ to 10⁻³ changes per base pair per cell cycle (Li *et al.*, 2004). A number of mechanisms are involved in SHM: Error-prone DNA synthesis is a mechanism of imperfect synthesis of DNA, causing a mismatch between the template DNA and replicated mutated DNA. The second mechanism targets hotspots that contain the amino acid motif 'RGYW'. Another mechanism is gene conversion between function and non-functional V sequences. SHM allows for affinity maturation, or tailoring of the immune response, to best fit the antigen presented (Steele *et al.*, 1997; Barbas *et al.*, 2001; Schroeder and Cavacini, 2010).

1.3.4 Recombinant antibodies

Recombinant antibodies (rAbs) are produced by genetically manipulating antibody-encoding genes. They offer a number of advantages over polyclonal and monoclonal antibodies; they can be expressed in robust bacterial expression systems to achieve high yields in the gram per litre scale. Tags, such as hexa-histidine (HIS6) and hemagglutinin (HA) tags, can be fused to the antibody to allow for affinity isolation and immobilisation. Antibody affinity can be improved to levels beyond what can be achieved *in vivo* through use of techniques such as targeted- or random-mutagenesis. Many different antibody-conjugates can be produced, such as antibody-enzyme (Tian *et*

al., 2015) and antibody-drug conjugates (Paulik *et al.*, 1999; Bouchard *et al.*, 2014; Gerber *et al.*, 2016) or indeed antibody fusions, that have specificities to multiple targets (Kontermann, 2005; Kontermann and Brinkmann, 2015; Spiess *et al.*, 2015).

The smallest antibody fragment that retains the antigen-binding function of a full-length Ig is the fragment variable (Fv), which is composed of the V_L and V_H domains of the Ig. These domains are brought together only by ionic interactions, thus, Fv molecules are generally unstable. To address this, the V domains can be connected by a disulfide bridge or by a polypeptide linker, creating a disulfide fragment variable (dsFv) or a single chain fragment variable (scFv), respectively (Glockshuber *et al.*, 1990). The small scFv (~27 kDa) is the most commonly developed rAb fragment, as it is considered the simplest rAb for cloning and expression. ScFv are also useful for characterising antibody-antigen binding kinetics due to their monovalent binding (as opposed to a full IgG that has divalent binding), which is required for 1:1 interaction studies (Leonard *et al.*, 2011). However, scFv sometimes exhibit lower affinity than the native Ig and often have lower stability. Due to the absence of the C domains, scFv cannot interact with Fc-receptors, and therefore, during therapeutic use they are characterised as having a short serum half-life (Chames *et al.*, 2009). Issues with scFv-expression include low product solubility, misfolding of protein product and protein aggregation (Frenzel *et al.*, 2013). A frequently-used strategy is to generate a scFv library for screening and characterisation of suitable candidates. Following this, chosen scFv molecules can be converted into full IgG or other formats that may exhibit improved stability and/or pharmacokinetics (Afanasieva *et al.*, 2003; Staelens *et al.*, 2006; Berger *et al.*, 2013; Bujak *et al.*, 2014; Steinwand *et al.*, 2014; Xu *et al.*, 2015) Other rAbs include Fab (composed of the V_L, V_H, C_L and C_{H1} domains of a native Ig; ~50 kDa) and single chain antibodies (scAb) (composed of the V regions and the C_L domain; ~38 kDa) are alternatives to scFv (see Figure 1.5) that have improved stability (due to the inclusion of C domains) and expression characteristics (Barbas *et al.*, 2001; Altshuler *et al.*, 2010).

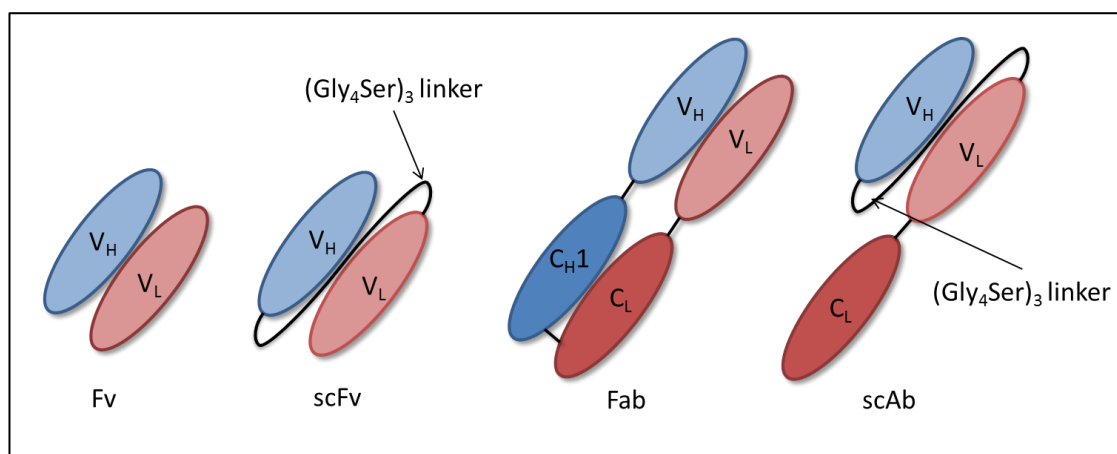


Figure 1.5: Recombinant antibody format examples. The Fv is the smallest antibody fragment that retains the antigen-binding capability of a full IgG. It is comprised of the antibody V_H and V_L domains. The scFv was developed to address the stability issues of the Fv fragment, which was achieved by connecting the variable domains by a flexible glycine-serine linker. The Fab fragment is comprised of the variable domains and the C_{H1} and C_L domains. These are joined by a disulfide bond. The scAb improves upon the stability of the scFv by incorporating the C_L domain attached to the V_L domain.

RABs are well established as biorecognition elements used in biosensors, due to their ability to bind to virtually any molecule with high affinity and specificity. They can also be rapidly expressed in bacterial expression systems at a low cost and a high yield. In order to tailor rABs to a specific target of interest, a frequently used strategy is to immunise a host animal with the target. When a sufficiently strong immune response is generated, the antibody-producing B-cells are harvested from the animal's spleen. The total RNA from these cells is extracted and converted to cDNA by reverse transcription. This cDNA provides a genetic template for the amplification of the antibody variable light and variable heavy genes.

The V_L and V_H genes are amplified by polymerase chain reaction (PCR) using sequence-specific sense and reverse primers. These primers contain extension tails that are non-complementary to the cDNA template. The V_L reverse primers and V_H sense primer tails are complementary to each other and form an overlap. When a Splice-by-overlap extension (SOE) PCR is carried out, the V_L and V_H overlapping sequences are read as a single template and are amplified as a single gene product. The V_L reverse primers also include a long-linker section which encodes a $(Gly_4Ser)_3$ linker. This flexible linker joins the V_L and V_H domains and forms a scFv molecule and this linker affords higher stability of the scFv compared to an Fv. A $(Gly_4Ser)_3$ linker is used as it tends not to form secondary structures and is well tolerated in phage display due to the fact that it is found naturally in the bacteriophage pIII protein (Kretschmar and Geiser,

1995; Barbas *et al.*, 2001; Conroy *et al.*, 2009). This scFv-encoding gene can be inserted into a phagemid vector and transformed into *E. coli* to allow for the production of scFv-pIII fusion proteins. When the *E. coli* are co-infected with helper phage, this scFv-pIII fusion protein is incorporated into new phage particles that ‘display’ the scFv on their surface, while the scFv-encoding phagemid is also encapsulated within the new phage particles; this forms a direct link between the antibody phenotype and genotype. These phage-displayed antibody libraries can then be screened by panning methods to enrich for target-binding antibodies (Barbas *et al.*, 2001).

1.3.5 Bacteriophage

Filamentous bacteriophage of the genus *Inovirus* are a class of virus that are frequently used for antibody-screening and -selection processes. The Ff class of bacteriophage, in particular M13, have been used extensively in this field (Kretschmar and Geiser, 1995; Ward *et al.*, 1996; Lamminmaki *et al.*, 1999; Baltrusch *et al.*, 2001; Ding *et al.*, 2005; Pan *et al.*, 2006; Nejatollahi *et al.*, 2008; Zare *et al.*, 2014). These viruses contain single-stranded DNA within a protein capsid cylinder and can infect *E. coli* via binding to the F pilus. Ff phage do not kill the host bacterium during the infection process. Their single-stranded genome, which contains the genetic information for constructing phage structural proteins and DNA replication, is inserted into the *E. coli* cell. Using the host’s cellular machinery and phage-encoded components, the single-stranded DNA is converted to double-stranded DNA and the phage capsid proteins are synthesised from this DNA template. During the replication process, viral DNA is extruded through a membrane-associated assembly site and newly synthesised capsid proteins are packaged around the DNA. The phage protein structure is described in Figure 1.6 (Barbas *et al.*, 2001; Marvin *et al.*, 2014).

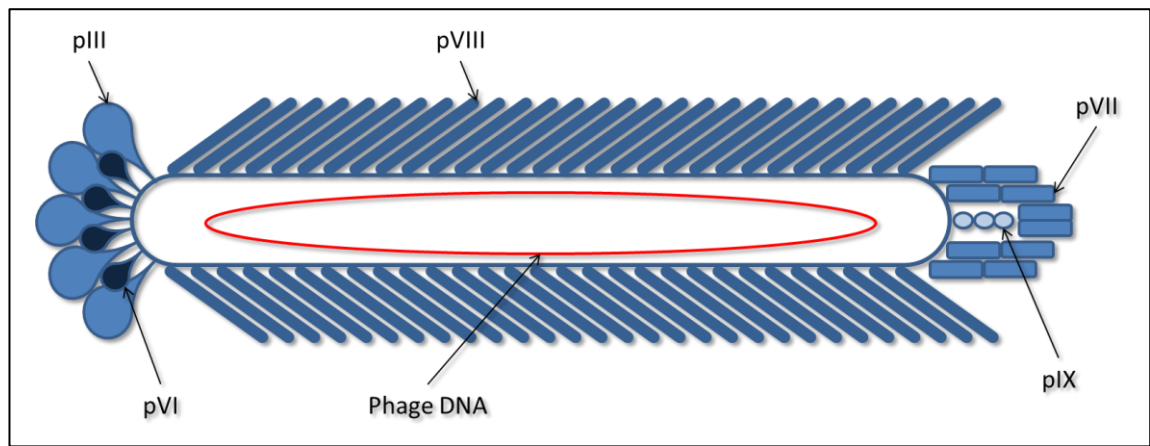


Figure 1.6: Structure of Ff bacteriophage. The Ff phage particle is ~930 nm in length and ~6.5 nm in diameter, with a molecular mass of ~16.3 MD. The DNA is encapsulated in a protein capsid that is mainly composed of the pVIII protein. One end of the particle contains ~5 molecules each of the pVII and pIX proteins. The other end contains ~5 molecules each of the pIII and pVI proteins. The pIII protein is involved in binding to the F pilus of *E. coli* and is also important in phage display methods, as described below. Figure adapted from Barbas *et al.* (2001).

1.3.6 Phage display

Phage display involves the displaying of rAb fragments on the surface of the M13 bacteriophage. This is achieved by the cloning of the antibody-encoding gene into a phagemid vector, such as pComb3XSS (see Figure 1.7), which places the rAb-encoding gene upstream of the pIII protein-encoding gene. When this phagemid vector is transformed into a suppressor strain of *E. coli*, such as XL1 Blue, the rAb is fused to the pIII protein. The phagemid vector does not encode for the other phage structural proteins. Therefore, to allow for expression of infectious phage particles, the *E. coli* are infected with Helper phage (such as M13KO7), which provide the required genomic information to produce complete phage particles. The phagemid and Helper phage DNA are both packaged into newly assembled phage particles. The rAb-pIII fusion protein is also assembled into these new phage particles. The coupling of the rAb DNA within the phage and the rAb protein displayed on the surface provides a physical link between the phenotype and genotype. This link is highly important for screening, as described below. In general, the antibody affinity derived from recombinant libraries is proportional to the library size; a library size of 10^7 - 10^8 clones can have affinity as high as 10 nM, and larger libraries can have sub-nanomolar affinity (Barbas *et al.*, 2001; Hoogenboom, 2005).

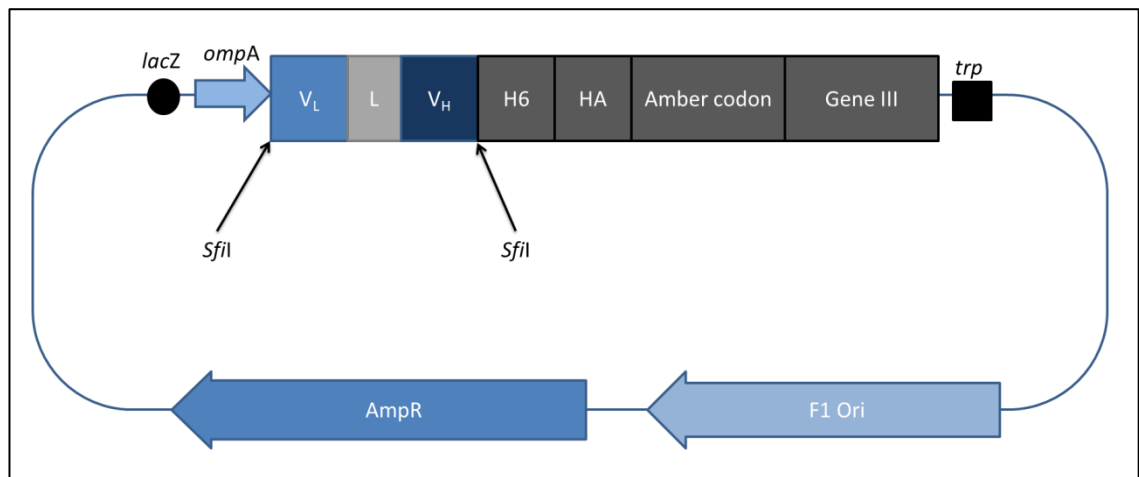


Figure 1.7: pComb3XSS phagemid map. Transcription is driven by a *lacZ* promoter. The expressed protein is directed to the periplasm by the *ompA* signal peptide. The scFv gene (V_L -Linker- V_H) is inserted into the vector via two *SfiI* cloning sites. Downstream of the scFv gene are a H6 and a HA tag that allow for affinity purification and detection. Between the scFv gene and Gene III fragment is an Amber stop codon; this allows for soluble scFv-expression in non-suppressor bacterial strains without the pIII protein. A *trp* terminator allows for transcription termination. The F1 Ori origin of replication allows for plasmid replication. Finally, the AmpR gene confers ampicillin resistance.

1.3.7 Panning

Panning is a process used for screening phage-displayed rAb libraries. Numerous formats have been described in the literature (Conroy *et al.*, 2009). The basic principle (summarised in Figure 1.8) involves the exposure of the phage library to the antigen of interest immobilised onto a surface (such as onto the surface of a multiwell plate, immunotube and/or magnetic bead). Non-specific phage are removed by repeated washing steps. The remaining phage are eluted (elution methods include protein digestion using trypsin and competitive elution using free antigen) and re-infected into *E. coli*. The *E. coli* are infected with Helper phage to produce a new batch of rAb-displaying phage which are subjected to another round of panning. In order to obtain rAb fragments with the highest binding affinities, a selective pressure is placed on them in the panning process. For example, using a limited and decreasing amount of immobilised antigen, the selection will favour antibody clones with lower K_d value (i.e. a lowest dissociation rate); using a short incubation time for antibodies to bind to antigens will favour clones with rapid on-rate kinetics; using long washing procedures and increasing the number of wash steps per round will favour clones with lower off-rate kinetics (Hoogenboom, 2005). Generally, 4-6 rounds of panning are sufficient to reduce the number of potential antibody leads from $>10^7$ clones down to a few hundred

clones. At this stage, the output phage from each round of panning can be characterised for antigen binding by ELISA. A polyclonal phage ELISA is used to determine the combined response of all phage-bound antibodies from each round to the antigen of interest. When the round(s) with the highest antigen-specific response have been identified, the output phage of these rounds are infected into a non-suppressor strain of *E. coli*, such as Top10F'. The pComb3XSS phagemid encodes an amber stop codon, TAG, between the protein of interest and the pIII genes. In suppressor strains of *E. coli* such as XL1 Blue, the TAG codon is read as glutamic acid, whereas in non-suppressor strains such as TOP10F', it is read as a stop codon (Qi *et al.*, 2012). This allows for the soluble expression of rAbs without the attached pIII protein. Each clone is grown up individually in a 96- or 384-well format and each respective rAb is expressed and used in a monoclonal ELISA. In this way, individual antibody clones with favourable characteristics can be identified and brought forward for further analysis (Barbas *et al.*, 2001). In the work described in this thesis, the processes of antibody library construction and screening by phage display and panning will be used to identify rAb fragments that bind with high affinity and specificity to AZA1 and *A. spinosum*. The long-term goal will be to incorporate these rAb fragments onto a biosensor platform and to be deployed onto a marine monitoring buoy at sea with the aim of monitoring AZA1 and *A. spinosum* levels in 'real-time', so as to mitigate the harmful effects of this toxin and harmful algal species.

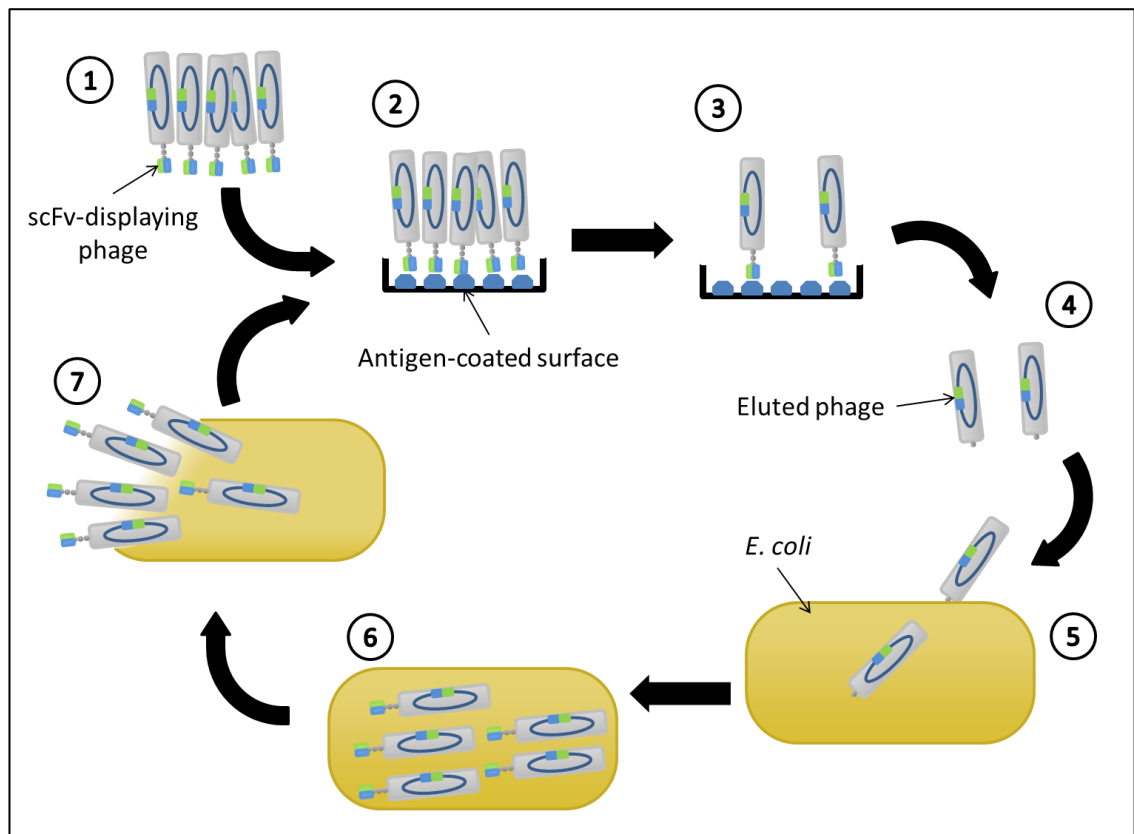


Figure 1.8: Concept of panning. (1) A scFv-displaying phage library is prepared by infection with Helper phage. (2) The phage library is added to a surface coated with the antigen of interest. (3) Non-specific or weaker-bound phage are removed by washing. (4) The remaining phage are eluted. (5) The eluted phage are infected into *E. coli*. (6) The *E. coli* are grown and co-infected with Helper phage to produce scFv-displaying phage. (7) The scFv-displaying phage are released and are subjected to another round of panning.

1.4 *Bacillus cereus*

Another focus of the work described in this thesis was the development of recombinant antibodies specific to the foodborne pathogen *Bacillus cereus*. Such antibodies would be incorporated into a flow cytometry-based assay to identify the harmful *B. cereus* present in dairy products. In this section, the background on *B. cereus* will be discussed, with particular attention to the potential hurdles associated with *B. cereus*-specific biomarkers.

B. cereus is a Gram-positive bacterial species that is ubiquitous in nature and is found in many types of soils, plants, sediments and dust (Kramer and Gilbert, 1989; von Stetten *et al.*, 1999). *B. cereus* is believed to exist as endospores in soil, but when brought into contact with organic matter or a potential host, it germinates and grows. *B. cereus* is adapted to use protein as a nutrient source more so than carbohydrates, but it can

metabolise a large number of carbohydrates (Mols *et al.*, 2007). This shows that *B. cereus* is well adapted to live in soil but also in a host, where it can exist as a pathogen or as part of the intestinal flora (Ceuppens *et al.*, 2013). There is not much data on the existence of *B. cereus* in water, however, cytotoxic strains have been isolated from a number of Norwegian surface waters (Ostensvik *et al.*, 2004).

The taxonomy of *B. cereus* and a number of similar species has been the topic of debate for a number of years. The '*B. cereus* group' is also known as *B. cereus sensu lato* and comprises six species: *B. cereus sensu stricto* (ATCC 14579), *B. anthracis*, *B. thuringiensis*, *B. mycoides*, *B. pseudomycoides* and *B. weihenstephanensis*, however, about 150 subspecies are listed (McIntyre *et al.*, 2008). While *B. anthracis*, *B. cereus* and *B. thuringiensis* have different phenotypic and pathological characteristics, they are closely related in terms of gene content and their 16S rRNA share >99% similarity (Ash *et al.*, 1991). Distinguishing characteristics between the species are encoded on plasmids. *B. thuringiensis* is distinguished in that it produces an insecticidal δ -endotoxin and can be used commercially for insect control in crop production and the insecticidal δ -endotoxin gene (*cry*) is plasmid-encoded (Aronson and Shai, 2001). *B. anthracis* causes anthrax poisoning, which is a fatal animal and human disease and is a known bioterrorism agent. Two plasmids encode the two main virulence factors of *B. anthracis*; pXO1 (anthrax toxin complex) and pXO2 (poly- γ -D-glutamic acid capsule) (Leppla, 2006). *B. mycoides* and *B. pseudomycoides* differ from *B. cereus* by their colony phenotype and fatty acid composition (Nakamura, 1998). Some strains of *B. cereus* can grow at temperatures as low as 4-6 °C (van Netten *et al.*, 1990), such as *B. weihenstephanensis* which is a psychrotolerant species that can grow below 7 °C but not above 43 °C (whereas *B. cereus* grows between 10 and 50 °C) and can also be distinguished by differences in 16S rRNA and cold-shock protein genes (Lechner *et al.*, 1998). *B. cereus sensu stricto* comprises the remainder of the *B. cereus* group members that do not show distinctive traits.

B. cereus strains form endospores that are resistant to heat, dehydration and other physical stresses. These endospores are highly adhesive, which allows them to spread and adhere to different types of food products (Stenfors Arnesen *et al.*, 2008). This bacterium is a contaminant of a wide range of food products and ingredients, including dairy products, spices, rice, dried foods and vegetables, with starchy foods and

vegetables being the food groups most frequently identified as vehicles for *B. cereus* (Kramer and Gilbert, 1989; Glasset *et al.*, 2016). Endospores can also be ‘cross-contaminated’ to other foods such as meat products. The ability of the spores to resist heat-deactivation and cleaning activities (due to characteristics such as hydrophobicity and the presence of exosporium and appendages) confers a significant evolutionary advantage over other potential foodborne bacteria. In addition, the ability of *B. cereus* to form biofilms provides effective resistance to inactivation by sanitising agents (Ryu and Beuchat, 2005) and the ability of vegetative *B. cereus* and *B. weihenstephanensis* to grow at low temperatures are added dangers that are presented by this bacterial group (Wong *et al.*, 1988; Te Giffel *et al.*, 1997; Larsen and Jørgensen, 1999). Some studies have shown that food poisoning ascribed to *B. cereus* was found to be caused by other members of the *Bacillus* group on closer inspection. Some outbreaks were associated with *B. thuringiensis* and *B. mycooides* (McIntyre *et al.*, 2008). The closely related nature of the *B. cereus* group species makes identification of different members a considerable challenge (Charni *et al.*, 2000).

In stark contrast to the *B. cereus* group, *B. subtilis* is a model Gram positive bacterium. It is part of the bacilli bacterial family and is closely linked to *B. licheniformis*; however, while *B. subtilis* is generally regarded as safe, some strains of *B. licheniformis* are known to cause food poisoning. *B. subtilis* is also closely related to the *B. cereus sensu lato* group and to *Listeria monocytogenes* (Danchin, 2001). *B. subtilis* is known to be ubiquitous in many environments. Its spore-forming property allows it to survive in many environments such as in soil (Earl *et al.*, 2008), in close contact with plant root surfaces (Bais *et al.*, 2004; Rudrappa *et al.*, 2007) and in the gastrointestinal tracts of many animals (Tam *et al.*, 2006; Leser *et al.*, 2008). In fact, this bacterium has been observed to convey beneficial probiotic effects on the host, helping to restore a healthy gut microbiome (Hong *et al.*, 2005).

1.4.1 Types of poisonings

B. cereus is associated with two types of foodborne disease, emetic disease and diarrhoeal syndrome. Emetic disease is caused by the toxin cereulide. This toxin is a cyclic dodecadepsipeptide (a depsipeptide is made up of acyl moieties linked by amide and ester bonds) with molecular mass 1.2 kDa (Figure 1.9) and is synthesized by cereulide synthetase, which is a heterodimer of the non-ribosomal peptide synthetase

(NRPS) proteins, Cesa and CesaB (Agata *et al.*, 1994; Ehling-Schulz *et al.*, 2004; Alonzo *et al.*, 2015). The toxin is resistant to proteolysis, and acidic conditions, so it is not destroyed in the gastric tract and, in addition, it can survive treatments of 126 °C for 90 min (FSAI, 2016). The main mechanism of cereulide poisoning is mediated by the serotonin 5-HT₃ receptor and via stimulation of the vagus afferent nerve (Agata *et al.*, 1995). It also acts as a cation ionophore which can inhibit fatty acid oxidation which in turn exerts toxic effects on the mitochondria (Agata *et al.*, 1994; Andersson *et al.*, 1998; Mikkola *et al.*, 1999). Cereulide is pre-formed in foods before ingestion. The symptoms of emetic disease are nausea and vomiting and can occur between 0.5 and 6 h after ingestion and can last between 6-24 h (Ehling-Schulz *et al.*, 2004). In extreme cases, cereulide toxin-associated food poisoning can lead to acute liver failure and death (Kotiranta *et al.*, 2000; Dierick *et al.*, 2005; Stenfors Arnesen *et al.*, 2008, Shiota *et al.*, 2010). Cereulide has been found to not be immunogenic (Andersson *et al.*, 1998; Rajkovic *et al.*, 2006), which may have implications for the detection of this toxin by immunoassay-based methods.

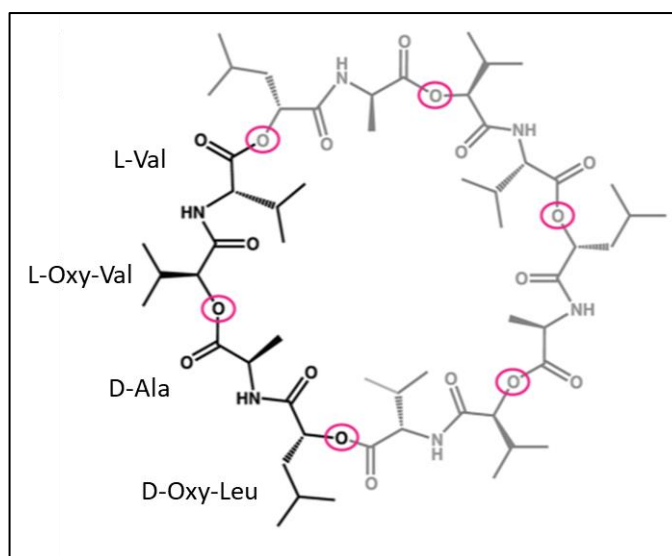


Figure 1.9: Structure of cereulide. The toxin is composed of three repeats of four amino acids; L-Val, L-Oxy-Val), D-Ala and D-Oxy-Leu. (Sourced from Alonzo *et al.* (2015)).

Diarrhoeal syndrome is believed to be a toxicoinfection caused by ingestion of viable cells or spores and the production of protein enterotoxins in the small intestine, which are thought to disrupt the plasma membrane integrity of intestinal epithelial cells (Granum *et al.*, 1993; Andersson *et al.*, 1998; Clavel *et al.*, 2004). Symptoms include diarrhoea and cramps and can occur in the range of 8-16 h after ingestion and the

duration of the syndrome is usually 12-24 h (Kramer and Gilbert, 1989). Three protein enterotoxins have been implicated with diarrhoeal syndrome, which are the pore-forming cytotoxins haemolysin BL (Hbl), nonhaemolytic enterotoxin (Nhe) and cytotoxin K₁ (CytK₁) and CytK₂ (Beecher and MacMillan, 1991; Lund and Granum, 1996; Lund *et al.*, 2000, Wehrle *et al.*, 2010; Glasset *et al.*, 2016).

The two forms of *Bacillus*-related foodborne diseases are generally mild and self-limiting, however, serious and even lethal cases have been reported (Granum, 1994; Mahler *et al.*, 1997; Lund *et al.*, 2000; Dierick *et al.*, 2005). A number of studies have been carried out to determine the prevalence of the different forms of *B. cereus* food-poisoning toxins. For example, Ankolekar *et al.* (2009) analysed 178 samples of raw rice from US retailers and found 52.8% of the samples contained *Bacillus* species spores. The authors analysed these isolates for the toxin-associated genes and found no presence of the cereulide synthetase gene, *ces*, but found that 56.6% of isolates were positive for Hbl-associated genes *hblA* and *hblD*, while 89.1% were positive for the Nhe-associated genes *nheA* and *nheB*. This is in alignment with a number of studies, which have shown that the majority of *B. cereus* strains harbour the *nhe* gene, whereas only ~50% harbour the *hbl* gene (in't Veld *et al.*, 2001; Hansen and Hendriks *et al.*, 2001; Ehling-Schulz *et al.*, 2005).

1.4.2 Biomarkers for *B. cereus*

As a target for detection and measurement, *B. cereus* is a challenging target. Unlike other Gram-positive food-poisoning bacteria, to date, no traditional serological, biochemical or morphological markers have been able to discriminate between *B. cereus* group members (Cronin and Wilkinson, 2010) (for example, the marker internalin A (InIA) is a known species-specific marker for *L. monocytogenes*). This is due to the fact that the distinction between the different members of the *B. cereus* group is difficult to define. As discussed earlier, the differences between group species are often defined by genes encoded on plasmids, which can be transferred by lateral gene transfer.

Despite these challenges, a great deal of work has been done to identify potential markers that may discriminate between the different *B. cereus* group members. For example, enterotoxin FM, (EntFM) is a protein that was first isolated from *B. cereus* FM1. The *entFM* gene is common to *B. thuringiensis* and *B. cereus* strains (Asano *et*

al., 1997). However, further analysis of EntFM by Tran *et al.* (2010) revealed that EntFM is related to a cell wall peptidase specific for *B. cereus* group members and proposed to rename it CwpFM. The authors showed that CwpFM is involved in bacterial motility and shape, adhesion to epithelial cells, the formation of biofilms, vacuolisation of macrophages and virulence (Tran *et al.*, 2010). This cell-surface marker presents as a promising biomarker for *B. cereus* and *B. thuringiensis*, however, further work is required to elucidate the expression of this marker and if it is also present in spores.

Due to the importance of *B. anthracis* in terms of bioterrorism and global safety, much work has focused on identifying biomarkers for this species. Daubenspeck *et al.* (2004) identified an oligosaccharide side chain of the *B. anthracis* exosporium protein, *Bacillus* collagen-like protein of *anthracis* (BclA). The oligosaccharide (designated anthrose) was shown to be specific for *B. anthracis* spores, and was not found on *B. cereus* or *B. thuringiensis* spores. Subsequent to this work, antibodies specific to anthrose were developed (Mehta *et al.*, 2006). Other work, undertaken by Loeff *et al.* (2009) studied cell wall polysaccharides of *B. cereus* and *B. anthracis*. The authors generated hydrogen fluoride (HF)-released cell wall polysaccharides (HF-PSs) from these species, as at this point carbohydrate antigens of vegetative *B. cereus* and *B. anthracis* had not been extensively studied. The authors attempted to determine if the carbohydrates either on the spores or on vegetative cells of these species were antigenic. The HF-PS helps to anchor cell surface proteins (such as S-layer proteins) to the peptidoglycan. The results of this study showed that *B. anthracis* produces a specific HF-PS structure that is identical in *B. anthracis* strains (Ames, Sterne and Pasteur) but was different from that of *B. cereus*. Antisera from rabbit were generated and could detect vegetative cells and spores. The antisera also showed cross-reactivity between *B. cereus* strains G9241, 03BB87, and 03BB102 and *B. anthracis*, but cross-reactivity was not observed for *B. cereus* ATCC 10987 or ATC 14579. It is possible that the HF-PS generated may have different epitopes that produce different antigenic profiles when immunised in an animal; the inner most portion that lies next to the cell wall may not be exposed to the host's immune system. The results suggest that this cryptic epitope near the cell wall may be the cross-reactive epitope. Therefore, the HF treatment effectively uncovers the epitope to the immune system. However, in order for this putative biomarker to be used

in a detection system, HF treatment would need to be incorporated into sample processing in order to make the cryptic portion of the biomarker available for binding.

An interesting study on this area of research (and that is highly relevant to the work in this chapter) was carried out by Mechaly *et al.* (2008). The work focused on the development of a recombinant scFv for *B. anthracis* spores, using a cell-based panning strategy. After identification of a potential scFv, the antibody was used to probe the solubilised exosporium fraction by immunoblot. A >250 kDa band was observed and it was presumed that this was likely the Bcl1 protein, which is the most immunogenic antigen in the exosporium fraction. Further analysis showed that the scFv could discern *B. anthracis* spores from *B. subtilis* spores.

Further evidence that cell wall polysaccharide structures may confer species-specificity in the *B. cereus* group was found by Kong *et al.* (2015). They observed that the endolysin of bacteriophage PBC1, designated LysPBC1, binds to distinct cell wall polysaccharides specific for the *B. cereus* group and it was also weakly active against the *B. subtilis* group and did not act on *Clostridium* and *Listeria* species. The authors commented that the specificity may be conferred by differences in cell wall carbohydrate structures. In terms of carbohydrate structures, the *B. subtilis* bacteria display wall teichoic acid (WTA), which contains a negatively charged phosphate group, whereas *B. cereus* lack WTA (Anderson *et al.*, 2005; Weidenmaier and Peschel, 2008). This information holds promise for the identification of biomarkers specific to *B. cereus*, and shows the merit in investigating not just the proteome, but also the glycoproteome.

Other work on the identification of *B. cereus*-specific markers has been carried out. Daou *et al.* (2009) identified a surface protein, called iron-regulated leucine rich surface protein (IlsA) that is specific to *B. cereus*. However, this protein is only expressed when the bacteria colonises an insect host or under simulated low-iron conditions *in vitro*. Unfortunately, this severely limits its applicability in the monitoring of *B. cereus* contamination in food products. Tagawa (2014) identified flagellar filaments of *B. cereus* strain ATCC 14579 as unique markers. Mouse mAbs were developed and the results showed that the flagellar filaments differ between strains. These mAbs would be useful in identifying vegetative motile *B. cereus* 14579 but the applicability of these mAbs for spores of this strain or for other strains of *B. cereus* has yet to be determined.

1.4.3 Current detection methods

European Commission (EC) regulations on *Bacillus* contamination in dried infant formula and dried dietary food states that *Bacillus* contamination should be “as low as possible”, with a limit of 500 cfu/g, based on a culture-based detection method (European Commission, 2005). There are no official EC guidelines for *Bacillus* levels in raw milk, but dairy companies impose a limit of 10 cfu/mL in raw milk (International Dairy Federation, 2016). Unfortunately, culture-based detection of *B. cereus* is time consuming, ranging from 2-7 days for confirmation, and it is labour- and time-intensive (Izadi *et al.*, 2016). Another disadvantage of culture-based methods is the inability to enumerate viable but non-culturable (VBNC) or non-viable cells (Cronin and Wilkinson, 2010). Other established methods for detection focus on toxin-measurement as an indicator of *B. cereus* contamination. For example, assays to measure cereulide include the HEp-2 cell assay (Hughes *et al.*, 1988; Mahler *et al.*, 1997; Szabo *et al.*, 1991) and the boar sperm motility bioassay (Andersson *et al.*, 1998; Jaaskelainen *et al.*, 2003), based on the mitochondrial toxicity of cereulide. However, disadvantages of the HEp-2 cell assay include the >15 h turnaround time and laborious nature of the method. Meanwhile, the boar sperm motility bioassay can detect cereulide in 5-20 min but suffers cross-reactivity to other mitochondrial toxins (Yamaguchi *et al.*, 2013). Therefore, over the last number of years, a myriad of alternative detection and measurement methods for *B. cereus* have been developed, that range from immunoassays and DNA-based detection to high performance analytical methods, as discussed in the following section.

A number of commercial kits are available for the detection of *B. cereus* enterotoxins. The Tecra™ *Bacillus* Diarrhoeal Enterotoxin VIA kit (3M™) (3M, 2018) is an immunoassay that can detect diarrhoeal enterotoxins in 4.5 h with a sensitivity of 1 ng/mL. The *B. cereus* enterotoxin-reversed passive latex agglutination (BCET-RPLA) kit (Oxoid) is an immunoassay based on latex bead agglutination with a sensitivity of 2 ng/mL in test extract (Oxoid, 2018). The Duopath® *Cereus* Enterotoxins test (Merck) is a lateral flow immunoassay that can detect enterotoxins with a sensitivity of 1 cfu/mL (Merck, 2018). Dietrich *et al.* (2005) also developed an immunoassay that utilises Abs that targets the three subunits of Nhe enterotoxin. These Abs were able to neutralise up to 98% of the cytotoxic activity of Nhe. However, as was noted by Ceuppens *et al.* (2012), preformed enterotoxins do not withstand passage through the stomach, which

suggests that preformed enterotoxins in food do not contribute to the diarrheal food poisoning syndrome. Instead, diarrhoeal syndrome is probably caused by *de novo* enterotoxin production by *B. cereus* cells located in the host's intestinal epithelium. Therefore, by measuring enterotoxins, these commercial assays should be used as an indirect measurement of *B. cereus* contamination.

A number of immunoassay-based methods have been also developed for the measurement of *B. cereus* vegetative cells and endospores. Quinlan and Foegeding (1997) developed mAbs against *Bacillus* spores and could detect the spores of *B. megaterim* ATCC 12872, *B. stearothermophilus* ATCC 7953, *B. subtilis* var. *globigii* and *B. cereus* T. The mAbs did not bind *B. subtilis* A, *B. coagulans* ATCC 56177 or *B. licheniformis* ATCC 9789 but they showed cross reactivity with other genera, including *Clostridium* and *Desulfotomaculum*. While the mAbs could bind to endospores, they could not detect vegetative cells. Meanwhile, Charni *et al.* (2000) developed mouse mAbs against *B. cereus* LMG 6923 that could detect vegetative cells but not spores. Using a capture ELISA approach, the mAbs could react with all *B. cereus* strains tested and with a number of *B. thuringiensis* and *B. mycoides* strains. Though it was not fully elucidated, the target antigen was likely to be a surface protein. The assay could detect vegetative cells with a LOD of 10^2 cells/mL, with no cross reactivity to *Salmonella enteritidis*, *E. coli*, *Proteus vulgaris*, *Citrobacter freundii*, *Micrococcus luteus*, *Pseudomonas stutzeri* or *L. monocytogenes*.

DNA-based methods show great promise for the identification of toxic *B. cereus* group species, as they utilise the exquisite sensitivity of DNA probes for the genetic markers of toxicity. Fricker *et al.* 2007 developed a reverse transcriptase polymerase chain reaction (RT-PCR) method to detect *B. cereus* cells in food. The target for PCR amplification was a highly specific section of the *ces* gene. With a 4-6 h enrichment step, the method could detect 10^0 cfu/g or, omitting the enrichment step, the method could detect 10^1 - 10^3 cfu/g in food samples. The assay could also discriminate *B. cereus* from *S. aureus* (Ehling-Schulz *et al.*, 2004). Izadi *et al.* (2016) developed an electrochemical DNA sensor for diarrhoeal syndrome-causing *B. cereus*. This sensor used a single stranded DNA (ssDNA) probe for the *nheA* gene immobilised on a gold nanoparticle-coated surface. Binding of the target DNA to the immobilised capture probe could then be detected as an electronic readout. The biosensor's sensitivity was

10^0 cfu/mL of *B. cereus* in pure culture. The advantages of this assay include rapidity, low cost and high sensitivity. The assay could also detect *B. cereus* vegetative cells and spores in dairy products without the need for PCR amplification. The *nhe* gene serves as an optimal DNA target for *B. cereus* identification as it is the most prevalent of the toxin genes in all *B. cereus* subspecies. By targeting the virulence-associated gene, this assay could discern virulent from non-virulent members of the same species.

Analytical methods present another means for measuring *B. cereus* toxins, with advantages of automation and high sensitivity. An LC-MS/MS method was developed by Yamaguchi *et al.* (2013) to detect cereulide with a LOD and LOQ of 0.1 and 0.5 ng/mL, respectively. However, to date no methods have been developed that can distinguish between the *B. cereus sensu lato* group species.

The aim of the work in DCU is to develop rAbs that are specific to *B. cereus* vegetative cells and spores and that have low cross-reactivity to *B. subtilis* (vegetative cells and spores). These rAbs will then be incorporated into a flow cytometry (FCM) assay in the University of Limerick that will quantify *B. cereus* cells and spores in dairy products with high sensitivity and specificity. In the following section, the use of FCM for measuring bacterial contaminants will be discussed.

1.4.4 Flow cytometry

As was discussed in the previous sections, markers of virulence (such as emetic or diarrhoeal syndrome toxins or genes) are ideal targets for discriminating toxic *Bacillus* species present in a food sample from non-toxic species. However, for a cell-labelling technique (required for FCM) that is specific for toxic species, these targets are not ideal; the toxins are secreted from cells into the surrounding medium. In addition, antibodies cannot penetrate the cell wall or membrane to target intracellular protein or DNA targets. Hence, a cell-surface marker that distinguishes *B. cereus* from *B. subtilis* would be ideal, as antibodies could bind to targets regardless of whether their cell membrane is intact or compromised. Combining this antibody-labelling with other live/dead counterstains, such as propidium iodide (PI), would allow for species-specific live/dead analysis of food products.

Currently, without the use of antibodies that are species-specific, FCM would not be able to discern between contaminating bacterial species or even genera, without

requiring further confirmatory testing. However, a panel of antibodies, specific for different bacteria could allow for multiplexed analyses of complex samples, enable multiple bacterial species to be enumerated in tandem. As FCM technology improves, it could easily be conceived that 10 or more simultaneous fluorescent detectors could monitor 10 separate bacterial species in a sample. Cronin and Wilkinson (2010) commented that strain-specific antibodies or probes for *B. cereus* incorporated into FCM analyses could negate the requirement for confirmatory tests that are otherwise required for slower growth-based methods. The tandem use of physiological dyes would allow for information on the physiological status of the identified vegetative cells or spores. Additionally, nucleic acid probes that target toxin genes could, in theory, allow for the detection of enterotoxigenic strains amongst the identified *B. cereus* population.

An example of the assay design envisioned for *B. cereus* measurement is an FCM method developed by Chiron *et al.* (2018). The authors tested five probiotic bacterial strains using pAbs that were specific to the subspecies level. Fluorescently-labelled pAbs in combination with SYTO® 24 and PI live/dead staining were used to quantify cell numbers in commercial products. FCM provided significantly higher cell counts than culturing methods, which is likely due to dormant or VBNC bacterial population. The turnaround time for the FCM method was <2 h and the potential of automated and high-throughput FCM equipment is a significant advantage of this technique over culture-based and molecular methods, the latter often requiring the extraction of genetic material (Schumacher *et al.*, 2008). FCM also has great versatility, due to the availability of different targeted dyes and probes, and the ability to measure up to 12 parameters per cell. This in turn can allow for the extraction of a myriad of data from a sample, such as DNA content and physiological state of the cells (for example, depending on the stains used, enzyme activity, redox activity, changes in membrane permeability and potential, and DNA damage can be assessed) (Cronin and Wilkinson, 2010).

Sporulation is a characteristic of *Bacillus* species that has implications for techniques such as ELISA, fluorescence *in-situ* hybridisation (FISH) and PCR, which have a tendency to overestimate cell numbers compared to the plate count method. FCM may present a viable alternative, as it can enumerate the number of suspended particles (cells or spores) in a solution. For example, Leser *et al.* (2008) used FCM with SYTO 13

staining to enumerate endospores and vegetative *B. subtilis* and *B. licheniformis* cells. FCM could be used to carry out 'real-time' analysis of sporulation, but this would require the development of fluorescent antibodies specific to the structural components of the exosporium or coat protein.

Schumacher *et al.* (2008) developed an FCM method that can identify *B. anthracis* from *B. cereus* and *B. thuringiensis*. Using peptide phage display, a peptide, abbreviated to ATYP, was found to specifically bind to *Bacillus anthracis* spores, but it cannot differentiate different strains of *B. anthracis* (Williams *et al.*, 2003). A marker specific to pXO1-harbouring strains of *B. anthracis*, called protective antigen (PA) was also identified and subsequently an anti-PA antibody was generated (Welkos *et al.*, 2001; Cote *et al.*, 2005). Using a combination of the fluorescently-labelled ATYP peptide and anti-PA antibody, a two-colour FCM assay was developed that could discriminate pXO1-harbouring strains of *B. anthracis* from non-pXO1 harbouring strains and from *B. cereus* and *B. thuringiensis* within heterogeneous populations.

Lee *et al.* (2012) used FCM to detect *B. cereus* and other bacterial species that were spiked into platelet products. They showed that 10 cfu/mL of *B. cereus* could be detected 8 h after spiking. However, the authors used only thiazole orange to stain the bacteria. This method would have the disadvantage of not being able to distinguish between the bacterial species present.

Other innovations in the area of FCM shows promise for the use of the technology to measure *Bacillus* toxins. Through use of multiplex-bead-array assays, proteins in solution can be measured. For such assays, microspheres are coated with antibodies specific to the target protein. After capture of the protein of interest onto the bead, a secondary fluorescently labelled antibody can bind to the target. FCM can then be used to measure the fluorescent intensity and hence concentration of the target. In addition, the use of differentially labelled antibodies against different targets can allow for high throughput multiplexed analyses (Elshal and McCoy, 2006).

Of course there are a number of disadvantages of FCM such as the cost of equipment and reagents, and requirement of expertise (Cronin and Wilkinson, 2010), but these disadvantages are certainly counter-balanced given the potential of multiplexed, real-time, species-specific detection of *Bacillus* contamination in food and the generation of vast amounts of data.

1.4.5 Cell-based panning

The approach used in the research described in this chapter to isolate *B. cereus*-specific rAbs was to use a whole-cell panning methodology. Whereas for traditional panning, a known, purified antigen is immobilised to a solid support, for whole-cell panning, the recombinant antibody-phage library is allowed to react with the cell targets in solution. Non-specific or low-affinity binders can be removed from the cells through a series of wash and centrifugation steps. The remaining antibodies can then be eluted using traditional elution steps.

There are a number of advantages of whole-cell panning (Stephenson *et al.*, 1998);

- The target antigen is in its native conformation, which is very important for membrane protein targets. Expressing membrane proteins in large amounts is difficult, due to their hydrophobic transmembrane domains. Outside of the hydrophobic environment of the cell membrane, these proteins can experience conformational changes and aggregation. In addition, when coated on a solid surface (i.e. plastic multiwell plate), these surface proteins can lose their natural conformational structures, hence they become structurally different from what exists in nature. Therefore, binders for such antigens will not be able to identify the antigen in its native form on the cell surface (Alfaleh *et al.*, 2017);
- Unlimited supply of the protein due to the ability to simply grow fresh stock of the bacterial target, and which also negates the need for protein purification;
- Prevents exclusion of epitopes that might be hidden or denatured in solid-based panning;
- Competition-driven elution. After completion of the wash steps to remove non-specific binders, the remaining antibodies can be competitively eluted by mixing with the *E. coli* used for phage-recovery; the number of F pili on the *E. coli* far outnumber the antigens to which the phage-bound antibodies bind. Using this method, it would be expected that even high affinity binders should be eluted.

Difficulties associated with cell-based panning include low receptor density, high background of irrelevant antigens and non-specific adsorption of phage onto the cell surface. The most critical step in any cell-based panning method is the appropriate exposure of target antigen on the cell surface. However, native cells usually have relatively low expression levels of desired antigens which make it difficult to capture

even high-affinity clones from a highly diverse library (Alfaleh *et al.*, 2017). Therefore, a number of steps were taken in order to improve the outcome of the cell-based panning;

- Depletion of the library using negative selection: During the panning regime, the scFv-phage library was sequentially exposed to negative and positive screening steps. The library was initially allowed to bind to *B. subtilis* cells. The cells were then centrifuged in order to remove any clones that would be specific to *B. subtilis* antigens. The remaining library, therefore, should have fewer clones reactive to *B. subtilis*. This remaining library would then be exposed to *B. cereus* for positive selection. (For illustration of this concept, see Figure 5.18 in Section 5.3).
- The nature of the antigen highly affects the likelihood of success. The immunogenicity and accessibility of the target antigen will have a significant impact on the success of panning. Antigens (e.g. a specific biomarker for *B. cereus*) exist at lower concentrations on the cell surface relative to the rest of the host cell proteins, i.e. there is a huge background of irrelevant proteins, which can lead to significant, undesirable non-specific binding events. Blocking agents, therefore, were applied to the target cells to help reduce non-specific binding between scFv-phage and the target cells.

A number of studies have been carried out that successfully used whole-cell panning for Gram-positive bacterial targets. For example, Paoli *et al.* (2004) used whole-cell panning of scFv phage library against *L. monocytogenes*. The library was reacted with *L. monocytogenes* for the positive selection step, followed by *L. innocua* and *L. ivanovii* for the negative selection. The resultant *L. monocytogenes*-specific scFv had no cross reactivity to any other *Listeria* species or any other Gram-positive and -negative bacteria tested. A recombinant anti-*Streptococcus parasanguis* Fab was generated by Stephenson *et al.* (1998). Traditional panning was initially used to isolate a Fab specific to the target protein, fimbriae-associated protein 1 (Fap1), but after 5 rounds of panning using purified antigen, no clones were identified. This may have been due to limited supply of the antigen or poor elution of high affinity binders. Following this, a whole-cell panning method was used and a Fab specific to the Fap1 target was successfully isolated. A novel screening method was developed by Tanaka *et al.* (2008), which

utilised bacterial magnetic particles (BacMPs) obtained from *Magnetospirillum magneticum*. These BacMPs were used in the screening of a phage-displayed peptide library and successfully identified peptides with antimicrobial activity against *B. subtilis* but not against *E. coli*. In addition, whole-cell panning of *Staphylococcus aureus* with peptide phage display was successfully used to identify peptides that bind to the *S. aureus* type 8 capsular polysaccharide (Lenkey, 2016). As was mentioned previously, Mechaly *et al.* (2008) used a cell-based panning approach to develop a scFv to detect *B. anthracis* spores. Thus, one of the aims of Chapter 5 was to use whole-cell panning to screen an anti-*B. cereus* scFv library for *B. cereus*-specific clones.

1.5 Antibody optimisation

In this thesis, one of the main focuses was on the optimisation of an anti-MC-LR scFv, designed in this research group. This scFv is designated 2G1 and its ability to binding to MC-LR and multiple MC congeners is well characterised (Murphy *et al.*, 2015). However, it is desired to refine our understanding of the interaction between the 2G1 scFv and MC-LR by identifying the amino acids (AAs) that are specifically involved in MC-LR binding and elucidating their specific role in this interaction, i.e. whether the residue is involved in direct antigen-binding or plays a secondary structural role. Furthermore, it was of significance to determine if beneficial AA substitutions could be made in order to improve antigen-binding ability.

In addition to improving the antigen-binding ability, it was also desired to improve the solubility and stability of the 2G1 scFv so as to improve the product yield from bacterial expression and the shelf-life of any assays incorporating this antibody. These optimisations were carried out by mutating surface-exposed hydrophobic residues on the antibody surface.

1.5.1 Protein solubility and stability

Protein solubility is a thermodynamic parameter that is defined as the concentration of a protein in a saturated solution that is in equilibrium with a solid phase at a given temperature, pH and solvent composition. It can also be defined as the maximum concentration of protein that remains in solution and that does not cause precipitation or aggregation (Arakawa and Timasheff, 1985; Schein, 1990; Ducruix and Riès-Kautt, 1990; Ahern and Manning, 1992). Solubility is influenced by extrinsic and intrinsic factors. Extrinsic factors include ionic strength, pH, temperature and the presence of solvent additives (Riès-Kautt and Ducruix, 1997). The primary intrinsic factor is the amino acid composition on the protein surface (Kramer *et al.*, 2012).

Protein solubility and stability are related properties. The stability of a protein is the net balance of forces that determine whether a protein will remain in its folded, native state or in its unfolded, denatured state. The interactions that stabilise protein structures are hydrophobic, hydrogen bonding, van der Waals, electrostatic and disulfide bonds. The net stability of proteins is generally very small, at approximately 5 – 10 kcal/mol (Gromiha, 2010). An interesting point is that the solubility and aggregation propensity of a protein *in vitro* are correlated with the abundance of that protein *in vivo*, i.e. low abundance proteins tend to have poorer solubility than high abundance proteins. This is suggested to be another level of controlling *in vivo* protein concentrations and homeostasis, even if gene-expression levels diverge (Tartaglia and Vendruscolo, 2009; Tartaglia *et al.*, 2009; Tartaglia and Vendruscolo, 2010; Castillo *et al.*, 2011). In recombinant protein applications, proteins are required at concentrations well above their native concentration in the cell. However, global correlations between protein abundance *in vivo* and protein solubility strongly suggest that proteins are operating close to the limit of their solubility (Tartaglia and Vendruscolo, 2010); thus, it is a considerable challenge to produce recombinant proteins to the extremely high concentrations required at industry scale. For example, antibody fragments tend to have poor biophysical properties, such as high aggregation propensity even at relatively low concentrations (Jespers *et al.*, 2004a, 2004b).

There are a number of advantages for increasing the stability of an over-expressed protein. Increasing stability can help with increase production yields (Kwon *et al.*, 1996; McLendon *et al.*, 1978). More stable proteins have a longer shelf-life (Sauerborn *et al.*,

2010; Manning *et al.*, 2010; Boulet-Audet *et al.*, 2014) and they show improved survival under unfavourable conditions such as high temperature, presence of solvents and proteases, and pH extremes (Boulet-Audet *et al.*, 2014); higher stability can also allow for the use of higher temperatures, which in turn can improve reaction rates and reduce the chance of bacterial contamination. The use of higher temperatures also has a benefit of further improving the solubility of the protein (Bommarius *et al.*, 2013; Magliery, 2015).

Another benefit of enhanced protein stability is the reduction in the formation of aggregates. Aggregation has implications for protein yield but it is only one of the major concerns for diagnostic and therapeutic antibodies, as it can have major effects on drug potency and drug safety, as aggregated protein therapeutics can cause immunological effects such as anaphylactic shock and cell cytotoxicity (Lawrence *et al.*, 2007; Sauerborn *et al.*, 2010; Manning *et al.*, 2010; Boulet-Audet *et al.*, 2014). In fact, the use of some proteins in a clinical setting is often hampered by aggregation, causing difficulty in handling and poor storage stability (Magliery, 2015). It was estimated that 90% of all potential protein pharmaceuticals are unsuitable for pre-clinical or clinical trials due to poor solubility (Trevino *et al.*, 2007). Protein aggregation is also associated with some human diseases, such as cystic fibrosis, Alzheimer's and Parkinson's (Cohen and Kelly, 2003; Chiti and Dobson, 2006, Perchiacca *et al.*, 2012). Protein aggregation can occur from chemical aggregation, which commonly occurs from nonspecific disulfide bond formation, and physical aggregation, caused by the formation of partially folded intermediates. Temperatures of 40 – 70 °C typically result in the loss of protein activity, which is due to protein unfolding and aggregation (Boulet-Audet *et al.*, 2014).

The solubility of a protein is highly concentration-dependent (Ganesan *et al.*, 2016). For example, mAbs can exhibit high folding stability and solubility while at low concentration, however, their properties can be highly variable and difficult to predict when used at high concentrations, such as those required for subcutaneous delivery (>50 mg/mL) (Shire, 2009). As previously mentioned, amino acid composition is an intrinsic factor that affects protein solubility and strong correlations have been found between a protein's average charge and aggregate formation (Wilkinson and Harrison, 1991). Further to this, noncovalent interactions, such as van der Waals, H-bonding,

hydrophobic and electrostatic interactions dictate the stability of proteins in solution. However, these interactions are highly context-dependent, which makes predicting their effects very challenging (Boulet-Audet *et al.*, 2014).

Generally, proteins are less stable around their isoelectric point and solubility increases with the absolute net charge value (Cohn and Edsall, 1943; Lawrence *et al.*, 2007). For example, Boulet-Audet *et al.* (2014) observed that screening at various pH and ionic strength conditions showed that IgG is less stable around the pI (which for IgG is generally between 5.5 – 6.0), which highlights the impact of electrostatic interactions on IgG stability. It was observed that the IgG was more stable at high pH but also at either low or high salinity.

In bacterial expression systems, the solubility of a protein is an important consideration, and proteins with poor solubility can be rapidly degraded in the periplasm of *E. coli*. Only 15-20% of known *E. coli* proteases reside in the periplasm, however, it has been reported that some exported proteins can be readily degraded in this compartment. The proteolysis of a target protein can lead to very low yield and this can be misinterpreted as poor expression. Kwon *et al.* (1996) reported that, for the protein barnase, it was found that increasing the thermodynamic stability *in vitro* improved the half-life *in vivo* and had the additional benefit of also improving the yield of the protein by 50% versus the wild type. McLendon and Radany (1978) also reported that the thermodynamic stability of the protein's folded structure is a key determinant of the half-lives of the proteins in the cytoplasm of *E. coli*. It was also observed that an increase in the stability of a Fab molecule correlated with higher expression yields and higher levels of correctly folded and functional antibody (Demarest *et al.*, 2006).

A number of methods can be used to estimate the solubility of a protein. SDS-PAGE and Western blotting can be used to qualitatively look at protein aggregation, as determined from the appearance of protein bands at molecular weights higher than the target protein. Other methods include size exclusion chromatography, dynamic light scattering, guanidine hydrochloride denaturation and dynamic scanning fluorescence. Circular dichroism is a frequently used method that can measure subtle conformation changes that occur during protein unfolding and subsequent aggregation (Schwehm *et al.*, 1998; Perl *et al.*, 2000; Pedone *et al.*, 2001; Loladze and Mekhatadze, 2002; Christ *et al.*, 2007; Lawrence *et al.*, 2007; Boulet-Audet *et al.*, 2014). Fourier transform infra-

red (FT-IR) spectroscopy is also useful for detecting aggregation, as folded, unfolded and aggregated protein states give characteristic FT-IR spectra. For example, Boulet-Audet *et al.* (2014) developed an FT-IR spectroscopic method that could distinguish monomeric IgG from aggregated form at high-throughput.

1.5.2 Hydrophobic to hydrophilic mutations

There is much evidence in the literature demonstrating that hydrophobic to hydrophilic mutations are beneficial for enhancing protein stability; there is a considerable bias in favour of solvent-exposed hydrophilic residues on most proteins (Bashford *et al.*, 1987). Studies have shown that hydrophilic amino acids at surface positions have a stabilising effect (Wigley *et al.*, 1987; Reidhaar-Olson and Sauer, 1990; Schwehm *et al.*, 1998). In hyperthermophiles, there is a higher proportion of surface-exposed hydrophilic residues compared to mesophilic species and there is a consistent increase in polar surface area and hydrogen bonds with increased thermostability (Argos *et al.*, 1979; Auerbach *et al.*, 1998; Vogt *et al.*, 1997). Unfortunately, there is no universal stabilisation method that can be applied to all proteins (Jaenicke, 1998), and so much protein-mutagenesis work must be carried out on an *ad hoc* basis.

Looking at antibody-engineering in particular, there are a number of advantages for using small recombinant antibody fragments such as scFv. Full length IgG molecules tend to experience greater difficulty than antibody fragments to correctly fold in bacterial expression systems. The improved folding ability of antibody fragments helps to improve protein yields in *E. coli* versus IgG. However, there are a number of challenges associated with the use of antibody fragments that lack the constant (C) domains, such as scFv and monomeric Fv fragments (also referred to as domain Abs (dAbs) or nanobodies). It is known that the C domains make the most important contributions for the stability of protein folding in Fabs; the interchain disulfide bonds between C domains play a substantial role in their stability (Rothlisberger *et al.*, 2005). The interfacial regions between the H and L domains of antibodies are important for solubility. These regions have complementary hydrophobic residues that can interact with each other. It is suggested that in full Ig molecules, these complementary surfaces are bigger and interact with a different angle than in VH and VL complementary pairs, thus conferring greater protein folding stability (Rothlisberger *et al.*, 2005; Perchiacca and Tessier, 2012). Furthermore, full-length IgG have more stable folding than antibody

fragments (Jager and Pluckthun, 1999; Rothlisberger *et al.*, 2005). This is due to a number of factors such as non-covalent interactions between complementary Ig domains, disulfide bonds between H and L chains and sugar interactions in glycosylated domains (Worn and Pluckthun, 2001). The instability of dAb and scFv is related to the absence of complementarity between domains and lack of interchain disulfide bonds (Shimba *et al.*, 1995). However, there are valuable lessons to be learned from the examples of shark and camelid antibodies.

The antibodies of sharks and camels are referred to as Heavy chain Abs (HCAs), and do not contain an L chain but utilise a single V_H domain for antigen-binding. The camelid V_H domain (V_HH) and the shark V_H domain (called Variable-novel antigen receptor, V-NAR) are highly stable nanobodies (of size 11 – 15 kDa) generated from the full-length antibodies of their respective hosts, that are conformationally stable without a complementary V_L (Perchiacca *et al.*, 2011). The amino acid sequences of the nanobodies reveal that they have more hydrophilic residues than human or mouse V_H domains (Hamers-Casterman *et al.*, 1993; Muyldermans *et al.*, 1994; Barthelemy *et al.*, 2008). A study by Muyldermans *et al.* (2001), whereby camelid and human antibodies were compared, led to the discovery of the so-called V_HH tetrad, which are four AA residues that represent substitutions of hydrophobic residues in human V_H domains for either less hydrophobic or charged residues in camelid antibodies. Three of these occur at the V_H-V_L interface of the human antibodies. In another study, (Ewert *et al.*, 2002) it was shown that camelid antibodies displayed two charged residues in the CDR3 that were occupied by hydrophobic residues in human V_H domains. Thus, in summary, it was found from studies of V-NAR and V_HH antibodies that the enhanced structural stability of these molecules was owed to the improved hydrophilic properties of their surfaces, which was attributed to the replacement of hydrophobic with charged residues.

In the following section, evidence of specific mutations that lead to improvements in protein solubility will be discussed in detail. In general, it was observed that substitutions to arginine and aspartic acid most frequently improved protein solubility.

A large number of methodologies have been applied to the improvement of protein stability and/or solubility. Most reports used bioinformatics to guide rational mutagenesis of surface hydrophobic sites (Leonis *et al.*, 2013; Magliery, 2015; Broom *et al.*, 2017). Some authors report the development of large mutant databases or

libraries, in which selected AA sites are mutated to all standard AAs. For example, Broom *et al.* (2007) developed a meta-predictor for protein solubility and folding. This molecular modelling approach encompassed a number of different modelling software packages to create a database of mutants of the ThreeFoil protein. It was observed that the poor solubility was due to increased hydrophobicity on the surface, which occurred due to the introduction of a hydrophobic residue or changing a charged residue to a polar one on the surface.

In their study, Lawrence *et al.* (2007) investigated the process they called ‘supercharging’, which involved drastically changing the charge of the protein surface by replacing certain residues with positive or negatively charged residues. The aim of this was to determine if ‘supercharging’ would affect the proteins function and how it would affect solubility and thermostability. Using green fluorescent protein (GFP), 29 highly solvent-exposed residues were mutated to Lys or Arg. It was observed that ‘supercharged’ GFP remained soluble when heated to 100 °C and also recovered fluorescence upon cooling. It also appeared to remain entirely soluble upon thermal or chemical denaturation. A ‘supercharged’ mutant of streptavidin was also generated; the mutants retained biotin-binding capacity, albeit at a reduced level. These mutants were more resistant to thermal aggregation than the wild type. Finally, glutathione-S-transferase (GST) was also supercharged and retained enzymatic activity whilst remaining soluble upon heating to 100 °C and it also retained 40% activity upon cooling. However, this strategy did not work for all the tested mutants, as one superpositive GST failed to express in *E. coli*.

Strub *et al.* (2004) examined the stability of the enzyme acetylcholinesterase to determine if mutations to surface hydrophobic residues could improve the resistance to denaturation by high temperature, urea, organic solvents and proteases. It was also anticipated that such mutations would have the additional advantage of stabilising the protein during synthesis, leading to higher yields. Fourteen solvent-exposed hydrophobic residues were mutated to Arg, which was chosen because the guanidinium group is the most polar of all the standard amino acid residues. Half of these mutations increased stability. It was suggested that this may be due to suppression of unfavourable interactions between nonpolar residues and water molecules, or from the addition of new H bonding with the solvent (Vogt *et al.*, 1997).

Interestingly, it was observed by Pedone *et al.* (2001) that the stability of the thioredoxin protein of *E. coli* could be improved by a single point mutation, mutating Glu85 to Arg. Generally, it would be expected that a number of mutations would need to be made in order to observe drastic changes in stability. Usually single amino acid substitutions do not significantly affect stability (Reidhaar-Olson and Sauer, 1990, Rennell *et al.*, 1991, Perchiacca *et al.*, 2014), although improvements have been reported for mutagenesis of a single solvent-exposed residue in other studies (Perl *et al.*, 2000).

Further evidence for the solubility-enhancing properties of charged AA residues was exhibited by Trevino *et al.* (2007), who mutated a ribonuclease (RNase) Sa at a highly solvent-exposed Threonine residue at position 76 to all 20 amino acids. They observed that mutations to Asp, Glu and Ser resulted in the greatest improvements in protein solubility. It was suggested that this may be due to the high water-binding ability of acidic residues. It was commented that carboxyl groups on the acidic residues have much greater water-binding abilities than the side-chains of any other AAs (Kuntz, 1971, Cacace *et al.*, 1990). Furthermore, it was observed by Fan *et al.* (2004) that mutating residues Trp264 and Val287 of the C-terminal domain of the human apolipoprotein E to arginine and glutamic acid, respectively, resulted in a 10-fold improvement in protein solubility. In addition, it was observed by Kramer *et al.* (2012) that high negative surface charge correlates strongly with increased protein solubility, which may be due to the strong water-binding ability of the glutamic acid and aspartic acid side chains.

It was observed in a number of reports that large libraries of mutant proteins could be generated and subsequently screened to isolate clones with desired properties. A novel method to screen antibody libraries for aggregation-resistant clones was developed by Dudgeon *et al.* (2009). This method was adapted from the phage display and panning method (as described in Section 1.3) but utilised the high temperature stability of bacteriophage. The authors mutated surface exposed residues on V_H and V_L domains and displayed them onto phage. The library was screened by heating to 80 °C and capturing folded antibodies using protein A or L, which rely on shape-complementarity for binding. It was observed that preselection of aggregation-resistant V_H domains resulted in a significant reduction in CDR diversity (Christ *et al.*, 2006, 2007; Dudgeon

et al., 2009), which raised the question of whether aggregation resistance and high affinity binding are mutually compatible. However, further investigations from that research group found that mutations to CDRH1 and CDRL2 could result in improvements in aggregation-resistance without affecting antigen-binding. The most pronounced changes were observed for negatively charged substitutions, with aspartic acid having a greater effect than glutamic acid. There was a strong preference for these negatively charged amino acids than positively charged lysine or arginine substitutions. The effects were mostly additive, with combinations of mutations leading to higher aggregation resistance. In addition to reducing aggregation, the mutations also improved refolding yields and elution volumes on gel filtration.

Beneficial mutations to protein surface residues are highly dependent on the location of the mutations as well as the net charge of the protein in question, as was concluded by Perchiacca *et al.* (2014). In this study, the authors examined a number of V_H domain antibodies (dAbs) with unique hydrophobic CDRs. One, two and three residues each of Asp, Glu and Arg were inserted at the N- and C-terminals of the CDR3. It was observed that the net charge of the dAb and the position of the insertions relative to the CDR had profound impacts on solubility; for negatively- or near-neutrally-charged V_H scaffolds, inserting negatively charged residues at the N-terminus of the CDRs inhibited aggregation. However, for a positively charged scaffold, positively charged residues more efficiently inhibited aggregation. Generally, insertions at the CDR N-terminus were beneficial while insertions at the C-terminus resulted in decreases in solubility and expression yields. However, this is dependent on the sequence of the CDR in question. For Asp and Glu mutants, the expression levels increased with increasing numbers of inserted residues. It was speculated that positively charged CDR mutations may be solubilising for positively charged antibody scaffolds (or indeed that negatively charged CDR mutations may be solubilising for negatively charged scaffolds), due to electrostatic repulsion between the charged residue and adjacent hydrophobic residues in the CDR (Perchiacca *et al.*, 2014).

Thus, based on the research outlined above, it was decided to investigate the 2G1 anti-MC-LR scFv structure using homology modelling to identify surface-exposed hydrophobic residues. As was evident in a number of reports, the hydrophilic residues most commonly used for substitution were arginine and aspartic acid. Thus, three

surface-exposed hydrophobic residues (L124, L153 and I255) were substituted with arginine and aspartic acid, creating six mutant clones. To determine if these mutations had any deleterious effect on the binding to the 2G1 antigen, MC-LR, ELISAs were carried out. These mutations were also investigated to elucidate the effect on protein expression and purification. In addition, experiments were carried out to measure the effect of the mutations on native and non-native solubility. Finally, experiments were performed to determine the effect of the mutations on the functional stability of the scFv, i.e. if the scFv could retain binding-ability after treatment to denaturing conditions.

1.6 Thesis aims

HABs and algal toxins are a global concern due to their widespread prevalence in freshwater and seafood for consumption and due to the acute effects elicited in humans and animals. In addition, *B. cereus* is a ubiquitous bacterial species capable of eliciting potent food poisoning symptoms via consumption of contaminated dairy, vegetable and meat products. Accordingly, national and international authorities recognise the need to eliminate the exposure to these harmful contaminants and strict legislative limits are imposed. The ability to accurately monitor and detect these contaminants is of paramount importance, and, thus, highly sensitive and specific methods are required to facilitate this.

It is also well established that exposure to MCs can elicit highly toxic effects in numerous cell lines. However, the effects of *M. aeruginosa* and AZA1 on human liver cells are not currently well established. Furthermore, the effects of co-exposure to these toxins/cyanobacteria had not yet been evaluated, which indicated that further research was required to address this gap in our knowledge.

The first aim of this research thesis was to generate novel recombinant antibody fragments specific to AZA1. Such antibodies would be incorporated into immunoassays to facilitate sensitive detection of this toxin.

The second aim of the research presented in this thesis was to investigate the binding interaction of a previously developed anti-MC-LR scFv, 2G1, with the MC-LR molecule. The aim was to use *in silico* modelling and docking techniques to identify a putative binding pocket. Following this, targeted mutagenesis was used to investigate

the role of individual amino acid residues in the 2G1-MC-LR binding interaction and to carry out substitutions to improve the binding interaction. Another aim of this section was to use these techniques to optimise surface-exposed amino acid residues so as to improve the long-term stability and expression characteristics of the 2G1 antibody.

A third aim of this work was to develop and characterise recombinant antibody fragments specific to *B. cereus*. It was desired to identify antibody fragments that could discern *B. cereus* from the closely related, but non-toxic, *B. subtilis* species. It was further desired that such antibodies would be incorporated into a flow cytometry assay to detect the harmful *B. cereus* in food samples.

The final aim of this work was to determine the toxic effects of individual and combined exposure to AZA1, MC-LR and *M. aeruginosa* on human hepatocellular carcinoma cells (HepG2). These toxic effects were investigated in terms of proliferation, apoptosis and necrosis using a number of different methods.

2 Materials and Methods

2.1 Materials

Table 2.1: Reagents.

Reagent	Supplier
Azaspiracid-1	Marine Institute, Rinville, Oranmore, Co. Galway, Ireland.
Bacteriological agar Greiner 96 Well Masterblock® plates Tryptone Yeast extract	Cruinn Diagnostics Ltd., Hume Centre, Parkwest Business Park, Nangor Road, Dublin 12, Ireland.
T4 DNA ligase, Antarctic Phosphatase, restriction enzymes (<i>Sfi</i> I, <i>Xba</i> I, <i>Xho</i> I).	Brennan and Co., Unit 61, Birch Ave, Stillorgan Industrial Park, Stillorgan, Co. Dublin, Ireland.
PCR Primers	Integrated DNA technologies, 1710 Commercial Park, Coralville, IA 52241, USA.
Dulbecco's Modified Eagle Medium (DMEM) Foetal bovine serum (FBS) Glycogen NuPAGE® LDS Sample Buffer (4x) Penicillin-Streptomycin RNAlater® RNaseZap® SOC Media Sodium acetate (3 M, pH 5.5) SuperScript® III First-Strand Synthesis kit SYBR® Safe DNA gel stain	Bio-Sciences Ltd., 3 Charlemont Terrace, Crofton Rd, Dún Laoghaire, Dublin, Ireland.
Ammonium persulfate BG-11 media (50x) Bromophenol Blue Camptothecin cOmplete™ ULTRA protease inhibitor	Sigma Aldrich Ireland Ltd., Vale Rd, Arklow, Co. Wicklow, Ireland.

cocktail Dimethyl sulfoxide Ethanol Glycine Hydrochloric acid Isopropanol Lugol's Iodine 2-mercaptoethanol MOPS Mouse anti-HA horseradish peroxidase (HRP)-labelled antibody (catalogue number H6533) Polyethylene glycol Potassium chloride Potassium phosphate dibasic Potassium phosphate monobasic Rabbit anti-mouse IgG HRP-labelled antibody (catalogue number A9044) Sodium chloride Sodium dodecyl sulfate Sodium phosphate dibasic Sodium phosphate monobasic Sulfuric acid TEMED Tetracycline TMB Liquid Substrate System for Membrane Tris Acetate EDTA buffer 10x Tris Base Tris HCl Tween 20 Trizma® hydrochloride	Sigma Aldrich Ireland Ltd., Vale Rd, Arklow, Co. Wicklow, Ireland.
--	---

<p>Agar</p> <p>Carbenicillin</p> <p>Carbenicillin</p> <p>Corning™ Costar™ round bottom culture plates</p> <p>Glycerol</p> <p>Hyclone Molecular Grade Water</p> <p>Isopropyl β-D-1-thiogalactopyranoside (IPTG)</p> <p>Kanamycin sulfate</p> <p>Mouse anti-M13-HRP-labelled monoclonal antibody (catalogue number 10723387)</p> <p>NucleoBond® Xtra Midi kit</p> <p>NucleoSpin® Gel and PCR Clean-up kit</p> <p>NucleoSpin® Plasmid kit</p> <p>Page Ruler Plus Ladder</p> <p>Pierce Bicinchoninic Acid (BCA) Protein Assay kit</p> <p>Pierce Imject™ BSA protein and EDC conjugation kit</p> <p>Pierce Imject™ Mariculture KLH and EDC conjugation kit</p> <p>Pierce OVA protein standard</p>	<p>Fisher Scientific Ireland, Suite 3, Plaza 212, Blanchardstown Corporate Park 2, Ballycoolin, Dublin 15, Ireland.</p>
<p>Amintra Ni-NTA</p> <p>Hyperladder™ 1kb</p> <p>Hyperladder™ 1kb Plus</p> <p>InstantBlue Protein stain</p> <p>MyTaq™ Red Mix</p>	<p>Medical Supply Company Ltd., Damastown, Mulhuddart, Dublin 15, Ireland.</p>
<p>HRP-labelled anti-M13 rat secondary antibody</p>	<p>GE Healthcare, Amersham Pl, Little Chalfont HP7 9NA, UK.</p>
<p>Microcystin-LR</p> <p>Lipopolysaccharide (LPS) from <i>E. coli</i>,</p>	<p>Enzo Biochem Inc. Farmingdale, New York, USA.</p>

Serotype R515	
QuikChange II Site-Directed Mutagenesis kit	Agilent Technologies Ireland Ltd., Unit 3, Euro House, Euro Business Park, Little Island, Co. Cork, Ireland.
IgY EggPress Purification Kit	Gallus Immunotech, Exalpha Biologicals, Inc., 2 Shaker Road, Unit B101, Shirley, MA, USA.
HRP-labelled donkey anti-chicken antibody	Abcam, 330 Cambridge Science Park Rd, Milton, Cambridge CB4 0FL, UK
Bio-Rad FAM-FLICA® Caspase-3/7 assay kit	Fannin Ltd Fannin House, South County Business Park, Leopardstown, Dublin 18, Ireland.
Human IL-1 beta/IL-1F2 DuoSet™ ELISA kit Human TNF-alpha DuoSet™ ELISA kit	R&D Systems, Bio-Techne 614 McKinley Place NE, Minneapolis, MN 55413, USA.

Table 2.2: Bacterial culture media composition.

Media	Composition	
Super broth (SB)	Tryptone	30 g/L
	Yeast Extract	20 g/L
	MOPS pH 7.0	10 g/L
Lysogeny broth (LB) agar	Tryptone	10 g/L
	Yeast Extract	5 g/L
	NaCl	10 g/L
	Agar	15 g/L

Table 2.3: Cell Lines.

Bacterial strains	Supplier
<i>Escherichia coli</i> TOP10 F' strain: { <i>lacI</i> ^q , Tn10(Tet ^R)} <i>mcrA</i> Δ(<i>mrr-hsd</i> RMS- <i>mcrBC</i>) ϕ80 <i>lacZ</i> ΔM15 Δ <i>lacX74</i> <i>recA1</i> <i>araD139</i> Δ(<i>ara-eu</i>)7697 <i>galU</i> <i>galK</i> <i>rpsL</i> (Str ^R) <i>endA1</i> <i>nupG</i> .	Bio-Sciences Ltd., 3 Charlemont Terrace, Crofton Rd, Dún Laoghaire, Dublin, Ireland.
<i>E. coli</i> XL1-Blue strain: <i>recA1</i> <i>endA1</i> <i>gyrA96</i> <i>thi-1</i> <i>hsdR17</i> <i>supE44</i> <i>relA1</i> <i>lac</i> [F' <i>proAB lacI</i> ^q ZΔM15 Tn10 (Tet ^R)].	Agilent Technologies Ireland Ltd., Unit 3, Euro House, Euro Business Park, Little Island, Co. Cork, Ireland.
Bacteriophage	Supplier
Ff Bacteriophage M13K07	Brennan and Co., Unit 61, Birch Ave, Stillorgan Industrial Park, Stillorgan, Co. Dublin, Ireland.
Algal strains	Supplier
<i>Azadinium spinosum</i> , <i>A. obesum</i> , <i>A. poporum</i> .	Marine Institute, Rinvilla, Oranmore, Co. Galway, Ireland.
<i>Microcystis aeruginosa</i>	Culture Collection of Algae and Protozoa, Scottish Association for Marine Sciences, OBAN Argyll PA37 1QA Scotland, United Kingdom.
Mammalian Cell Lines	Supplier
Human Hepatoma (HepG2) Cells (ATCC® HB-8065™)	LGC Standards, Queens Road, Teddington, Middlesex, TW11 0LY, UK.

Table 2.4: General Buffers.

Buffer	Reagent	Composition
Phosphate-buffered saline (PBS) (150 mM, pH 7.4)	NaCl	8 g/L
	KCl	0.2 g/L
	Na ₂ PO ₄	1.44 g/L
	KH ₂ PO ₄	0.24 g/L

Phosphate-buffered saline Tween (PBS-T) (150 mM, pH 7.4)	1L PBS Tween 20	0.05% (v/v)
Tris HCl (1 M, pH 6.8)	Tris HCl pH adjusted to 6.8	157.6 g/L
Tris base (1 M, pH 8.8)	Tris Base pH adjusted to 8.8	121.14 g/L
10x Electrophoresis buffer	SDS Tris Base Glycine	10 g/L 30 g/L 154 g/L
4x Loading dye	Tris 0.5M, pH 6.8 Glycerol 2-mercaptoethanol 20% SDS Bromophenol Blue dH ₂ O	2.5 mL 2 mL 0.5 mL 2.5 mL 20 ppm 2.5 mL
5x PEG/NaCl	PEG NaCl	20% (w/v) 2.5 M
TAE Buffer	1 Litre, pH 7.0 Tris Base 17.4 M Glacial Acetic Acid Ethylenediaminetetraacetic acid (EDTA) dH ₂ O	1X 4.84 g/L 1.14 mL/L 0.37 g/L Make up to 1 Litre

Table 2.5: Chromatography buffers.

Buffer	Reagent	Composition
Equilibration Buffer	500 mL, pH 8 50 mM NaH ₂ PO ₄ (mono) 300 mM NaCl 10 mM imidazole dH ₂ O	2.99 g/500 mL 8.76 g/500 mL 0.34 g/500 mL Make up to 500 mL

Wash Buffer A	500 mL, pH 7.5 0.5 M NaCl 0.1% (v/v) Tween 40 mM Imidazole dH ₂ O	14.6 g/500 mL 0.5 mL/500 mL 1.36 g/500 mL Make up to 500 mL
Wash Buffer B	500 mL, pH 7.5 0.5 M NaCl 0.1% (v/v) Tween 50 mM Imidazole dH ₂ O	14.6 g/500 mL 0.5 mL/500 mL 1.7 g/500 mL Make up to 500 mL
Elution Buffer	500 mL, pH 7.5 50 mM NaH ₂ PO ₄ (mono) 300 mM NaCl 250 mM Imidazole dH ₂ O	2.99 g/500 mL 8.76 g/500 mL 8.51 g/500 mL Make up to 500 mL

Table 2.6: Antibiotic and IPTG stocks.

Chemical	Composition
Tetracycline	5 mg/mL in ethanol
Carbenicillin	100 mg/mL in dH ₂ O
Kanamycin	50 mg/mL in dH ₂ O
Isopropyl β-D-1-thiogalactopyranoside (IPTG)	2.39 g/10 mL of dH ₂ O

Table 2.7: SDS-PAGE gel compositions.

Separating gel	Quantity per 6 mL gel
Tris base (1 M, pH 8.8)	1.5 mL
30% (w/v) Acrylagel	2.5 mL
2% (w/v) Bis-acrylagel	1.0 mL
10% (w/v) SDS	30 μL
10% (w/v) APS	30 μL
TEMED	6 μL

dH ₂ O	934 µL
Stacking gel	Quantity per 2.5 mL gel
Tris HCl (1 M, pH 6.8)	300 µL
30% (w/v) Acrylagel	375 µL
2% (w/v) Bis-acrylagel	150 µL
10% (w/v) SDS	24 µL
10% (w/v) APS	24 µL
TEMED	2.5 µL
dH ₂ O	1.625 mL

Table 2.8: Equipment.

Equipment	Manufacturer
Rotor-Gene 6000 Thermal Cycler	Qiagen, Skelton House, Lloyd St N, Manchester M15 6SH, UK.
Nanodrop™ ND-1000	NanoDrop Technologies Inc., 3411, Silverside Rd 100BC, Wilmington DE19810-4803, USA.
Gene Pulser Xcell™ electroporation system Gel Doc™ EZ Imager PowerPac® Basic SDS-PAGE Gel Dock Gel Doc™ EZ system and Image Lab™	Bio-Rad Laboratories Inc., 2000 Alfred Nobel Drive, Hercules, California 94547, USA.
Safire ² Plate-Reader	Tecan Group Ltd., Seestrasse 103, Mannedorf CH-8708, Switzerland.
Darkreader® Transluminator	Clare Chemical Research.
Hermle Z233MK-2 Centrifuge Rotor: 220.87 V05	Hermle, Siemensstrasse, Wehingen, 78564, Germany.
Pierce™ G2 Fast Blotter	Thermo Fisher Scientific, Manor Park, Tudor. Rd, Blacon, Runcorn, WA7 1TA, UK.

Chyo JK-180 Balance Mettler PJ300 Balance Orion 3 Star pH meter	Medical Supply Company Ltd., Damastown, Mulhuddart, Dublin 15, Ireland.
Ultra-Turrax Homogeniser	IKA-Werke GmbH & Co. KG., 10 Janke & Kunkel-Str., 79219, Stauffern, Germany.
Stuart Roller Mixer – SRTI	Lennox Laboratory Supplies Ltd., John F. Kennedy Drive, Naas Road, Dublin 12, Ireland.
Eppendorf 5810R refrigerated centrifuge Rotors: F45-30-11; A-4-62.	Eppendorf UK Ltd., Endurance House, Vision Park, Histon, Cambridge, CB24 9ZR, UK.
New Brunswick Scientific Excella® E25 Temperature-controlled shaker. Branson Sonifer™ S-450 Digital Sonicator	VWR International Co., Orion Business Campus, Northwest Business Park, Ballycoolin, Dublin 15, Ireland.
Heraeus Hera-safe laminar flow cabinet Thermo Scientific Heraeus BB15 Carbon Dioxide incubator Binder C170 Carbon Dioxide incubator	Thermo Scientific, 12-16 Sedgeway Business Park, Witchford, Cambridgeshire CB6 2HY, UK.
OPTIKA XDS-2FL inverted HBO Fluorescence Microscope	OPTIKA SRL, Via Rigla, 30 -24010 Ponteranica (BG), Italy

2.2 Methods

2.2.1 General Methods

2.2.1.1 Ethanol precipitation of DNA/RNA

Ethanol precipitation of DNA/RNA was carried out by the addition of 2x volume 100% (v/v) ethanol, 0.1x volume 3 M sodium acetate (pH 5.5) and 1 μ L 5 mg/mL glycogen.

2.2.1.2 Gel purification of DNA

Gel purification of DNA was carried out using a NucleoSpin® Gel and PCR Clean-up kit according to the manufacturer's instructions (Macherey-Nagel, 2014a). Briefly, a DNA band of interest was excised from an agarose gel and placed into a sterile tube. Buffer NTI was added to the gel slice (200 μ L per 100 mg gel). The gel was melted at 50 °C in a waterbath for 10 – 15 min. A NucleoSpin® Gel and PCR Clean-up Column was placed into a collection tube. The sample was added to the column and centrifuged at 11,000 x g for 30 s in a benchtop centrifuge (Hermle Z233MK-2). The column flow-through was discarded. The column was washed in duplicate by the addition of 700 μ L Buffer NT3 and centrifugation at 11,000 x g for 30 s. The flow-through was discarded. Residual NT3 buffer was removed from the column by centrifugation at 11,000 x g for 1 min. The column was then placed into a new 1.5 mL tube. Molecular grade H₂O was heated to 60 °C and 15 – 30 μ L was added to the column membrane. The column was incubated at 60 °C for 2 min and then centrifuged at 11,000 x g for 1 min. The eluted DNA was quantified at 260 nm using a Nanodrop™ ND-1000.

2.2.1.3 Purification of plasmid DNA from bacterial cells

Purification of plasmid DNA from bacterial cells was carried out using a NucleoSpin® Plasmid QuickPure kit according to the manufacturer's instructions (Macherey-Nagel, 2014b). Briefly, the cultivated cells were harvested by centrifugation at 11,000 x g for 30 s using a benchtop centrifuge (Hermle Z233MK-2). The supernatant was discarded and the cell pellet was lysed by the addition of 250 μ L Buffer A1 and 250 μ L Buffer

A2. This was incubated at room temperature for 5 min and, following this, 300 μ L Buffer A3 was added. The lysate was clarified by centrifugation at 11,000 x g for 5 min using a benchtop centrifuge (Hermle Z233MK-2). The supernatant containing the plasmid DNA was loaded onto a silica membrane column and centrifuged at 11,000 x g for 1 min using a benchtop centrifuge (Hermle Z233MK-2). The column was washed by the addition of 450 μ L Buffer AQ and was centrifuged at 11,000 x g for 3 min using a benchtop centrifuge (Hermle Z233MK-2). Finally, the DNA was eluted by the addition of 50 μ L Buffer AE, incubation at 60 °C for 2 min and centrifugation at 11,000 x g for 1 min using a benchtop centrifuge (Hermle Z233MK-2). The eluted DNA was quantified at 260 nm using a Nanodrop™ ND-1000.

2.2.1.4 Bicinchoninic Acid (BCA) assay

Protein quantification was carried out using a Pierce BCA Protein Assay kit as per the manufacturer's instructions (Thermo Scientific, 2015). Briefly, BSA standards were prepared in PBS for a concentration range of 25 – 2,000 μ g/mL. Unknown samples were diluted at 1:5 and 1:25 dilutions to ensure the concentrations of the unknowns lie within the range of the standard curve. Working reagent (WR) was prepared by the addition of the BCA assay reagents A and B at a ratio of 50:1. Each standard and unknown was added to a Nunc Maxisorb™ 96 well plate at 25 μ L per well. Following this, 200 μ L of WR was added to each well and the plate was incubated at 37 °C for 30 min. The absorbance was measured at 562 nm using a Tecan Safire² plate-reader.

2.2.2 Generation of murine scFv library for AZA1

2.2.2.1 Preparation of AZA1 conjugates

AZA1 contains a terminal carboxyl group and is suitable for conjugation via N-ethyl-N'-(dimethylaminopropyl)-carbodiimide (EDC) coupling chemistry. Conjugates were prepared through use of Pierce EDC conjugation kits (Thermo Scientific, 2014). Briefly, 2 mg of keyhole limpet hemocyanin (KLH)/bovine serum albumin (BSA) was dissolved in 400 μ L ultrapure water. 250 μ g of AZA1 was dissolved in 450 μ L conjugation buffer with 15% (v/v) dimethyl sulfoxide (DMSO). This 450 μ L AZA1 solution was added to 200 μ L carrier protein solution. In the case of AZA1-KLH

conjugation, 50 μL of 10 mg/mL EDC was added to the 650 μL AZA1-carrier protein solution. In the case of AZA1-BSA conjugation, the 650 μL of AZA1-carrier protein solution was added directly to 10 mg EDC powder. The two reactions were incubated at room temperature on a bench-top mixer for 2 h.

The two conjugate reactions were purified using Zeba™ Spin Desalting Columns provided with the Pierce EDC conjugation as follows: Purification buffer salts were dissolved in 10 mL ultrapure water with 15% (v/v) DMSO. The desalting column was placed into a collection tube and centrifuged at 1,000 x g for 2 min in an Eppendorf 5810R centrifuge (rotor: A-4-62) to remove the storage solution. One mL of purification buffer was added to the column and centrifuged at 1,000 x g for 2 min in an Eppendorf 5810R centrifuge (rotor: A-4-62). This step was repeated two more times. The column was placed into a new collection tube and the conjugate sample was added to the resin. The sample was passed through the desalting column by centrifugation at 1,000 x g for 2 min an Eppendorf 5810R centrifuge (rotor: A-4-62). The desalted conjugate sample was filtered through a 0.2 μm filter and stored at -20 °C until use. A small amount of each conjugate sample was used for protein quantification using the BCA assay. Table 2.9 describes the overall conjugation reaction and the theoretical molar ratio.

Table 2.9: Molar ratios for AZA1 conjugate syntheses.

Reaction	Molar Ratio	Reagent	Molecular weight (Da)	Mass (mg)	mmol
AZA1:BSA	19.8:1	AZA1	842	0.25	2.97×10^{-4}
		BSA	66,463	1	1.5×10^{-5}
AZA1:KLH	4.64:1	AZA1	842	0.25	2.97×10^{-4}
		KLH	5×10^6	1	6.4×10^{-5}

2.2.2.2 Immunisation schedule

This immunisation work performed in this thesis was carried under license number B100/2705. Three female BALB/c mice aged 4 weeks were immunised with AZA1-KLH. The immunisation schedule is outlined below (Table 2.10). For the initial immunisation, each mouse was administered an intraperitoneal (IP) injection of 200 μL of 100 $\mu\text{g}/\text{mL}$ AZA1-KLH mixed at a ratio of 1:1 with Freund's complete adjuvant (Freund's complete adjuvant was used for only the first immunisation as it promotes a

strong immune response, but repeated exposure may promote the formation of tumours and/or inflammatory lesions (Barbas *et al.*, 2001)). For the subsequent boosts, each mouse was administered an IP injection of 200 μ L of 100 μ g/mL AZA1-KLH mixed at a ratio of 1:1 with Freund's incomplete adjuvant. The conjugate-adjuvant mixture was prepared by vortexing at room temperature for 1 h until a thick white-coloured emulsion was formed. Bleeds were collected through cheek bleeding. They were allowed to clot at 4 °C overnight. They were then centrifuged at 3,200 x g for 20 min in a benchtop centrifuge (Hermle Z233MK-2). The serum was removed and stored at -20 °C.

Table 2.10: Immunisation schedule of BALB/C mice.

Event	Day
Pre-bleed	0
Immunisation	0
Bleed	7
Boost	14
Bleed	21
Boost	35
Bleed	42
Boost	48
Bleed	56
Boost	70
Bleed	77
Boost	84
Bleed	97
Boost	114
Bleed	121
Boost	136
Bleed	142
Boost	177
Boost	199
Sacrifice	206

BALB/c mice were administered an immunisation/boost at an interval of at least three weeks. Approximately 6 – 7 days after each immunisation/boost a bleed was taken.

2.2.2.3 Determination of murine immune response to AZA1 by indirect ELISA

The purpose of this experiment was to determine the immune response of each mouse towards AZA1, as indicated by the serum titre. The serum titre is defined as the lowest detectable concentration of antibodies present in the serum that can bind to the target at 2 – 3 standard deviations above the blank. A 96-well Nunc Maxisorb™ plate was coated with 100 µL per well of 5 µg/mL of AZA1-BSA. The plate was incubated at 37 °C for 1 h. The liquid was then removed. Each well was blocked with 200 µL of 5% (w/v) Milk Marvel (MM) in PBS (150 mM, pH 7.4) and incubated at 37 °C for 1 h. The liquid was then removed. Each mouse serum was diluted in doubling dilutions from 1:200 to 1:51,200 in 5% (w/v) MM. A negative control was also included, which omitted the serum. One hundred µL of each serum dilution and negative control was added to the plate in triplicate. The plate was incubated at 37 °C for 1 h. The wells were then rinsed three times with PBS-T (150 mM, pH 7.4, 0.05% (v/v) Tween 20) and PBS (150 mM, pH 7.4). HRP-labelled anti-mouse IgG was diluted at 1:10,000 in 5% (w/v) MM and 100 µL was placed into each well. The plate was incubated at 37 °C for 1 h. The wells were then rinsed three times with PBS-T (150 mM, pH 7.4, 0.05% (v/v) Tween 20) and PBS (150 mM, pH 7.4). 3,3',5,5'-Tetramethylbenzidine (TMB) was added at 100 µL per well. The plate was incubated at 37 °C for 15 min. Ten percent (v/v) H₂SO₄ was added at 50 µL per well to stop the colourimetric reaction. The absorbance was measured at 450 nm using a Tecan Safire² plate-reader.

2.2.2.4 Isolation of RNA from BALB/c mouse spleen

After completion of the immunisation process, the BALB/c mice were sacrificed by cervical dislocation. A significant response was observed from the sera of mice A and B against AZA1, and thus the spleens of these mice were used for RNA extraction. The spleens of all three mice were stored in RNAlater® at -80 °C until required for use. Spleens A and B were centrifuged for 10 min at 3,200 x g in an Eppendorf 5810R centrifuge (rotor: A-4-62) to remove the RNAlater®. The spleens were placed in fresh 'RNase-free' tubes. Ten mL of Trizol® was added to the samples and each spleen was homogenised at 50% output for 1 min. Trizol® maintains RNA integrity, inhibits RNase activity and dissolves cell components during homogenisation. The samples were allowed to stand at room temperature for 5 min to allow larger tissue debris to settle to

the bottom of the tubes. The samples were centrifuged at 3,200 x g for 10 min at 4 °C in an Eppendorf 5810R centrifuge (rotor: A-4-62) to pellet the cell debris. The supernatants were carefully removed, transferred to fresh 80 ml Oakridge tubes and 2 mL of chloroform was added to each supernatant. The samples were mixed well by shaking for 15 s to evenly distribute the chloroform in the samples. They were then incubated at room temperature for 15 min and centrifuged at 15,500 x g for 25 min at 4 °C in an Eppendorf 5810R centrifuge (rotor: F45-30-11) to allow for the formation of an upper aqueous phase (which contains RNA), an interphase and lower red phenol-chloroform phase (which contains protein and DNA). The upper, aqueous layer was removed from each sample. These were transferred to fresh 80 mL tubes, 5 mL of isopropanol was added to each tube and they were vortexed for 15 s. The addition of isopropanol allows for the precipitation of RNA. The tubes were incubated at room temperature for 10 min. The tubes were centrifuged at 15,500 x g for 20 min at 4 °C in an Eppendorf 5810R centrifuge (rotor: F45-30-11) to pellet the precipitated RNA. The supernatant was carefully removed and the RNA pellet was washed by the addition of 30 mL of 75% (v/v) ice-cold ethanol, being careful not to disturb the pellet. The tubes were centrifuged at 15,500 x g for 20 min at 4 °C in an Eppendorf 5810R centrifuge (rotor: F45-30-11) and the supernatant was removed and discarded. The pellet was air-dried for 10 min until the ethanol had fully evaporated. The pellet was resuspended in 800 µL of 'RNase-free' water. The RNA concentration was quantified using a Nanodrop™ ND-1000 at 260 nm. A small amount of RNA from samples A and B was kept for cDNA synthesis. The remaining RNA was precipitated as per Section 2.2.1.1 and was stored at -80 °C.

2.2.2.5 Synthesis of cDNA from RNA by reverse transcriptase PCR (RT-PCR)

Total RNA was transcribed to cDNA by RT-PCR, using a Superscript™ III First Strand synthesis kit as per the manufacturer's instructions (Invitrogen, 2013). Briefly, RNA from samples A and B were amplified separately, using 4 tubes each. To the sample A tubes, the following was added: 2.5 µL Oligo dT (50 µM), 2.5 µL dNTPs (10 mM), 12.65 µL RNA and 27.5 µL molecular grade H₂O. To the sample B tubes, the following was added: 2.5 µL Oligo dT (50 µM), 2.5 µL dNTPs (10 mM), 21.8 µL RNA and 18.18 µL molecular grade H₂O. The tubes were incubated at 65 °C for 5 min followed by 1

min incubation on ice. To each of the A and B tubes, 25 μ L of mixture 2 (see Table 2.11) was added. They were incubated at 50 °C for 50 min followed by 85 °C for 5 min in a Rotor-Gene 6000 Thermal Cycler. Five μ L RNase H was added to each mixture and incubated at 37 °C for 20 min. The eight aliquots were combined and vortexed. Total cDNA was quantified at 260 nm using a Nanodrop™ ND-1000.

Table 2.11: Superscript™ III mixture 2 composition.

Mixture 2	Volume (μL)
10x RT Buffer	40
25 mM MgCl ₂	80
0.1 M DTT	40
RNase out	20
Superscript III	20

2.2.2.6 Amplification of antibody variable light and heavy genes

Following cDNA synthesis, the IgG variable regions were amplified by PCR. There is a high degree of variability in the murine DNA regions flanking the variable light and heavy chains, thus, 17 forward and 3 reverse primers are required for V _{κ} amplification, a single forward and reverse primer are required for V _{λ} amplification, and 19 forward and 3 reverse primers are required for V_H amplification. Primer sequences are listed in Table 2.12.

Table 2.12: Murine scFv primer sequences.

V_κ5' Sense Primers

MSCVK-1

5' GGG CCC AGG CGG CCG AGC TCG AYA TCC AGC TGA CTC AGC C 3'

MSCVK-2

5' GGG CCC AGG CGG CCG AGC TCG AYA TTG TTC TCW CCC AGT C 3'

MSCVK-3

5' GGG CCC AGG CGG CCG AGC TCG AYA TTG TGM TMA CTC AGT C 3'

MSCVK-4

5' GGG CCC AGG CGG CCG AGC TCG AYA TTG TGY TRA CAC AGT C 3'

MSCVK-5

5' GGG CCC AGG CGG CCG AGC TCG AYA TTG TRA TGA CMC AGT C 3'

MSCVK-6

5' GGG CCC AGG CGG CCG AGC TCG AYA TTM AGA TRA MCC AGT C 3'

MSCVK-7

5' GGG CCC AGG CGG CCG AGC TCG AYA TTC AGA TGA YDC AGT C 3'

MSCVK-8

5' GGG CCC AGG CGG CCG AGC TCG AYA TYC AGA TGA CAC AGA C 3'

MSCVK-9

5' GGG CCC AGG CGG CCG AGC TCG AYA TTG TTC TCA WCC AGT C 3'

MSCVK-10

5' GGG CCC AGG CGG CCG AGC TCG AYA TTG WGC TSA CCC AAT C 3'

MSCVK-11

5' GGG CCC AGG CGG CCG AGC TCG AYA TTS TRA TGA CCC ART C 3'

MSCVK-12

5' GGG CCC AGG CGG CCG AGC TCG AYR TTK TGA TGA CCC ARA C 3'

MSCVK-13

5' GGG CCC AGG CGG CCG AGC TCG AYA TTG TGA TGA CBC AGK C 3'

MSCVK-14

5' GGG CCC AGG CGG CCG AGC TCG AYA TTG TGA TAA CYC AGG A 3'

MSCVK-15

5' GGG CCC AGG CGG CCG AGC TCG AYA TTG TGA TGA CCC AGW T 3'

MSCVK-16

5' GGG CCC AGG CGG CCG AGC TCG AYA TTG TGA TGA CAC AAC C 3'

MSCVK-17

5' GGG CCC AGG CGG CCG AGC TCG AYA TTT TGC TGA CTC AGT C 3'

V_κ3' Reverse Primers

MSCJK12-BL

5' GGA AGA TCT AGA GGA ACC ACC CCC ACC ACC GCC CGA GCC ACC GCC
ACC AGA GGA TTT KAT TTC CAG YTT GGT CCC 3'

MSCJK4-BL

5' GGA AGA TCT AGA GGA ACC ACC CCC ACC ACC GCC CGA GCC ACC GCC
ACC AGA GGA TTT TAT TTC CAA CTT TGT CCC 3'

MSCJK5-BL

5' GGA AGA TCT AGA GGA ACC ACC CCC ACC ACC GCC CGA GCC ACC GCC
ACC AGA GGA TTT CAG CTC CAG CTT GGT CCC 3'

V_λ5' Sense Primer

MSCVL-1

5' GGG CCC AGG CGG CCG AGC TCG ATG CTG TTG TGA CTC AGG AAT C 3'

V_λ3' Reverse Primer

MSCJL-BL

5' GGA AGA TCT AGA GGA ACC ACC CCC ACC ACC GCC CGA GCC ACC GCC
ACC AGA GGA GCC TAG GAC AGT CAG TTT GG 3'

V_H5' Sense Primers

MSCVH1

5' GGT GGT TCC TCT AGA TCT TCC CTC GAG GTR MAG CTT CAG GAG TC 3'

MSCVH2

5' GGT GGT TCC TCT AGA TCT TCC CTC GAG GTB CAG CTB CAG CAG TC 3'

MSCVH3

5' GGT GGT TCC TCT AGA TCT TCC CTC GAG GTG CAG CTC AAG SAS TC 3'

MSCVH4

5' GGT GGT TCC TCT AGA TCT TCC CTC GAG GTC CAR CTG CAA CAR TC 3'

MSCVH5

5' GGT GGT TCC TCT AGA TCT TCC CTC GAG GTY CAG CTB CAG CAR TC 3'

MSCVH6

5' GGT GGT TCC TCT AGA TCT TCC CTC GAG GTY CAR CTG CAG CAG TC 3'

MSCVH7

5' GGT GGT TCC TCT AGA TCT TCC CTC GAG GTC CAC GTG AAG CAG TC 3'

MSCVH8

5' GGT GGT TCC TCT AGA TCT TCC CTC GAG GTG AAS STG GTG GAA TC 3'

MSCVH9

5' GGT GGT TCC TCT AGA TCT TCC CTC GAG GTG AWG YTG GTG GAG TC 3'

MSCVH10

5' GGT GGT TCC TCT AGA TCT TCC CTC GAG GTG CAG SKG GTG GAG TC 3'

MSCVH11

5' GGT GGT TCC TCT AGA TCT TCC CTC GAG GTG CAM CTG GTG GAG TC 3'

MSCVH12

5' GGT GGT TCC TCT AGA TCT TCC CTC GAG GTG AAG CTG ATG GAR TC 3'

MSCVH13

5' GGT GGT TCC TCT AGA TCT TCC CTC GAG GTG CAR CTT GTT GAG TC 3'

MSCVH14

5' GGT GGT TCC TCT AGA TCT TCC CTC GAG GTR AAG CTT CTC GAG TC 3'

MSCVH15

5' GGT GGT TCC TCT AGA TCT TCC CTC GAG GTG AAR STT GAG GAG TC 3'

MSCVH16

5' GGT GGT TCC TCT AGA TCT TCC CTC GAG GTT ACT CTR AAA GWG TST G 3'

MSCVH17

5' GGT GGT TCC TCT AGA TCT TCC CTC GAG GTC CAA CTV CAG CAR CC 3'

MSCVH18

5' GGT GGT TCC TCT AGA TCT TCC CTC GAG GTG AAC TTG GAA GTG TC 3'

MSCVH19

5' GGT GGT TCC TCT AGA TCT TCC CTC GAG GTG AAG GTC ATC GAG TC 3'

V_H3' Reverse Primers

MSCG1ab-B

5' CCT GGC CGG CCT GGC CAC TAG TGA CAG ATG GGG STG TYG TTT TGG C 3'

MSCG3-B

5' CCT GGC CGG CCT GGC CAC TAG TGA CAG ATG GGG CTG TTG TTG T 3'

MSCGM-B

5' CCT GGC CGG CCT GGC CAC TAG TGA CAT TTG GGA AGG ACT GAC TCT C 3'

Overlap Extension Primers

RSC-F (sense)

5' GAG GAG GAG GAG GAG GAG GCG GGG CCC AGG CGC CCG AGC TC 3'

RSC-B (reverse)

5' GAG GAG GAG GAG GAG GAG CCT GGC CGG CCT GGC CAC TAG TG 3'

Sequencing Primers

OmpSeq (sense)

5' AAG ACA GCT ATC GCG ATT GCA G 3'

Gback (reverse)

5' GCC CCC TTA TTA GCG TTT GCC ATC 3'

2.2.2.6.1 V_κ gene amplification

The V_κ genes were amplified as follows; it was decided to pool the V_κ reverse primers in a ratio of 2:1:1 for the primers MSCJK12-BL, MSCJK4-BL, MSCJK5-BL, respectively, as recommended by Barbas *et al.* (2001). A master mix of MyTaq Red Mix (which included *Taq* polymerase, buffer, dNTPs and MgCl₂) was prepared according to Table 2.13 and was vortexed. A control reaction was prepared by taking 47 μL of the master mix and adding to a control tube and by also adding 1 μL of MSCVK-1 and 2 μL molecular grade H₂O. To the remaining master mix, 38 μL of cDNA was added. The master mix was then divided into seventeen 49 μL aliquots. Each of the 17 forward primers was added to its designated tube at 1 μL per reaction. The PCR was run in a Rotor-Gene 6000 Thermal Cycler according to the conditions described in Table 2.14. The completed PCR was separated on a 1% (w/v) agarose gel stained with SYBR® Safe at 100 V for 45 min. A Hyperladder™ 1 kb Plus was used as molecular size markers.

Table 2.13: V_κ PCR master mix composition.

Component	Volume (μL)	Working concentration
2x MyTaq Red Mix	500	1x
MSCJK12-BL	10	1 μM
MSCJK4-BL	5	0.5 μM
MSCJK5-BL	5	0.5 μM
Molecular grade H ₂ O	420	-

Table 2.14: PCR thermal cycler conditions.

PCR stage	Temperature (°C)	Time
Initialisation	94	5 min
Denaturation	94	15 s
Annealing	56	15 s
Extension	72	90 s
Final Extension	72	10 min

} x 30 cycles

2.2.2.6.2 V_λ gene amplification

The V_λ gene was amplified as follows; a master mix was prepared according to Table 2.15. This was divided into three 49 μL aliquots. To the control tube, 1 μL of molecular grade H₂O was added. To two test tubes, 1 μL of cDNA was added. The PCR was run in a Rotor-Gene 6000 Thermal Cycler according to the conditions described in Table 2.14. The completed PCR was separated on a 1% (w/v) agarose gel stained with SYBR® Safe at 100 V for 35 min. A Hyperladder™ 1 kb Plus was used as molecular size markers. The two amplified V_λ reactions were pooled with the seventeen successfully amplified V_κ reactions and gel-purified according to Section 2.2.1.2. The DNA concentration was determined by spectrophotometric measurement at 260 nm using a Nanodrop™ ND-1000. The combined V_λ and V_κ DNA are hereafter referred to as V_L.

Table 2.15: V_λ PCR master mix composition.

Component	Volume (μL)	Working concentration
2x MyTaq Red Mix	75	1x
MSCVL-1	1.5	1 μM
MSCJL-BL	1.5	1 μM
Molecular grade H ₂ O	69	-

2.2.2.6.3 V_H gene amplification

The V_H region was amplified as follows; it was decided to pool the V_H reverse primers in a ratio of 3:1:1 for the primers MSCG1ab-B, MSCG3-B, MSCGM-B, respectively, as recommended by Barbas *et al.* (2001). A master mix was prepared according to Table 2.16. A control reaction was prepared by taking 48.5 μL of the master mix and adding to a control tube and by also adding 0.5 μL of MSCVH-1 and 1 μL molecular grade H₂O. To the remaining master mix, 21 μL of cDNA was added. This was divided into nineteen 49.5 μL aliquots. Each of the 19 forward primers was added to its designated tube at 0.5 μL per reaction. The PCR was run in a Rotor-Gene 6000 Thermal Cycler according to the conditions described in Table 2.14. The completed PCR was separated on a 1% (w/v) agarose gel stained with SYBR® Safe at 100 V for 35 min. A Hyperladder™ 1 kb Plus was used as molecular size markers. The successfully amplified reactions were pooled and gel-purified according to Section 2.2.1.2. The DNA concentration was determined by spectrophotometric measurement at 260 nm using a Nanodrop™ ND-1000.

Table 2.16: V_H PCR master mix composition.

Component	Volume (μL)	Working concentration
2x MyTaq Red Mix	550	1x
MSCG1ab-B	6.6	0.6 μM
MSCG3-B	2.2	0.2 μM
MSCGM-B	2.2	0.2 μM
Molecular grade H ₂ O	506	-

2.2.2.7 scFv gene construction

2.2.2.7.1 Splice-by-overlap extension (SOE) PCR

The full length scFv gene was constructed via SOE PCR as follows; a reaction mix was prepared according to Table 2.17. The control reaction was prepared, as described in Table 2.17, but omitted the V_H and V_L DNA and, instead, included 0.83 μL of molecular grade H_2O . The PCR was run in a Rotor-Gene 6000 Thermal Cycler according to the conditions described in Table 2.18. The completed PCR was separated on a 1% (w/v) agarose gel stained with SYBR® Safe at 100 V for 45 min. A Hyperladder™ 1 kb Plus was used as molecular size markers.

Table 2.17: SOE PCR reaction composition.

Component	Volume (μL)	Working concentration
2x MyTaq Red Mix	25	1x
RSC-F	0.5	1 μM
RSC-B	0.5	1 μM
V_H DNA	0.58	2 ng/ μL
V_L DNA	0.25	2 ng/ μL
Molecular grade H_2O	23.17	-

Table 2.18: SOE PCR conditions.

PCR stage	Temperature ($^{\circ}\text{C}$)	Time
Initialisation	94	5 min
Denaturation	94	30 s
Annealing	65* *Decreased by 0.2 $^{\circ}\text{C}$ per cycle	30 s
Extension	72	90 s
Final Extension	72	10 min

2.2.2.7.2 Large-scale SOE PCR

In order to have sufficient DNA material to ligate into the pComb3XSS vector, a large-scale SOE PCR was carried out as follows. A master mix was prepared according to Table 2.19. The control reaction was prepared by removing 49.17 μL of the master mix

and placing it into the control tube with 0.83 μL of molecular grade H_2O . V_H and V_L DNA were added to the remaining master mix at 13.34 μL and 5.75 μL , respectively. The master mix was divided into twenty two 50 μL aliquots. The PCR was run in a Rotor-Gene 6000 Thermal Cycler according to the conditions described in Table 2.18. Four test SOE tubes were selected at random and, with the control tube, separated on a 1% (w/v) agarose gel stained with SYBR® Safe at 100 V for 35 min. A Hyperladder™ 1kb Plus was used as molecular size markers. The successfully amplified reactions were pooled and gel-purified according to Section 2.2.1.2. The DNA concentration was determined by spectrophotometric measurement at 260 nm using a Nanodrop™ ND-1000.

Table 2.19: Large-scale SOE PCR reaction composition.

Component	Volume (μL)	Working concentration
2x MyTaq Red Mix	575	1x
RSC-F	11.5	1 μM
RSC-B	11.5	1 μM
Molecular grade H_2O	532.9	-

2.2.2.8 Preparation of pComb3XSS plasmid

Escherichia coli cells containing the pComb3XSS plasmid were inoculated into 5 mL Super Broth (SB) containing 100 $\mu\text{g}/\text{mL}$ carbenicillin and grown overnight at 37 °C at 200 rpm in an Excella® E25 shaking incubator. This overnight culture was subcultured at 1:100 into 100 mL SB containing 100 $\mu\text{g}/\text{mL}$ carbenicillin and grown overnight at 37 °C at 200 rpm. Plasmid DNA was purified from the cells using a NucleoBond® Xtra Midi kit according to the manufacturer’s instructions (Macherey-Nagel, 2014c). Briefly, the cells were centrifuged at 3,200 x g for 15 min at 4 °C in an Eppendorf 5810R centrifuge (rotor: A-4-62). The supernatant was discarded. The pellet was resuspended in 8 mL Resuspension buffer. Following this, 8 mL Lysis buffer was added to the sample and mixed by inversion. This was incubated at room temperature for 5 min. The column filter was inserted into a NucleoBond® Xtra column and equilibrated by the addition of 12 mL Equilibration buffer. After the incubation step, 8 mL Neutralisation buffer was added to the sample and mixed by inversion. This lysate was added to the column filter and allowed to flow through. The column was washed by the addition of 5

mL Equilibration buffer. The filter was removed and discarded. The column was washed by the addition of 8 mL Wash buffer. The plasmid DNA was then eluted by the addition of 5 mL Elution buffer into a 15 mL tube. Following this, 3.5 mL isopropanol was added to the eluted DNA and centrifuged at 3,200 x g for 30 min at 4 °C in an Eppendorf 5810R centrifuge (rotor: A-4-62). The supernatant was discarded and 2 mL 70% (v/v) ethanol was added and the sample was centrifuged at 3,200 x g for 10 min at 4 °C in an Eppendorf 5810R centrifuge (rotor: A-4-62). The ethanol was fully removed and the DNA pellet was dissolved in 100 µL molecular grade H₂O. The purified DNA was quantified at 260 nm using a Nanodrop™ ND-1000.

2.2.2.9 Restriction enzyme digestion of SOE and pComb3XSS

It was determined that 10 µg and 20 µg of SOE and pComb3XSS vector, respectively, would be sufficient to provide enough material to transform into *E. coli*, as recommended by Barbas *et al.* (2001).

The SOE digestion was performed in duplicate as follows; a reaction mixture was prepared according to Table 2.20. The reaction was incubated at 50 °C for 3 h followed by an inactivation step at 65 °C for 20 min in a Rotor-Gene 6000 Thermal Cycler. The digested SOE products were pooled and ethanol-precipitated according to Section 2.2.1.1. They were centrifuged at 14,000 x g for 35 min in a benchtop centrifuge (Hermle Z233MK-2) and resuspended in 50 µL of molecular grade water. They were stored overnight at -20 °C.

Table 2.20: SOE digestion reaction mixture composition.

Component	Volume (µL)	Working concentration
H ₂ O	13.6	-
SOE (5 µg)	29.4	100 ng/µL
10x NEB Buffer	5	1x
<i>Sfi</i> I	2	0.8 U/µL

The pComb3XSS digestion was performed in duplicate as follows; a reaction mixture was prepared according to Table 2.21. The reaction was incubated at 50 °C for 3 h followed by an inactivation step at 65 °C for 20 min in a Rotor-Gene 6000 Thermal

Cycler. Four μL each of *Xba*I and *Xho*I was added and the reaction was incubated at 37 °C for 1 h. Following this, 5.8 μL of 10x AP buffer and 2 μL AP enzyme was added and the reaction was incubated at 37 °C for 15 min followed by an inactivation step at 70 °C for 5 min. The digested pComb3XSS products were pooled and ethanol-precipitated according to Section 2.2.1.1. They were centrifuged at 14,000 x g for 35 min in a benchtop centrifuge (Hermle Z233MK-2) and resuspended in 50 μL of molecular grade water. They were stored overnight at -20 °C.

Table 2.21: pComb3XSS digestion reaction mixture composition.

Component	Volume	Working concentration
H ₂ O	38.85	-
Vector (10 μg)	2.15	200 ng/ μL
10x NEB Buffer	5	1x
<i>Sfi</i> I	4	1.6 U/ μL

The digested SOE and pComb3XSS products were gel-purified according to Section 2.2.1.2 on a 1% (w/v) and 0.7% (w/v) agarose gel, respectively. The 800 bp SOE and 3,300 bp pComb3XSS products were isolated. The purified SOE and pComb3XSS DNA concentrations were determined by spectrophotometric measurement at 260 nm using a Nanodrop™ ND-1000.

2.2.2.10 Ligation of SOE insert into pComb3XSS vector

It was deemed pertinent to use the maximum amount of digested pComb3XSS product in a ligation reaction, as any remaining product may re-ligate over time in storage. Therefore, a 33x ligation reaction was prepared according to Table 2.22. The reaction was incubated at room temperature for 20 min and was inactivated by incubating at 65 °C for 10 min in a Rotor-Gene 6000 Thermal Cycler. The reaction tubes were combined into three 220 μL aliquots and ethanol-precipitated according to Section 2.2.1.1. This constructed library was stored at -20 °C until required for use.

Table 2.22: Ligation reaction composition.

Component	Volume (μL)	Working concentration
H ₂ O	514	-
Vector (140 ng/reaction)	27.39	7 ng/ μL
SOE (70 ng/reaction)	19.14	3.5 ng/ μL
10x Ligase buffer	66	1x
T4 ligase	33	20 U/ μL

2.2.2.11 Electroporation of SOE-pComb3XSS into XL1 Blue electrocompetent *E. coli*

The three 220 μL aliquots of ethanol-precipitated library were centrifuged at 14,000 x g for 30 min at 4 °C in a benchtop centrifuge (Hermle Z233MK-2). The supernatant was removed and the pellets were air-dried at room temperature. The pellets were each resuspended in 20 μL of molecular grade water. Following this, 4 μL of this library was mixed with 1 μL of 5x DNA loading buffer and run on a 0.7% (w/v) agarose gel stained with SYBR® Safe. The remaining library was placed on ice with electroporation cuvettes. Six 100 μL aliquots of XL1 Blue electrocompetent *E. coli* were thawed on ice. Ten μL of library was added to 100 μL of *E. coli* in a cuvette. This was mixed and stored on ice for 1 min. Electroporation was carried out in a Bio-Rad GenePulser XCell™ with the following conditions; 2.5 kV, 25 μF , 200 Ω , $\tau \sim 4$ ms. The cuvette was immediately flushed with a total of 3 mL pre-warmed SOC media and added to a 50 mL Falcon tube. The tube was incubated at 37 °C and 250 rpm for 1 h in an Excella® E25 shaking incubator.

A titre of the transformed bacteria was performed by taking 2 μL of the culture and adding to 200 μL of SB. The titre plates were prepared by plating 100 μL and 10 μL of the diluted culture onto Lysogeny Broth (LB) agar plates containing 100 $\mu\text{g}/\text{mL}$ carbenicillin and these were incubated overnight at 37 °C. The following day the colonies were counted in order to calculate the library size. The plates were also kept for colony pick PCR analysis (see Section 2.2.2.12).

To the remaining culture, 10 mL of pre-warmed SB and 13 μL of 100 mg/mL carbenicillin were added. The culture was incubated at 37 °C, 250 rpm for 2 h in an Excella® E25 shaking incubator. The culture was centrifuged at 3,200 x g for 20 min in

an Eppendorf 5810R centrifuge (rotor: A-4-62). The supernatant was removed and the pellet was resuspended in 50 μ L SB containing 100 μ g/mL carbenicillin. This was spread on a LB agar plate containing 100 μ g/mL carbenicillin and incubated overnight at 37 °C. The colonies were scraped in 5 mL SB. Glycerol was added to a final concentration of 15% (v/v) and the culture was divided into aliquots and stored at -80 °C.

2.2.2.12 Colony pick PCR of transformed XL1 Blue *E. coli*

To determine the efficiency of the ligation and transformation experiments, a colony pick PCR was carried out as follows. A master mix was prepared according to Table 2.23 and divided into 11x 50 μ L aliquots. A single colony from the transformation titre plates was added to each of the 10 reaction tubes. No colony was added to the control tube. The PCR was carried out using the conditions described in Table 2.18 in a Rotor-Gene 6000 Thermal Cycler. The PCR products were separated on a 1% (w/v) agarose gel stained with SYBR® Safe at 100 V for 35 min. A Hyperladder™ 1kb Plus was used as molecular size markers.

Table 2.23: Colony pick PCR master mix composition.

Component	Volume (μ L)	Working concentration
2x MyTaq Red Mix	275	1x
RSC-F	5.5	1 μ M
RSC-B	5.5	1 μ M
Molecular grade H ₂ O	264	-

2.2.2.13 Screening the anti-AZA1 scFv library by phage display and panning

Two hundred and fifty μ L of anti-AZA1 *E. coli* library was added to 250 mL SB containing 100 μ g/mL carbenicillin in duplicate. These cultures were grown at 37 °C and 200 rpm for ~6 h in an Excella® E25 shaking incubator until OD₆₀₀ reached approximately 0.5. The two cultures were pooled and 2x10¹² M13KO7 helper phage added. The culture was incubated, while static, at 37 °C for 1 h. The culture was centrifuged at 3,200 x g for 10 min at 4 °C in an Eppendorf 5810R centrifuge (rotor: A-4-62). The supernatant was discarded and the pellet was resuspended in 100 mL SB containing 100 μ g/mL carbenicillin. The culture was incubated at 30 °C, 250 rpm for 1.5 – 2 h. Kanamycin was then added to a final concentration of 50 μ g/mL and the

culture was incubated overnight at 30 °C and 250 rpm. An immunotube was coated with AZA1-BSA overnight at 4 °C at the concentrations described in Table 2.24.

Table 2.24: Panning conditions used for screening the anti-AZA1 scFv library.

Round	Coating concentration (µg/mL AZA1-BSA)	Number of washes (PBS-T:PBS)
1	100	3:3
2	50	4:4
3	25	5:5
4	10	6:6

The following day, an overnight XL1 Blue *E. coli* culture was sub-cultured at the following dilutions: 1:50, 1:100, 1:500, 1:1,000, and 1:2,000. While these were growing, the immunotube was blocked with 5% (w/v) MM and the overnight library was centrifuged at 3,200 x g for 30 min in an Eppendorf 5810R centrifuge (rotor: A-4-62). Forty mL of the library supernatant, which contained the bacteriophage, was added to an Oakridge tube with 10 mL 5x polyethylene glycol (PEG)/NaCl in duplicate. These were incubated on ice for 1 h and centrifuged at 13,000 x g for 20 min, with the brake off, in an Eppendorf 5810R centrifuge (rotor: F45-30-11). The supernatant was discarded and the pellet, which contained the precipitated bacteriophage, was resuspended in 1 mL of sterile PBS (150 mM, pH 7.4). This was then centrifuged at 11,600 x g for 10 min in a benchtop centrifuge (Hermle Z233MK-2). The phage-rich supernatant was kept and 3% (w/v) BSA solution was added to a final concentration of 1% (w/v).

The coated and blocked immunotube was washed once by filling with PBS (150 mM, pH 7.4). 1 mL of the phage-BSA was added to 1 mL 5% (w/v) MM. This was mixed and added to the immunotube. The immunotube was incubated at room temperature on a benchtop roller for 1 h and then static for 1 h. The immunotube was washed as described in Table 2.24. To elute the remaining phage from the immunotube, 1 mL of 10 mg/mL trypsin was added and the tube was incubated on a benchtop roller for 1 h.

The growing XL1 Blue *E. coli* cultures prepared earlier were used for reinfection of the eluted phage and for phage input and output titres. The culture that had reached OD₆₀₀

of approximately 0.5 was used. Serial dilutions of the input and output phage were prepared from 10^{-1} to 10^{-10} and from 10^{-1} to 10^{-7} , respectively, using the XL1 Blue *E. coli* as the diluent. The remaining eluted phage was added to ~5 mL of XL1 Blue *E. coli*. All cultures were infected at 37 °C for 0.5 – 1 h. The input and output cultures were plated onto separate LB agar plates containing 100 µg/mL carbenicillin at 100 µL per plate and incubated overnight at 37 °C. The ~5 mL culture was centrifuged at 3,200 x g for 20 min in an Eppendorf 5810R centrifuge (rotor: A-4-62) and resuspended in 500 µL SB containing 100 µg/mL carbenicillin. This was plated onto six LB agar plates containing 100 µg/mL carbenicillin at 100 µL per plate and incubated overnight at 37 °C.

The following day, the input and output titre plate colonies were counted. The six LB agar plates were scraped into SB containing 100 µg/mL carbenicillin. 75% of this SB culture was used for further rounds of panning. Glycerol was added to the remaining culture to a final concentration of 15% (v/v) and this was stored at -80 °C.

2.2.2.14 Polyclonal phage ELISA of panning output phage

The precipitated phage from each round of panning and the un-panned library were tested in an indirect ELISA format against AZA1-BSA and BSA. This was carried out to determine the overall response towards the antigen and carrier protein after each round. The test wells and control wells were coated with 5 µg/mL AZA1-BSA and 5 µg/mL BSA, respectively, for 1 h at 37 °C. The liquid was then removed. Each well was blocked with 200 µL of 5% (w/v) MM and incubated for 1 h at 37 °C. The wells were then washed 2x with PBS (150 mM, pH 7.4). The phage from each round was diluted at 1:4 in 5% (w/v) MM and added to the designated wells in triplicate at 90 µL per well. To the negative control wells, 5% (w/v) MM was added. The plate was incubated at room temperature on a benchtop shaker for 1.5 h. The plate was then washed three times with PBS-T (150 mM, pH 7.4, 0.05% (v/v) Tween 20) and PBS (150 mM, pH 7.4). HRP-labelled anti-M13 secondary antibody was prepared at 1:5,000 dilution in 5% (w/v) MM and added to each well at 100 µL per well. The plate was then washed three times with PBS-T (150 mM, pH 7.4, 0.05% (v/v) Tween 20) and PBS (150 mM, pH 7.4). One hundred µL TMB was added to each well and the plate was incubated at room temperature on a benchtop shaker for 7 min. The reaction was stopped by the addition

of 50 μL 10% (v/v) H_2SO_4 to each well. The absorbance was measured at 450 nm using a Tecan Safire² plate-reader.

2.2.2.15 Soluble expression of scFv library in non-suppressor strain Top10F' *E. coli*

Top10F' *E. coli* were grown in SB containing 10 $\mu\text{g}/\text{mL}$ tetracycline at 37 °C until the OD_{600} reached a value of 0.5. 20 μL each of output phage from rounds 3 and 4 of panning were added to 2 mL of Top10F' *E. coli* and incubated, while static, at 37 °C for 1 h. The *E. coli* were diluted over a serial dilution range from 10^{-1} to 10^{-8} in SB containing 100 $\mu\text{g}/\text{mL}$ carbenicillin. They were then plated onto LB agar plates containing 100 $\mu\text{g}/\text{mL}$ carbenicillin at 100 μL per plate. The plates were incubated at 37 °C overnight to allow for the growth of visible colonies.

The following day, 192 colonies were picked each from the round 3 and 4 plates (384 colonies in total) into 4x 96 round bottom culture plates (hereafter referred to as the master plates), each well containing 100 μL SB with 100 $\mu\text{g}/\text{mL}$ carbenicillin. The plates with visible colonies were kept for colony pick PCR analysis (see Section 2.2.2.17). The plates were incubated overnight at 37 °C and 220 rpm in an Excella® E25 shaking incubator. To allow for antibody-expression, 20 μL was taken from each well of the 'overnight-cultures' and added to its corresponding well in a deep-well plate, each well containing 1 mL auto-induction media with 100 $\mu\text{g}/\text{mL}$ carbenicillin. These deep-well plates were incubated overnight at 37 °C, 220 rpm. The following additions were made to the master plates; 21.8 μL of 70% (v/v) glycerol was added to each well (giving a final glycerol concentration of 15% (v/v)). The plates were mixed on a benchtop mixer to ensure even distribution of glycerol. The master plates were stored at -80 °C for long-term storage.

2.2.2.16 Monoclonal ELISA of solubly expressed clones

In this experiment a plate from rounds 3 and 4 of panning were tested in an indirect ELISA. Each well was coated with 100 μL of 5 $\mu\text{g}/\text{mL}$ AZA1-BSA in PBS (150 mM, pH 7.4) for 1.5 h, while shaking, at room temperature. The liquid was then removed. The wells were blocked with 200 μL 5% (w/v) MM for 1.5 h, while shaking, at room temperature. The liquid was then removed. The deep-well plates were freeze-thawed three times (each freeze-thaw cycle consisted of 30 min at -80 °C followed by 30 min in a waterbath at 37 °C) to lyse the bacterial cells and centrifuged at 3,200 x g for 20 min

in an Eppendorf 5810R centrifuge (rotor: A-4-62) to pellet the cell debris. The deep-well plate supernatants were diluted at 1:4 by adding 25 μL of supernatant to 75 μL 5% (w/v) MM in the test plate. The plates were incubated for 1.5 h, while shaking, at room temperature. The wells were washed three times with PBS-T (150 mM, pH 7.4, 0.05% (v/v) Tween 20) and PBS (150 mM, pH 7.4). HRP-labelled anti-HA secondary antibody was diluted at 1:2000 dilution in 5% (w/v) MM and 100 μL was added to each well and incubated for 1.5 h, while shaking, at room temperature. The wells were washed three times with PBS-T (150 mM, pH 7.4, 0.05% (v/v) Tween 20) and PBS (150 mM, pH 7.4). One hundred μL TMB was added to each well for 30 min, while shaking, at room temperature. Fifty μL of 10% (v/v) H_2SO_4 was added to each well to stop the colourimetric reaction. The absorbance was measured at 450 nm using a Tecan Safire² plate-reader. No signal was observed in any of the test wells.

This experiment was repeated with the following amendments; non-diluted lysate supernatant was added to the coated and blocked test plates at 100 μL per well and incubated at 4 °C overnight. The HRP-labelled anti-HA antibody concentration was increased to a 1:1000 dilution. Again, no signal was observed. To address this, the soluble-expression method was adjusted by expressing each clone in 1 mL SB containing 50 $\mu\text{g}/\text{mL}$ carbenicillin at 37 °C for 6 h. At this time, IPTG was added to a final concentration of 1 mM and the plates were incubated overnight at 30 °C and 220 rpm in an Excella® E25 shaking incubator. The monoclonal ELISA was performed according to the above amended protocol. However, no signal was observed in any of the test wells.

2.2.2.17 Colony pick PCR of panning input and output phage

This experiment was performed in order to determine if the scFv gene-insert remained present before and after round 4 of panning. Using the soluble expression plates from Section 2.2.2.15, 8 colonies were picked each from round 4 input and round 4 output plates and grown separately in 200 μL SB containing 100 $\mu\text{g}/\text{mL}$ carbenicillin overnight at 37 °C. This was done to ensure that enough DNA template would be available for PCR analysis. A PCR master mix was prepared as described in Table 2.25. The master mix was divided into seventeen 49 μL aliquots. Eight tubes were labelled Round 4 Input and another 8 tubes were labelled Round 4 Output. One tube was used as a negative control. A 1 μL sample was taken from each of the overnight cultures and added to its

designated tube. For the negative control reaction, 1 μL of SB containing 100 $\mu\text{g}/\text{mL}$ carbenicillin was added to the negative control tube. The PCR was carried out as per the conditions described in Table 2.18 in a Rotor-Gene 6000 Thermal Cycler. The PCR products were separated on a 1% (w/v) agarose gel stained with SYBR® Safe at 100 V for 35 min. A Hyperladder™ 1kb Plus was used as molecular size markers.

Table 2.25: Colony pick PCR master mix composition.

Component	Volume (μL)	Working concentration
2x MyTaq Red Mix	425	1x
RSC-F	8.5	1 μM
RSC-B	8.5	1 μM
Molecular grade H_2O	408	-

2.2.2.18 Determination of wtM13 response towards AZA1 by indirect ELISA

The purpose of this experiment was to determine the extent of the binding of wtM13 to AZA1 by indirect ELISA. Using a Nunc Maxisorb™ 96-well plate, the test wells and control wells were coated with 5 $\mu\text{g}/\text{mL}$ AZA1-BSA and 5 $\mu\text{g}/\text{mL}$ BSA, respectively, for 1 h at 37 °C. The liquid was then removed. Each well was blocked with 200 μL of 5% (w/v) MM and incubated for 1 h at 37 °C. The wells were washed 1x with PBS (150 mM, pH 7.4). A 1:5 serial dilution range of wtM13 and the eluted phage of Round 4 were prepared in 5% (v/v) MM from 1:10 to 1:6,250. Furthermore, as another point of comparison, the response of a phage library that was raised against pancreatic tumour markers was also tested against AZA1-BSA, i.e. an scFv library that was heavily biased towards pancreatic tumour marker antigens that was displayed on M13 phage. This anti-pancreatic cancer phage library was diluted from 1:20 to 1:1,280 in 5% (w/v) MM. Each dilution of phage was added to its designated well in triplicate at 100 μL per well. To each of the negative control wells, 100 μL of 5% (w/v) MM without phage was added. The plate was incubated at 37 °C for 1 h. The plate was then washed three times with PBS-T (150 mM, pH 7.4, 0.05% (v/v) Tween 20) and PBS (150 mM, pH 7.4). HRP-labelled anti-M13 secondary antibody was prepared at a 1:5,000 dilution in 5% (w/v) MM and added to each well at 100 μL per well. The plate was then washed three times with PBS-T (150 mM, pH 7.4, 0.05% (v/v) Tween 20) and PBS (150 mM, pH 7.4). One hundred μL TMB was added to each well and the plate was incubated at room

temperature on a benchtop shaker for 15 min. The reaction was stopped by the addition of 50 μL 10% (v/v) H_2SO_4 to each well. The absorbance was measured at 450 nm using a Tecan Safire² plate-reader.

2.2.2.19 Conjugation of AZA1 to ovalbumin

The purpose of this experiment was to develop a new AZA1 conjugate to use for further testing of the non-specific binding of non-displaying phage. For this conjugate, ovalbumin (OVA) was used as a carrier protein. It was determined that the non-specific binding interaction observed may have been due to conjugation chemistry used to develop the previous conjugate. Thus, in collaboration with researchers in the School of Chemical Sciences in DCU, the following conjugation method was developed. This method was a modified version of the previous conjugation (Section 2.2.2.1) but included a number of amendments to improve the efficiency of conjugation. Firstly, when used alone, EDC forms a highly reactive intermediate when coupled to the carboxylic acid-containing reagent (AZA1) but the reaction efficiencies are low. The inclusion of *N*-hydroxysuccinimide (NHS) or sulfo-NHS (which is the water-soluble analogue) allows for the formation of a semi-stable ester intermediate upon reaction with EDC and the carboxylic acid. There are issues with the use of NHS intermediates, as they begin to hydrolyse rapidly at elevated pH levels (especially greater than pH 8). The solution to this issue was to perform the coupling in two steps. The first step involved stably forming the NHS-intermediate in water-free organic solvents. The use of DMSO allows for direct miscibility of the NHS-intermediate reaction solution with the buffer which contains the protein. In the second step a buffer with a pH > 7 must be used to promote reaction of neutral amines on the protein, thus PBS (150 mM, pH 7.4) was used.

Three hundred μg of AZA1 (1 molar equivalent) was dried under nitrogen stream in a glass vial. Next, 775 μg sulfo-NHS (10 molar equivalent) and 1,400 μg EDC (20 molar equivalent) were dissolved in 200 μL DMSO and added to the reaction vial. The reaction was stirred to ensure full dissolution of the reagents before 100 μL pyridine was added to raise the pH to > 7. The reaction was left to stir overnight in the sealed vial at room temperature in the dark. The mixture was then diluted with 600 μL sterile filtered PBS (150 mM, pH 7.4) and allowed to mix thoroughly. To the reaction vial was added 80 μL of 20 mg/mL OVA in PBS (150 mM, pH 7.4) (1,600 μg OVA, 0.1 molar

equivalent). The molar ratio of AZA1 to the OVA carrier protein was 10:1 to ensure high coupling efficiency, i.e. to ensure that AZA1 would be presented on a large number of sites per OVA molecule. The vial was sealed and the mixture was stirred overnight at room temperature in the dark. Membrane ultrafiltration was carried using a 10,000 MWCO Viva spin-column out to remove any reaction by-products (such as urea) and retain the AZA1-OVA conjugate. The conjugate was reconstituted into PBS (150 mM, pH 7.4) with 15% (v/v) glycerol. The protein concentration of the AZA1-OVA conjugate was determined by BCA assay (as per Section 2.2.1.4).

2.2.2.20 Testing AZA1-OVA conjugate with mouse B antiserum and wtM13

The purpose of this experiment was to determine if the AZA1-OVA conjugation reaction was successful. This was determined by measuring the response of the mouse B antiserum to the AZA1-OVA conjugate. In addition, the response of wtM13 towards the new AZA1-OVA conjugate was measured to evaluate any non-specific binding of the phage to the conjugate. A 96-well Nunc MaxisorbTM plate was coated with 100 μ L per well of 5 μ g/mL of AZA1-OVA. The control wells were coated with 100 μ L per well of 5 μ g/mL OVA. The plate was incubated at 37 °C for 1 h. The liquid was then removed. Each well was blocked with 200 μ L of 5% (w/v) MM and incubated at 37 °C for 1 h. The liquid was then removed. The mouse B antiserum was diluted in doubling dilutions from 1:400 to 1:12,800 in 5% (w/v) MM. The wtM13 phage was diluted in doubling dilutions from 1:100 to 1:800. A negative control was also included, which omitted the serum and wtM13. One hundred μ L of each dilution and negative control was added to the plate incubated at 37 °C for 1 h. The wells were then rinsed three times with PBS-T (150 mM, pH 7.4, 0.05% (v/v) Tween 20) and PBS (150 mM, pH 7.4). HRP-labelled anti-mouse IgG was diluted at 1:10,000 in 5% (w/v) MM and 100 μ L was placed into the mouse B antiserum wells. HRP-labelled anti-M13 secondary antibody was prepared at a 1:5,000 dilution in 5% (w/v) MM and added to the wtM13 wells at 100 μ L per well. The plate was incubated at 37 °C for 1 h. The wells were then rinsed three times with PBS-T (150 mM, pH 7.4, 0.05% (v/v) Tween 20) and PBS (150 mM, pH 7.4). TMB was added at 100 μ L per well. The plate was incubated at 37 °C for 15 min. Ten percent (v/v) H₂SO₄ was added at 50 μ L per well to stop the colourimetric reaction. The absorbance was measured at 450 nm using a Tecan Safire² plate-reader.

2.2.2.21 Re-construction of anti-AZA1 scFv library

Given that the first antibody library was relatively small (of the order of 10^5 clones), it was decided to re-construct the anti-AZA1 scFv library, so as generate a larger library with greater diversity. The antibody library was constructed as per Sections 2.2.2.6 – 2.2.2.11. After transformation of the scFv-pComb3XSS vector into *E. coli*, the antibody library size was determined and a colony pick PCR was carried out as per Section 2.2.2.12 but included the following amendment; in place of the CSC-F and CSC-B primers, the OmpSeq and Gback primers were used.

2.2.2.22 Re-screening the new anti-AZA1 scFv library by panning using AZA1-OVA

This experiment used the same method as Section 2.2.2.13 above but included the following amendment; the AZA1-OVA coating concentration for rounds 1 – 4 was 50, 25, 10 and 5 $\mu\text{g/mL}$, respectively.

2.2.2.23 Polyclonal ELISA of panning output phage

Following 4 rounds of panning, a polyclonal phage ELISA was carried out. The test wells were coated with 5 $\mu\text{g/mL}$ AZA1-OVA for 1 h at 37 °C. The liquid was then removed. Each well was blocked with 200 μL of 5% (w/v) MM and incubated for 1 h at 37 °C. The wells were then washed 2x with PBS (150 mM, pH 7.4). The phage from each round and wtM13 were diluted to 10^{10} pfu/mL in 5% (w/v) MM and 100 μL was added to the designated wells in triplicate. The negative control consisted of 5% (w/v) MM without phage. The plate was incubated at room temperature on a benchtop shaker for 1.5 h. The plate was then washed three times with PBS-T (150 mM, pH 7.4, 0.05% (v/v) Tween 20) and PBS (150 mM, pH 7.4). HRP-labelled anti-M13 secondary antibody was prepared at 1:5,000 dilution in 5% (w/v) MM and added to each well at 100 μL per well. The plate was then washed three times with PBS-T (150 mM, pH 7.4, 0.05% (v/v) Tween 20) and PBS (150 mM, pH 7.4). One hundred μL TMB was added to each well and the plate was incubated at room temperature on a benchtop shaker for 10 min. The reaction was stopped by the addition of 50 μL 10% (v/v) H_2SO_4 to each well. The absorbance was measured at 450 nm using a Tecan Safire² plate-reader. Data was analysed by one-way analysis of variance (ANOVA) using GraphPad Prism. If the ANOVA table was significant ($P < 0.05$), post-hoc analysis was performed using Newman-Keuls' test.

2.2.2.24 Development of an assay to measure AZA1 using polyclonal mouse antiserum

The purpose of these experiments was to develop an assay to measure AZA1 in solution using the polyclonal antiserum obtained from Mouse B.

2.2.2.24.1 Optimisation of Mouse B antiserum dilution and AZA1-OVA coating concentration by checkerboard ELISA

The purpose of this experiment was to determine an optimal dilution factor of the mouse B antiserum and an optimal coating concentration of AZA1-OVA. The aim was to find a concentration of each of these components that would produce a response that was significantly different to the negative control and that allowed for the most economical use of the limited antiserum and toxin stocks. A series of dilutions of AZA1-OVA were prepared in PBS (150 mM, pH 7.4), ranging from 10 to 0.625 µg/mL and a 0 µg/mL solution was also prepared, which served as a negative control. A 96-well Nunc Maxisorb™ plate was coated with 100 µL per well of each AZA1-OVA dilution. The plate was incubated at 37 °C for 1 h. The liquid was then removed. Each well was blocked with 200 µL of 5% (w/v) MM and incubated at 37 °C for 1 h. The liquid was then removed. A dilution series of the Mouse B antiserum was prepared in 5% (w/v) MM, ranging from 1:200 to 1:12,800. One hundred microlitres of each antiserum dilution was placed into each well and the plate was incubated at 37 °C for 1 h. The wells were then rinsed three times with PBS-T (150 mM, pH 7.4, 0.05% (v/v) Tween 20) and PBS (150 mM, pH 7.4). HRP-labelled anti-mouse IgG was diluted at 1:10,000 in 5% (w/v) MM and 100 µL was placed into each well. The plate was incubated at 37 °C for 1 h. The wells were then rinsed three times with PBS-T (150 mM, pH 7.4, 0.05% (v/v) Tween 20) and PBS (150 mM, pH 7.4). TMB was added at 100 µL per well. The plate was incubated at 37 °C for 15 min. Ten percent (v/v) H₂SO₄ was added at 50 µL per well to stop the colourimetric reaction. The absorbance was measured at 450 nm using a Tecan Safire² plate-reader.

2.2.2.24.2 Development of competitive assay to detect AZA1 using polyclonal murine IgG

The purpose of this experiment was to develop a competitive assay to determine the binding characteristics of the antiserum obtained from the final bleed of Mouse B. A 96-well Nunc Maxisorb™ plate was coated with 100 µL per well of 5 µg/mL of AZA1-

OVA. The plate was incubated at 37 °C for 1 h. The liquid was then removed. Each well was blocked with 200 µL of 5% (w/v) MM and incubated at 37 °C for 1 h. The liquid was then removed. The Mouse B antiserum and free AZA1 were mixed in equal volumes and allowed to incubate at room temperature for 1 h before being added onto the ELISA plate at 100 µL per well in triplicate. The final dilution factor of the Mouse B antiserum was 1:200 in 5% (w/v) MM. The final AZA1 concentrations ranged from 1,400 to 0.015 ng/mL. The wells were then rinsed three times with PBS-T (150 mM, pH 7.4, 0.05% (v/v) Tween 20) and PBS (150 mM, pH 7.4). HRP-labelled anti-mouse IgG was diluted at 1:10,000 in 5% (w/v) MM and 100 µL was placed into each well. The plate was incubated at 37 °C for 1 h. The wells were then rinsed three times with PBS-T (150 mM, pH 7.4, 0.05% (v/v) Tween 20) and PBS (150 mM, pH 7.4). TMB was added at 100 µL per well. The plate was incubated at 37 °C for 15 min. Ten percent (v/v) H₂SO₄ was added at 50 µL per well. The absorbance was measured at 450 nm using a Tecan Safire² plate-reader.

2.2.3 Elucidating Microcystin-LR-antibody interactions by *in silico* docking and *in vitro* mutagenesis

2.2.3.1 SwissModel and CASTp modelling of anti-MC-LR scFv (2G1)

A 3D model of the 2G1 scFv was generated using SwissModel (Guex *et al.*, 2009; Biasini *et al.*, 2014) using PDB 4p48.1.A as a template, which shared 85.41% sequence identity. 4p48.1.A is a chicken anti-cardiac Troponin I scFv, the crystal structure of which was elucidated using X-ray diffraction to a resolution of 1.35 Å (Conroy *et al.*, 2014). The SwissModel-generated 2G1 model was saved as .pdb format and uploaded to Computed Atlas of Surface Topography of proteins (CASTp) database to determine the location and size of the pockets in the 3D structure (Dundas *et al.*, 2006).

2.2.3.2 Docking MC-LR into anti-MC-LR scFv (2G1) using AutoDock

All docking experiments were carried out using AutoDock Vina according to Huey *et al.* (2012). The 2G1.pdb file from SwissModel was opened in AutoDock Tools (ADT). To process the .pdb model for docking, the following edits were made; water molecules were deleted, hydrogen atoms were added and non-polar hydrogens were subsequently merged, and charges were computed using the Gasteiger method. The MC-LR 3D

structure .pdb file was acquired from PDB (code: 1LCM) (Troger *et al.*, 1996). 1LCM.pdb was inputted into ADT and the Torsion Tree root was detected. 2G1 and 1LCM were saved as .pdbqt files. A grid box was set up to encompass the pocket identified by CASTp. The grid box XYZ dimensions were 20, 20, and 20 Å, respectively, with the grid centre XYZ coordinates at 47.65, 9.37 and 3.91, respectively. For flexible side chain docking, the residues L-Y49, H-E101 and H-E102 were assigned flexibility. The highest ranked, lowest energy docking pose was used as the basis for further work.

2.2.3.3 Preparation of MC-LR-BSA conjugate

MC-LR-BSA conjugates were prepared using an Imject™ EDC BSA Spin Kit, as per the manufacturer's instructions. Briefly, 500 µg MC-LR was dissolved in Imject™ EDC conjugation buffer and mixed with 10 mg/mL BSA solution. This hapten-carrier solution was added to 10 mg EDC and incubated at room temperature with constant mixing for 2 h. The conjugate was purified by desalting using the provided desalting spin column. The purified MC-LR-BSA was aliquoted and stored at -20 °C until used.

2.2.3.4 Targeted Mutagenesis of 2G1 DNA sequence

The wild type 2G1 clone plasmid was purified using a NucleoSpin® Plasmid kit, as per Section 2.2.1.3. The 2G1 scFv DNA was analysed by Sanger Sequencing (Source Bioscience plc, Nottingham, UK). Site-directed mutagenesis was carried out using a QuikChange II Mutagenesis kit, as per the manufacturer's instructions. The site-specific primers were designed based on the manufacturer's guidelines and the primer sequences are shown in Table 2.26. The targeted mutagenesis reactions were prepared according to Table 2.27 and reactions were run in a Rotor-Gene 6000 Thermal Cycler as described in Table 2.28. Following the mutagenesis reaction, the reaction tubes were placed on ice to reduce the temperature to below 37 °C. One µL of *DpnI* restriction enzyme was added directly to each completed reaction and incubated at 37 °C for 1 h to digest the template DNA plasmid. The mutant plasmids were transformed into XL1 *E. coli* by heat-shock treatment as follows. XL1 *E. coli* were gently thawed on ice. For each reaction, 50 µL of thawed *E. coli* were placed into a 15 mL tube. Following this, 1 µL of *DpnI*-digested DNA was added to the *E. coli* and incubated on ice for 30 min. The tube was heat-pulsed for 45 s at 42 °C and placed on ice for 2 min. To rescue the heat-pulsed *E. coli*, 0.5 mL of NZY⁺ broth that was preheated to 42 °C was added to the cells and incubated

at 37 °C for 1 h with shaking at 250 rpm in an Excella® E25 shaking incubator. The transformed cells were streaked onto LB agar plates supplemented with 100 µg/mL carbenicillin (250 µL of transformed cells per plate) and incubated at 37 °C overnight. Colonies were picked and the presence of the scFv gene insert was confirmed by PCR as per Section 2.2.2.12. The mutant plasmids were purified using the NucleoSpin® Plasmid kit as per Section 2.2.1.3 and these were analysed by Sanger Sequencing to confirm the amino acid residue changes. These DNA sequences were aligned using Clustal Omega (Sievers *et al.*, 2014).

Table 2.26: Binding site mutagenesis primer sequences.

Primer name	Primer sequence
L-Y49A F	5' – TTCACCTTCAGCAGTGCCAACATGGGTTGGGTG – 3'
L-Y49A R	5' – CACCCAACCCATGTTGGCACTGCTGAAGGTGAA – 3'
L-P55A F	5' – CAAAACACCAAGAGGGCCTCGGACATCCCTTCA – 3'
L-P55A R	5' – TGAAGGGATGTCCGAGGCCCTCTTGGTGTTTTG – 3'
L-S56A F	5' – AACACCAAGAGGCCCGCGGACATCCCTTCACGA – 3'
L-S56A R	5' – TCGTGAAGGGATGTCCGCGGGCCTCTTGGTGTT – 3'
L-D57A F	5' – ACCAAGAGGCCCTCGGCCATCCCTTCACGATTCTCC – 3'
L-D57A R	5' – GGAGAATCGTGAAGGGATGGCCGAGGGCCTCTTGGT – 3'
H-L2A F	5' – GGTGGCTCTTCCGCCGCGACGTTGGACGAGTCC – 3'
H-L2A R	5' – GGACTCGTCCAACGTCGCGGCGGAAGAGCCACC – 3'
H-Y32A F	5' – TTCACCTTCAGCAGTGCCAACATGGGTTGGGTG – 3'
H-Y32A R	5' – CACCCAACCCATGTTGGCACTGCTGAAGGTGAA – 3'
H-E101A F	5' – GCCAAAGGTAATATTAACATCGCAGAATGGGGCCACG GGACCGAA – 3'
H-E101A R	5' – TTCGGTCCCGTGGCCCCATTCTGCGATGTTAATATTAC CTTTGGC – 3'
H-E102A F	5' – GCCAAAGGTAATATTAACATCGAAGCATGGGGCCAC GGGACCGAA – 3'
H-E102A R	5' – TTCGGTCCCGTGGCCCCATGCTTCGATGTTAATATTAC CTTTGGC – 3'
L-D57N F	5' – ACCAAGAGGCCCTCGAACATCCCTTCACGATTCTCC – 3'

L-D57N R	5' – GGAGAATCGTGAAGGGATGTTTCGAGGGCCTCTTGGT – 3'
L-D57Y F	5' – CCAAGAGGCCCTCGTACATCCCTTCACGATTCTCC – 3'
L-D57Y R	5' – GGAGAATCGTGAAGGGATGTACGAGGGCCTCTTGG – 3'
H-E102Q F	5' – GCCAAAGGTAATATTAACATCGAACAATGGGGCCAC GGGACCGAA – 3'
H-E102Q R	5' – TTCGGTCCCGTGGCCCCATTGTTTCGATGTTAATATTAC CTTTGGC – 3'

Table 2.27: QuikChange Mutagenesis reaction composition.

Component	Volume (μL)	Working concentration
10x Reaction Buffer	5	1x
dsDNA template	2.5	1 ng/ μL
Forward primer	0.9	2.5 ng/ μL
Reverse Primer	0.9	2.5 ng/ μL
dNTP mix	1	-
Molecular grade H ₂ O	36.7	-
QuikSolution	3	-
<i>PfuUltra</i> High Fidelity DNA polymerase	1	0.05 U/ μL

Table 2.28: QuikChange Mutagenesis reaction conditions.

Stage	Temperature ($^{\circ}\text{C}$)	Time
Initialisation	95	60 s
Denaturation	95	30 s
Annealing	60	60 s
Extension	68	4 min
Final Extension	68	7 min

} x 18 cycles

2.2.3.5 Expression of 2G1 wild type and mutant scFv

Overnight cultures of the 2G1 wild type and mutant clones were prepared by inoculating individual colonies into 5 mL SB with 100 $\mu\text{g}/\text{mL}$ carbenicillin. These cultures were grown at 37 $^{\circ}\text{C}$, 220 rpm overnight. The following day, these overnight

cultures were subcultured at a ratio of 1:100 into 50 mL SB supplemented with 100 µg/mL carbenicillin, 0.5% (v/v) glycerol and 0.05% (w/v) glucose. The cultures were grown at 37 °C, 220 rpm until an OD₆₀₀ of 0.4 was reached. At this point, the cultures were induced with 1 mM isopropyl β-D-1-thiogalactopyranoside (IPTG) and were incubated at 30 °C, 220 rpm for 16 h. The cells were collected by centrifugation at 3,200 x g in an Eppendorf 5810R centrifuge (rotor: A-4-62) for 20 min. The pellet was resuspended in PBS (150 mM phosphate buffer saline, pH 7.2) supplemented with cOmplete™ ULTRA protease inhibitor cocktail. To lyse the cells and release the intracellular scFv, the resuspended pellets were sonicated using a Branson Digital Sonifier (Emerson Electric, St. Louis, MO, USA) at 40% output for 3 min, with a pulse duration of 6 s on and 6 s off. The lysed cell debris was pelleted at 15,500 x g in an Eppendorf 5810R centrifuge (rotor: F45-30-11) for 20 min. The supernatant was collected and stored at -20 °C until used.

2.2.3.6 SDS-PAGE and Western blotting

In order to confirm the presence of the 2G1 wild type and mutant scFv in lysates, they were tested by sodium dodecyl sulfate-polyacrylamide gel electrophoresis (SDS-PAGE) and Western blotting. Briefly, each lysate was diluted to 1:5 in PBS (150 mM, pH 7.2) (representing the lowest dilution tested in an indirect ELISA). PBS (150 mM, pH 7.2) without lysate was included as a negative control. Equal volumes of the lysates were loaded and separated on 12.5% (v/v) acrylamide gels at 110 V for 1.5 h. For SDS-PAGE, the gel was treated with Instant Blue stain at room temperature on a plate rocker for 15 min. The stained gel was imaged using a BioRad EZ Imager. For the Western blots, the proteins were transferred to a nitrocellulose membrane using a Pierce G2 Fast Blotter. After the transfer, the membrane was blocked using 5% (w/v) MM at room temperature on a plate rocker for 1 h. The membrane was probed with HRP-labelled anti-HA secondary antibody diluted to 1:2,000 in MM at room temperature on a plate rocker for 1 h. The membrane was washed three times each with PBS-T (150 mM, pH 7.2, 0.05% (v/v) Tween-20) and PBS (150 mM, pH 7.2). TMB was added to the membrane and incubated at room temperature for 5 min until colour formation was observed.

2.2.3.7 Indirect ELISA of 2G1 mutant lysates

A Nunc MaxiSorp™ 96-well plate was coated with 5 µg/mL MC-LR-BSA in PBS (150 mM, pH 7.2) (100 µL/well) and incubated at 37 °C for 1 h. The plate was blocked with 5% (w/v) MM (200 µL/well) and incubated at 37 °C for 1 h. The antibody lysates were serially diluted from 1:5 to 1:1.95 x 10⁶ in 5% (w/v) MM. For a negative control, 5% (w/v) MM without lysate was used. The lysate samples were incubated on the coated and blocked multiwell plates (100 µL/well) for 1 h at 37 °C. Following this, the wells were washed three times each with PBS-T (150 mM, pH 7.2, 0.05% (v/v) Tween-20) and PBS (150 mM, pH 7.2). A HRP-labelled anti-HA secondary antibody diluted to 1 in 2,000 in 5% (w/v) MM was added to each well (100 µL/well) and incubated at 37 °C for 1 h. A wash step was performed as above. TMB was added to each well (100 µL/well) and incubated at room temperature on a plate shaker for 15 min. 10% (v/v) HCl was added to each well (50 µL/well) to stop the colourimetric reaction. The absorbance was measured using a Tecan Safire² at 450 nm.

2.2.3.8 Competitive ELISA of 2G1 mutant lysates

A Nunc MaxiSorp™ 96-well plate was coated with 5 µg/mL MC-LR-BSA in PBS (150 mM, pH 7.2) (100 µL/well) and incubated at 37 °C for 1 h. The plate blocked with 5% (w/v) MM (200 µL/well) and incubated at 37 °C for 1 h. Each antibody lysate solution was diluted in 5% (w/v) MM such that it should produce a maximum absorbance of 1, as determined by indirect ELISA. Tests for 2G1 wild type and mutants were carried out in triplicate (n = 3). MC-LR standard (free MC-LR) was used in the competition step at a range of concentrations from 5,000 to 0.76 ng/mL. A 0 ng/mL MC-LR sample was also prepared in order to determine the maximum absorbance of each antibody. In order to ensure solubility of MC-LR at this range of concentrations, each antibody-MC-LR sample included methanol at a final concentration of 0.5% (v/v). The antibody-MC-LR samples were incubated on the coated and blocked multiwell plates (100 µL/well) for 1 h at 37 °C. Following this, the wells were washed three times each with PBS-T (150 mM, pH 7.2, 0.05% (v/v) Tween-20) and PBS (150 mM, pH 7.2). A HRP-labelled anti-HA secondary antibody diluted to 1 in 2,000 in 5% (w/v) MM was added to each well (100 µL/well) and incubated at 37 °C for 1 h. A wash step was performed as above. TMB was added to each well (100 µL/well) and incubated at room temperature on a plate shaker for 15 min. To stop the colourimetric reaction, 10% (v/v) HCl was added to each well (50 µL/well). The absorbance was measured using a Tecan Safire² at 450 nm.

2.2.4 Optimisation of anti-MC-LR scFv stability and solubility by targeted mutagenesis

2.2.4.1 *In silico* modelling

The 3D 2G1 scFv model was generated according to Section 2.2.3.1. To identify surface-exposed hydrophobic amino acid (AA) residues, the 2G1 model surface was coloured according to the Kyte-Doolittle hydrophobicity scale using University of California, San Francisco (UCSF) Chimera 1.12 software (Pettersen *et al.*, 2004). The theoretical isoelectric point (pI) values for the wild type, single mutant and triple mutants were determined using the Protein-Sol online tool (Hebditch *et al.*, 2017).

2.2.4.2 QuikChange mutagenesis

The aim of this experiment was to introduce charged residue mutations into the 2G1 structure at positions of surface-exposed hydrophobic residues. This experiment was carried out as per Section 2.2.3.4, but using the mutagenesis primers listed in Table 2.29.

Table 2.29: Stability mutagenesis primer sequences.

Primer name	Sequence
L124D – F	5' – GGACAACCCTGACCGTCGATGGTGGTTCCTCTGGAT CTTCC – 3'
L124D – R	5' – GGAAGATCCAGAGGAACCACCATCGACGGTCAGGG TTGTCC – 3'
L124R – F	5' – CAACCCTGACCGTCCGAGGTGGTTCCTCTGG – 3'
L124R – R	5' – CCAGAGGAACCACCTCGGACGGTCAGGGTTG – 3'
L153D – F	5' – CGAGTCCGGGGGCGGCGACCAGACGCCCCGGAGG AGC – 3'
L153D – R	5' – GCTCCTCCGGGCGTCTGGTCGCCGCCCCGGAC TCG – 3'
L153R – F	5' – GAGTCCGGGGGCGGCCGCCAGACGCCCCGGAGG – 3'
L153R – R	5' – CCTCCGGGCGTCTGGCGGCCGCCCCGGACTC – 3'
I255D – F	5' – CCACGGGACCGAAGTCGACGTCTCCTCCACTA GTGG – 3'

I255D – R	5' – CCACTAGTGGAGGAGACGTCGACTTCGGTCCCG TGG – 3'
I255R – F	5' – CACGGGACCGAAGTCCGCGTCTCCTCCACTAG – 3'
I255R – R	5' – CTAGTGGAGGAGACGCGGACTTCGGTCCCGTG – 3'

2.2.4.3 Small-scale expression of 'stability mutant' scFv fragments

The small-scale expression of each 'stability mutant' clone was carried out as per Section 2.2.3.5.

2.2.4.4 Indirect ELISA of 2G1 'stability mutant' lysates

The purpose of this experiment was to determine the binding response of each mutant lysate and to determine a suitable dilution factor to provide a binding response of ≈ 1 absorbance unit. This dilution factor would then be subsequently used in a competitive ELISA.

A 96-well Nunc Maxisorb™ plate was coated with 100 μ L per well of 5 μ g/mL MC-LR-BSA. The plate was incubated at 37 °C for 1 h. The liquid was then removed. Each well was blocked with 200 μ L of 5% (w/v) MM and incubated at 37 °C for 1 h. The liquid was then removed. A dilution series of each mutant lysate from Section 2.2.4.3 was prepared in 5% (w/v) MM, ranging from 1:5 to 1:1.95 x 10⁶. One hundred microlitres of each lysate dilution was placed into each well in triplicate. The plate was incubated at 37 °C for 1 h. The wells were then rinsed three times with PBS-T (150 mM, pH 7.2, 0.05% (v/v) Tween-20) and PBS (150 mM, pH 7.2). HRP-labelled anti-HA secondary antibody was diluted at 1:2,000 in 5% (w/v) MM and 100 μ L was placed into each well. The plate was incubated at 37 °C for 1 h. The wells were then rinsed three times with PBS-T (150 mM, pH 7.2, 0.05% (v/v) Tween-20) and PBS (150 mM, pH 7.2). TMB was added at 100 μ L per well. The plate was incubated at 37 °C for 15 min. Ten percent (v/v) H₂SO₄ was added at 50 μ L per well. The absorbance was measured at 450 nm using a Tecan Safire² plate-reader.

2.2.4.5 Competitive ELISA

The introduction of mutations into the framework regions of the 2G1 wild type may cause changes in the overall scFv structure, which may impact the binding-ability of the antibody. The purpose of this experiment was to determine if any of the mutations

carried out had any deleterious effects on the binding response of the antibody to MC-LR.

A 96-well Nunc Maxisorb™ plate was coated with 100 µL per well of 5 µg/mL MC-LR-BSA in PBS (150 mM, pH 7.2). The plate was incubated at 37 °C for 1 h. The liquid was then removed. Each well was blocked with 200 µL of 5% (w/v) MM and incubated at 37 °C for 1 h. The liquid was then removed. Each antibody lysate solution from 2.2.4.3 was diluted such that it should produce a maximum absorbance of 1, as determined by indirect ELISA. Free MC-LR was used in the competition step at a range of concentrations from 5,000 to 0.76 ng/mL. A 0 ng/mL MC-LR sample was also prepared in order to determine the maximum absorbance of each antibody. In order to ensure solubility of MC-LR at this range of concentrations, each antibody-MC-LR sample included methanol at a final concentration of 0.5% (v/v). Each lysate sample and free MC-LR dilution was placed into each well in triplicate. The plate was incubated at 37 °C for 1 h. The wells were then rinsed three times with PBS-T (150 mM, pH 7.2, 0.05% (v/v) Tween-20) and PBS (150 mM, pH 7.2). HRP-labelled anti-HA secondary antibody was diluted at 1:2,000 in 5% (w/v) MM and 100 µL was placed into each well. The plate was incubated at 37 °C for 1 h. The wells were then rinsed three times with PBS-T (150 mM, pH 7.2, 0.05% (v/v) Tween-20) and PBS (150 mM, pH 7.2). TMB was added at 100 µL per well. The plate was incubated at 37 °C for 15 min. Ten percent (v/v) H₂SO₄ was added at 50 µL per well. The absorbance was measured at 450 nm using a Tecan Safire² plate-reader.

2.2.4.6 Large-scale expression and purification

The aim of this procedure was to express and purify each of the ‘stability mutant’ clones in order to determine the effect of the mutations on protein yield. In addition, it was desired to produce enough antibody to facilitate further experiments.

The expression of each clone was carried out as per Section 2.2.4.3, but included the following amendments:

- After culturing each clone in 5 mL SB overnight, they were sub-cultured into 200 mL SB supplemented with 100 µg/mL carbenicillin, 0.5% (v/v) glycerol and 0.05% (w/v) glucose.

- For resuspending the centrifuged cell pellet, in place of PBS (150 mM, pH 7.2), equilibration buffer was used and it was supplemented with cOmplete™ ULTRA protease inhibitor cocktail.

After resuspending the lysate in equilibration buffer, the scFv was purified from the lysate as follows. One millilitre of IMAC resin (1:1 mixture of resin with 20% (v/v) ethanol) was added to a plastic column. The resin was allowed to settle and the ethanol storage solution was removed, producing a final resin volume of 500 μ L. The IMAC column was equilibrated by the addition of 10 mL equilibration buffer. The resuspended lysate was applied to the equilibrated IMAC column. The column was sealed and mixed on a benchtop roller for 2 h at room temperature to allow the HIS-tagged scFv molecules to bind to the nickel resin in solution. Following this, the resin was settled and the lysate was passed through. Eight millilitres of wash buffer A was passed through the column followed by 8 mL of wash buffer B to remove non-specifically bound proteins from the resin. Five millilitres of elution buffer was applied to the column and 0.5 mL fractions were collected. The protein concentration was measured at 280 nm using a NanoDrop ND-1000. The elution fractions containing observable levels of protein were pooled and buffer exchanged with 0.2 μ m-filtered PBS (150 mM, pH 7.2) using a 10,000 MWCO VivaSpin column.

A BCA assay was carried out to determine the concentration of each antibody sample as per Section 2.2.1.4. Protein yields were determined by multiplying the concentration measured by the volume of sample. SDS-PAGE and Western blot analyses were also carried out on the lysate, flow through, wash A, wash B, elution and concentrated elution samples as per Section 2.2.3.6. Following imaging of the SDS-PAGE gels, the images were processed and analysed using the ‘enhance contrast’ feature in ImageJ software (Schindelin *et al.*, 2012) in order to quantitatively measure the pixel intensity of the protein bands. In the concentrated elution lanes from each sample, the bands observed at approximately 25 kDa and 55 kDa, (corresponding to the monomeric scFv and the aggregated dimerised scFv, respectively) were analysed for pixel intensity. For the six clones, between 25,000 and 50,000 pixels were analysed and the mean pixel intensity was determined. The ratio of band intensity was determined as the mean pixel intensity of the ~25 kDa band divided by the mean pixel intensity of the ~55 kDa band.

2.2.4.7 Measurement of the solubility of the 2G1 wild type and ‘stability mutant’ clones

The aim of this experiment was to determine the solubility of each antibody mutant when exposed to different conditions. The theory was that, as each mutant came out of solution it would be removed by high speed centrifugation. The protein concentration of the remaining solution would then be measured to determine the amount of remaining soluble protein. To determine the native solubility, each clone was incubated at 25 °C for a set duration, ranging from 0 – 6 days. To determine the non-native solubility, each clone was incubated at a set temperature, ranging from 25 – 95 °C, for 20 min followed by cooling to 25 °C for 20 min.

Each antibody clone solution was diluted to 300 µg/mL and 30 µL was aliquoted per tube. Each sample was exposed to the various treatments in triplicate. Each sample was centrifuged at 10,000 x g for 20 min in an Eppendorf 5810R centrifuge (rotor: F45-30-11). Twenty five microlitres of the supernatant was transferred to a multiwell plate and a BCA assay was carried out as per Section 2.2.1.4. Data were analysed by ANOVA using GraphPad Prism 5.0. If the ANOVA table was significant ($P < 0.05$), post-hoc analysis was performed using Dunnett’s test.

2.2.4.8 Measurement of the functional stability of 2G1 wild type and ‘stability mutant’ clones by ELISA

The purpose of this experiment was to determine if the mutation to each surface hydrophobic residue changed the functional stability of the antibody; i.e. to test if the mutation changed the ability of the antibody to bind to MC-LR at different temperatures.

A 96-well Nunc Maxisorb™ plate was coated with 100 µL per well of 5 µg/mL MC-LR-BSA in PBS (150 mM, pH 7.2). The plate was incubated at 37 °C for 1 h. The liquid was then removed. Each well was blocked with 200 µL of 5% (w/v) MM and incubated at 37 °C for 1 h. The liquid was then removed. In order to reduce the chance of protease digestion of the scFv molecules, each antibody was diluted to a final concentration of 10 µg/mL in PBS (150 mM, pH 7.2) supplemented with cOmplete™ ULTRA protease inhibitor cocktail. Following this, each clone was treated at a range of temperatures, from 4 °C to 70 °C for 1 h. One hundred microlitres of each treated antibody was applied to the coated and blocked multiwell plate in triplicate. The plate was incubated

at 37 °C for 1 h. The wells were then rinsed three times with PBS-T (150 mM, pH 7.2, 0.05% (v/v) Tween-20) and PBS (150 mM, pH 7.2). HRP-labelled anti-HA secondary antibody was diluted at 1:2,000 in 5% (w/v) MM and 100 µL was placed into each well. The plate was incubated at 37 °C for 1 h. The wells were then rinsed three times with PBS-T (150 mM, pH 7.2, 0.05% (v/v) Tween-20) and PBS (150 mM, pH 7.2). TMB was added at 100 µL per well. The plate was incubated at 37 °C for 15 min. Ten percent (v/v) H₂SO₄ was added at 50 µL per well. The absorbance was measured at 450 nm using a Tecan Safire² plate-reader. Data was analysed by ANOVA using GraphPad Prism 5.0. If the ANOVA table was significant (P < 0.05), post-hoc analysis was performed using Dunnett's test.

2.2.5 Generation of an avian scFv library for *Bacillus cereus*

2.2.5.1 Immunisation of White Leghorn chicken with *B. cereus* vegetative cells

The purpose of this immunisation process was to raise an immune response in the host towards *B. cereus* antigens and to allow for subsequent development of polyclonal and recombinant anti-*B. cereus* antibodies. This work was carried out under license number B100/2705. For this work, the host was a female White Leghorn Chicken, designated 'ABG035'. A pre-bleed was taken 7 d before the initial immunisation. The host was immunised via subcutaneous injection with a total of 1 mL of immunogen over 5 locations on the chicken. The initial immunogen contained 1 x 10⁸ formaldehyde-inactivated *B. cereus* cells prepared in a 1:1 mixture with Freund's Complete Adjuvant. All subsequent booster immunogens contained 1 x 10⁸ formaldehyde-inactivated *B. cereus* cells prepared in a 1:1 mixture with Freund's Incomplete Adjuvant. In total, an initial immunisation and 3 booster immunisations were administered. Bleeds were taken 7 d after each immunisation/booster. To isolate serum from each bleed, the bleed sample was allowed to clot at 4 °C overnight. The sample was then centrifuged at 3,200 x g for 20 min in a benchtop centrifuge (Hermle Z233MK-2). The serum was removed and stored at -20 °C until required for use.

2.2.5.2 Determination of avian immune response to *B. cereus* by indirect ELISA

After the third booster immunisation, a serum titre ELISA was carried out to determine the response of the chicken using the sera obtained from the pre-bleed and bleed 3. The

response was measured against formaldehyde-inactivated *B. cereus* vegetative cells. A 96-well Nunc Maxisorb™ plate was coated with 100 µL per well of 8×10^7 cells/mL in PBS (150 mM, pH 7.4). The plate was incubated at room temperature for 2 h. The liquid was then removed. Each well was blocked with 200 µL of 3% (w/v) BSA in PBS (150 mM, pH 7.4) and incubated at 4 °C overnight. The liquid was then removed. Each serum sample was diluted to the following dilutions in 1% (w/v) BSA in PBS (150 mM, pH 7.4); 1:1,000, 1:5,000, 1:10,000, 1:50,000 and 1:100,000. A negative control was also included, which omitted the serum. One hundred µL of each serum dilution and negative control was added to the plate in duplicate. The plate was incubated at 37 °C for 1 h. The wells were then rinsed three times with PBS-T (150 mM, pH 7.4, 0.05% (v/v) Tween 20) and PBS (150 mM, pH 7.4). HRP-labelled anti-chicken secondary antibody was diluted at 1:2,000 in 1% (w/v) BSA in PBS (150 mM, pH 7.4) and 100 µL was placed into each well. The plate was incubated at 37 °C for 1 h. The wells were then rinsed three times with PBS-T (150 mM, pH 7.4, 0.05% (v/v) Tween 20) and PBS (150 mM, pH 7.4). TMB was added at 100 µL per well. The plate was incubated at 37 °C for 15 min. Ten percent (v/v) H₂SO₄ was added at 50 µL per well to stop the colourimetric reaction. The absorbance was measured at 450 nm using a Tecan Safire² plate-reader.

2.2.5.3 Purification of polyclonal IgY from an egg of the *B. cereus*-immunised chicken

An egg from chicken ABG035 was obtained 8 d after the third booster immunisation. In order to isolate pure IgY from this egg, an IgY EggPress Purification Kit was used, according to the manufacturer's instructions. Briefly, the egg yolk was separated from the white using the egg separator. The yolk was drained into a beaker. 5x volumes of cold Reagent A was slowly added to the yolk and this was incubated at 4 °C for 2 h. The solution was gently mixed before being centrifuged at 4,000 x g for 15 min in an Eppendorf 5810R centrifuge (rotor: A-4-62). The supernatant was removed and an equal volume of cold Reagent B was added with continuous stirring for 2 min. This solution was incubated at 4 °C for 2 h and centrifuged at 4,000 x g for 15 min in an Eppendorf 5810R centrifuge (rotor: A-4-62). The supernatant was discarded and the pellet was resuspended in PBS (150 mM, pH 7.4). This IgY solution was passed through a 0.2 µm filter and the concentration was measured by absorbance at 280 nm

using a Nanodrop™ ND-1000. The IgY solution was dispensed into 1 mL aliquots and stored at -80 °C until required for use.

2.2.5.4 Measurement of specificity of purified polyclonal IgY by ELISA

The purpose of this experiment was to determine the specificity of the purified IgY by indirect ELISA. This was done by measuring the response of multiple concentrations of the antibody to formaldehyde-inactivated *B. cereus* and *B. subtilis* vegetative cells and spores coated onto a multiwell plate. A 96-well Nunc Maxisorb™ plate was coated with 50 µL per well of 1×10^7 cells or spores per mL in PBS (150 mM, pH 7.4). The plate was incubated overnight at 4 °C. The liquid was then removed. Each well was blocked with 200 µL of 3% (w/v) BSA in PBS (150 mM, pH 7.4) and incubated at 37 °C for 1 h. The liquid was then removed. A series dilution of the IgY was prepared in 1% (w/v) BSA in PBS (150 mM, pH 7.4) from 500 µg/mL to 7.8 µg/mL. As a negative control, IgY from the egg of a non-immunised chicken was used. Limited stocks of this negative control IgY were available at the time of testing, therefore, it was diluted to 31.3, 15.6 and 7.8 µg/mL. A negative control was also included, which consisted of 1% (w/v) BSA in PBS (150 mM, pH 7.4) without IgY. Fifty microlitres of each IgY dilution was added to the plate. Due to the limited stocks of the *B. cereus* and *B. subtilis* cells and spores available, each test was measured singly. The plate was incubated at 37 °C for 1 h. The wells were then rinsed three times with PBS-T (150 mM, pH 7.4, 0.05% (v/v) Tween 20) and PBS (150 mM, pH 7.4). HRP-labelled donkey anti-chicken antibody (Abcam) was diluted to 1:2,000 in 1% (w/v) BSA in PBS (150 mM, pH 7.4) and 50 µL was placed into each well. The plate was incubated at 37 °C for 1 h. The wells were then rinsed three times with PBS-T (150 mM, pH 7.4, 0.05% (v/v) Tween 20) and PBS (150 mM, pH 7.4). TMB was added at 100 µL per well. The plate was incubated at 37 °C for 15 min. Ten percent (v/v) H₂SO₄ was added at 50 µL per well. The absorbance was measured at 450 nm using a Tecan Safire² plate-reader.

2.2.5.5 Affinity preparation of IgY polyclonal antibody

The aim of this experiment was to determine if it is feasible to optimise the affinity of the polyclonal IgY using a technique similar to phage display. Due to the high quantity of IgY obtained from the purification from egg yolk (60 mL of 5.97 mg/mL IgY = 358.2 mg of IgY), this could have been a time- and cost-saving exercise. The principle applied was that the stock IgY would be exposed to a negative selection step, consisting

of *B. subtilis* spores. Once *B. subtilis*-specific IgY bound, the spores would be centrifuged to remove these IgY (negative selection). The supernatant would then be exposed to *B. cereus* spores to allow *B. cereus*-specific IgY to bind. These IgY would then be isolated by centrifuging the *B. cereus* spores and discarding the supernatant. The *B. cereus* spores and any bound IgY would then be washed to remove non-specific IgY (positive selection). The remaining IgY would then be eluted (positive elution). After each step, (negative selection, positive selection, positive elution) a small sample was taken to analyse for protein concentration by BCA assay. The response of equal concentrations of each sample would then be determined by ELISA.

A 1.5 mL tube was blocked by the addition of 1 mL of 5% (w/v) MM. The tube was incubated at 4 °C overnight on a benchtop roller. The liquid was then discarded. Five hundred microlitres of the IgY stock was combined with 500 µL of 1×10^6 *B. subtilis* spores in the blocked tube. This was incubated at room temperature for 2 h on a benchtop roller. The tube was then centrifuged at 4,000 x g for 15 min in an Eppendorf 5810R centrifuge (rotor: A-4-62) to pellet the *B. subtilis* spores along with any IgY that bound to them. The supernatant was removed and the pellet was discarded. A sample of this supernatant was retained for BCA and ELISA (negative selection). The supernatant was mixed with 1×10^6 *B. cereus* spores in a 1.5 mL tube that was blocked with 5% (w/v) MM. This was incubated at room temperature for 2 h on a benchtop roller. The tube was then centrifuged at 4,000 x g for 15 min in an Eppendorf 5810R centrifuge (rotor: A-4-62) to pellet the *B. cereus* spores. The supernatant was removed, being careful not to disturb the pellet. A small sample of this supernatant was retained for BCA and ELISA (positive selection). The pellet was washed by resuspending in 1 mL PBS-T (150 mM, pH 7.4, 0.05% (v/v) Tween 20) and centrifuging at 4,000 x g in an Eppendorf 5810R centrifuge (rotor: A-4-62) for 15 min. The supernatant was discarded. The pellet was resuspended in 50 µL 0.1 M glycine, pH 2.5 and incubated at room temperature for 10 min to elute IgY from the *B. cereus* spores. The elution buffer was neutralised by the addition of 50 µL 1 M Tris, pH 8.0. The sample was centrifuged at 4,000 x g for 15 min Eppendorf 5810R centrifuge (rotor: A-4-62) to separate the *B. cereus* spores. The supernatant was retained for BCA and ELISA analysis (positive elution).

2.2.5.6 Measurement of affinity-matured polyclonal IgY by BCA assay

The protein concentrations of the stock IgY, the negative selection, positive selection and positive elution samples from the Section 2.2.5.5 were determined using a Pierce BCA Protein Assay kit as per Section 2.2.1.4. Single measurements of each protein sample were made.

2.2.5.7 Measurement of the specificity of the affinity-matured polyclonal IgY by ELISA

The purpose of this experiment was to determine the specificity of the affinity-matured IgY by indirect ELISA. This was carried out by measuring the response of equal concentrations of the stock IgY, negative selection, positive selection and positive elution samples obtained from Section 2.2.5.5 to formaldehyde-inactivated *B. cereus* and *B. subtilis* vegetative cells and spores coated onto a multiwell plate. A 96-well Nunc Maxisorb™ plate was coated with 50 µL per well of 1×10^7 cells or spores per mL in PBS (150 mM, pH 7.4). The plate was incubated at 37 °C for 1 h. The liquid was then removed. Each well was blocked with 200 µL of 3% (w/v) BSA in PBS (150 mM, pH 7.4) and incubated at 37 °C for 1 h. The liquid was then removed. Each sample from the affinity preparation process was diluted to give a working concentration of 16.7 µg/mL of IgY in 1% (w/v) BSA in PBS (150 mM, pH 7.4). Fifty microlitres of each sample was added to the plate in triplicate. The plate was incubated at 37 °C for 1 h. The wells were then rinsed three times with PBS-T (150 mM, pH 7.4, 0.05% (v/v) Tween-20) and PBS (150 mM, pH 7.4). HRP-labelled donkey anti-chicken antibody was diluted to 1:2,000 in 1% (w/v) BSA in PBS (150 mM, pH 7.4) and 50 µL was placed into each well. The plate was incubated at 37 °C for 1 h. The wells were then rinsed three times with PBS-T (150 mM, pH 7.4, 0.05% (v/v) Tween-20) and PBS (150 mM, pH 7.4). TMB was added at 100 µL per well. The plate was incubated at 37 °C for 15 min. Ten percent (v/v) H₂SO₄ was added at 50 µL per well to stop the reaction. The absorbance was measured at 450 nm using a Tecan Safire² plate-reader.

2.2.5.8 RNA extraction from White Leghorn Chicken spleen

The purpose of this experiment was to extract high quality RNA from the spleen of the *B. cereus*-immunised chicken, which will encode the genes required for the expression of the antibody variable fragments. Due to the susceptibility of RNA to degradation, prior to the extraction procedure, several preparatory steps were taken. Oakridge tubes

were cleaned with Virkon®, washed with ‘RNase-free’ water (Sigma), sprayed with RNase zap® (Sigma) and left overnight to ensure no contaminating RNases remained. The homogenizer used was incubated in Precept™, washed thoroughly with ‘RNase-free’ water, autoclaved and then baked in an oven at 60 °C overnight. Ethanol (75% (v/v) in ‘RNase-free’ water) was prepared in ‘RNase-free’ tubes and stored at -20°C. A laminar flow hood was de-contaminated by cleaning with 70% (v/v) Ethanol, 70% (v/v) IMS (both in ‘RNase-free’ water) and RNase Zap. Materials and reagents to be used during the extraction procedure were also decontaminated. Chicken ABG035 was sacrificed by cervical dislocation. The spleen was removed, placed in 15 mL RNAlater® in an ‘RNase-free’ tube and stored at -80 °C until use. On the day of the RNA extraction, the spleen was thawed and removed from RNAlater® and the excess RNAlater® was removed.

In a fresh ‘RNase-free’ tube, the spleen was homogenised in 30 mL of TriZol® reagent (Sigma) using a sterile homogenizer (Ultra-Turrax) at 50% output for 1 min. The sample was centrifuged in an Eppendorf 5810R centrifuge (rotor: A-4-62) at 1,575 x g for 20 min at 4 °C. The supernatant was transferred into 50 mL Oakridge tubes containing 6 mL of chloroform. This was mixed well by shaking and was incubated at room temperature for 15 min. The sample was then centrifuged at 17,500 x g in an Eppendorf 5810R centrifuge (rotor: F45-30-11) for 20 min at 4 °C. Following this centrifugation step, three visible layers were produced. The upper aqueous layer was carefully removed (ensuring that none of the organic layer containing protein was transferred from the interphase) and added to a 50 mL Oakridge tube with 15 mL of isopropanol to aid in RNA precipitation. This was mixed and left at room temperature for 10 min. It was then centrifuged at 17,500 x g for 40 min at 4 °C in an Eppendorf 5810R centrifuge (rotor: F45-30-11). The supernatant was carefully removed and discarded ensuring that the pellet was not disrupted. The RNA pellet was washed by adding 10 mL of 75% (v/v) ethanol. This was centrifuged once again at 17,500 x g for 10 min at 4 °C in an Eppendorf 5810R centrifuge (rotor: F45-30-11) and the supernatant was discarded. The pellet was air dried in the laminar flow cabinet and then gently resuspended in 500 µL of molecular grade water (Sigma). The RNA was subsequently quantified in triplicate at 260 nm using the Nanodrop™ ND-1000 and cDNA synthesis was performed.

2.2.5.9 Synthesis of cDNA from RNA by reverse transcriptase PCR (RT-PCR)

Total RNA was transcribed to cDNA by reverse transcriptase PCR, using the Superscript™ III First Strand Synthesis Supermix kit (Invitrogen) according to the manufacturer's instructions. Briefly, the reaction components of Mixture 1 was combined in a tube according to the Table 2.30. Mixture 1 was split into 21x 8µL aliquots and incubated at 65 °C for 5 min followed by incubation on ice for 1 min. Mixture 2 was prepared in a separate tube according to Table 2.30. Twelve µL of mixture 2 was added to each 8 µL aliquot of Mixture 1. This was incubated at 50 °C for 50 min followed by 85 °C for 5 min. The reaction was finally cooled on ice for 5 min. The 21 aliquots were combined. Total cDNA was quantified at 260 nm using a Nanodrop™ ND-1000. They were then distributed into 50 µL aliquots and stored at -80 °C.

Table 2.30: Composition of Superscript™ reaction Mixtures 1 and 2.

Mixture 1	Volume (µL)	Mixture 2	Volume (µL)
Total RNA (5 µg/reaction)	10.2	First Strand	220
Oligo dT	22	Reaction Mix	
10mM dNTP	22	Superscript III	44
Molecular grade water	121.8		

2.2.5.10 Amplification of antibody variable light and heavy genes

Following cDNA synthesis, the immunoglobulin variable regions were amplified by PCR. Due to the highly conserved framework regions of avian antibodies, a single pair of primers were required for the amplification of the V_L and V_H genes. In addition, for the formation of a scFv-encoding gene, the V_L and V_H amplicons can be joined and amplified by SOE PCR using a single pair of overlap extension primers. The primer sequences used for the amplification of the V_L and V_H genes are presented in Table 2.31.

Table 2.31: Avian scFv primer sequences.

<u>V_L Primers</u> CSCVK (sense) 5' GTG GCC CAG GCG GCC CTG ACT CAG CCG TCC TCG GTG TC 3' CKJo-B (reverse) 5' GGA AGA TCT AGA GGA CTG ACC TAG GAC GGT CAG G 3'
<u>V_H Primers</u> CSCVHo-FL (sense) 5' GGT CAG TCC TCT AGA TCT TCC GGC GGT GGT GGC AGC TCC GGT GGT GGC GGT TCC GCC GTG ACG TTG GAC GAG 3' CSCG-B (reverse) 5' CTG GCC GGC CTG GCC ACT AGT GGA GGA GAC GAT GAC TTC GGT CC 3'
<u>Overlap extension primers</u> CSC-F (sense) 5' GAG GAG GAG GAG GAG GAG GTG GCC CAG GCG GCC CTG ACT CAG 3' CSC-B (reverse) 5' GAG GAG GAG GAG GAG GAG CTG GCC GGC CTG GCC ACT AGT GGA GG 3'

2.2.5.10.1 Small scale V_L and V_H amplification

The V_L and V_H and control PCRs were prepared according to Table 2.32. For the V_L test and control PCRs, the forward and reverse primers were CSCVK and CKJo-B, respectively. For the V_H test and control PCRs, the forward and reverse primers were CSCVHo-FL and CSCG-B, respectively. To the control tubes, 0.5 µL of molecular grade H₂O was added. To V_L and V_H test reactions, 0.5 µL of cDNA was added. The PCR was run in a Rotor-Gene 6000 Thermal Cycler according to the conditions described in Table 2.33. The completed PCR products were separated on a 1% (w/v) agarose gel stained with SYBR® Safe at 100 V for 35 min. A Hyperladder™ 1 kb was used as molecular size markers.

Table 2.32: V_L and V_H PCR reaction composition.

Component	Volume (μL)	Working concentration
2x MyTaq Red Mix	75	1x
F Primer	0.5	1 μM
R Primer	0.5	1 μM
Molecular grade H ₂ O	23.5	-

Table 2.33: V_L and V_H PCR amplification conditions.

PCR stage	Temperature (°C)	Time
Initialisation	94	5 min
Denaturation	94	15 s
Annealing	56	15 s
Extension	72	90 s
Final Extension	72	10 min

} x 30 cycles

2.2.5.10.2 Large scale V_L amplification

For the amplification of the V_L gene, a 20x large scale PCR was carried out. The V_L gene was amplified as follows; a master mix was prepared according to Table 2.34. This was divided into 21x 49.5 μL aliquots. To the control tube, 0.5 μL of molecular grade H₂O was added. To test samples, 0.5 μL of cDNA was added. The PCR was run in a Rotor-Gene 6000 Thermal Cycler according to the conditions described in Table 2.33. The completed PCR was separated on a 1% (w/v) agarose gel stained with SYBR® Safe at 100 V for 35 min. A Hyperladder™ 1 kb was used as molecular size markers. The amplified V_L fragments were gel-purified according to Section 2.2.1.2. The DNA concentration was determined by spectrophotometric measurement at 260 nm using a Nanodrop™ ND-1000.

Table 2.34: Large scale V_L PCR master mix composition.

Component	Volume (μL)	Working concentration
2x MyTaq Red Mix	525	1x
CSCVK	10.5	1 μM
CKJo-B	10.5	1 μM
Molecular grade H ₂ O	493.5	-

2.2.5.10.3 V_H amplification optimisation

The V_H amplification was optimised to determine the optimal primer concentration. The forward and reverse primers were optimised by varying the working concentration to 0.5, 1 and 1.5 μM. For the control reaction, a primer concentration of 1 μM was used. The reactions were prepared according to Table 2.35. The PCR was run in a Rotor-Gene 6000 Thermal Cycler according to the conditions described in Table 2.33. The completed PCR was separated on a 1% (w/v) agarose gel stained with SYBR® Safe at 100 V for 35 min. A Hyperladder™ 1 kb was used as molecular size markers.

Table 2.35: V_H PCR optimisation reaction composition.

Component	Reaction 1	Reaction 2	Reaction 3	Control
	(0.5 μM Primer)	(1 μM Primer)	(1.5 μM Primer)	
	(μL)	(μL)	(μL)	(μL)
2x MyTaq Red				
Mix	25	25	25	25
CSCVHo-FL	0.25	0.5	0.75	0.5
CSCG-B	0.25	0.5	0.75	0.5
cDNA	0.5	0.5	0.5	0
H ₂ O	24	23.5	23	24

2.2.5.10.4 Large Scale V_H amplification

For the amplification of the V_H gene, a 10x large scale PCR was carried out. The V_H gene was amplified as follows; a master mix was prepared according to Table 2.36. This was divided into 11x 49.5 μL aliquots. To the control tube, 0.5 μL of molecular grade H₂O was added. To test samples, 0.5 μL of cDNA was added. The PCR was run in a Rotor-Gene 6000 Thermal Cycler according to the conditions described in Table 2.33.

The completed PCR was separated on a 1% (w/v) agarose gel stained with SYBR® Safe at 100 V for 35 min. A Hyperladder™ 1 kb was used as molecular size markers. The amplified V_L fragments were gel-purified according to Section 2.2.1.2. The DNA concentration was determined by spectrophotometric measurement at 260 nm using a Nanodrop™ ND-1000.

Table 2.36: Large Scale V_H PCR master mix composition.

Component	Volume (μL)	Working concentration
2x MyTaq Red Mix	275	1x
CSCVH ₀ -FL	2.75	0.5 μM
CSCG-B	2.75	0.5 μM
Molecular grade H ₂ O	264	-

2.2.5.11 scFv gene construction by SOE PCR

The full length scFv-encoding gene was constructed via SOE PCR as follows; a reaction mix was prepared according to Table 2.37. The control reaction was prepared, as described in Table 2.37, but omitted the V_H and V_L DNA and, instead, included 1 μL of molecular grade H₂O. The PCR was run in a Rotor-Gene 6000 Thermal Cycler according to the conditions described in Table 2.38. The completed PCR was separated on a 1% (w/v) agarose gel stained with SYBR® Safe at 100 V for 45 min. A Hyperladder™ 1 kb Plus was used as molecular size markers.

Table 2.37: SOE PCR composition.

Component	Volume (μL)	Working concentration
2x MyTaq Red Mix	25	1x
CSC-F	0.25	0.5 μM
CSC-B	0.25	0.5 μM
V _H DNA	0.5	-
V _L DNA	0.5	-
Molecular grade H ₂ O	23.5	-

Table 2.38: SOE PCR amplification conditions.

PCR stage	Temperature (°C)	Time
Initialisation	94	5 min
Denaturation	94	15 s
Annealing	56	15 s
Extension	72	120 s
Final Extension	72	10 min

} x 30 cycles

After successfully amplifying the scFv gene by SOE PCR, a large scale SOE PCR was prepared according to Table 2.39. This master mix was divided into 21x 49 μ L aliquots. To the test reactions, 0.5 μ L each of V_H and V_L DNA was added. To the control reaction, 1 μ L of molecular grade H_2O was added. The PCR was run in a Rotor-Gene 6000 Thermal Cycler according to the conditions described in Table 2.38. The completed PCR was separated on a 1% (w/v) agarose gel stained with SYBR® Safe at 100 V for 45 min. A Hyperladder™ 1 kb Plus was used as molecular size markers.

Table 2.39: Large-scale SOE PCR composition.

Component	Volume (μ L)	Working concentration
2x MyTaq Red Mix	525	1x
CSC-F	5.25	0.5 μ M
CSC-B	5.25	0.5 μ M
Molecular grade H_2O	493.5	-

2.2.5.12 pComb3XSS preparation

The pComb3XSS stock from the AZA library chapter was used.

2.2.5.13 Restriction enzyme digestion of SOE and pComb3XSS

It was suggested by Barbas *et al.* (2001) that 10 μ g and 20 μ g of SOE PCR product and pComb3XSS vector, respectively, would be sufficient to provide enough material to transform into *E. coli*.

The SOE digestion was performed in duplicate as follows; a reaction mixture was prepared according to Table 2.40. The reaction was incubated at 50 °C for 3 h in a Rotor-Gene 6000 Thermal Cycler. The digested SOE products were pooled and ethanol-

precipitated according to 2.2.1.1. They were centrifuged at 14,000 x g for 35 min in a benchtop centrifuge (Hermle Z233MK-2) and resuspended in 50 μ L of molecular grade water. They were stored overnight at -20 °C.

Table 2.40: SOE DNA digestion reaction mixture composition.

Component	Volume (μ L)	Working concentration
H ₂ O	18.9	-
SOE DNA (5 μ g)	24.1	100 ng/ μ L
10x NEB Buffer	5	1x
<i>Sfi</i> I	2	0.8 U/ μ L

The pComb3XSS digestion was performed in duplicate as follows; a reaction mixture was prepared according to Table 2.41. The reaction was incubated at 50 °C for 3 h in a Rotor-Gene 6000 Thermal Cycler. Four μ L each of *Xba*I and *Xho*I was added and the reaction was incubated at 37 °C for 1 h to facilitate digestion of the Stuffer fragment. Following this, 5.8 μ L of 10x AP buffer and 2 μ L AP enzyme was added and the reaction was incubated at 37 °C for 15 min followed by an inactivation step at 70 °C for 5 min. The digested pComb3XSS products were pooled and ethanol-precipitated according to Section 2.2.1.1. They were centrifuged at 14,000 x g for 35 min in a benchtop centrifuge (Hermle Z233MK-2) and resuspended in 50 μ L of molecular grade water. They were stored overnight at -20 °C.

Table 2.41: pComb3XSS digestion reaction mixture composition.

Component	Volume (μ L)	Working concentration
H ₂ O	38.85	-
Vector (10 μ g)	2.15	200 ng/ μ L
10x NEB Buffer	5	1x
<i>Sfi</i> I	4	1.6 U/ μ L

The digested pComb3XSS products were gel-purified according to 2.2.1.2 on a 0.7% (w/v) agarose gel. The 3,300 bp pComb3XSS product was isolated. The purified pComb3XSS DNA concentration was determined by spectrophotometric measurement at 260 nm using a NanodropTM ND-1000.

2.2.5.14 Ligation of SOE DNA insert into pComb3XSS vector

A 20x ligation reaction was set up according to Table 2.42. The reaction was incubated at room temperature for 20 min. The reaction was inactivated by incubating at 65 °C for 10 min in a Rotor-Gene 6000 Thermal Cycler. The reaction product was ethanol-precipitated according to Section 2.2.1.1. This constructed library was stored at -20 °C until required for use.

Table 2.42: Ligation reaction composition.

Component	Volume (µL)	Working concentration
H ₂ O	326.8	-
Vector (140 ng/reaction)	8.96	7 ng/µL
SOE DNA (70 ng/reaction)	4.2	3.5 ng/µL
10x Ligase buffer	40	1x
T4 ligase	20	20 U/µL

2.2.5.15 Electroporation of SOE-pComb3XSS into XL1 Blue *E. coli*

The precipitated library was resuspended in 30 µL of molecular grade water and was placed on ice along with electroporation cuvettes. Three 100 µL aliquots of XL1 Blue electrocompetent *E. coli* were thawed on ice. Ten µL of ligated library from Section 2.2.5.14 was added to 100 µL of *E. coli* in a cuvette. This was mixed and stored on ice for 1 min. Electroporation was carried out in a Bio-Rad GenePulser XCell™ using the following conditions; 2.5 kV, 25 µF, 200 Ω, τ ~ 4 ms. The cuvette was immediately flushed with a total of 3 mL pre-warmed SOC media and added to a 50 mL Falcon tube. This was repeated for a total of three electroporations. The Falcon tube was incubated at 37 °C at 250 rpm for 1 h in an Excella® E25 shaking incubator.

A titre of the transformed bacteria was performed by taking 2 µL of the culture and adding to 200 µL of SB. The titre plates were prepared by plating 100 µL and 10 µL of the diluted culture onto LB agar plates containing 100 µg/mL carbenicillin and these were incubated overnight at 37 °C. The following day the colonies were counted. The plates were also kept for colony pick PCR analysis (see Section 2.2.5.16).

To the remaining culture, 10 mL of pre-warmed SB was added. Carbenicillin was added to a final concentration of 100 µg/mL. The culture was incubated at 37 °C, 250 rpm for 2 h in an Excella® E25 shaking incubator. The culture was centrifuged at 3,200 x g for

20 min in an Eppendorf 5810R centrifuge (rotor: A-4-62). The supernatant was removed and the pellet was resuspended in 50 μ L SB containing 100 μ g/mL carbenicillin. This was spread on LB agar plates containing 100 μ g/mL carbenicillin and incubated overnight at 37 °C. Five mL of SB containing 100 μ g/mL carbenicillin was placed onto each plate and the colonies were collected using a cell scraper. Glycerol was added to a final concentration of 15% (v/v) and the culture was mixed and divided into aliquots and stored at -80 °C.

2.2.5.16 Colony pick PCR of transformed XL1 Blue *E. coli*

To determine the efficiency of the ligation and transformation experiments, a colony pick PCR was carried out as follows. A master mix was prepared according to Table 2.42 and divided into 13x 25 μ L aliquots. A single colony from the transformation titre plates was added to each of the 12 reaction tubes. No colony was added to the control tube. The PCR was carried out using the conditions described in Table 2.39 in a Rotor-Gene 6000 Thermal Cycler. The PCR products were separated on a 1% (w/v) agarose gel stained with SYBR® Safe at 100 V for 35 min. A Hyperladder™ 1kb was used as molecular size markers.

Table 2.43: Colony pick PCR master mix composition.

Component	Volume (μ L)	Working concentration
2x MyTaq Red Mix	162.5	1x
CSC-F	3.25	1 μ M
CSC-B	3.25	1 μ M
Molecular grade H ₂ O	156	-

2.2.5.17 Screening of the anti-*B. cereus* recombinant scFv library by whole-cell panning

The aim of this screening approach was to enrich for *B. cereus*-specific antibodies through a series of negative depletion and positive selection steps. The library was negatively depleted by exposure to *B. subtilis* cells, which should remove any antibodies that cross-react to both *B. cereus* and *B. subtilis*. The remaining depleted library was then exposed to *B. cereus* cells to allow any specific clones to bind.

Two hundred μL of *E. coli* library was added to 200 mL SB containing 100 $\mu\text{g}/\text{mL}$ carbenicillin. This culture was grown at 37 °C and 200 rpm for ~6 h in an Excella® E25 shaking incubator until OD_{600} reached approximately 0.5, at which point 1×10^{11} M13KO7 helper phage were added. The culture was incubated, while static, at 37 °C for 0.5 h, followed by incubation at 37 °C and 200 rpm for 1 h. Kanamycin was then added to a final concentration of 50 $\mu\text{g}/\text{mL}$ and the culture was incubated overnight at 30 °C and 200 rpm. Two mL tubes were blocked overnight with 5% (w/v) MM.

The following day, an overnight XL1 Blue *E. coli* culture was sub-cultured at the following dilutions: 1:50, 1:100, 1:500, 1:1,000, and 1:2,000. The overnight library culture was centrifuged at 3,200 x g for 30 min in an Eppendorf 5810R centrifuge (rotor: A-4-62). The supernatant was returned to the culture flask and PEG and NaCl were added to a final concentration of 4% (w/v) and 3% (w/v), respectively. This was incubated on ice for 1 h and centrifuged at 15,000 x g for 20 min, with the brake off, in an Eppendorf 5810R centrifuge (rotor: F45-30-11). The supernatant was discarded and the pellet was resuspended in 1 mL of sterile PBS (150 mM, pH 7.4). This was then centrifuged at 11,600 x g for 10 min in a benchtop centrifuge (Hermle Z233MK-2). The phage-rich supernatant was kept and 3% (w/v) OVA solution was added to a final concentration of 1% (w/v).

The blocked 2 mL tube was washed once by filling with PBS (150 mM, pH 7.4). Twenty million *B. subtilis* cells were resuspended in 500 μL 5% (w/v) MM and were added to the tube followed by 1 mL of the phage-OVA. The tube was incubated at room temperature on a benchtop roller for 1 h. The tube was centrifuged at 11,000 x g for 10 min in an Eppendorf 5810R centrifuge (rotor: F45-30-11) to pellet the *B. subtilis* cells. The supernatant was removed and was added to a second blocked tube. *B. cereus* cells at the cell concentration described in Table 2.44 was prepared in 500 μL 5% (w/v) MM) and was added to the tube. The tube was incubated at room temperature on a benchtop roller for 1 h. The tube was centrifuged at 11,000 x g for 10 min in an Eppendorf 5810R centrifuge (rotor: F45-30-11) to pellet the *B. cereus* cells and the supernatant was discarded. A series of wash steps was performed as follows; after centrifugation, the cell pellet was resuspended in 1 mL of wash solution. This was mixed at room temperature for 5 min followed by centrifugation at 11,000 x g for 10 min in an Eppendorf 5810R centrifuge (rotor: F45-30-11). This was repeated for the number of washes described in

Table 2.44. After the final wash, the cell pellet was resuspended in 1 mL PBS (150 mM, pH 7.4).

Table 2.44: Conditions used for the screening of the anti-*B. cereus* scFv library

Round	<i>B. cereus</i> cell concentration (cells/mL)	Number of washes (PBS-T:PBS)
1	2×10^7	3:3
2	1×10^7	4:4
3	5×10^6	5:5

The growing XL1 Blue *E. coli* cultures prepared earlier were used for reinfection of the eluted phage and for phage input and output titres. The 1 mL of washed cell pellet was added to 5 mL XL1 Blue *E. coli* at $OD_{600} = 0.5$. This method of competitive elution is based on the theory that the phage will be competitively eluted off *B. cereus* by the disproportionate number of infection sites on *E. coli* (Stephenson *et al.*, 1998). Serial dilutions of the input and output phage were also prepared from 10^{-1} to 10^{-12} and from 10^{-1} to 10^{-6} , respectively, using the XL1 Blue *E. coli* as the diluent. All cultures were infected at 37 °C for 0.5 – 1 h. The input and output cultures were plated onto separate LB agar plates containing 50 µg/mL carbenicillin at 100 µL per plate and incubated overnight at 37 °C. The 5 mL culture was centrifuged at 3,200 x g for 20 min in an Eppendorf 5810R centrifuge (rotor: A-4-62) and resuspended in 500 µL SB containing 100 µg/mL carbenicillin. This was plated onto 6 LB agar plates containing 50 µg/mL carbenicillin at 100 µL per plate and incubated overnight at 37 °C.

The following day, the input and output titre plate colonies were counted. These counting plates were also retained in order to carry out colony pick PCR analysis, as per Section 2.2.5.17. The six LB agar plates were scraped into SB containing 100 µg/mL carbenicillin. 75% of this SB culture was used for further rounds of panning. Glycerol was added to the remaining culture to a final concentration of 15% (v/v) and this was stored at -80 °C. After 2 rounds of panning, the output phage from round 2 were infected into Top10F' *E. coli* to allow for soluble expression of the scFv molecules.

2.2.5.18 Monoclonal ELISA of solubly expressed clones

The purpose of this experiment was to determine the response of individual scFv-phage clones for *B. cereus* and *B. subtilis* vegetative cells. Top10F' *E. coli* were grown in SB containing 10 µg/mL tetracycline at 37 °C until the OD₆₀₀ reached a value of 0.5. Twenty microlitres of output phage from round 2 of panning was added to 2 mL of Top10F' *E. coli* and incubated, while static, at 37 °C for 1 h. The *E. coli* were diluted over a serial dilution range from 10⁻¹ to 10⁻⁸ in SB containing 100 µg/mL carbenicillin. They were then plated onto LB agar plates containing 100 µg/mL carbenicillin at 100 µL per plate. The plates were incubated at 37 °C overnight to allow for the growth of visible colonies.

The following day, 192 colonies were picked each from the agar plates into 2x 96 well sterile culture plates (hereafter referred to as the master plates), each well containing 100 µL SB supplemented with 100 µg/mL carbenicillin. The plates with visible colonies were kept for colony pick PCR analysis (see Section 2.2.1.19). The plates were incubated overnight at 37 °C and 220 rpm in an Excella® E25 shaking incubator. To allow for antibody-expression, 20 µL was taken from each well of the master plates and added to its corresponding well in a deep-well plate, each well containing 1 mL auto-induction media with 100 µg/mL carbenicillin. These deep-well plates were incubated overnight at 37 °C, 220 rpm. To the master plates, glycerol was added to each well to a final glycerol concentration of 15% (v/v). The plates were mixed on a benchtop mixer to ensure even distribution of glycerol. These master plates were stored at -80 °C for long-term storage.

Ninety six-well Nunc Maxisorb™ plates were coated with whole *B. cereus* and *B. subtilis* vegetative cells. Fifty microlitres of 9.5 x 10⁵ cells/mL in PBS (150 mM, pH 7.4) was added to each well and the plates were incubated for 1.5 h, while shaking, at room temperature. The liquid was then removed. The wells were blocked with 200 µL 5% (w/v) MM for 1.5 h, while shaking, at room temperature. The liquid was then removed. The overnight-incubated deep-well plates were freeze-thawed three times (each freeze-thaw cycle consisted of 30 min at -80 °C followed by 30 min in a waterbath at 37 °C) to lyse the bacterial cells and centrifuged at 3,200 x g for 20 min in an Eppendorf 5810R centrifuge (rotor: A-4-62) to pellet the cell debris. One hundred microlitres of deep-well plate supernatants were added to its designated well on the

ELISA plate. To reduce non-specific binding, 50 μL of 5% (w/v) MM was added to each well. The plates were incubated for 1.5 h, while shaking, at room temperature. The wells were washed three times with PBS-T (150 mM, pH 7.4, 0.05% (v/v) Tween-20) and PBS (150 mM, pH 7.4). HRP-labelled anti-HA secondary antibody was diluted at 1:2,000 dilution in 5% (w/v) MM and 50 μL was added to each well and incubated for 1.5 h, while shaking, at room temperature. The wells were washed three times with PBS-T (150 mM, pH 7.4, 0.05% (v/v) Tween-20) and PBS (150 mM, pH 7.4). One hundred μL TMB was added to each well for 30 min, while shaking, at room temperature. Fifty μL of 10% (v/v) H_2SO_4 was added to each well. The absorbance was measured at 450 nm using a Tecan Safire² plate-reader.

2.2.5.19 Colony pick PCR of the chosen scFv clones

The purpose of this experiment was to determine the presence of the scFv-encoding gene in the nine *E. coli* clones chosen after the monoclonal ELISA analysis. A master mix was prepared according to Table 2.45 and divided into 11x 25 μL aliquots. Two microlitres of the culture media containing each chosen clone was added to each of the 9 reaction tubes. Two microlitres of sterile SB media was added to the control tube. The PCR was carried out using the conditions described in Table 2.39 in a Rotor-Gene 6000 Thermal Cycler. The PCR products were separated on a 1% (w/v) agarose gel stained with SYBR® Safe at 100 V for 35 min. A Hyperladder™ 1kb was used as molecular size markers.

Table 2.45: Colony pick PCR master mix composition.

Component	Volume (μL)	Working concentration
2x MyTaq Red Mix	137.5	1x
CSC-F	2.75	1 μM
CSC-B	2.75	1 μM
Molecular grade H_2O	110	-

2.2.6 Investigation into the toxic effects of MC-LR, *M. aeruginosa* and AZA1 on the Hepatocellular Carcinoma cell line, HepG2

2.2.6.1 Determination of the effects of MC-LR, *M. aeruginosa* cells and AZA1 on HepG2 cell proliferation

The aim of this experiment was to determine:

1. The effect of MC-LR alone and in tandem with 100 ng/mL lipopolysaccharide (LPS) on HepG2 cell proliferation.
2. The effect of whole and lysed *M. aeruginosa* cells on HepG2 cell proliferation.
3. The effect of AZA1 on HepG2 cell proliferation

For all assays, a 96 well culture plate was coated with 100 μL of 1×10^6 HepG2 cells/mL in Dulbecco's Modified Eagle Medium (DMEM) (supplemented with 10% (v/v) foetal bovine serum (FBS) and 100 U/mL penicillin-streptomycin) (hereafter referred to as DMEM, unless specified otherwise) overnight. The media was removed and replaced with fresh DMEM. For the 'cells alone' control, 100 μL DMEM was added ($n = 12$). The vehicle control consisted of 100 μL DMEM + 0.5% (v/v) EtOH (corresponding to the EtOH concentration of the highest MC-LR test concentration) ($n = 6$). The positive control consisted of 100 μL DMEM + 10% (v/v) DMSO ($n = 9$). For the MC-LR alone and MC-LR + LPS assays, MC-LR dilutions were prepared in DMEM and DMEM supplemented with 100 ng/mL LPS, respectively. The MC-LR working concentrations ranged from 5 – 0.008 μM , with 1:5 dilutions. One hundred microlitres of each dilution was added to the plate ($n = 3$). The HepG2 cells were exposed for 24 h at 37 °C with 5% CO_2 .

To facilitate the investigation into the effects of *M. aeruginosa* on HepG2 cells, *M. aeruginosa* was grown in BG-11 media at 25 °C, with 16 h/8 h light/dark cycles. The cyanobacterial cells were counted and prepared at a cell count of 1×10^7 *M. aeruginosa* cells/mL in DMEM. This stock solution was split in half, with one half of this volume remaining untreated and the other half was lysed. The lysis method involved sonication using a Branson Digital Sonifier (Emerson Electric, St. Louis, MO, USA) at 40% output for 2 min, with a pulse duration of 6 s on and 6 s off. Both the untreated and lysed *M. aeruginosa* cells were diluted to concentrations ranging from 1×10^7 – 1.6×10^4

cells/mL in DMEM. One hundred microlitres of each dilution was applied to each well (n = 3). The vehicle control consisted of 100 μ L DMEM + 1.1% (v/v) BG-11 media (corresponding to the BG-11 concentration of the highest *M. aeruginosa* test) (n = 3). The positive control consisted of 100 μ L DMEM + 10% (v/v) DMSO (n = 9). The HepG2 cells were exposed for 24 h at 37 °C with 5% CO₂.

For the AZA1 assay, AZA1 was diluted in DMEM to a working concentration range of 10 – 0.0001 μ M. The vehicle control consisted of 100 μ L DMEM + 0.76% (v/v) MeOH per well (corresponding to the MeOH concentration in the highest AZA1 test). The positive control consisted of 100 μ L DMEM + 10% (v/v) DMSO per well. The HepG2 cells were exposed for 24 and 48 h at 37 °C with 5% CO₂.

After the exposure, the media was removed. For plates with *M. aeruginosa*, in order to reduce interference from live *M. aeruginosa* in the MTT assay, all wells were gently rinsed twice with Dulbecco's phosphate buffered saline (DPBS). To determine cell proliferation, a 3-[4,5-dimethylthiazol-2-yl]-2,5 diphenyl tetrazolium bromide (MTT) assay was carried out using a Trevigen TACS® MTT Cell Proliferation Assay (Bio-Techne, Minneapolis, MN, USA). One hundred microlitres of fresh DMEM supplemented with 10% (v/v) MTT reagent was added to each well. The plate was incubated at 37 °C with 5% CO₂ for 2 h. One hundred microliters of detergent reagent was then added and the plate was incubated at 37 °C with 5% CO₂ for 2 h. The absorbance was measured at 570 nm with a reference subtraction at 650 nm using a Tecan Safire². Data was analysed by ANOVA using GraphPad Prism. If the ANOVA table was significant (P < 0.05), post-hoc analysis was performed using Newman-Keuls' test.

2.2.6.2 High Content Analysis (HCA) of the effects of AZA1 on HepG2

This work was carried out in collaboration with researchers in Queen's University Belfast. HCA was performed as per Meneely *et al.* (2018). Briefly, HepG2 cells were cultured in Modified Eagle's Media (MEM) supplemented with 10% (v/v) FBS, 1% (w/v) penicillin-streptomycin, 1 mM sodium pyruvate and 2 mM L-glutamine at 37 °C with 5% CO₂. The cells were seeded into Corning® BioCoat™ Collagen I, 96 well microwell plates in 100 μ L per well at a concentration of 1 x 10⁵ cells/mL. The cells adhered to the surface of the well for 24 h at 37 °C with 5% CO₂. AZA1 solutions and the controls were prepared in MEM supplemented with 10% (v/v) FBS, 1% (w/v)

penicillin-streptomycin, 1 mM sodium pyruvate and 2 mM L-glutamine. AZA1 was prepared with a working concentration ranging from 5 μM to 0.0005 μM . The vehicle control consisted of 0.38% (v/v) MeOH. The positive control consisted of 60 μM valinomycin. The adhered HepG2 cells were exposed to all test conditions for 18 h at 37 °C with 5% CO_2 .

Two fluorescent probes were used to assess cell health. A working concentration of 100 nM MitoTracker® Orange CMTMRos was prepared in DMEM without FBS, as the dye is susceptible to degradation by oxidases in serum. This stain was used to label the mitochondria. A working concentration of 2 μM Hoechst nuclear stain in PBS (150 mM, pH 7.4) was used to label cellular DNA. Following 18 h of exposure, the media was carefully removed from all wells. Fifty microlitres of MitoTracker® Orange CMTMRos was added to each well and incubated (protected from light) at 37 °C for 30 min. The mitochondrial dye was removed and the cells were fixed to the multiwell plate with 150 μL per well of 10% (v/v) formalin solution, while protected from light, at room temperature for 15 min. The formalin solution was removed and each well was gently washed with 200 μL PBS (150 mM, pH 7.4). Following the wash step, 100 μL of Hoechst DNA stain was added to each well and incubated at room temperature for 20 min and protected from light. The nuclear stain solution was removed and each well was gently washed with 200 μL PBS (150 mM, pH 7.4). Two hundred microlitres of fresh PBS (150 mM, pH 7.4) was added to each well before sealing the plate with black vinyl film to protect the samples from light.

The samples were analysed using a CellInsight™ NXT High Content Screening (HCS) platform (Thermo Fisher Scientific, UK). This instrument uses automated fluorescence microscopy and advanced imaging software to carry out quantitative analysis of five parameters i.e. cell number (CN), nuclear area (NA), nuclear intensity (NI), mitochondrial mass (MM) and mitochondrial membrane potential (MMP). In each well, data was captured at 10x objective magnification and five field of view images were captured. The excitation and emission wavelengths for the Hoechst nuclear stain and MitoTracker® Orange CMTMRos were 361/497 nm and 554/576 nm, respectively.

Exposures were performed in triplicate. Data was analysed by ANOVA using GraphPad Prism. If the ANOVA table was significant ($P < 0.05$), post-hoc analysis was performed using Dunnett's test.

2.2.6.3 Investigation of the combined effects of MC-LR with AZA1 and MC-LR with *M. aeruginosa* on HepG2 proliferation

It was shown in Section 2.2.6.1 that a wide range of effects were observed after exposure of HepG2 cells to MC-LR, *M. aeruginosa* and AZA1 individually, with differing degrees of significance. However, very little is known about the potential effects on HepG2 cells when binary combinations of these toxins/cyanobacteria are present. Therefore, the aim of this section was to expose HepG2 cells to levels of the toxins/cyanobacteria that, when present alone, do not have a highly significant effect on HepG2 proliferation. The following concentrations of MC-LR, lysed *M. aeruginosa* and AZA1 were chosen; 0, 0.2 and 1 μM MC-LR; 0, 1.6×10^4 and 8×10^4 *M. aeruginosa* cells/mL; and 0, 0.1 and 1 μM AZA1. These experiments were carried out in duplicate and within each experiment at least three biological replicates for each test were carried out.

For all assays, a 96 well culture plate was coated with 100 μL of 1×10^6 HepG2 cells/mL in DMEM overnight. The media was removed and replaced with fresh media containing the various test components. For the cells alone control, 100 μL DMEM was added ($n = 24$). In the MC-LR + *M. aeruginosa* exposure, the vehicle control consisted of 100 μL DMEM + 0.2% (v/v) EtOH + 1% (v/v) BG-11 (corresponding to the EtOH and BG-11 concentration of the highest MC-LR + *M. aeruginosa* test) ($n = 6$). In the MC-LR + AZA1 exposure, the vehicle control consisted of 100 μL DMEM + 0.2% (v/v) EtOH + 0.15% (v/v) MeOH (corresponding to the EtOH and MeOH concentrations of the highest MC-LR + AZA1 test) ($n = 6$). For both assays, the positive control consisted of 100 μL DMEM + 10% (v/v) DMSO ($n = 12$). For *M. aeruginosa* assays, lysed *M. aeruginosa* was prepared as per Section 2.2.6.1. For all test assays, MC-LR, *M. aeruginosa* and AZA1 were diluted to the required concentrations and combinations in DMEM and 100 μL was added to each designated well ($n = 6$). The HepG2 cells were exposed for 24 h at 37 °C with 5% CO₂.

After this exposure, the media was removed. To measure cell proliferation, an MTT assay was carried out using a Trevigen TACS® MTT Cell Proliferation Assay. One hundred microlitres of fresh DMEM supplemented with 10% (v/v) MTT reagent was added to each well. The plate was incubated at 37 °C with 5% CO₂ for 2 h. One hundred microliters of detergent reagent was then added and the plate was incubated at 37 °C

with 5% CO₂ for 2 h. The absorbance was measured at 570 nm with a reference subtraction at 650 nm using a Tecan Safire². Data was analysed by ANOVA using GraphPad Prism. If the ANOVA table was significant (P < 0.05), post-hoc analysis was performed using Dunnett's test.

In addition to carrying out MTT assays on these samples, the supernatants were also kept for testing for the levels of IL-1 β and TNF- α (see Section 2.2.6.6).

2.2.6.4 Investigation of the combined effects of MC-LR with AZA1 and MC-LR with *M. aeruginosa* on HepG2 cell health using HCA

HCA was performed as described in Section 2.2.6.2 but included the following amendments:

For exposures to combinations of AZA1 and MC-LR, the working concentrations of AZA1 were 0.5, 0.05 and 0 μ M, while the working concentrations of MC-LR were 2.5, 0.5 and 0 μ M. The vehicle control consisted of 0.29% (v/v) MeOH. For exposures to combinations of lysed *M. aeruginosa* and MC-LR, the working concentrations of *M. aeruginosa* were 2 x 10⁵, 4 x 10⁴ and 0 cells/mL, while the working concentrations of MC-LR were 2.5, 0.5 and 0 μ M. The vehicle control consisted of 0.038% (v/v) MeOH. The positive control for all assays consisted of 60 μ M valinomycin. The adhered HepG2 cells were exposed to all test conditions for 18 h at 37 °C with 5% CO₂. The post-exposure procedure was carried out as described in Section 2.2.6.2.

Exposures were performed in experimental triplicates. Data was analysed by ANOVA using GraphPad Prism. If the ANOVA table was significant (P < 0.05), post-hoc analysis was performed using Dunnett's test.

2.2.6.5 Determination of the effect of MC-LR-, AZA1- and *M. aeruginosa*-exposure on caspase-dependent apoptosis in HepG2 cells

The aim of this experiment was to determine if MC-LR and AZA1 activate caspases 3 and 7, which are effector enzymes in the apoptosis cell death pathway.

HepG2 cells were diluted to a concentration of 10⁶ cells/mL in DMEM. The cells were seeded into 6 well plates in a volume of 1 mL per well and allowed to adhere to the plate for 24 h at 37 °C with 5% CO₂. The media was removed and replaced with fresh media containing the various test components. For MC-LR and AZA1 assays, the

vehicle controls consisted of 1 mL DMEM + 0.5% (v/v) EtOH and 0.38% (v/v) MeOH, respectively. For both assays, the positive control consisted of 1 mL DMEM + 4 µg/mL camptothecin (CAM). For MC-LR and AZA1 assays, the toxins were tested at 5 µM and 1 µM with and without 100 ng/mL LPS. For each test, the required volumes of MC-LR, AZA1 and LPS stocks were added directly to 1 mL DMEM on the plate and mixed. The HepG2 cells were exposed for 24 h at 37 °C with 5% CO₂.

Caspase 3/7 assays were carried out using a Bio-Rad FAM-FLICA® Caspase-3/7 assay kit according to the manufacturer's instructions, with minor adjustments. Briefly, a vial of FLICA was reconstituted in 50 µL of DMSO. Before use, this stock was diluted 1:5 by the addition of 200 µL of DPBS (30x FAM-FLICA stock). The apoptosis wash buffer 10x stock solution was diluted 1:10 in sterile diH₂O. After the exposure, the media was carefully removed from each well (this media was also retained for testing for levels of IL-1β and TNF-α cytokines by ELISA; see Section 2.2.6.6). Any cells in this media were retained by centrifugation at 200 x g for 10 min at 25 °C in an Eppendorf 5810R centrifuge (rotor: A-4-62). Cells that remained adhered to the 6 well culture plate were scraped into 1 mL fresh DMEM. These cells were retained by centrifugation at 200 x g for 10 min at 25 °C in an Eppendorf 5810R centrifuge (rotor: A-4-62) and combined with the non-adherent cells from the previous centrifugation step in a total volume of 290 µL of fresh DMEM. To stain each cell sample, 10 µL of 30x FAM-FLICA stock was added to each sample and incubated, while protected from light, at 37 °C, 5% CO₂ for 1 h, with gentle mixing every 15 min. Following this staining step, three wash steps were performed to remove any residual FAM-FLICA dye. Each wash step consisted of the resuspension of the cell pellet in 2 mL of 'apoptosis wash buffer' provided with the kit, gentle mixing and centrifugation at 200 x g for 10 min at 25 °C in an Eppendorf 5810R centrifuge (rotor: A-4-62). Following the third wash, each sample was resuspended in 300 µL of apoptosis wash buffer. One hundred microlitres of each sample was added to a black, flat-bottom Nunc™ 96 well plate in triplicate. The fluorescence output was measured with excitation and emission wavelengths of 488 and 530 nm, respectively, using a Tecan Safire².

In order to account for differing cell numbers per well, cell counts were performed on each sample prior to fluorescence measurement; the fluorescent output was then divided by the corresponding cell number. These values were normalised against the vehicle

control in order to represent the data as a fold-change relative to the vehicle. Data was analysed by ANOVA using GraphPad Prism. If the ANOVA table was significant ($P < 0.05$), post-hoc analysis was performed using Dunnett's test.

2.2.6.6 IL-1 β and TNF- α ELISAs

The supernatants from the experiments in Sections 2.2.6.3 and 2.2.6.5 were kept and were analysed for concentrations of IL-1 β and TNF- α , which are indicators of cell stress. For the measurement of IL-1 β and TNF- α , R&D Systems® Human IL-1 beta/IL-1F2 DuoSet™ ELISA and Human TNF-alpha DuoSet™ ELISA kits were used according to the manufacturer's instructions.

For the TNF- α ELISA, a 96-well Nunc Maxisorb™ plate was coated with 100 μ L per well of 4 μ g/mL capture antibody. The plate was incubated at room temperature for 2 h. The liquid was then removed. Each well was blocked with 200 μ L of 1% (w/v) BSA in PBS and incubated at room temperature for 2 h. The liquid was then removed. TNF- α standards were prepared in 1% (w/v) BSA in PBS from 1000 – 15.6 pg/mL and a negative control was included which consisted of 1% (w/v) BSA in PBS. For the samples obtained from Section 2.2.6.3, the following replicates were tested; cells alone (n = 12); vehicles (n = 3); positive control (n = 6); test exposures with different toxin/cyanobacteria combinations (n = 3). The supernatants from Section 2.2.6.5 were added to the plate in triplicate. One hundred microlitres of each sample was added to the plate neat. One hundred microlitres of each standard was added to the plate in triplicate and the plate was incubated at 4 °C overnight. The wells were then rinsed three times with PBS-T and thoroughly dried. The detection antibody was diluted to 50 pg/mL in 1% (w/v) BSA in PBS and 100 μ L was placed into each well. The plate was incubated at room temperature for 2 h. The wells were then rinsed three times with PBS-T and thoroughly dried. HRP-labelled streptavidin was diluted 1:40 in 1% (w/v) BSA in PBS and 100 μ L was placed into each well. The plate was incubated at room temperature for 20 min. The wells were then rinsed three times with PBS-T and thoroughly dried. One hundred microlitres of TMB was added to each well. The plate was incubated at room temperature for 30 min. Ten percent (v/v) H₂SO₄ was added at 50 μ L per well. The absorbance was measured at 450 nm using a Tecan Safire² plate-reader.

A similar method was used for the IL-1 β ELISA but included the following amendments; the capture antibody was diluted to 4 $\mu\text{g}/\text{mL}$; the IL-1 β standards were prepared in 1% (w/v) BSA in PBS from 1000 – 15.6 pg/mL ; and the detection antibody was diluted to 500 ng/mL .

3 Generation of a murine anti-AZA1 scFv antibody fragment

3.1 Introduction

This chapter describes the development of recombinant antibody fragments targeting azaspiracid-1 (AZA1). The algal toxin group AZAs are emerging food-borne contaminants that can cause severe gastrointestinal disorders such as vomiting, nausea and diarrhoea. ‘Knock-on’ effects of AZA shellfish contamination include economic losses due to massive shellfish recalls, fishery closures and job losses (GESAMP, 2001). Also, due to factors such as increasing ocean temperatures from global warming, and eutrophication, HABs are expected to increase in intensity and AZA toxin levels are expected to rise (Paerl and Huisman, 2008; Michalak *et al.*, 2013; Paerl and Otten, 2013). Current regulations for AZA toxins legislate only for AZAs in food, and do not cover toxin and algal levels in the sea. Monitoring toxin levels in the sea may allow for mitigation of the effects of these toxins, by alerting coastal authorities of areas containing high levels and this may help in avoiding harvesting of contaminated shellfish. The current regulated detection method for AZA1 is reliant on LC-MS/MS which is a labour-intensive, laboratory-based analytical method with high costs associated (European Commission, 2011). Therefore, there is a pressing need for a ‘real-time’, ‘on-site’, inexpensive monitoring device that can be deployed in the sea and monitor toxin levels and relay the data ashore to coastal authorities. Biosensors are a potential means to sensitively and specifically detect toxins at low levels at the point-of-need (PON), with a low cost and a rapid turnaround time (TAT) (Murphy *et al.*, 2015) and may present a promising solution to this issue.

The aim of this research was to develop recombinant antibodies (rAbs) specific to AZA1 through the process of host-immunisation, library building, and screening via phage display and panning. The intended use of any identified rAbs was to incorporate them onto a microfluidic lab-on-a-disk (LOAD) platform that would be deployed on a marine-monitoring buoy in the sea. There, this biosensor platform would autonomously measure AZA1 concentration levels *in situ* and in ‘real-time’.

In this chapter, an immune response was generated in mice towards AZA1. The highest serum titre was observed for Mouse A and was determined to be 1:20,000 by serum titre ELISA. Following this, the host spleen RNA was converted to cDNA and the antibody variable regions were amplified by PCR. These V regions were then fused by SOE PCR to form a scFv-encoding gene that was subsequently restriction-digested and ligated into

a phagemid vector. This vector was transformed into *E. coli* to form an antibody library, with a size in the order of 10^5 clones. This library was then screened by phage display and panning. Unfortunately, AZA1-specific antibodies were not identified, and anomalous polyclonal phage ELISA results were also observed. It was later determined that the M13 phage used in the phage-display system bound to the AZA1-Bovine Serum Albumin (BSA) conjugate used for screening, which obstructed the identification of AZA1-specific antibodies. Subsequently, a new AZA1-Ovalbumin (OVA) conjugate was developed that eliminated the non-specific phage binding. The scFv library was reconstructed. This newly constructed library was screened using the new AZA1-OVA conjugate. However, this screening process using the new AZA1-OVA conjugate was not successful in isolating AZA1-specific scFv from the library. Therefore, a competitive assay was subsequently developed and optimised to detect AZA1 using polyclonal antiserum obtained from the immunised-mice bleeds, with an IC_{50} value of 3.59 ng/mL. This showed the potential of the antibody library to isolate AZA1-specific scFv, but future work would need to involve more refined screening methodologies, such as single cell analysis, to sensitively screen the antibody library for the rare AZA1-specific scFv.

3.2 Results

This results chapter describes the results of the construction (Sections 3.2.1 – 3.2.9) and screening (Section 3.2.10 – 3.2.13) of an anti-AZA1 scFv library. The initial attempt at screening the library involved the use of an AZA1-BSA conjugate. However, anti-AZA1 scFv were not isolated with this initial screening process, as shown by the lack of response in a monoclonal ELISA. In this screening section, results are also presented that show non-specific interactions between the M13 phage, used in the phage display system, and the AZA1-BSA conjugate used for screening. Following this, Section 3.2.14 describes the generation of a new AZA1-OVA conjugate. It was shown that no non-specific interactions occurred between M13 phage and this AZA1-OVA conjugate. In addition, Section 3.2.14 describes the construction of a new anti-AZA1 scFv library, which had a 10-fold greater library size than the previous library. This new library was screened using the AZA1-OVA conjugate; however, no anti-AZA1 scFv were isolated.

Finally, Section 3.2.17 describes the development of an assay to measure AZA1 using polyclonal mouse anti-serum.

3.2.1 Determination of AZA1-BSA and AZA1-KLH protein concentration by BCA assay

In order to accurately determine the protein concentration of the AZA1 conjugates synthesised in Section 2.2.2.1, a BCA assay was carried out according to the manufacturer's guidelines. A BSA standard curve was generated (Figure 3.1) and using the equation of the line, the protein content of the AZA1-BSA and AZA1-KLH conjugates were measured as 2.72 mg/mL and 2.41 mg/mL, respectively.

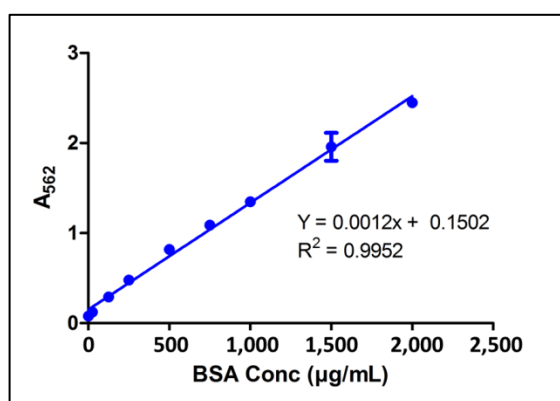


Figure 3.1: BCA standard curve. BSA protein standards were diluted from 25 to 2,000 µg/mL and measured in triplicate. Error bars = standard error of mean (SEM) (n = 3).

3.2.2 Determination of murine immune response to AZA1 by indirect ELISA

In order to determine the level of immune response exhibited by each immunised mouse towards AZA1, a serum titre was performed. The mice were immunised with AZA1-KLH. So as to avoid the carrier protein-specific response, AZA1-BSA was used to determine the serum titre. The serum titres of Mouse A, Bleed 8 (Figure 3.2), and Mouse B and C, Bleed 10 (Figure 3.3) are shown. Mouse A, Bleed 8 appeared to titre at ~1:20,000, Mouse B, Bleed 10 at ~1:10,000 and Mouse C, Bleed 10 at ~1:6,000.

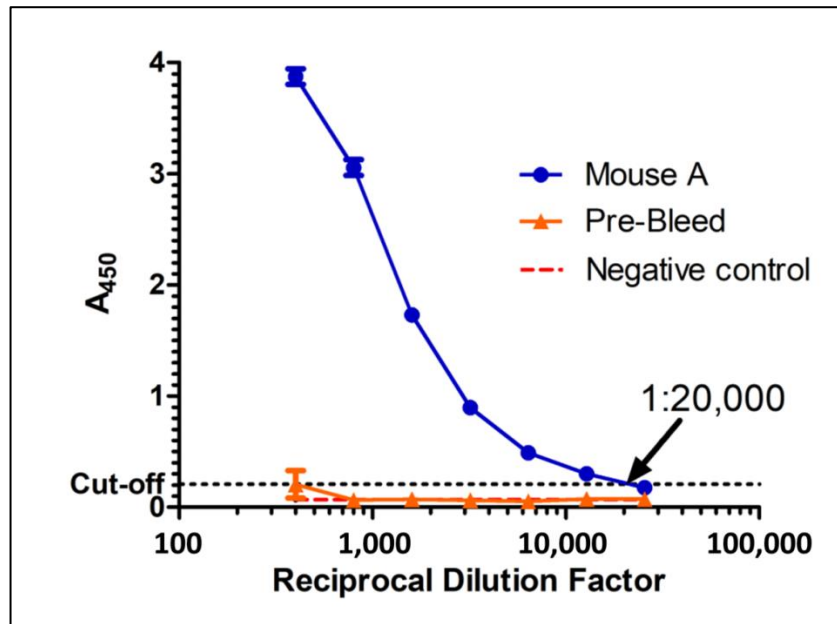


Figure 3.2: Serum titre of Mouse A Bleed 8. This figure displays the response of the serum obtained from bleed 8 of Mouse A towards AZA1-BSA. The wells of the multiwell plate were coated with 5 $\mu\text{g}/\text{mL}$ AZA1-BSA. In triplicate, the serum was added to the plate in doubling dilutions from 1:400 to 1:25,600. In the negative control wells, the same conditions as the test wells were used but the serum was omitted. The cut-off was determined at three times the negative control (i.e. the lowest signal that can be distinguished from background). Error bars = SEM (n = 3).

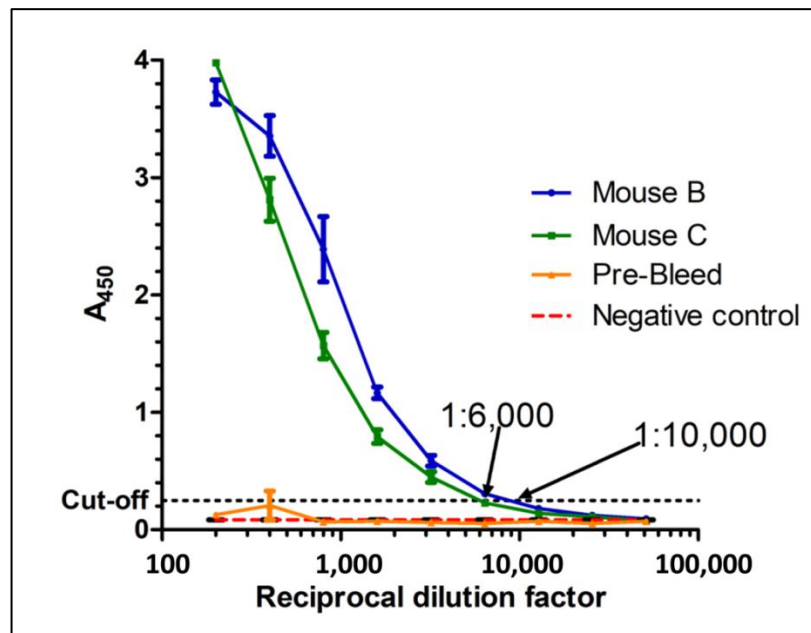


Figure 3.3: Serum titre of Mouse B and C, Bleed 10. This figure displays the response of the serum obtained from bleed 10 of Mouse B and Mouse C towards AZA1-BSA. The wells of the multiwell plate were coated with 5 $\mu\text{g}/\text{mL}$ AZA1-BSA. In triplicate, the serum was added to the plate in doubling dilutions from 1:400 to 1:25,600. In the negative control wells, the same conditions as the test wells were used but the serum was omitted. The cut-off was determined at three times the negative control (i.e. the lowest signal that can be distinguished from background). Error bars = SEM (n = 3).

3.2.3 Spectrophotometric determination of extracted mouse RNA concentration

After the total RNA was extracted from each mouse spleen, the RNA concentration is required in order to correctly perform cDNA-synthesis. The purpose of this experiment was to determine the concentration of the RNA extracted from the spleens of mice A, B and C. The RNA concentration was quantified using the Nanodrop® ND-1000 at 260 nm. The RNA concentrations of samples A-C are shown in Table 3.1.

Table 3.1: Extracted mouse spleen RNA concentrations

Sample	Concentration (ng/ μ L)
A	1,975
B	1,145
C	1,830

3.2.4 Spectrophotometric determination of synthesised cDNA concentration

The purpose of this experiment was to determine the concentration of the cDNA synthesised from the RNA of Mouse A and Mouse B. This cDNA would then serve as a template for amplification of the antibody V genes. The cDNA concentration was quantified using the Nanodrop® ND-1000 at 260 nm as 1078 ng/ μ L.

3.2.5 Amplification of antibody genes; variable light and variable heavy chain genes

The purpose of these experiments was to amplify the variable light (V_{κ} and V_{λ}) and heavy (V_H) antibody genes from the synthesised cDNA template using sequence-specific primers (outlined in Table 2.12). The amplified variable light and heavy chain DNA was used in further experiments to produce a scFv-encoding gene by SOE PCR using SOE primers (Section 2.2.2.7). All PCR products were separated on 1% (w/v) agarose gels stained with SYBR® Safe. The gel images of V_{κ} , V_{λ} , and V_H are presented in Figures 3.4, 3.5 and 3.6, respectively. PCR products are visible in all lanes, with the exception of the lane that contained MSCVH18 (Figure 3.6, lane 18). After amplification, the PCR products were gel-purified. The V_{κ} and V_{λ} products were combined at a ratio of 17:2 (V_{κ} : V_{λ}), so as to approximately reflect the predominance of V_{κ} genes in mouse antibody repertoires (Almagro *et al.*, 1998) (this product is hereafter

referred to as V_L). The DNA concentrations of V_L and V_H were determined by spectrophotometric measurement at 260 nm (summarised in Table 3.2).

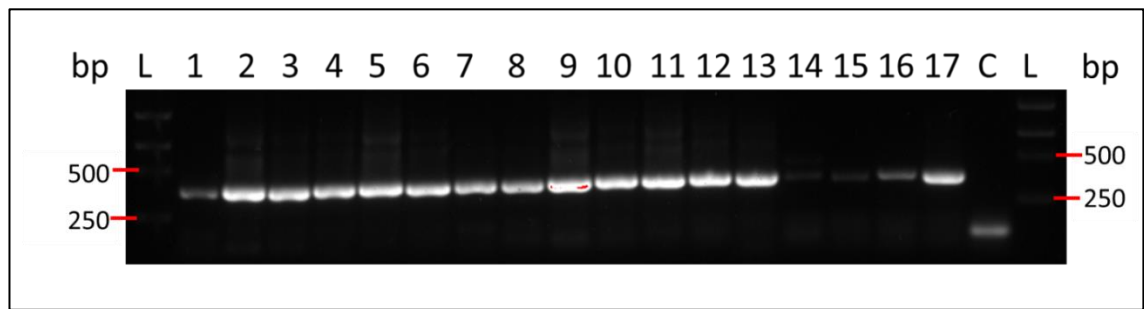


Figure 3.4: V_κ gene amplification. V_κ PCR products were observed at ~350 bp. Additional bands were also observed at ~500-700 bp. L = Hyperladder 1kb Plus; Lanes 1 – 17 = PCR products using primers MSCVK-1 – MSCVK-17; C = control. (The control reaction included all reaction components except cDNA).

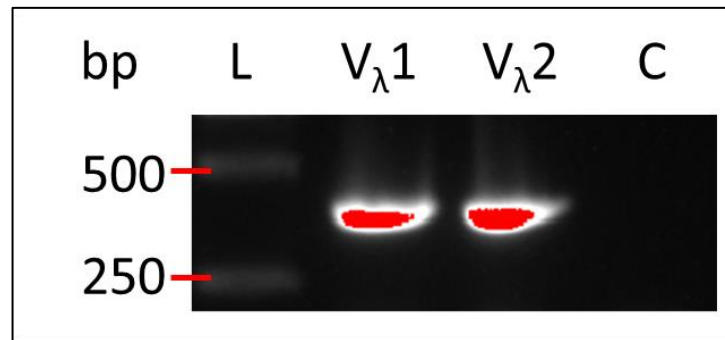


Figure 3.5: V_λ gene amplification. V_λ PCR products were observed at ~350 bp. L = Hyperladder 1kb Plus; C = control. (The control reaction included all reaction components except cDNA).

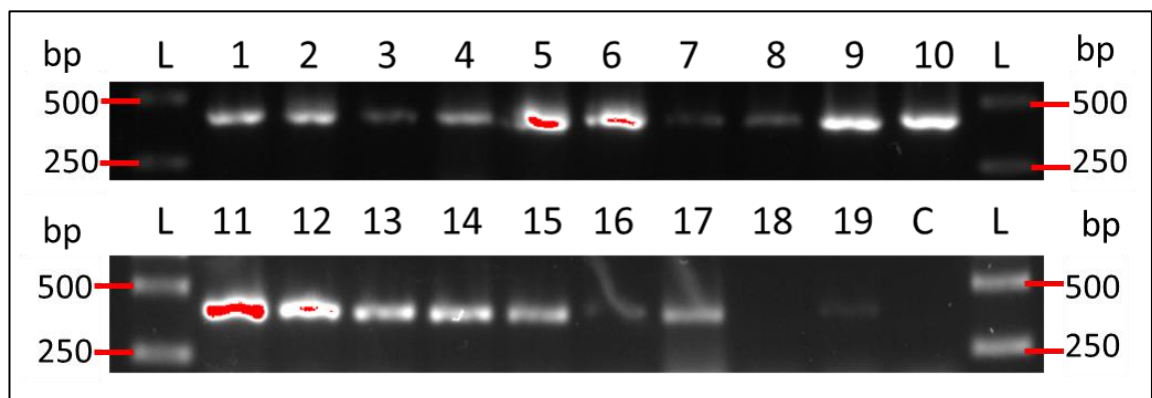


Figure 3.6: V_H gene amplification. V_H PCR products were observed at ~400 bp. L = Hyperladder 1kb Plus; Lanes 1 – 19 = PCR products using primers MSCVH-1 – MSCVH-19; C = control. (The control reaction included all reaction components except cDNA).

3.2.6 Generation of scFv-encoding gene by SOE PCR

The purpose of these experiments was to fuse and amplify the V_L and V_H PCR products to form a complete scFv-encoding DNA fragment. A small-scale SOE PCR was carried out initially (Figure 3.7) followed by a large scale SOE PCR in order to have sufficient scFv-encoding DNA for restriction enzyme digestion and ligation into a phagemid vector. The large-scale SOE PCR product was gel-purified and the DNA concentration was determined by spectrophotometric measurement at 260 nm (see Table 3.2).

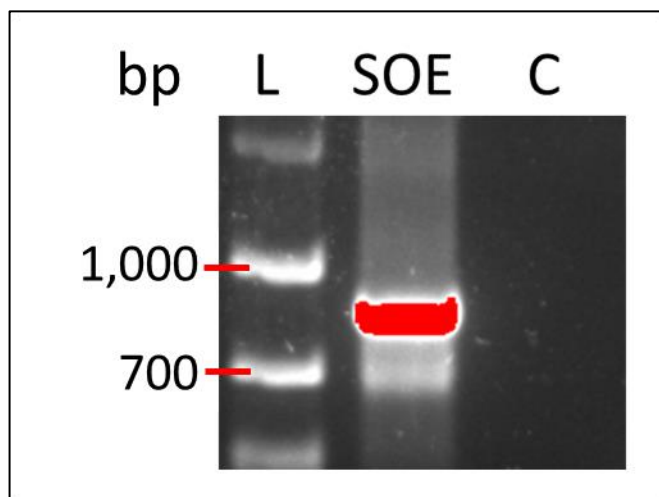


Figure 3.7: SOE PCR. The SOE PCR product was observed at ~800 bp. A smear was also observed at sizes above and below the band of interest. L = Hyperladder 1kb Plus; C = control. (The control reaction included all reaction components except V_L and V_H DNA).

Table 3.2: DNA concentration measurements of V_L , V_H and SOE PCR products.

Product	DNA concentration (ng/ μ L)
V_L	406.8
V_H	171.9
SOE	170.0

3.2.7 pComb3XSS concentration measurement

The *E. coli* containing the pComb3XSS vector was grown in a small-scale culture and the plasmid was purified. In order to accurately carry out subsequent digestion experiments, the plasmid DNA concentration is required. The purified plasmid DNA was quantified by spectrophotometric measurement at 260 nm as 4653.1 ng/ μ L.

3.2.8 Restriction enzyme digestion and ligation of scFv DNA and pComb3XSS

The purpose of this experiment was to digest the scFv DNA and pComb3XSS products using the *Sfi*I restriction enzyme in order to form complementary ‘sticky’ ends that will facilitate the insertion of the scFv DNA into the plasmid. The pComb3XSS was also digested with *Xba*I and *Xho*I, which act on restriction sites within the plasmid’s Stuffer fragment. This was carried out in order to reduce the chance of the Stuffer fragment being re-ligated back into the plasmid. The digested scFv DNA and pComb3XSS products were separated on agarose gels (see Figures 3.8 and 3.9) and subsequently gel-purified. The DNA concentrations of the purified digested scFv DNA and pComb3XSS vector were determined by spectrophotometric measurement as 119.9 ng/μL and 167.9 ng/μL, respectively. After the ligation was carried out, a small amount of ligated product was separated on an agarose gel to check the extent of the ligation reaction (see Figure 3.10).

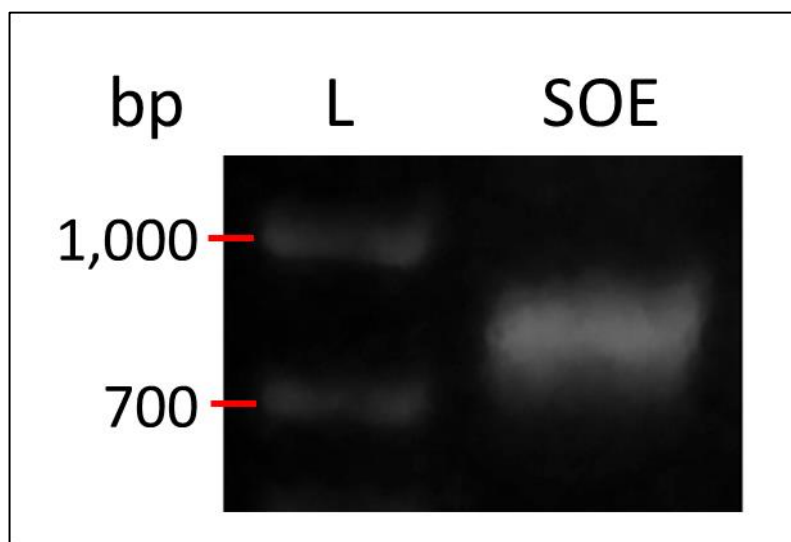


Figure 3.8: Digested SOE product. The digested SOE product was observed at ~800 bp. L = Hyperladder 1kb Plus.

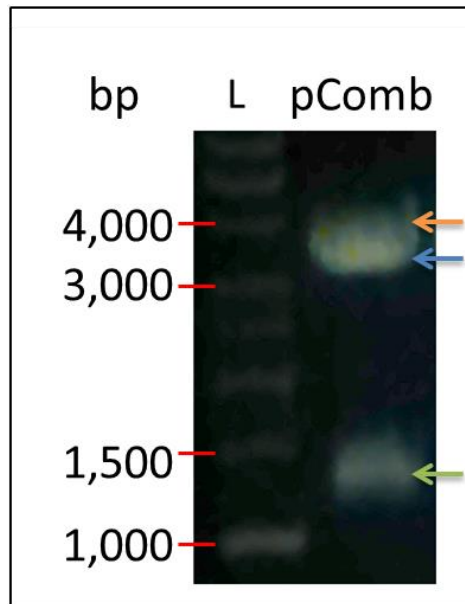


Figure 3.9: Digested pComb3XSS product. The digested pComb3XSS product was observed at ~3,300 bp (as indicated by the blue arrow). This band was subsequently gel-purified. Additional bands were observed at ~4,000 bp (which is difficult to observe in this image, but is indicated by the orange arrow) and 1,200 bp (green arrow), corresponding to single-cut plasmid and the Stuffer fragment, respectively. L = Hyperladder 1kb Plus.

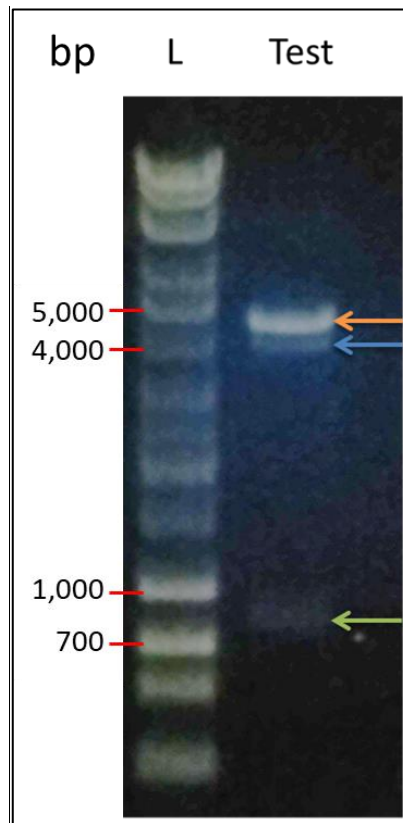


Figure 3.10: Ligated pComb3XSS plasmid with SOE insertion. The circularised plasmid containing the SOE insert was observed at ~4,100 bp (blue arrow). A band was visible at ~4,800bp which was likely a linearised scFv-containing plasmid (orange arrow). The non-ligated SOE was observed at ~800 bp (green arrow). L = Hyperladder 1kb Plus.

3.2.9 Electroporation of SOE-pComb3XSS into XL1 Blue electrocompetent *E. coli*

The pComb3XSS plasmid containing the scFv gene insert was electroporated into XL1 Blue *E. coli* to allow for expression of the scFv-pIII fusion protein. A titre was carried out to determine the approximate library size. This titre was determined to be of the order of 10^5 clones, which is a relatively small library size in comparison to previous work in this research group. A colony pick PCR was carried out to determine the proportion of the transformed clones that contained the scFv insert (see Figure 3.11). Of the ten picked colonies, all contained the scFv insert, indicating that all of the transformed clones have the potential to express scFv fragments.

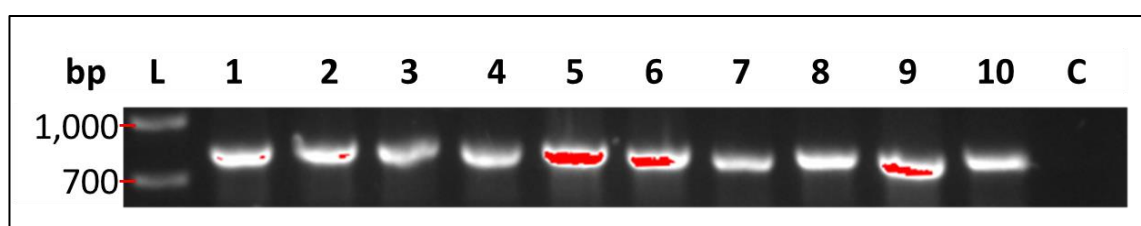


Figure 3.11: Colony pick PCR. The scFv gene insert was observed in 10 out of 10 lanes at ~800 bp. L = Hyperladder 1kb Plus; 1-10 = 10 PCR reactions; C = control. (The control reaction included all reaction components except a picked bacterial colony).

3.2.10 Screening the anti-AZA1 scFv phage library by panning

The purpose of the panning experiments was to screen and enrich the constructed antibody library for potential AZA1-binding clones. In order to determine if the screening process is selectively enriching the antibody library, after each round, the input and output phage were re-infected into *E. coli* and grown on LB agar plates supplemented with kanamycin. Only clones containing the re-infected phagemid vector will be resistant to kanamycin and so only these clones will be permitted to grow. Titres were determined by counting the *E. coli* colonies grown on titre plates (see Table 3.3).

Table 3.3: Input and output phage titres from each round of panning.

Round	Input titre (cfu/mL)	Output titre (cfu/mL)
1	3.2×10^{13}	2×10^9
2	8.3×10^{10}	*
3	1.9×10^{10}	2×10^5
4	5.6×10^{12}	1.4×10^7

(*Note: An output phage titre was not acquired for round 2 due to no observed growth on these plates).

3.2.11 Polyclonal phage ELISA of panning output phage

The purpose of this experiment was to determine the response of the phage pool acquired from each round of panning towards AZA1 and to also investigate if any response was directed towards the carrier protein, BSA. The responses from each round of panning and the un-panned library towards AZA1-BSA and BSA are shown in Figure 3.12.

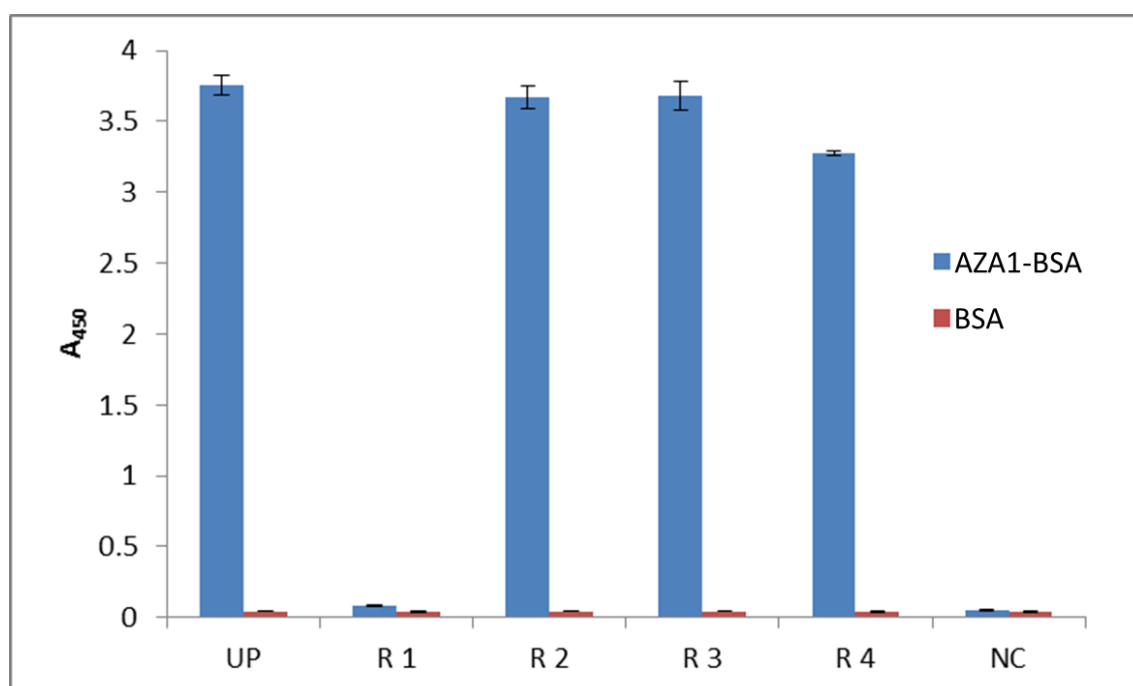


Figure 3.12: Response of polyclonal phage pools towards AZA1-BSA and BSA. A high response was observed in the un-panned library and rounds 2-4 against AZA1-BSA. Very low response was observed in round 1 towards AZA1-BSA. Baseline response was observed from each round towards BSA. The negative control wells were treated the same as the test wells but omitted any phage. UP = Un-panned library; R 1 – 4 = Rounds 1 – 4; NC = Negative Control. The negative control consisted of 5% (w/v) MM without any phage.

3.2.12 Colony pick PCR of panning input and output phage

In order to determine if the scFv gene insert was still present within the input and output phage library after round 4 of panning, a colony pick PCR was carried out on a number of colonies. Eight input and eight output colonies were tested and separated on an agarose gel (see Figure 3.13).

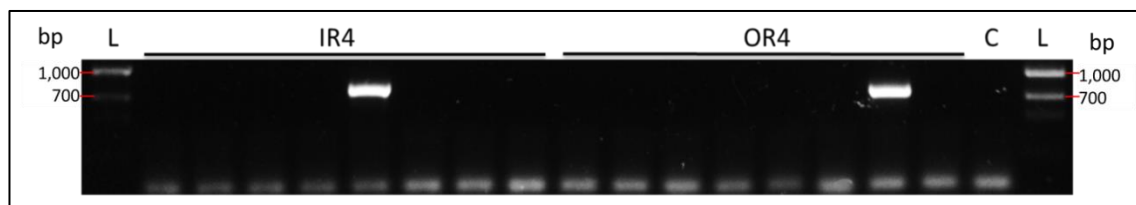


Figure 3.13: Colony pick PCR of panning input and output phage. A PCR product of 800 bp was expected in each of the round 4 input and output reactions. One scFv out of eight round 4 input products and one out of eight round 4 output products were observed. The negative control consisted of all reaction components but omitted a picked colony. No DNA product was observed in the negative control lane. Primer dimers were observed at sizes smaller than 250 bp in all lanes. L = Hyperladder 1kb Plus. IR4 = Input round 4; OR4 = Output round 4; C = Negative control.

3.2.13 Determination of wild type M13 response towards AZA1 by indirect ELISA

The purpose of this experiment was to test the response of the output phage from round 4 of panning to AZA1-BSA and compare this to the binding response of wild type M13 helper phage (wtM13), i.e. M13 phage that do not present an antibody on their surface (Figure 3.14). Furthermore, for another point of comparison, the response of a phage library that was raised against pancreatic tumour markers was also tested against AZA1-BSA, i.e. an scFv library that was heavily biased towards pancreatic tumour marker antigens that was displayed on M13 phage. The phage output from round 4 showed a low response towards AZA1-BSA, with a titre of ~1:50. The wtM13 showed a higher response towards AZA1-BSA, with a titre of ~1:1,000. The highest response was displayed by the anti-pancreatic tumour scFv-phage library, with a titre >1:1,280. Negligible response was displayed towards BSA for any of the phage pools tested.

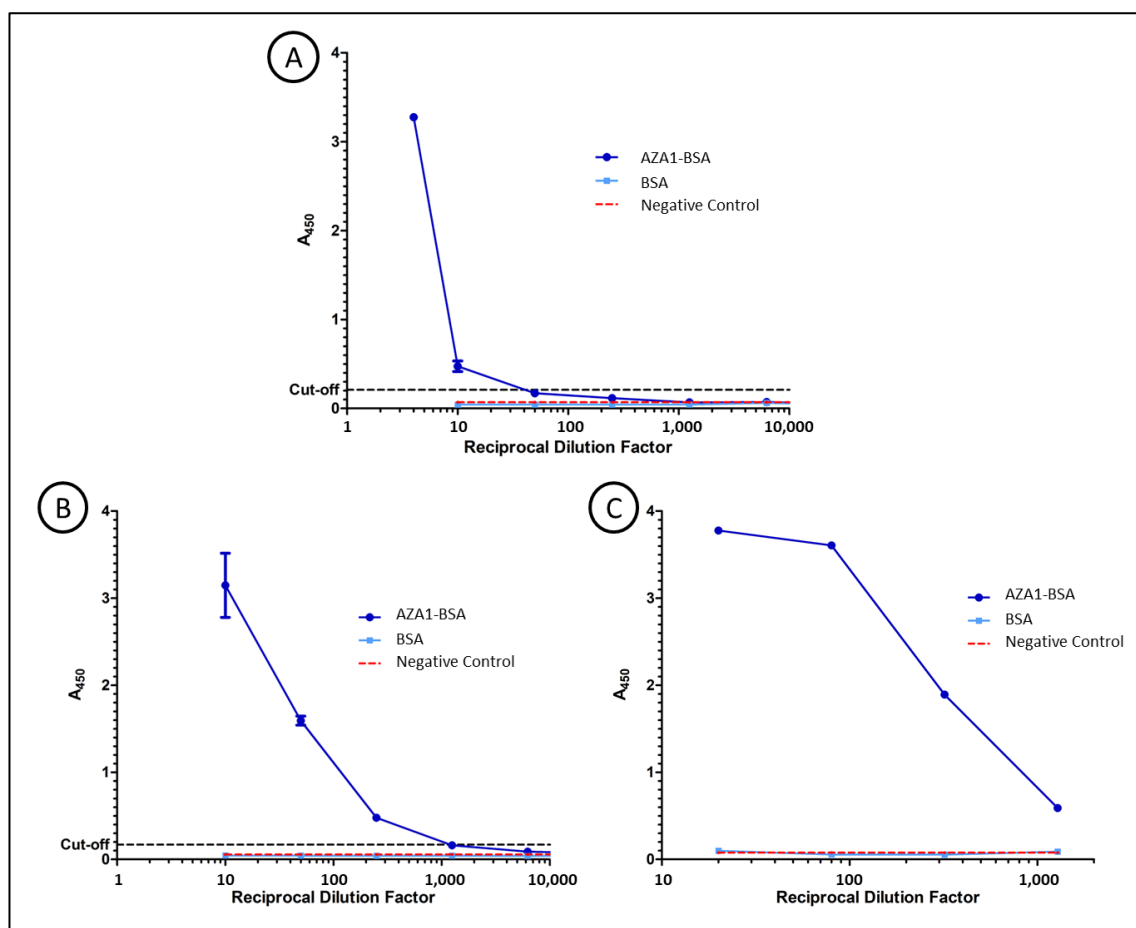


Figure 3.14: M13 phage exhibited non-specific binding to AZA1-BSA. (A) The binding response of the phage pool isolated from Round 4 of panning. (B) The binding response of wtM13 helper phage to AZA1-BSA. (C) The binding response of a non-screened anti-pancreatic tumour marker phage library towards AZA1-BSA. The negative control in each assay included the same conditions as the test wells but the phage was omitted. Error bars = SEM (n = 3).

3.2.14 Generation of a new AZA1-OVA conjugate and construction of a new anti-AZA1 scFv library

3.2.14.1 Measurement of AZA1-OVA protein concentration by BCA assay

Following un-successful screening using the AZA1-BSA conjugate, a new AZA1-OVA conjugate was synthesized using a new conjugation process. The purpose of this experiment was to determine the protein concentration of this new conjugate for use in further experiments. The protein concentration of the newly synthesized AZA1-OVA conjugate was measured by BCA assay to be 1,532 $\mu\text{g/mL}$.

3.2.14.2 Binding response of mouse B antiserum and wtM13 to AZA1-OVA

The purpose of this experiment was to determine if the conjugation of AZA1 to OVA was successful. This was determined by measuring the binding response of mouse B antiserum to AZA1-OVA. In addition, the response of wtM13 to the new conjugation was also measured, so as to determine if the non-specific interaction persisted. The results of these ELISAs are presented in Figure 3.15 below. As can be seen from Figure 3.14(A), a strong response was observed from mouse B antiserum to AZA1-OVA, with negligible response towards OVA. This indicates that the conjugation was successful. From Figure 3.15(B), it can be seen that wtM13 exhibited no binding towards AZA1-OVA or OVA, indicating that the non-specific interaction had ceased with the new conjugate.

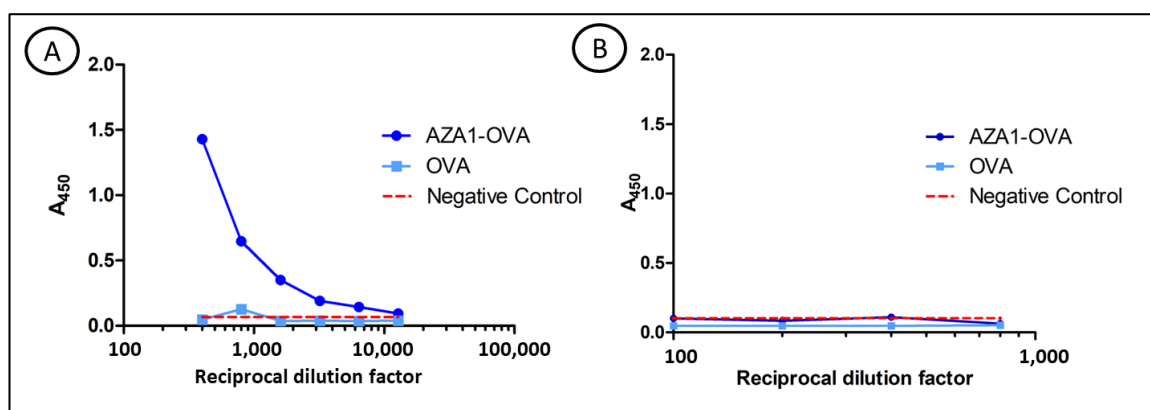


Figure 3.15: Binding response of (A) mouse B antiserum and (B) wtM13 towards AZA1-OVA. The mouse B antiserum and wtM13 were also tested against OVA as a control. The negative control consisted of all reaction components except antiserum or phage sample.

3.2.14.3 Transformation of re-constructed anti-AZA1 antibody library

The anti-AZA1 scFv library was re-constructed with the aim of increasing the size and diversity of the scFv library so as to improve the likelihood of isolating an AZA1-specific scFv. After transforming the newly constructed library into *E. coli*, the library size was determined to be of the order of 2.5×10^6 clones, which was a 10-fold improvement over the previous library. A colony pick PCR was performed on 10 clones, the result of which is presented below in Figure 3.16. Using the OmpSeq and Gback primer pair, it is expected to observe the scFv insert at ~1,000 bp. The 1,000 bp gene was amplified in 9 out of the 10 tested clones, indicating 90% transformation efficiency.

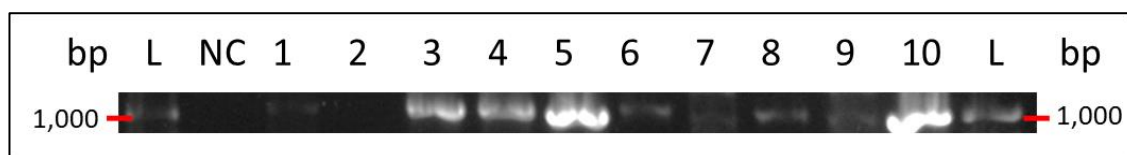


Figure 3.16: Colony pick PCR of 10 clones from the re-constructed anti-AZA1 scFv library. The scFv gene, as amplified using the OmpSeq and Gback primers, was observed at 1,000 bp in 9 out of 10 tested colonies. L = Hyperladder 1kb; 1-10 = 10 PCR reactions; NC = negative control. (The negative control reaction included all reaction components except a picked bacterial colony).

3.2.15 Screening the re-constructed anti-AZA1 scFv library

The purpose of this experiment was to screen and enrich the re-constructed anti-AZA1 antibody library for potential AZA1-binding clones using the newly synthesized AZA1-OVA conjugate. The progress of the panning experiment was monitored by determining the input and output phage titres of each panning round (see Table 3.4), as was carried out previously in Section 3.2.10.

Table 3.4: Input and output phage titres from each round of panning.

Round	Input titre (cfu/mL)	Output titre (cfu/mL)
1	5.2×10^{13}	2.71×10^8
2	6.2×10^{12}	2.08×10^9
3	1.24×10^{13}	5.35×10^6
4	2.96×10^{13}	1×10^5

3.2.16 Polyclonal phage ELISA

After carrying out 4 rounds of panning on the anti-AZA1 scFv phage library, the response of the phage output pools from each round was determined by indirect ELISA. The response of the wtM13 phage was also tested and served as a point of comparison. The result of the ELISA is presented in Figure 3.17 below. As can be seen from Figure 3.17, there was no statistically significant difference in response between any of the tested samples ($P > 0.05$). This indicates that no enrichment occurred during the panning process.

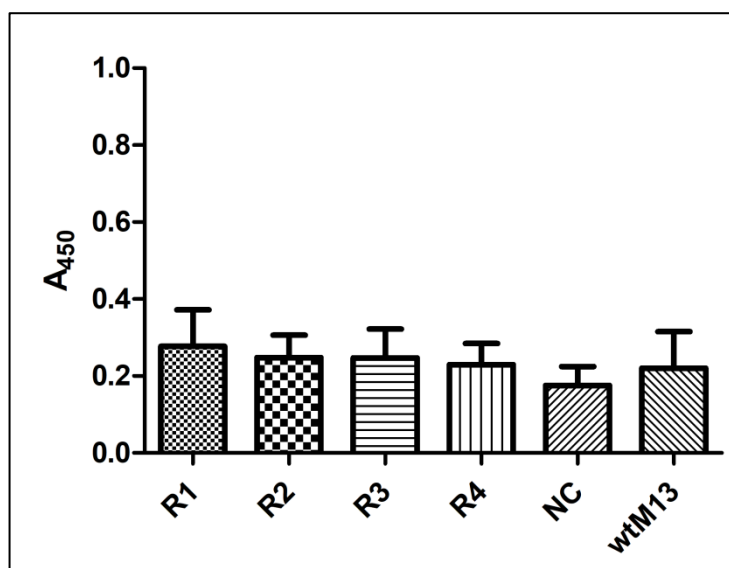


Figure 3.17: Response of polyclonal phage pools towards AZA1-OVA. The phage outputs from each round of panning were tested against AZA1-OVA to determine if any enrichment of response was observed. No statistically significant changes in binding response were observed. NC = negative control.

3.2.17 Development of an assay to measure AZA1 using polyclonal mouse antiserum

In these experiments, the aim was to develop a competitive assay using the polyclonal antiserum from mouse B to measure AZA1. In order to optimise the appropriate antiserum dilution and AZA1-OVA conjugate dilution to use in a competitive assay, a checkerboard assay was first carried out (Section 3.2.17.1). Following this optimisation, three independent competitive assays were carried out to measure free AZA1 in solution (Section 3.2.17.2).

3.2.17.1 Optimisation of Mouse B antiserum dilution and AZA-OVA coating concentration by checkerboard ELISA

The purpose of this experiment was to determine a suitable dilution of the mouse B antiserum and the AZA1-OVA coating concentration for carrying out subsequent competitive assays. The aim was to identify an antiserum dilution and AZA1-OVA coating concentration that would produce a response significantly different to the negative control. A range of AZA-OVA concentrations were coated onto a plate surface and a series of mouse B antiserum dilutions were applied. The responses observed are presented in Figure 3.18. From the result of this experiment, a coating concentration of 5 µg/mL AZA1-OVA and an antiserum dilution of 1:200 were chosen for further experiments.

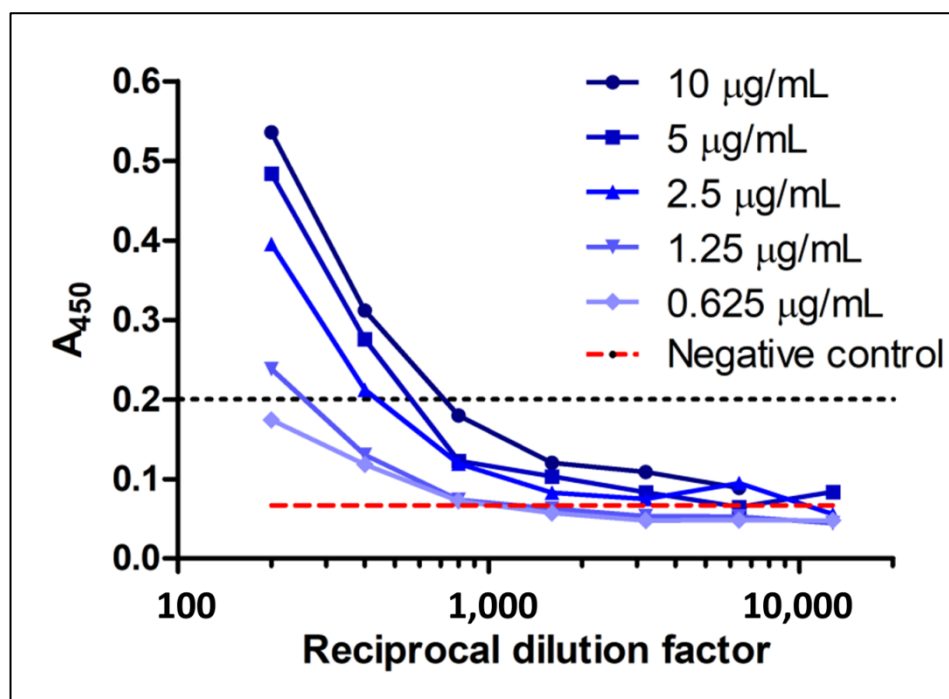


Figure 3.18: Checkerboard ELISA of various AZA1-OVA coating concentrations and Mouse B antiserum dilutions. The wells of a multiwell plate were coated with AZA1-OVA at concentrations ranging from 0.625 µg/mL to 10 µg/mL. The antiserum was diluted from 1:200 to 1:12,800. The negative control consisted of all test components but omitted the AZA1-OVA coating and any antiserum. The ‘cut-off’ (dotted line) was determined at three times the negative control (i.e. the lowest signal that can be distinguished from background).

3.2.17.2 Development of competitive assay to detect AZA1 using polyclonal murine IgG

The purpose of this experiment was to develop a competitive assay to determine the binding characteristics of the Mouse B antiserum, i.e. to determine the IC_{50} of this polyclonal Ab sample. Triplicate assays were conducted. The results of these three experiments are presented in Figure 3.19. As can be seen, there was considerable variation in the observed IC_{50} values and the R^2 values would suggest a poor curve fit. The average IC_{50} value was $3.59 \text{ ng/mL} \pm 2.00$ (SEM).

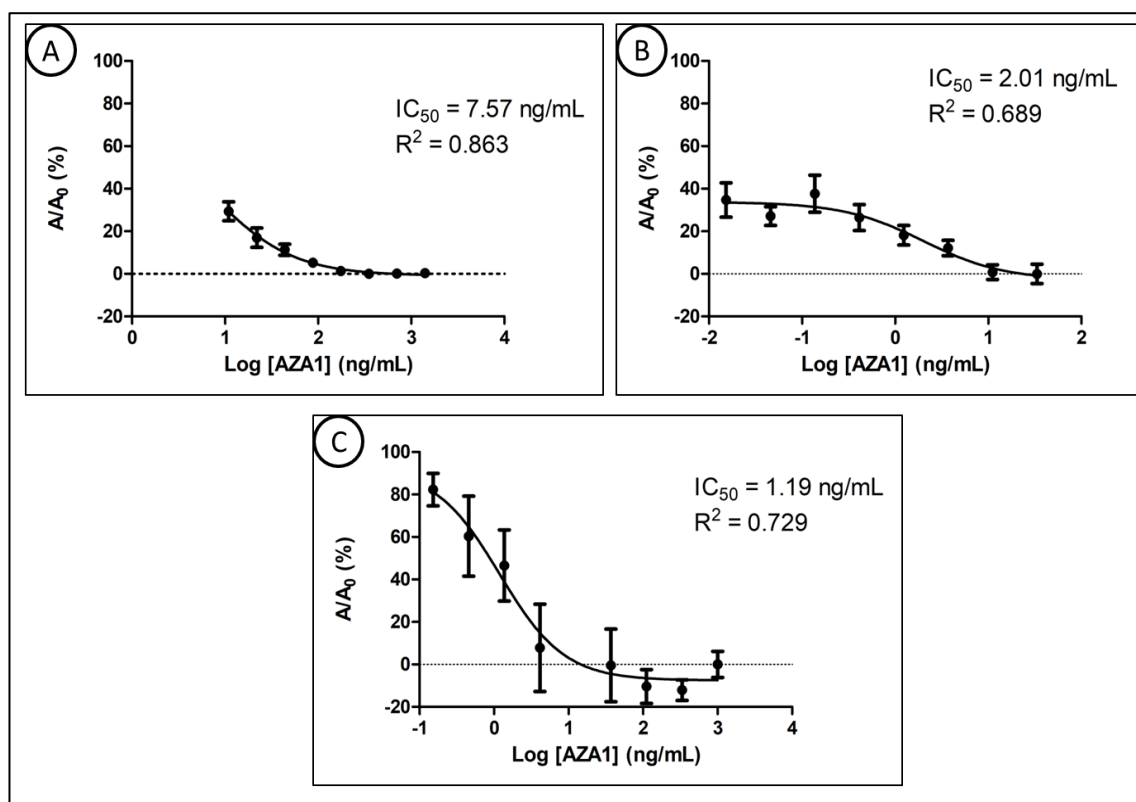


Figure 3.19: Competitive ELISA results of Mouse B antiserum for free AZA1. Assays A, B and C were carried out sequentially, i.e. assay A was carried out first, followed by B and then C. As can be observed from the error bars, each subsequent iteration of the assay appeared to introduce greater variability. Error bars = SEM (n = 3).

3.3 Discussion

There is a pressing need for on-site, real-time monitoring systems for AZA1 to ensure consumer safety and mitigate the harmful economic effects of this phycotoxin. The focus of this chapter was on the development of anti-AZA1 recombinant antibody fragments. RAb engineering affords an effective means to produce antibody fragments for diagnostic and therapeutic use in a relatively short time-frame and with relatively low cost. Such recombinant antibody fragments can be incorporated into PON biosensors to facilitate on-site detection and monitoring of toxins and offer a solution to the issue of monitoring AZA1-contamination in seafood.

As AZA1 is a poorly immunogenic hapten molecule, in order to generate an immune response to this target it was conjugated to an immunogenic carrier protein. KLH is a large protein (molecular mass ranging from 0.5 – 13 MDa) isolated from keyhole limpets (*Megathura crenulata*). This organism is phylogenetically very distant from mice (*Mus musculus*). Thus, KLH is very ‘foreign’ to a mouse’s immune system and,

combined with its high molecular mass and complex structure, elicits a strong immune response. KLH also contains hundreds of primary amine groups that can be targeted for conjugation with the carboxyl-containing AZA1 by EDC-crosslinking. Carbodiimide conjugation reactions mediate the formation of amide bonds between carboxyl groups with primary amines. Carbodiimides are ‘zero-length’ linkers because no additional chemical structure is introduced between the conjugating molecules. A zero-length linker is useful for immunization strategies in certain circumstances as this eliminates the chance of linker-specific antibodies being generated within the host. However, they may be undesirable if steric hindrance becomes a factor (Bieniarz *et al.*, 1996; Hermanson, 2008).

BSA and OVA are other frequently used carrier proteins for hapten molecules. The large size of BSA and OVA (66.5 kDa and 42.7 kDa, respectively) and the high number of amine groups on their surfaces allowed for effective EDC conjugation with AZA1. The use of these secondary proteins as non-relevant carrier proteins is highly useful in determining serum titres in ELISA and in screening, as the use of a non-relevant carrier protein will reduce the binding of antiserum to the carrier, ensuring that the response observed is that directed towards the hapten (Hermanson, 2013).

The development of an anti-AZA1 scFv was undertaken by the successive immunisation of three BALB/c mice with AZA1 conjugated to KLH, which promotes somatic hypermutation (SHM) of the antibody variable regions and the development of high-specificity antibodies. A serum titre is an effective means to determine the extent of the immune response in an immunised host, as it is used to measure the level of antibodies present in the serum that are specific to the target of interest. In this work, after a total of ten immunisations, serum titres of 1:20,000, 1:10,000 and 1:6,000 were observed for mice A, B and C, respectively. This is a moderate immune response that can be somewhat expected for such a non-immunogenic target as AZA1. This is reflected in other published work, as it was reported by Samdal *et al.* (2015) that a similar response was observed after a total of eleven host immunisations. Generally, it is recommended to establish an immune titre in the order of $1:10^5$ before commencing library construction (Barbas *et al.*, 2001). However, due to pressing time constraints (a total of 10 immunisations required 28 weeks) and the high consumption of valuable and highly limited AZA1 materials, and despite the moderate antibody titre established, it

was decided to develop the antibody libraries of mice A and B. The spleens were harvested from mice A and B as the spleen is a rich source of antibody-producing B cells. The RNA from these spleens was extracted and reverse transcribed to cDNA. The V_L and V_H genes were amplified from this cDNA using sequence-specific sense and reverse primers. When amplifying the V_k genes, additional bands were visible on the agarose gel at sizes between 500 – 700 bp (Figure 3.4). These products may have occurred due to product dimerisation. In the V_H PCR, the MSCVH18 product was not produced, which may be due to the under-representation of this V_H gene in the mouse antibody repertoire. Using SOE PCR, the V_L and V_H genes were spliced together and amplified to obtain a high yield of scFv-encoding gene template. When carrying out SOE PCRs, a smear was observed at sizes above and below the target band on the agarose gels. Such smearing can sometimes occur due to the presence of too much DNA template, incomplete polymerisation, or dimerization of PCR products (Bio-Rad, 2018). However, the ~800 bp band was excised from the agarose gel and gel-purified, which omitted most of these smeared products. The scFv gene and the pComb3XSS vector were restriction digested with the restriction enzyme *SfiI*, which facilitates the formation of ‘sticky’ ends and directional cloning upon ligation of the scFv gene into the vector. The pComb3XSS vector was also restriction digested with *XbaI* and *XhoI*, which cleave the stuffer fragment at two points within its sequence. This was done in order to reduce the chance of the stuffer fragment from re-ligating into the vector. The digested scFv gene and pComb3XSS vector were ligated and subsequently electroporated into XL1 Blue *E. coli*. The resulting library size was of the order of 10^5 clones. Ideally, a library size of $>10^7$ clones would increase the likelihood of isolating high affinity antibodies. However, previous work from this research group yielded highly specific antibodies from libraries of $\sim 10^5$ clones in size. Therefore, this library was used for phage display and panning to screen for potential anti-AZA1 antibody fragments.

The XL1 Blue *E. coli* library was infected with M13 helper phage in order to convert this bacterial library into a phage-display library, where each encoded antibody is displayed on the phage surface. This phage library was screened by panning with decreasing coating concentrations of AZA1-BSA and increasing number of wash steps per round of panning. This was done in order to put selective pressure on the library so as to enrich for antibodies that bind strongly to AZA1 and exclude non-specific and weaker binders. This enrichment was shown by the decreasing output titres after each

round of panning (with the exception of Round 4) (Table 3.3). However, the result of the polyclonal phage ELISA (Figure 3.12) shows a high response in the un-panned library and a decreasing response from round 2 to round 4. This is a highly anomalous result, as it would be expected that a low response would be observed from the un-panned library, where the antibody diversity is high and the proportion of potential AZA1-binding antibodies is relatively low. It would also be expected that the response towards AZA1-BSA would increase with further rounds of panning, when the AZA1-binding clones are enriched and become more prevalent in the phage pool (Byrne *et al.*, 2009).

To further investigate this, the phage outputs from rounds 3 and 4 were infected into non-suppressor strain Top10F' *E. coli* to allow for soluble expression of the encoded scFv fragments. Unfortunately, when tested in a monoclonal ELISA format, no response was observed from any of the tested samples (results not shown). A possible reason for this is that the colonies picked may have contained an empty pComb3XSS vector, which would confer carbenicillin-resistance and allow colonies to grow, but without the scFv gene insert. This was investigated by means of a colony pick PCR.

A colony pick PCR was carried out to determine if the scFv gene insert remained present before and after the final round of panning. The result indicates that the gene insert remained in only one of the eight tested input colonies and in one of the eight tested output colonies. This result suggests the scFv-encoding gene was present in only a very small proportion of the phage pool while the majority of the phage pool contained empty phagemid vector. Such clones would have less of a burden of expressing a deleterious gene and would have a competitive advantage over those clones that did express the gene (Hibbing *et al.*, 2010). Therefore, the majority of the clones picked after soluble-expression in Top10F' *E. coli* could not express scFv product, which would explain the result of the monoclonal ELISA. It is possible that the bacteria excised the scFv gene out of the phagemid vector but retained the carbenicillin-resistance gene (Kliman, 2016). This would explain why colonies could grow in the presence of carbenicillin but not produce any scFv product. Bacteriophage are notoriously 'sticky' and so another possible explanation of these results is that perhaps wtM13 was interacting with the AZA1-BSA-coated immunotube surface, perhaps via a non-specific binding interaction of phage coat proteins with the conjugate (Miersch *et*

al., 2015; Hakami *et al.*, 2015). This would allow non-scFv-displaying phage to be retained through the rounds of selection. This theory was investigated by comparing the response of phage from the round 4 of panning to that of wtM13 and to the response of an scFv-displaying phage library that was developed against pancreatic tumour markers; the binding of these phage pools was measured against AZA1-BSA and BSA using indirect ELISA (Figure 3.14).

The result shown in Figure 3.14(A) clearly shows a high response for round 4 phage at 1/4 dilution but declines rapidly with increasing dilutions. By comparison, a high response was observed from wtM13 towards AZA1-BSA with a titre observed at ~1:1,000 (Figure 3.14(B)). Further, a negligible response was observed towards BSA, which would suggest that wtM13 binds to AZA1. This was further shown by the high binding response of the anti-pancreatic tumour marker scFv-phage pool towards AZA1-BSA (Figure 3.14(C)). The likelihood of this response occurring due to the binding of the displayed scFv fragments is very low; the anti-pancreatic cancer antibody library was raised in BALB/c mice that would have never been exposed to AZA1. Furthermore, it should be stressed again how weak AZA1 is as an effective immunogen, requiring 10 administrations of the AZA1-KLH immunogen to raise the BALB/c immune response to a modest level. Thus, the response observed in Figure 3.14(C) is likely not due to antibody-antigen binding. Therefore, the results presented in Figure 3.14 suggest a non-specific binding interaction between the M13 phage and the AZA1-BSA conjugate, which is similar to other published work (Miersch *et al.*, 2015; Hakami *et al.*, 2015). There are considerable negative implications with the non-specific binding of the phage-carrier system to the target of interest.

Firstly, it is important to note that the process of panning relies on two critical steps that affect library diversity; the selection step, which based on affinity to a target; and the amplification step in which eluted phage compete for a limited number of host cells to allow for propagation. As was noted by Derda *et al.* (2011), the amplification step in panning contributes a significant loss of diversity in phage libraries. This occurs due to the ability of faster growing clones to out-compete the slower growing clones; thus, the output from each round of panning is a function of the scFv affinity and also the propagation rate of each clone. This was exemplified by Derda *et al.* (2010); a 40%

difference in infection time between a rapid-growing phage (R) and a slower-growing phage (S) can lead to a R:S ratio of 300:1 after five hours of growth.

It is well established that in a pool of *E. coli* clones, clones that do not have to over-express a protein-of-interest will have a growth advantage over those that do, due to the devotion of energy and cellular resources into growth (Hibbing *et al.*, 2010). In the present study, the scFv-expressing *E. coli* will be at a growth-disadvantage and will be quickly out-competed by the faster growing non-expressing clones. Furthermore, the fact that non-displaying M13 phage can bind to the AZA1-BSA target means that such clones can be retained through the wash steps in each round of panning, allowing them to be retained. With each subsequent propagation step, the non-displaying phage numbers will increase. This concept is presented in Figure 3.20 below. Therefore, the likely explanation of the high binding response observed in the polyclonal phage ELISA is that the response was related to the abundance and binding ability of the phage particles to the AZA1-BSA coated surface and not to the affinity of displayed antibodies for AZA1-BSA. Perhaps a number of clones lost the redundant scFv-encoding gene, as this would confer a higher growth rate, and binding to the AZA1-BSA surface would still be retained by the binding ability of wtM13. This may also explain the absence of scFv-inserts in the majority of clones tested in the colony pick PCR.

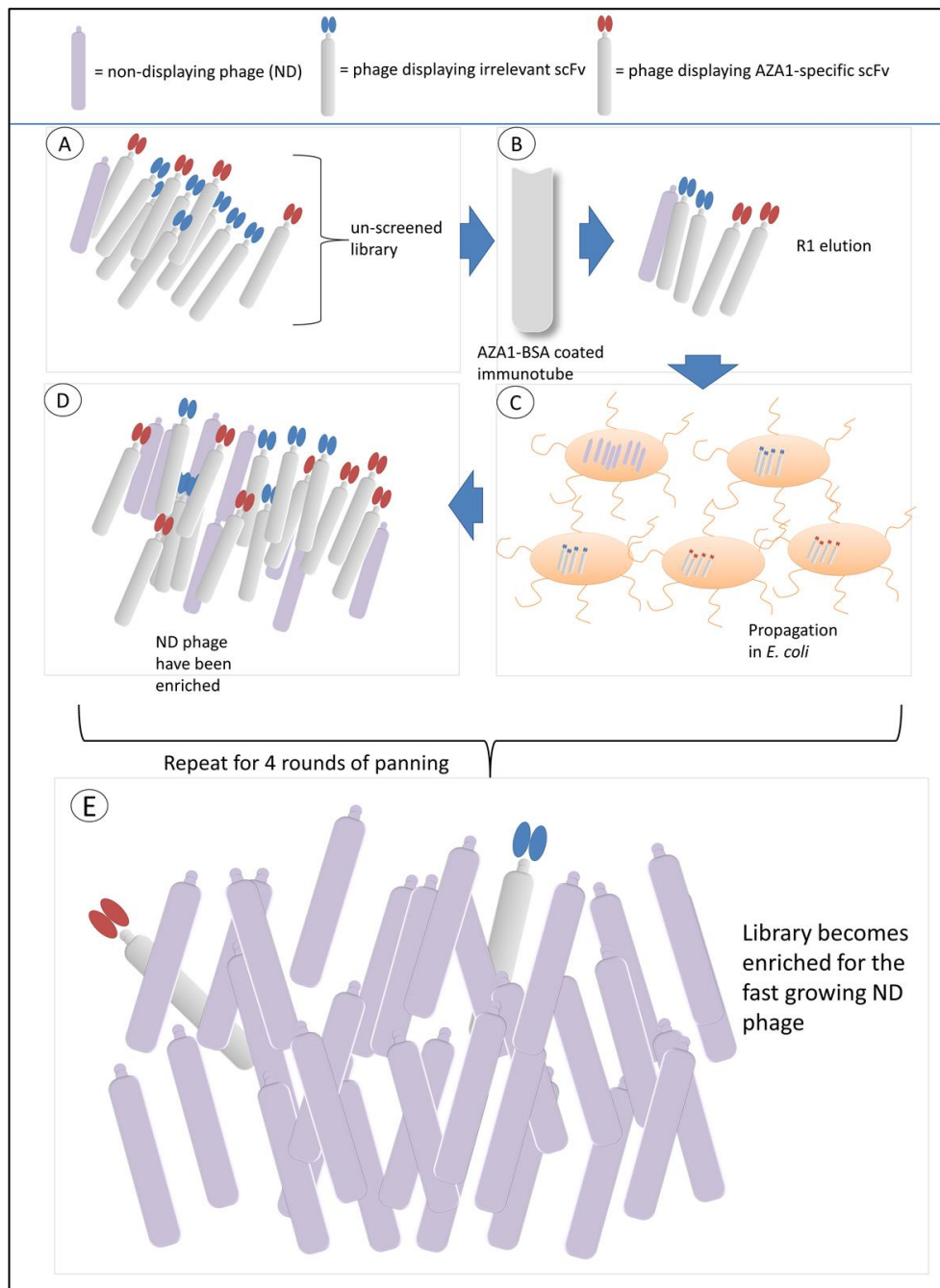


Figure 3.20: Concept of the enrichment of non-displaying M13 phage during panning. (A) The AZA1 scFv-phage library is made up of many clones that bind to AZA1 (red) and clones that bind to irrelevant antigen targets (blue). In addition, there are a small number of M13 phage (purple) that were transformed with phagemid lacking the scFv gene, thus they do not display an scFv on the surface (non-displaying (ND) phage). (B) During the first round of panning, a number of red AZA1-specific clones are retained because of their affinity to AZA1. However, some non-specific blue clones and ND phage are also retained because of the non-specific binding interaction between the M13 phage and the AZA1-BSA conjugate. (C) Upon transfection of the output library into *E. coli*, ND phage grow much faster as they do not need to over-express a recombinant protein, while AZA1-specific and non-specific phage lag behind as they must devote energy and resources into over-expressing the encoded scFv. (D) The levels of ND phage post-round 1 have grown relative to the amount pre-round 1. (E) When this process is repeated for several rounds, the ND phage levels have grown to the point that they now heavily out-number any scFv-displaying phage.

It was attempted to circumvent this issue by developing a new AZA1 conjugate, using an altered conjugation reaction. AZA1 was conjugated to OVA using a more efficient and better controlled EDC-NHS conjugation reaction. The binding of mouse B antiserum to AZA1-OVA (Figure 3.15) demonstrated that the conjugation was successful. Furthermore, the lack of binding between wtM13 and AZA1-OVA indicated that the non-specific binding interaction was successfully suppressed. This indicated that this new conjugate would be a viable target to use for phage-display and panning. Following this, the anti-AZA1 scFv library was successfully re-constructed with the aim of increasing the library size and diversity. This was achieved with the library size measured at 2.5×10^6 clones, indicating a 10-fold increase in size versus the previous library. This library was confirmed to have 90% insert efficiency by colony pick PCR.

Following successfully re-constructing the anti-AZA1 scFv library, panning was carried out using the new AZA1-OVA conjugate. After four rounds of panning, a polyclonal phage ELISA was carried out to determine if any enrichment of AZA1-specific clones occurred. Unfortunately, no significant difference was observed for any of the phage outputs versus the negative control, which indicated that no AZA1-specific clones were present in the outputs.

When it appeared that no significant increase in response towards AZA1-OVA was observed after four rounds of panning, it was decided to develop a competitive assay to measure AZA1 using the polyclonal antiserum isolated from mouse B. First, a checkerboard assay was carried out, varying the AZA1-OVA coating-concentration and the dilution factor for the mouse B antiserum. The aim was to identify a combination of the two factors that produced a binding response of $\sim 0.5 - 1$ absorbance units. Thus, a coating concentration of $5 \mu\text{g/mL}$ AZA1-OVA and an antiserum dilution of 1:200 were chosen for further experiments. These parameters were used to develop a competitive ELISA to measure free AZA1 in solution. Three independent competitive ELISAs are presented in Figure 3.19. As can be seen, a range of IC_{50} and R^2 values were observed between the three assays, which indicates high variability between assays. The variability observed in the assays may have been due to the use of polyclonal antiserum. The presence of other serum components may have interfered with the assay causing the variability observed (Cox *et al.*, 2004). In addition, the inter-assay variability observed may have been due to the inherent heterogeneous nature of polyclonal antibodies

(Seida, 2017). It would be preferable to use purified IgG instead of antiserum but unfortunately the extremely limited quantity of antiserum meant that purification was impossible. Despite this, the average IC_{50} value obtained from the assays was $3.59 \text{ ng/mL} \pm 2.00$ (SEM) which indicates good sensitivity of the polyclonal antiserum. Currently, the regulatory limit of AZA1 is $160 \text{ } \mu\text{g/kg}$ of tested shellfish and there is no limit related to the levels of toxin in water. However, Samdal *et al.* (2015) reported the development of polyclonal anti-AZA1 antiserum with a similar IC_{50} of 1.9 ng/mL in buffer and a limit of quantification in shellfish of $57 \text{ } \mu\text{g/kg}$, well below the regulatory limit. Thus, the result of this competitive assay indicates that the antibody repertoire indeed contains AZA1-specific antibody clones, which are of high sensitivity and have good potential to meet the regulatory required detection limits.

Unfortunately, the considerable difficulty that was exemplified in this research is successfully isolating such clones. It could be speculated that the failure to isolate AZA1-specific clones from the scFv library could be due to the relatively low immune response generated during the immunisation regime. After a total of ten immunisations, an antiserum titre of 1:20,000 was observed for the best-responding mouse. By comparison, it was observed in the *Bacillus cereus* chapter of this thesis that an antiserum response of 1:86,000 was observed after just three immunisations; it could be envisioned that if this latter immunisation regime was continued for longer, an even stronger immune titre could have been attained. Furthermore, the scFv library that was subsequently generated was of a moderate size, with 2.5×10^6 clones. By comparison, other studies have reported antibody library sizes in excess of $10^{10} - 10^{12}$ clones (Van Blarcom *et al.*, 2015; Sun *et al.*, 2016). It is likely that this initial poor response from the immunised hosts to AZA1 was the reason for the moderate scFv library size of 2.5×10^6 clones being generated. Perhaps in future work, the issue of poor immunogenicity could be addressed by the development of synthetic AZA1 epitopes, as was reported previously (Forsyth *et al.*, 2006; Frederick *et al.*, 2009; Samdal *et al.*, 2015).

3.4 Future work

The major issue presented by hapten targets with poor immunogenicity, such as AZA1, is the requirement of a carrier protein to elicit an immune response. However, because the carrier protein is more immunogenic than the hapten, this in turn can lead to the generation of antibodies with an extended binding site that recognise the hapten with a

portion of the protein carrier. Such antibodies would bind more tightly to the hapten-protein conjugate than soluble haptens due to the greater number of interactions at the binding site. Hence, antibodies with high affinity to the soluble antigen are very rare in the immunised antibody repertoire (Sun *et al.*, 2016). In this work, it was shown that AZA1 is not very immunogenic, as indicated by the prolonged immunisation regime, which is in agreement with the literature (Frederick *et al.*, 2009; Stack *et al.*, 2011; Samdal *et al.*, 2015). The disadvantage associated with the use of bulk-screening of heterogeneous libraries with panning is that rare clones, such as those binding to AZA1 can easily be lost due to the bias for enriching the faster growing clones with no preference for those expressing desirable antibodies (Fitzgerald *et al.*, 2015; Fitzgerald and Leonard, 2016). A potential path that could circumvent these disadvantages of whole-library-screening is the use of single cell analysis (SCA). A number of SCA systems have been devised to specifically circumvent the significant disadvantages of panning. One of the most prominent SCA systems is the coupling of yeast display with fluorescence-activated cell sorting (FACS).

Yeast display utilises a similar strategy as phage display in that the scFv is presented on the surface of *Saccharomyces cerevisiae* (albeit with much higher numbers of antibodies per cell) while the scFv-encoding gene is contained within the yeast cell, thereby allowing for the recovery of the genetic material of any positively selected clones. However, an important distinguishing feature is that yeast display can be coupled with FACS. This can potentially allow for the analysis of 10,000 individual cells per second (Harriman *et al.*, 2009). This in turn facilitates characterisation of individual candidates within vast quantities of cells, allowing for the isolation of rare antibodies. This is a prime reason for the wide adoption of this technology within the biopharmaceutical industry (Meehl and Stadheim, 2014; Doerner *et al.*, 2014). Such a method was successfully applied by Tasumi *et al.* (2009) to identify mAbs specific to cholera toxin with high affinity. This technique utilised mAbs displayed on the surface of *S. cerevisiae* and fluorescently-labelled cholera toxin. Clones specific to cholera-toxin could be identified by the fluorescent signal when analysed by FACS and subsequently sorted and isolated. This system was further used by Van Blarcom *et al.* (2015) to identify mAbs with high affinity to *Staphylococcus aureus* alpha toxin. Another instance of successfully applying yeast display was reported by Sun *et al.* (2016) and presented quite a similar situation as the current study; an scFv library of 4.4

$\times 10^6$ clones was raised against a poorly immunogenic polyaromatic hydrocarbon (PAH) hapten target. Yeast display and FACS were successfully used to isolate rare antibodies specific to the target. It was calculated that using this approach improved the chances of isolating hapten-specific scFv from 0.005% in the original library to 35% in the final pool.

Unfortunately, a significant caveat associated with this system is the requirement of considerable investment into FACS equipment and the requirement to reformat the phage display library into a yeast display library, which are not readily accessible in the research group. However, a potential system that would not require reformatting the current library and that can allow for SCA was recently developed within DCU. The direct clone analysis and selection technology (DiCAST) was reported by Fitzgerald *et al.* (2015). This system is amenable to phage displayed antibody libraries and utilises microcapillary plates to analyse millions of putative antibody clones simultaneously. It is the author's opinion that future work on this project should first investigate the use of DiCAST to screen the anti-AZA1 library for rare AZA1-specific scFv. If this should not prove successful, other SCA systems such as yeast display and FACS should be investigated.

4 Optimisation of anti-MC-LR scFv binding site and stability

4.1 Introduction

This chapter describes the optimisation of an anti-MC-LR scFv, designated 2G1, which was previously developed in the Applied Biochemistry Group. 2G1 is a well characterised antibody that exhibits high affinity for MC-LR, with a limit of detection of 0.19 ng/mL. It also shows high cross-reactivity to a number of MC congeners (Murphy *et al.*, 2015). These properties make this antibody very attractive for the incorporation in biosensor systems to facilitate the monitoring of water bodies for the hazardous MC toxins. However, the 2G1-MC-LR antibody-antigen interaction had not yet been thoroughly investigated, thus, this afforded a valuable opportunity to investigate and learn more about the interactions between a recombinant antibody and its hapten target. The information and knowledge gained could be applied to improve the antibody-hapten interactions of other anti-toxin recombinant antibodies. Indeed, it is possible that the information gained could be used to further improve the binding sensitivity of the 2G1 antibody.

Thus, in Section 4.2 of the chapter, the focus was on refining our understanding of the interaction between the 2G1 scFv and MC-LR by identifying the amino acids (AAs) that are specifically involved in MC-LR-binding and elucidating their specific role in this interaction, i.e. whether the residue is involved in direct antigen-binding or plays a secondary structural role. Firstly, *in silico* modelling of the antibody-antigen interaction was carried out to identify putative AAs central to the 2G1-MC-LR interaction. A 3D model of the avian 2G1 scFv was developed by homology modelling using another avian scFv developed in the Applied Biochemistry Group (Conroy *et al.*, 2014). Owing to the highly conserved structure of avian antibody frameworks, this pairing allowed for high homology between these structures. Following this, 3D docking of the MC-LR molecule into the binding site of the 2G1 3D model was carried out using AutoDock Vina software using flexible side-chain docking. This allowed for the identification of 8 putative AA residues in the 2G1 binding site. This, in turn, guided rational targeted mutagenesis, using alanine scanning to investigate the *in vitro* role of each AA residue (see Figure 4.1). Many of the mutations resulted in considerable decreases in binding affinity for the MC-LR antigen, indicating the likely antigen-binding role of the mutated residues. Of particular note, a glutamic acid residue was identified as having a critical role in binding, with the mutation of heavy (H) chain glutamic acid 102 (H-E102) (located in complementarity determining region heavy 3 (CDRH3)) to alanine resulting

in a drop in relative affinity to 1.2% compared to the wild type scFv. A number of mutations were carried out to improve the binding affinity between 2G1 and MC-LR. Interestingly, the alanine mutations of light chain serine 56 (L-S56) and light chain aspartic acid 57 (L-D57) resulted in the improvement in relative affinity to 347% and 219%, respectively. The work in this chapter highlights the benefits of using modern computational methods and protein engineering strategies to gain greater insight into how an avian antibody interacts with its hapten target. The information gathered here should help serve the wider antibody engineering community in the future, and should contribute towards a rational approach of developing recombinant antibodies for binding specific targets.

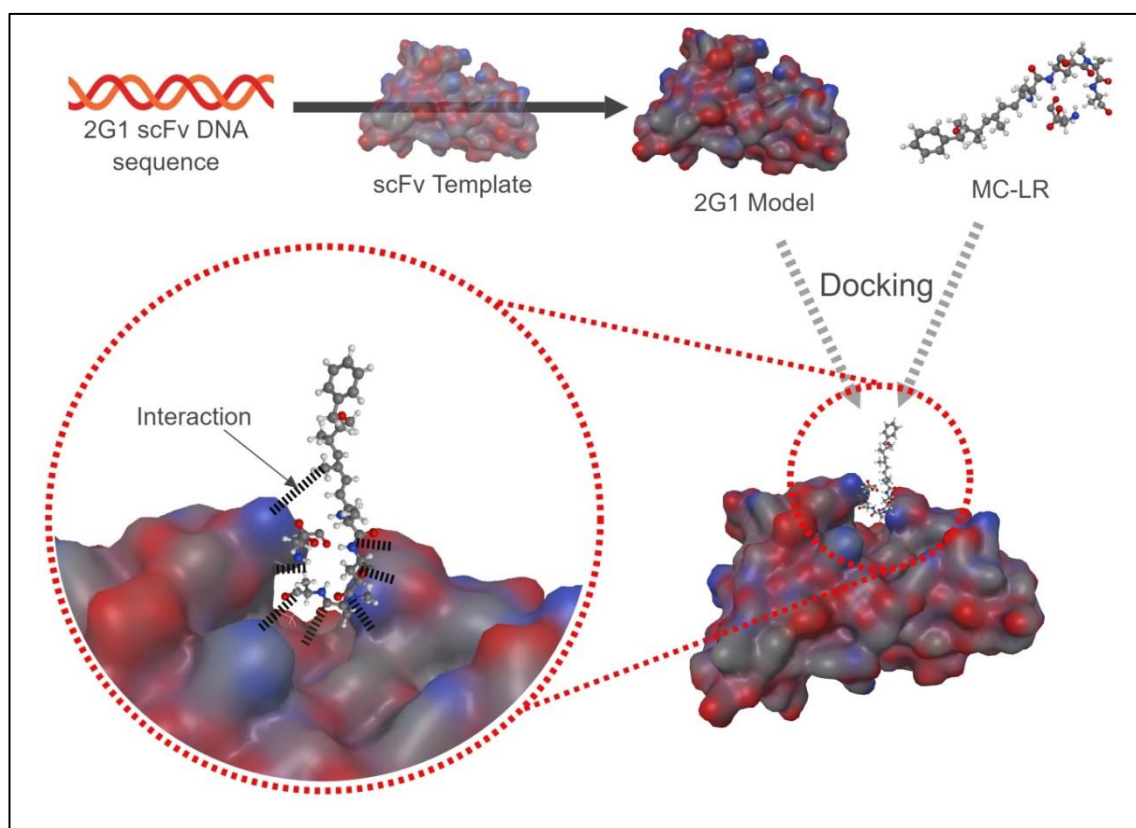


Figure 4.1: Concept of the approach used in this work. The 2G1 scFv DNA sequence was uploaded to SwissModel and, using a scFv template, a 2G1 model was developed. Next, using a combination of CASTp and AutoDock, the MC-LR structure was docked into a putative binding pocket of 2G1. This allowed for observation of potential interactions between the toxin and amino acids (AAs) in the binding pocket. In order to elucidate the nature of these interactions, these AAs were targeted for mutation by alanine scanning.

In addition to identifying important AA residues in the antigen-binding site, it was the aim of the second part of this chapter (Section 4.5) to improve the stability and

solubility of the 2G1 scFv. The 2G1 scFv is a viable antibody to incorporate onto a number of *in situ*, water-monitoring biosensor platforms to tests for the presence of MCs in water, as was discussed earlier. One of the aims of this chapter was to improve the shelf-life of the antibody to facilitate long-term deployment of biosensors that incorporate this antibody. In addition, much literature has discussed the benefits of enhanced protein stability and solubility leading to better performance in different matrices, which is an important consideration given the environmental monitoring application of this antibody. A potential added benefit of improving the protein stability and solubility is the potential to improve protein expression yields, which has important cost benefits for protein manufacturing.

A large number of previously published articles were investigated in order to determine the most frequently occurring beneficial mutations to improve protein stability. The most common stability- and/or solubility-enhancing mutations were hydrophobic-to-hydrophilic mutations of surface exposed hydrophobic residues. It was evident in a number of reports that the hydrophilic residues most commonly used for substitution were arginine and aspartic acid (see Section 1.5.2). In order to identify putative surface-exposed hydrophobic residues on the 2G1 scFv surface, the 2G1 3D model developed in the first part of the chapter was analysed and three surface-exposed hydrophobic residues were identified; L124, L153 and I255. These residues were each substituted with arginine and aspartic acid, creating six mutant clones each with single point mutations. To determine if these mutations had any deleterious effect on the binding to the 2G1 antigen, MC-LR, indirect and competitive ELISAs were carried out to determine the binding affinity of each mutant. These mutations were also investigated to elucidate the effect on protein expression and purification. Unfortunately, none of the mutations appeared to improve the overall protein yield, however, a number of mutations, in particular the mutation L153D, appeared to greatly reduce the aggregation propensity of the antibody mutants versus the wild type. In addition, experiments were carried out to measure the effect of the mutations on native and non-native solubility but it was determined that none of the mutations improved upon the solubility of the wild type. Finally, experiments were performed to determine the effect of the mutations on the functional stability of the scFv, i.e. if the scFv could retain binding-ability after treatment to denaturing conditions. Interestingly, three of the tested mutants, L124D, L124R and L153R exhibited improved thermal stability versus the wild type. In future

experiments, the individual mutations should be combined to develop double and triple mutant clones in order to determine if the hydrophilic mutations could exhibit cumulative benefits to antibody stability and solubility.

4.2 Results – Binding Site Optimisation

This results section describes the optimisation work carried out on the 2G1 scFv binding site. In Section 4.2.1, the results of *in silico* work for identifying the putative binding site are presented. In Section 4.2.2, the results of the *in vitro* mutagenesis for elucidating the role of each AA residues are presented.

4.2.1 Identification of the potential 2G1 binding site and associated binding residues

4.2.1.1 *In silico* modelling of 2G1 scFv using SwissModel and CASTp

SwissModel was used to generate a 3D model of 2G1. This model was based on the crystal structure PDB: 4p48.1.A, an avian anti-cardiac troponin I scFv. This scFv shared high sequence homology with the 2G1 sequence, with a value of 85.41% homology, which suggests that the generated model should be reliable for further computational analysis (Roy *et al.*, 2017). CASTp was used to predict the location of putative binding pockets on the scFv molecule, as this server provides identification and measurements of surface accessible pockets of proteins and can be used to guide protein-molecule interactions. The MC-LR 3D structure has a solvent accessible surface area (SASA) of 1240.0 Å². The largest pocket identified by CASTp located has a SASA of 479.6 Å². Therefore, this pocket was chosen for molecular docking, as it was the most viable to accommodate the MC-LR structure.

4.2.1.2 Molecular Docking of MC-LR into 2G1 scFv using AutoDock

After CASTp was used to identify the potential binding pocket, 3D docking of MC-LR into the CASTp-predicted pocket was carried out using AutoDock Vina. The highest ranked docking pose was chosen as this represents the most probable binding conformation. The binding energy of the highest ranked docking pose was -7.8 kcal/mol. The AutoDock Tools program was used to display the binding site interactions of this highest ranked docking pose, specifically displaying AA residues of the 2G1 wild type scFv that were in close contact and that shared hydrogen bonds with

MC-LR. The ‘van der Waals scaling factor’ was kept at the default setting of 1.00. The result of this displayed the following AA residues; L-Y49, L-P55, L-S56, L-D57, H-L2, H-Y32, H-E101 and H-E102. Figure 4.2 shows these residues in context to the CDRs of the 2G1 sequence. Figure 4.3 below and the videos in the supplementary material present these residues in close contact to MC-LR in the lowest energy docked pose. Following docking of MC-LR into 2G1, the shortest distances between the identified 2G1 residues and the MC-LR structure were measured (see Table 4.1).

L																				H																			
1	2	3	4	5	6	7	8	9	10	11	12	13	14	15	16	17	18	19	20	1	2	3	4	5	6	7	8	9	10	11	12	13	14	15	16	17	18	19	20
Q	A	A	L	T	Q	P	S	S	-	V	S	A	N	L	G	G	T	V	E	A	<u>L</u>	T	L	D	E	S	G	G	G	L	Q	T	P	G	G	A	L	S	L
21	22	23	24	25	26	27	28	29	30	31	32	33	34	35	36	37	38	39	39A	21	22	23	24	25	26	27	28	29	30	31	32	33	34	35	36	37	38	39	40
I	T	C	<u>S</u>	<u>G</u>	<u>G</u>	<u>S</u>	-	-	-	<u>N</u>	<u>N</u>	<u>Y</u>	<u>G</u>	W	Y	Q	Q	K	S	V	C	K	G	S	<u>G</u>	<u>F</u>	<u>T</u>	<u>F</u>	<u>S</u>	<u>S</u>	<u>Y</u>	<u>N</u>	<u>M</u>	<u>G</u>	W	V	R	Q	A
40	41	42	43	44	45	46	47	48	49	50	51	52	53	54	55	56	57	58	59	41	42	43	44	45	46	47	48	49	50	51	52	52A	53	54	55	56	57	58	59
P	G	S	A	P	V	T	V	I	<u>Y</u>	<u>Q</u>	<u>N</u>	<u>T</u>	<u>K</u>	<u>R</u>	<u>P</u>	<u>S</u>	<u>D</u>	I	P	P	G	K	G	L	E	F	V	A	<u>S</u>	<u>I</u>	<u>D</u>	<u>K</u>	<u>T</u>	<u>G</u>	<u>S</u>	<u>R</u>	<u>T</u>	<u>W</u>	<u>Y</u>
60	61	62	63	64	65	66	67	68	69	70	71	72	73	74	75	76	77	78	79	60	61	62	63	64	65	66	67	68	69	70	71	72	73	74	75	76	77	78	79
S	R	F	S	G	A	L	S	G	S	T	V	T	L	T	I	T	G	V	Q	<u>G</u>	<u>A</u>	<u>A</u>	<u>V</u>	<u>K</u>	<u>G</u>	R	A	T	I	S	R	D	N	G	Q	S	T	V	R
80	81	82	83	84	85	86	87	88	89	90	91	92	93	94	95	95A	96	97	98	80	81	82	82A	82B	82C	83	84	85	86	87	88	89	90	91	92	93	94	95	96
A	E	D	E	A	V	Y	F	C	<u>A</u>	<u>K</u>	<u>F</u>	<u>D</u>	<u>G</u>	<u>S</u>	<u>T</u>	<u>D</u>	<u>D</u>	<u>L</u>	F	L	H	L	N	N	L	R	P	E	D	T	A	I	Y	Y	C	A	K	<u>G</u>	<u>N</u>
99	100	101	102	103	104	105	106	107	97	98	99	100	101	102	103	104	105	106	107	108	109	110	111	112	113														
G	A	G	T	T	L	T	V	L	<u>I</u>	<u>N</u>	<u>I</u>	<u>E</u>	<u>E</u>	W	G	H	G	T	E	V	I	V	S	S															

Figure 4.2: 2G1 scFv sequence highlighting the CDRs and putative binding residues. The 2G1 scFv was numbered and the CDR residues were identified according to Kabat numbering. L = Light chain; H = Heavy chain. CDRL1 = blue, CDRL2 = green, CDRL3 = light green, CDRH1 = light orange, CDRH2 = dark orange, CDRH3 = red, and the residues identified by AutoDock are underlined.

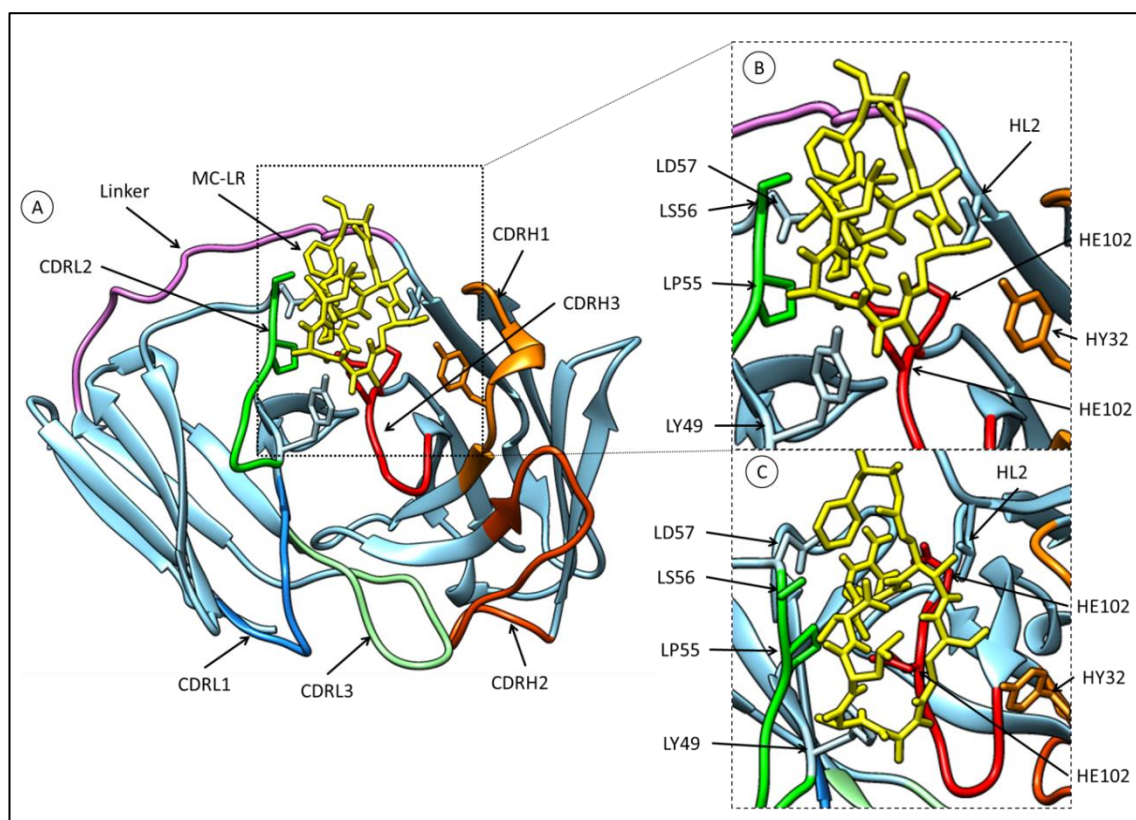


Figure 4.3: 3D structure of the 2G1 scFv in complex with MC-LR. A = highest ranked docking pose of MC-LR (yellow) docked into binding site of 2G1. B = zoomed in image of A with the investigated AAs labelled. C = 90° rotation of B. The antibody residues in closest contact with MC-LR are labelled and the atoms are shown in the stick depiction. The regions were designated as follows: CDRL1, blue; CDRL2, green; CDRL3, light green; CDRH1, light orange; CDRH2, dark orange; CDRH3, red, and the linker as pink. Images were generated using UCSF Chimera 1.12 (Pettersen *et al.*, 2004).

Table 4.1: This table shows the region of each identified residue. The shortest distances of each residue from MC-LR according to the highest ranked docking pose are also shown. Residue nomenclature: For each residue, the first letter, L or H, refers to the light or heavy chain, respectively. The letter following this refers to the AA code and the number designates the residue's position. FR = Framework region; CDR = complementarity determining region.

Residue	Region	Distance (Å)
L-Y49	FRL2	1.98
L-P55	CDRL2	3.41
L-S56	CDRL2	2.75
L-D57	FRL3	2.15
H-L2	FRH1	3.29
H-Y32	CDRH1	3.49
H-E101	CDRH3	3.55
H-E102	CDRH3	2.53

4.2.2 *In vitro* targeted mutagenesis of 2G1

To investigate the importance of each of the identified binding pocket residues, they were each in turn substituted to alanine. Alanine has been shown to have the highest helix propensity of the 20 standard AAs (Pace and Scholtz, 1998) and, therefore, alanine mutations should have minimal effects on the stability and structural integrity as compared to the wild type protein (Ni *et al.*, 2011). In addition to alanine mutations, mutations were made to L-D57 and H-E102 in order to determine the mode of interaction at these locations. These residues were chosen for further analysis due to the structural similarity shared between aspartic acid and glutamic acid with asparagine and glutamine, respectively, but the latter residues have a neutral charge at physiological pH. These mutations were carried out to determine if any electrostatic interactions were occurring at these positions. When it was determined that L-D57 was not playing any role in direct binding of the MC-LR antigen (as shown in Figure 4.7), an L-D57Y mutation was carried out in an attempt to improve the binding towards MC-LR, as tyrosine has been shown to greatly contribute to antigen-binding, allowing for a number of favourable binding interactions, such as hydrophobic and hydrogen bonding interactions (see Section 4.3). The targeted mutagenesis of the 2G1 scFv was confirmed by Sanger Sequencing (see Figure 4.4).

E247Q	MKKTAIAIAVALAGFATVAQAALTOPSSVSANLGGTVEITCSGGSNMYGHWYQQKSPGSAP	60
D73Y	MKKTAIAIAVALAGFATVAQAALTOPSSVSANLGGTVEITCSGGSNMYGHWYQQKSPGSAP	60
D73N	MKKTAIAIAVALAGFATVAQAALTOPSSVSANLGGTVEITCSGGSNMYGHWYQQKSPGSAP	60
E247A	MKKTAIAIAVALAGFATVAQAALTOPSSVSANLGGTVEITCSGGSNMYGHWYQQKSPGSAP	60
E246A	MKKTAIAIAVALAGFATVAQAALTOPSSVSANLGGTVEITCSGGSNMYGHWYQQKSPGSAP	60
Y174A	MKKTAIAIAVALAGFATVAQAALTOPSSVSANLGGTVEITCSGGSNMYGHWYQQKSPGSAP	60
L144A	MKKTAIAIAVALAGFATVAQAALTOPSSVSANLGGTVEITCSGGSNMYGHWYQQKSPGSAP	60
D73A	MKKTAIAIAVALAGFATVAQAALTOPSSVSANLGGTVEITCSGGSNMYGHWYQQKSPGSAP	60
S72A	MKKTAIAIAVALAGFATVAQAALTOPSSVSANLGGTVEITCSGGSNMYGHWYQQKSPGSAP	60
P71A	MKKTAIAIAVALAGFATVAQAALTOPSSVSANLGGTVEITCSGGSNMYGHWYQQKSPGSAP	60
2G1wt	MKKTAIAIAVALAGFATVAQAALTOPSSVSANLGGTVEITCSGGSNMYGHWYQQKSPGSAP	60

E247Q	VTVIYQNTKRPSDIPSRFSGALSGSTVTLTITGVQAEDEAVYFCAKFDGSTDDLFGAGTT	120
D73Y	VTVIYQNTKRPSYIPSRFSGALSGSTVTLTITGVQAEDEAVYFCAKFDGSTDDLFGAGTT	120
D73N	VTVIYQNTKRPSNIPSRFSGALSGSTVTLTITGVQAEDEAVYFCAKFDGSTDDLFGAGTT	120
E247A	VTVIYQNTKRPSDIPSRFSGALSGSTVTLTITGVQAEDEAVYFCAKFDGSTDDLFGAGTT	120
E246A	VTVIYQNTKRPSDIPSRFSGALSGSTVTLTITGVQAEDEAVYFCAKFDGSTDDLFGAGTT	120
Y174A	VTVIYQNTKRPSDIPSRFSGALSGSTVTLTITGVQAEDEAVYFCAKFDGSTDDLFGAGTT	120
L144A	VTVIYQNTKRPSDIPSRFSGALSGSTVTLTITGVQAEDEAVYFCAKFDGSTDDLFGAGTT	120
D73A	VTVIYQNTKRPSAIPSRFSGALSGSTVTLTITGVQAEDEAVYFCAKFDGSTDDLFGAGTT	120
S72A	VTVIYQNTKRPSDIPSRFSGALSGSTVTLTITGVQAEDEAVYFCAKFDGSTDDLFGAGTT	120
P71A	VTVIYQNTKRPSDIPSRFSGALSGSTVTLTITGVQAEDEAVYFCAKFDGSTDDLFGAGTT	120
2G1wt	VTVIYQNTKRPSDIPSRFSGALSGSTVTLTITGVQAEDEAVYFCAKFDGSTDDLFGAGTT	120
***** ; *****		
E247Q	LTVLGGSSGSSGGGSSGGGSSALTLDSEGGGLQTPGGALS LVCKGSGFTFSSYNMGWNR	180
D73Y	LTVLGGSSGSSGGGSSGGGSSALTLDSEGGGLQTPGGALS LVCKGSGFTFSSYNMGWNR	180
D73N	LTVLGGSSGSSGGGSSGGGSSALTLDSEGGGLQTPGGALS LVCKGSGFTFSSYNMGWNR	180
E247A	LTVLGGSSGSSGGGSSGGGSSALTLDSEGGGLQTPGGALS LVCKGSGFTFSSYNMGWNR	180
E246A	LTVLGGSSGSSGGGSSGGGSSALTLDSEGGGLQTPGGALS LVCKGSGFTFSSYNMGWNR	180
Y174A	LTVLGGSSGSSGGGSSGGGSSALTLDSEGGGLQTPGGALS LVCKGSGFTFSSYNMGWNR	180
L144A	LTVLGGSSGSSGGGSSGGGSSAALTLDSEGGGLQTPGGALS LVCKGSGFTFSSYNMGWNR	180
D73A	LTVLGGSSGSSGGGSSGGGSSALTLDSEGGGLQTPGGALS LVCKGSGFTFSSYNMGWNR	180
S72A	LTVLGGSSGSSGGGSSGGGSSALTLDSEGGGLQTPGGALS LVCKGSGFTFSSYNMGWNR	180
P71A	LTVLGGSSGSSGGGSSGGGSSALTLDSEGGGLQTPGGALS LVCKGSGFTFSSYNMGWNR	180
2G1wt	LTVLGGSSGSSGGGSSGGGSSALTLDSEGGGLQTPGGALS LVCKGSGFTFSSYNMGWNR	180
***** *****		
E247Q	QAPGKLEFVASIDKTGSRTWYGAAVKGRATISRDNQSTVRLHLNLRP EDTAIYYCAK	240
D73Y	QAPGKLEFVASIDKTGSRTWYGAAVKGRATISRDNQSTVRLHLNLRP EDTAIYYCAK	240
D73N	QAPGKLEFVASIDKTGSRTWYGAAVKGRATISRDNQSTVRLHLNLRP EDTAIYYCAK	240
E247A	QAPGKLEFVASIDKTGSRTWYGAAVKGRATISRDNQSTVRLHLNLRP EDTAIYYCAK	240
E246A	QAPGKLEFVASIDKTGSRTWYGAAVKGRATISRDNQSTVRLHLNLRP EDTAIYYCAK	240
Y174A	QAPGKLEFVASIDKTGSRTWYGAAVKGRATISRDNQSTVRLHLNLRP EDTAIYYCAK	240
L144A	QAPGKLEFVASIDKTGSRTWYGAAVKGRATISRDNQSTVRLHLNLRP EDTAIYYCAK	240
D73A	QAPGKLEFVASIDKTGSRTWYGAAVKGRATISRDNQSTVRLHLNLRP EDTAIYYCAK	240
S72A	QAPGKLEFVASIDKTGSRTWYGAAVKGRATISRDNQSTVRLHLNLRP EDTAIYYCAK	240
P71A	QAPGKLEFVASIDKTGSRTWYGAAVKGRATISRDNQSTVRLHLNLRP EDTAIYYCAK	240
2G1wt	QAPGKLEFVASIDKTGSRTWYGAAVKGRATISRDNQSTVRLHLNLRP EDTAIYYCAK	240

E247Q	GNINIEQWGHGTEVIVSSTSGQAGQH HHHH	271
D73Y	GNINIEEWGHGTEVIVSSTSGQAGQH HHHH	271
D73N	GNINIEEWGHGTEVIVSSTSGQAGQH HHHH	271
E247A	GNINIEAWGHGTEVIVSSTSGQAGQH HHHH	271
E246A	GNINIAEWGHGTEVIVSSTSGQAGQH HHHH	271
Y174A	GNINIEEWGHGTEVIVSSTSGQAGQH HHHH	271
L144A	GNINIEEWGHGTEVIVSSTSGQAGQH HHHH	271
D73A	GNINIEEWGHGTEVIVSSTSGQAGQH HHHH	271
S72A	GNINIEEWGHGTEVIVSSTSGQAGQH HHHH	271
P71A	GNINIEEWGHGTEVIVSSTSGQAGQH HHHH	271
2G1wt	GNINIEEWGHGTEVIVSSTSGQAGQH HHHH	271

Figure 4.4: Sequence alignment of the 2G1 wild type with mutants. The 2G1 wild type and each mutant were sequenced by Sanger Sequencing. Sequence alignment was performed using Clustal Omega (Sievers *et al.*, 2014). Note on nomenclature: the numbering of the AA sequence in this case is different than that of the Kabat numbering system. In this case, numbering begins from the methionine residue. For referencing to the Kabat numbering used in the bulk of the chapter: P71 = L-P55; S72 = L-S56; D73 = L-D57; L144 = H-L2; Y174 = H-Y32; E246 = H-E101; E247 = H-E102. 2G1wt = Wild type 2G1 scFv.

4.2.2.1 Evaluation of 2G1 mutant clones by Western blot and indirect ELISA

The expression of the wild type 2G1 scFv and mutants was checked qualitatively by Western blotting. Figure 4.5 shows that, with the exception of scFv L-Y49A, all clones were expressed. Interestingly, a band at ~55 kDa was observed for clone L-Y49A (data not shown). This clone was tested repeatedly for expression of the encoded scFv, but as the scFv could not be detected by Western blotting and by indirect ELISA (Figure 4.6), this clone was omitted from further testing. It is possible that this mutation led to instability of the scFv molecule and caused aggregation to occur. The binding of the wild type 2G1 scFv and the 2G1 mutants to MC-LR was determined by indirect ELISA. Figure 4.6 shows the binding of each clone to MC-LR over a series of lysate dilutions. A 'cut-off' was established as three times the mean of the negative control (i.e. the lowest signal that can be distinguished from the background). The titre for each scFv clone lysate was determined as the dilution factor that produced an absorbance value equal to the 'cut-off'. The titres of 2G1 wild type and mutants are presented in Table 4.2. The indirect ELISAs were carried out for each antibody in order to determine a dilution that should produce an absorbance value of 1; this dilution was then used for competitive ELISAs.

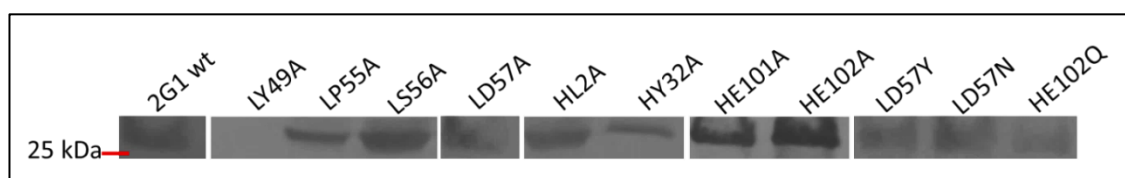


Figure 4.5: Western blot of 2G1 scFv wild type and mutant lysates. The 27 kDa scFv was observed in the lysates of all clones except clone L-Y49A. The position of the 25 kDa band of the molecular weight ladder is indicated by the red mark.

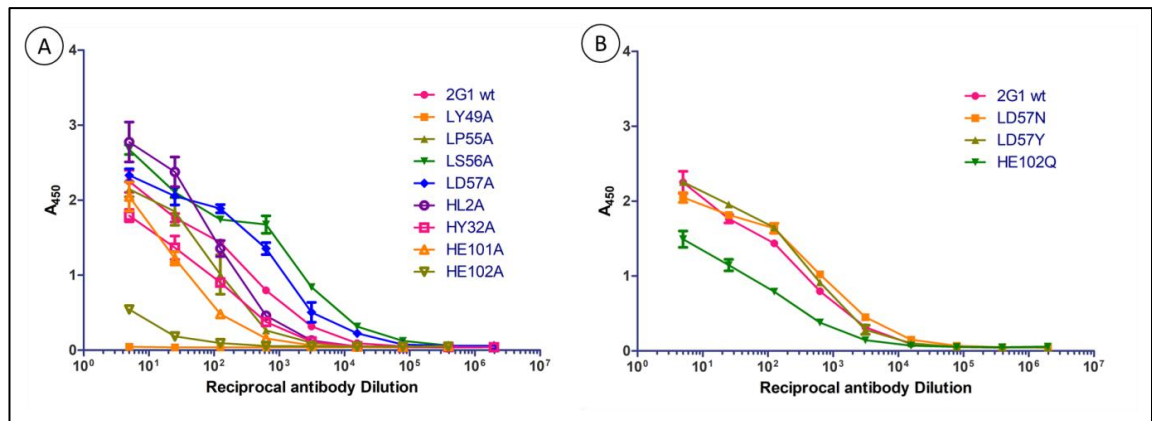


Figure 4.6: Indirect ELISA comparing the binding profiles of 2G1 wild type and 2G1 alanine mutant lysates (A) and the 2G1 special case mutants (B). The wells of a multiwell plate were coated with 5 µg/mL MC-LR-BSA. For each clone, the lysate was diluted from 1:5 to 1:1.95 x 10⁶. The negative control and ‘cut-off’ were not presented so as to improve clarity of the images. The negative control consisted of all test components but omitted the bacterial lysate. The ‘cut-off’ was determined as three times the value of the negative control. Error bars represent the standard error of the mean (SEM) (n = 3).

Table 4.2 Titres of 2G1 wild type and mutant lysates as determined by indirect ELISA. The titre values were determined as the dilution factors that produced an absorbance value equal to the ‘cut-off’ (i.e. the lowest signal that can be distinguished from background).

Clone	Titre
2G1 wild type	1:50,000
L-Y49A	N/A
L-P55A	1:41,000
L-S56A	1:1.9 x 10 ⁶
L-D57A	1:110,000
H-L2A	1:26,000
H-Y32A	1:50,000
H-E101A	1:2,600
H-E102A	1:275
L-D57N	1:75,000
L-D57Y	1:78,000
H-E102Q	1:15,000

4.2.2.2 Comparison of the 2G1 wild type and mutants by competitive ELISA

In order to more accurately compare the binding responses of the wild type 2G1 scFv and the mutant clones, competitive ELISAs were carried out on each antibody lysate. Figure 4.7 below show the response of each clone at a fixed lysate dilution with a range of concentrations of free MC-LR, from 5,000 to 0.76 ng/mL. The IC_{50} of each clone is compared in Table 4.3.

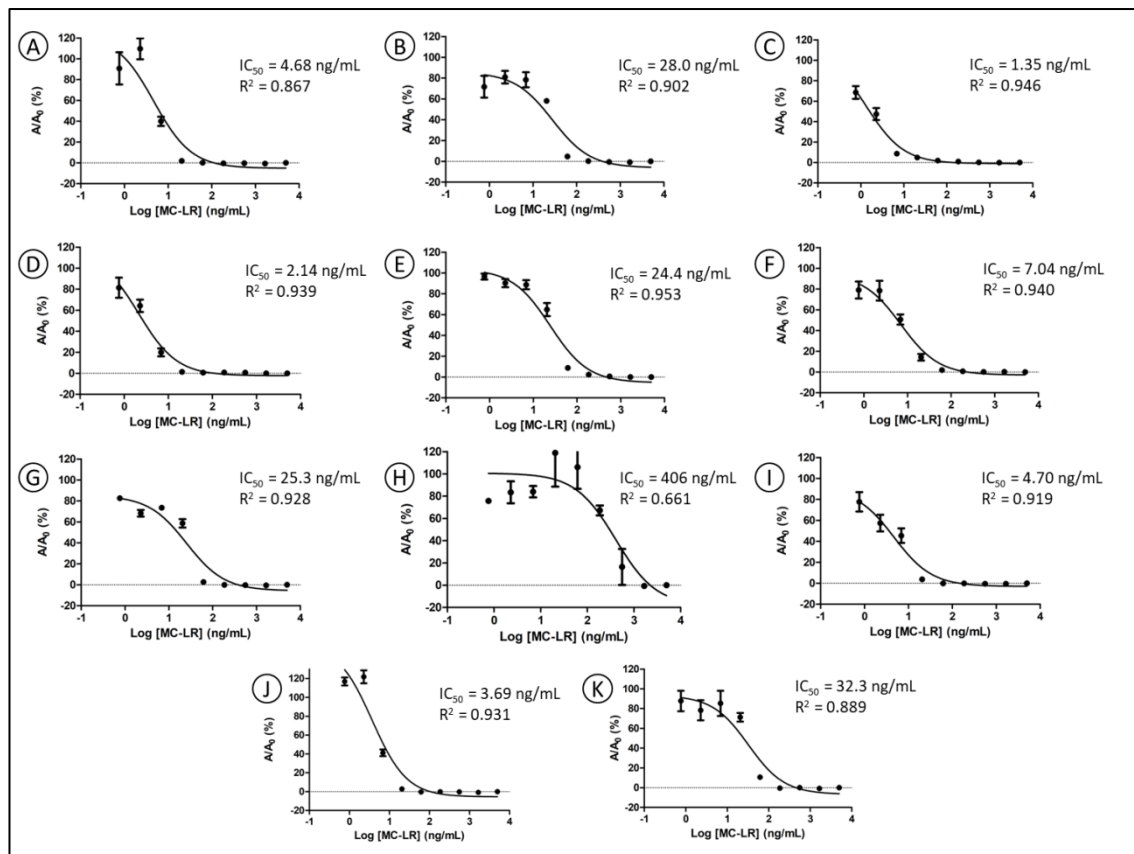


Figure 4.7: Competitive ELISAs of 2G1 wild type and mutants. The wells of a multiwell plate were coated with 5 μ g/mL MC-LR-BSA. The lysates of each antibody clone were diluted such that they should produce an absorbance value ≈ 1 . The diluted lysates were mixed 1:1 with free MC-LR that was diluted to concentrations ranging from 5,000 to 0.76 ng/mL. Following this, the lysate-free MC-LR mixtures were applied to the multiwell plate. Error bars represent the standard error of the mean (SEM) ($n = 3$). A = 2G1 wild type; B = L-P55A; C = L-S56A; D = L-D57A; E = H-L2A; F = H-Y32A; G = H-E101A; H = H-E102A; I = L-D57N; J = L-D57Y; K = H-E102Q.

Table 4.3: Comparison of IC₅₀ values for the 2G1 wild type and mutants. Relative affinity was calculated as the IC₅₀ value of the wild type divided by that of the clone, multiplied by 100. Clones that are of particular note are marked by an asterisk (*).

Clone	IC ₅₀ (ng/mL)	Relative affinity (%)
2G1	4.68	100
L-P55A	28.0	16.7
L-S56A	1.35	347*
L-D57A	2.14	219*
H-L2A	24.4	19.2
H-Y32A	7.04	66.5
H-E101A	25.3	18.5
H-E102A	406	1.2*
L-D57N	4.70	99.6
L-D57Y	3.69	127
H-E102Q	32.3	14.5

4.3 Discussion – Binding Site Optimisation

In this work, the anti-MC-LR scFv 2G1 was modelled using SwissModel and the crystal structure of a chicken scFv was used as a template. A putative binding pocket was identified using the CASTp server, which is a freely available online server that readily identifies and measures the SASA of protein pockets. In this case, it identified the largest pocket of 2G1 with a SASA of 480 Å², which appeared to be the most viable pocket to accommodate the MC-LR structure, which has a SASA of 1240 Å². This putative binding pocket was then targeted as the docking site for the 3D structure of MC-LR. AutoDock Vina was used for docking as it is a highly cited, freely available docking software package and has proven to be a valuable tool for researchers, guiding investigations into protein-protein and protein-compound interactions (Shityakov and Forster, 2014; Li *et al.*, 2016). While there is a considerable learning curve associated with this software package, with the use of methods papers such as Huey *et al.* (2012) and the video tutorial by Trott (2012), AutoDock Vina is relatively accessible for the first-time user and can provide highly useful information about the binding interaction between a protein and ligand and the orientation of the ligand within the protein's

binding pocket. AutoDock Vina was used to identify the amino acids in closest contact with MC-LR, based on the highest ranked docking pose. The role of each of these residues was subsequently investigated *in vitro* through the use of targeted mutagenesis, bacterial expression, and the analysis of the mutant clones by ELISA and Western blotting.

It was decided to use non-purified bacterial lysates for testing each mutation. The results of the competitive ELISA for the 2G1 wild type showed that the IC₅₀ value for this lysate (IC₅₀ = 4.68 ng/mL) was consistent with the reported IC₅₀ of the purified antibody, as reported by Murphy *et al.*, (2015) (IC₅₀ = 4.80 ng/mL) and also according to the authors' own testing of this purified antibody (data not shown). In addition, it was shown elsewhere that avian antibody libraries can be efficiently screened, even when present in crude bacterial lysates (Leonard *et al.*, 2007), which suggests that the bacterial lysate may not considerably negatively impact the antibody-antigen interaction. Therefore, testing the bacterial lysates may be a reliable measure of the each antibody mutant's binding characteristics.

Figure 4.2 shows the location of each residue with respect to the CDRs (as identified by the Kabat numbering). Five out of the eight residues were situated within CDRs, specifically, CDRL2 (L-P55, L-S56), CDRH1 (H-Y32) and CDRH3 (H-E101, H-E102). The remaining three residues identified were associated with the framework regions; FRL2 (L-Y49), FRL3 (L-D57) and FRH1 (H-L2). Binding residues from non-CDRs is not uncommon. In the study by Osajima *et al.*, (2014), for antibody-antigen complexes, direct H bonds from non-CDR residues were observed in 6 out of 20 complexes, and for one of these complexes, between Mouse IgG1 κ and Streptococcal Protein G, all direct H bonds were from non-CDR residues.

The importance of non-CDR residues was also observed by Murphy *et al.*, (2015) who also modelled this scFv 2G1 using a murine anti-interleukin (IL)-1 β scFv template (PDB code: 2KH2B) and, using the Maximum Entropy based Docking (MEdock) program, determined that residue H-R66 (which resides in FR3) was important for binding to MC-LR, however, it was not fully determined if this residue played a direct antigen-binding role or a secondary, structural role of the antibody. It is interesting that in this current study, H-R66 was not identified by AutoDock Vina. A potential reason for this is due to the different antibody templates used for modelling 2G1, which could

easily have led to a different 3D structure being generated. In addition, the cavity on the protein surface differed to that investigated in this study. In that study, when observing that the docked pose of MC-LR appears to reside in close contact primarily with the heavy chain, this highlights the effect that different templates (and hence 3D model structures) and docking approaches can have. Another possible explanation for this is that perhaps H-R66 is indeed playing more of a role in the overall 3D conformation of the antibody structure and less of a direct antigen-binding role. Thus, the beneficial H-R66S mutation that was observed by Murphy *et al.* (2015), which is a change from a bulky positively charged side chain to a less bulky uncharged side chain, may have allowed for better conformational stability of the scFv structure. It was noted elsewhere that serine allows for space and conformational flexibility, and plays an auxiliary role in allowing for productive contacts between other residues and the antigen (Bogan and Thorn, 1998; Fellouse *et al.*, 2004). It should be noted that the primary focus of the work of Murphy *et al.* (2015) was on the optimisation of 2G1 for use in an *in situ* biosensor and less on the specific role of the AA residue in binding; the focus of this work, however, is to elucidate the role of each identified AA in the scFv-toxin interaction through use of alanine scanning. In the following sub-sections, the role of each identified AA will be discussed and the potential nature of each interaction will be suggested.

4.3.1 The role of tyrosine

When observing the identified AA residues in 2G1, it is perhaps unsurprising that tyrosine was well represented in the binding site of 2G1, accounting for 25% of the identified residues. Tyrosine is highly abundant in antigen-binding sites, accounting for ~10% of the total CDR composition and for ~25% of antigen contacts (Mian *et al.*, 1991). In their paper, compiling a database of alanine-scanning studies of protein-protein interactions, Bogan and Thorn (1998) observed that tryptophan, tyrosine, arginine and aspartic acid (with 3.91-, 2.47-, 2.29- and 1.67-fold enrichment over the database as whole, respectively) were much more likely to be located in interaction ‘hot-spots’ than valine, leucine and serine (with fold enrichment values of 0, 0.01 and 0.21, respectively). Energetically-unimportant residues, however, can serve a purpose in occluding the bulk solvent from the binding interface. Osajiima *et al.*, (2014) analysed 20 antibody crystal structures and identified that tyrosine has the second highest appearance in CDR loops, after serine. Tyrosine has the capacity for the formation of

the highest number of hydrogen bond, followed by asparagine, aspartic acid, and serine. The average number of direct H bonds for protein-protein interactions was 15.0 ± 7.8 (st. dev.). For protein-compound interactions there are far fewer H bonds (e.g. 5-9 direct H bonds between HIV-1 protease and its inhibitors (Leonis *et al.*, 2013)) which is due to the comparatively smaller contact area. Tyrosine is capable of making multiple types of favourable interactions; it offers a hydrophobic surface, it can form aromatic π -interactions and it can form non-polar H bonds via its 4-hydroxyl group. Its rigidity can also be an advantage because a small loss in conformational entropy occurs when a side chain is immobilised in the binding interface. The rigidity may also contribute to specificity, as tyrosine-rich interfaces are less likely to accommodate non-specific interactions (Koide and Sidhu, 2009).

According to the highest ranked docking model generated in AutoDock Vina, the hydroxyl group of L-Y49 (FRL2) is 1.98 Å from the H atom of the D-Alanine group of MC-LR. This distance should allow for short range H bonding. Unfortunately, the role of L-Y49 could not be elucidated by *in vitro* testing, due to the unsuccessful expression of this mutant. Further, Western blot analysis showed a band at ~55 kDa (data not shown), which may constitute an aggregated form of the scFv. This L-Y49A mutation may inhibit native protein expression or it may have caused a loss in conformational stability, which in turn may cause the formation of aggregates. Paul *et al.* (2017) showed that single point mutations can lead to profound changes in aggregation propensity. Sanjeev and Mattaparthi (2017) observed that in Parkinson's disease, a Y39A mutation of α -synuclein accelerates protein aggregation whereas a Y133A mutation slows down the aggregation, highlighting the capacity of a tyrosine single point mutation to alter a protein's structure. In any case, further work is required to fully elucidate the role of L-Y49 in the 2G1-MC-LR interaction.

With respect to other identified residues in the putative 2G1 binding pocket, H-Y32 (CDRH1) appeared to play a comparatively minor role in the binding of MC-LR. The H-Y32A mutation resulted in a relatively small change in the relative affinity with a drop to 66.5%. This suggests that H-Y32 may be interacting with MC-LR via weak H bonding or, given the distance of 3.49 Å between this residue and the toxin, perhaps H-Y32 is interacting via water-mediated indirect H bonds. However, as with L-Y49,

further work is required to fully elucidate the binding interaction between L-Y32 and MC-LR.

4.3.2 L-P55 appears to maintain 2G1 tertiary structure

The appearance of proline in a potential antigen-binding ‘hot-spot’ is not surprising, given its reported 1.25-fold enrichment in the ‘hot-spot’ database compiled by Bogan and Thorn (1998). It is well established that proline is important for protein-protein interactions, with proline-rich regions appearing in the Src homology 3 (SH3) domain of the intracellular signalling proteins Src and Abl (Weng *et al.*, 1995) and in the ligase Itch (Desrochers *et al.*, 2017). While Desrochers *et al.* (2017) showed that the proline-rich region of the Itch protein can interact with numerous target residues via hydrophobic interactions, salt bridges and H bonds, however, at a distance of 3.41 Å from MC-LR, it is unlikely that L-P55 is interacting via H bonds. The result of the competitive ELISA for L-P55A (CDRL2) showed a decrease in relative affinity to 16.7% versus the wild type. A similar loss of function was observed by Consler *et al.* (1991), in which they showed that in *lac* permease of *E. coli* a P28A mutation abolishes lactose transport through the membrane protein. In 2G1, L-P55 could play more of a role in the tertiary structure, restricting backbone flexibility (Adib-Conquy *et al.*, 1998), forming molecular hinges (Ni *et al.*, 2011), stabilising the scaffolding motifs (Augustine *et al.*, 2001), or allowing binding residues to be better orientated to bind to MC-LR.

4.3.3 L-S56 and L-D57 appear to sterically hinder the antibody-toxin interaction

The result of the L-S56A (CDRL2) mutation appears to have improved upon the antigen-binding of the 2G1 wild type, with a change in relative affinity to 347%. This result suggests that L-S56 was not well optimised in this position in the wild type. While it has been noted in several studies that serine is highly abundant in natural antigen-binding sites, it rarely makes direct contacts with the antigen (Bogan and Thorn, 1998; Fellouse *et al.*, 2004), and, as was discussed earlier in this section, serine can allow for greater space and conformational flexibility. In the current situation for the 2G1 residue L-S56, it is likely that the residue was not engaging in direct contact with the antigen and may have allowed for flexibility, however, the AA side chain may have sterically hindered the arginine residue of MC-LR. The mutation from serine to alanine would retain flexibility and would effectively remove the AA side chain and thus would

allow for greater space for antigen docking, thereby improving the binding to the toxin (Koide and Sidhu, 2009).

In a similar way to L-S56, L-D57 (FRL3) appeared to be poorly optimised in its position in the wild type scFv, as a mutation to alanine resulted in a change in relative affinity to 219%. It was reported by Fellouse *et al.* (2004) that Asp residues within CDRs were not observed to make many antigen contacts, being almost entirely excluded from the binding interface, with less than 10% making contact with the antigen (as compared to tyrosine, which ~50% made contact with the antigen). However, the nearby, structurally related H-E102 was shown to be critical for binding, probably via electrostatic interactions with the Arg residue of MC-LR, L-D57 was shown to be deleterious to the scFv's interaction with MC-LR. It is possible that the carboxylate group of L-D57 in this instance is unprotonated, which is generally accepted as ineffective for binding (Leonis, 2013) and, hence, the side chain may have sterically hindered efficient docking of MC-LR into the binding site, as was possible for the adjacent L-S56. This proposition was further backed up by the mutation L-D57N. Asparagine was chosen as it is the most structurally similar AA to aspartic acid but has no charge at physiological pH (Popovic *et al.*, 2017). The relative affinity for this mutant was 99.6%. This result shows that even by changing the charge of the molecule from negative to neutral there was no effect on the binding capacity compared to the wild type. This finding could support the possibility of L-D57 not being protonated, which means that L-D57 would not be able to engage in any electrostatic interactions with MC-LR. When it was observed that L-D57 was playing no direct role in antigen-binding, it was attempted to improve the binding to MC-LR through the mutation of L-D57 to tyrosine. While this appeared to result in an improvement in relative affinity to 127%, it did not surpass the improvement observed from the L-D57A mutation. This suggests that alleviating the steric hindrance at this location was more beneficial than introducing a new functional side chain to the region.

4.3.4 H-L2 appears to engage in a hydrophobic interaction with MC-LR

The mutation implemented at position H-L2 (FRH2) suggests that this leucine residue indeed plays a role in binding MC-LR, albeit a less critical role than H-E102, as discussed below. The H-L2A mutation resulted in a drop in relative affinity to 19.2%. It is possible that H-L2 is interacting with the benzene ring of MC-LR via hydrophobic

interactions. Carter *et al.* (1999) showed that leucine plays an important role in the binding between Type-1 Parathyroid Hormone (PTH) Receptor and PTH. Mutations of this residue to hydrophilic residues caused a 20-fold weakening of the response, suggesting hydrophobic interactions were involved. In addition, Kim *et al.* (2016) observed that a leucine residue of B-cell receptor associated protein 31 (BAP31) appeared to interact with a phenylalanine side chain of a monoclonal antibody (MAb), establishing a hydrophobic interaction. Perhaps the evidence that would most back up this potential interaction can be interpreted from the crystal structure of PP2A in complex with MC-LR Cho and Xu (2007). The crystal structure (PDB code: 2IAE) shows that the benzene ring of MC-LR appears to reside in a hydrophobic pocket of PP2A, which is made up of tryptophan 200 and isoleucine 123 of the PP2A catalytic domain. Therefore, with the structural similarity between isoleucine and leucine, it is plausible that H-L2 of 2G1 is interacting via hydrophobic interactions with the benzene ring of MC-LR.

4.3.5 The critical role of glutamic acid

The appearance of two simultaneous glutamic acid residues in 2G1 is interesting. Osajima *et al.* (2016) showed that in 20 analysed antibody-antigen interactions (PDB crystal structures), of all the charged, polar AA residues, glutamic acid appears the least frequently, with the highest average appearance of 3% found in CDRH2, and with the average appearance of 1.0% in CDRH3. Bogan and Thorn (1998) observed a 0.68-fold enrichment of glutamic acid in ‘hot-spots’. This would suggest that the appearance of two tandem glutamic acid residues in CDRH3 is rare. It may be speculated that this occurrence could be due to the nature of the target antigen, MC-LR, with its positively charged arginine residue; hence a highly negatively charged core of the antibody binding pocket would be optimal for interacting with such a target.

The mutation H-E101A (CDRH3) had a similar effect on relative affinity as the L-P55A and H-L2A mutations, resulting in a drop of relative affinity to 18.5%. However, due to the 3.55 Å distance between the H-E101 side chain and the nearest MC-LR group, the role of H-E101 in 2G1 is more likely indirect bonding with MC-LR, i.e. potentially interacting with MC-LR via a long range ion pair or water-mediated H bonding (Jeffrey, 1997; Leonis *et al.*, 2013). In addition, as was speculated above, H-E101 may contribute with H-E102 to forming a highly negatively charged core of the antibody binding

pocket, with the specific function of binding to the positively charged guanidinium group of the MC-LR arginine residue.

The result of the H-E102A (CDRH3) mutation has revealed that this residue plays a key role in the binding of MC-LR. The mutation to alanine led to a drop in relative affinity to 1.2%. It should be noted that for this competitive ELISA, the lysate was diluted to the relatively low dilution of 1/4. This was due to the fact that, despite being well expressed in this clone (see Figure 4.5), there was very low response observed in the indirect ELISA. It is likely that this poor binding and relatively high proportion of lysate contributed to the poor R^2 value of 0.661. Despite this, this is quite a considerable drop in binding with just a single AA mutation. It was shown previously that despite the potential large size of binding interfaces, it is possible that single residues can contribute a substantial portion of the binding free energy at an interface (Clarkson and Wells, 1995; Bogan and Thorn, 1998). Glutamic acid was shown to play a critical role in other protein-small molecule interactions; mutating glutamic acid 338 of ornithine 4,5-aminomutase to glutamine, aspartic acid or alanine lead to 90-, 380- and 670-fold reductions in catalytic activity, respectively (Matkin *et al.*, 2013). Kusharyoto *et al.* (2002) investigated the binding interaction between a fragment antigen-binding (Fab) and the hapten atrazine. In this Fab, H-E50 (in CDRH2) plays a key role in binding the chlorine atom of the atrazine molecule. It also interacts with an adjacent L-Y96, forming a hydrogen bond, and also forms a salt bridge with H-R52. Furthermore, in that study it was observed that mutating H-E50 to glutamine and to any other residue lead to a reduction of relative affinity to 14% and <2%, respectively, compared with the wild-type Fab. Falco *et al.* (2010) showed, through site-directed mutagenesis, that in Natural Killer cells, killer cell Ig-like receptors (KIRs) contain a glutamic acid at site 35 that is important for recognition by two mAbs. It should also be noted that when observing the crystal structure of the PP2A-MC-LR complex the arginine of MC-LR appears to share no interactions with PP2A and instead appears to reside in the bulk solution away from the PP2A structure (Cho and Xu, 2007). This was a striking difference between that PP2A-MC-LR complex and the 2G1-MC-LR complex, i.e. that the MC-LR arginine residue is not involved in binding PP2A but is critical for binding to 2G1.

In order to more fully elucidate the interaction at residue H-E102, and similar to the L-D57N mutation, a H-E102Q mutation was carried out. This mutation replaced glutamic

acid for structurally-similar glutamine, albeit with the change in the side chain's charge. Leonis *et al.* (2013) observed that in compound-protein interactions, van der Waals forces contribute more to the binding free energy than electrostatic energy. However, the result of the mutation H-E102Q would suggest the reverse is true in this case. The H-E102Q mutation would effectively remove the electrostatic interaction, but would maintain van der Waals interactions. This mutation caused a reduction in relative affinity to 14.5%, whereas the removal of both electrostatic and van der Waals interactions (i.e. the H-E102A mutation) caused a reduction in relative affinity to 1.2%. This would suggest that the electrostatic interaction was the dominant one in this position.

4.4 Future work – binding site optimisation

The work outlined in this chapter demonstrated the power of using modern computational tools and recombinant DNA techniques to investigate the interaction between an antibody and its hapten target. The findings made in this study lay a good groundwork for future investigations. In particular, the mutant clones L-S56A and L-D57A should be investigated in greater detail, i.e. further antibody characterisations should be carried out, ideally using surface plasmon resonance (SPR) analysis to accurately determine the binding kinetics of these mutants and to compare to the wild type. It would also be very useful to carry out full assay development experiments to determine how these mutations affected the dynamic range and limits of detection of the assay. Provided that these mutants display improved binding characteristics versus the wild type, they could be incorporated into biosensors (such as that reported by Murphy *et al.*, 2015) to allow for higher sensitivity detection of MC-LR in environmental settings. Furthermore, other future work should investigate the effects of multiple mutations on MC-LR-binding; for example, mutations to both L-S56 and L-D57 should be investigated to determine if further improvements in antigen-binding could be observed.

4.5 Results – stability optimisation

In this section, the results of the optimisation work on the 2G1 scFv stability and solubility are presented.

4.5.1 Amino acid residues targeted for mutation

The 2G1 scFv model was generated as described in Section 4.2.1.1. Using UCSF Chimera 1.12 software, the 2G1 model molecular surface was coloured according to the Kyte-Doolittle hydrophobicity scale. Three surface-exposed hydrophobic AA residues were identified, namely L124, L153 and I255, as illustrated in Figure 4.8 below. (Note that the numbering of these residues is based on the AA numbering starting from the methionine residue and is not based on the Kabat numbering used in Section 4.2). The three identified AA residues were each subsequently mutated to Asp and Arg by targeted mutagenesis, producing a total of six mutant clones; L124D, L124R, L153D, L153R, I255D and I255R. The DNA sequences of the six mutant clones were sequenced by Sanger sequencing, which are presented in Figure 4.9 below. The theoretical isoelectric point (pI) values for the wild type, single mutant and triple mutants were determined using the ‘Protein-Sol’ online tool (Hebditch *et al.*, 2017) and are presented in Table 4.4.

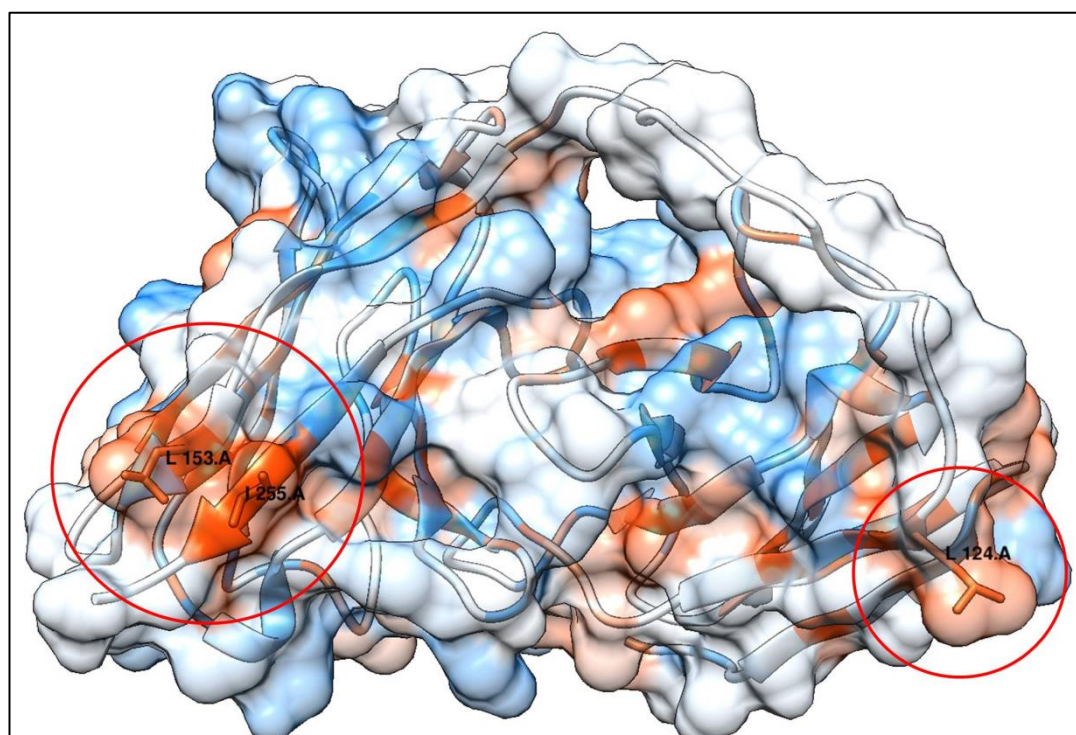


Figure 4.8: Illustration of 2G1 scFv model. The model is represented in the ribbon format and the solvent accessible surface is shown. The amino acid sequence and surface are coloured by the Kyte-Doolittle hydrophobicity scale, where hydrophilic residues are coloured blue, neutral residues are white and hydrophobic residues are orange. Labelled and circled are the three residues targeted in this study, L124, L153 and I255.

I255R	MKKTAIAIAVALAGFATVAQAL TQPSSV SANLGGTVEITCSGGSNNYGWYQQKSPGSAP	60
I255D	MKKTAIAIAVALAGFATVAQAL TQPSSV SANLGGTVEITCSGGSNNYGWYQQKSPGSAP	60
L153R	MKKTAIAIAVALAGFATVAQAL TQPSSV SANLGGTVEITCSGGSNNYGWYQQKSPGSAP	60
L153D	MKKTAIAIAVALAGFATVAQAL TQPSSV SANLGGTVEITCSGGSNNYGWYQQKSPGSAP	60
2G1wt	MKKTAIAIAVALAGFATVAQAL TQPSSV SANLGGTVEITCSGGSNNYGWYQQKSPGSAP	60
L124D	MKKTAIAIAVALAGFATVAQAL TQPSSV SANLGGTVEITCSGGSNNYGWYQQKSPGSAP	60
L124R	MKKTAIAIAVALAGFATVAQAL TQPSSV SANLGGTVEITCSGGSNNYGWYQQKSPGSAP	60

I255R	VTVIYQNTKRPSDIPSRFSGALSGSTVLTITGVQAEDEAVYFCAKFDGSTDDLFAGTT	120
I255D	VTVIYQNTKRPSDIPSRFSGALSGSTVLTITGVQAEDEAVYFCAKFDGSTDDLFAGTT	120
L153R	VTVIYQNTKRPSDIPSRFSGALSGSTVLTITGVQAEDEAVYFCAKFDGSTDDLFAGTT	120
L153D	VTVIYQNTKRPSDIPSRFSGALSGSTVLTITGVQAEDEAVYFCAKFDGSTDDLFAGTT	120
2G1wt	VTVIYQNTKRPSDIPSRFSGALSGSTVLTITGVQAEDEAVYFCAKFDGSTDDLFAGTT	120
L124D	VTVIYQNTKRPSDIPSRFSGALSGSTVLTITGVQAEDEAVYFCAKFDGSTDDLFAGTT	120
L124R	VTVIYQNTKRPSDIPSRFSGALSGSTVLTITGVQAEDEAVYFCAKFDGSTDDLFAGTT	120

I255R	LTVLGGSSGSSGGGSSGGGSSAL TDESGGGLQTPGGALSLVCKGSGFTFSSYNMGWVR	180
I255D	LTVLGGSSGSSGGGSSGGGSSAL TDESGGGLQTPGGALSLVCKGSGFTFSSYNMGWVR	180
L153R	LTVLGGSSGSSGGGSSGGGSSAL TDESGGGRQTPGGALSLVCKGSGFTFSSYNMGWVR	180
L153D	LTVLGGSSGSSGGGSSGGGSSAL TDESGGGDQTPGGALSLVCKGSGFTFSSYNMGWVR	180
2G1wt	LTVLGGSSGSSGGGSSGGGSSAL TDESGGGLQTPGGALSLVCKGSGFTFSSYNMGWVR	180
L124D	LTVLGGSSGSSGGGSSGGGSSAL TDESGGGLQTPGGALSLVCKGSGFTFSSYNMGWVR	180
L124R	LTVRGGSSGSSGGGSSGGGSSAL TDESGGGLQTPGGALSLVCKGSGFTFSSYNMGWVR	180
*** *****		
I255R	QAPGKLEFVASIDKTGSR TWYGA AVKGRATISRDNQSTVRLHLNLRP EDTAIYYCAK	240
I255D	QAPGKLEFVASIDKTGSR TWYGA AVKGRATISRDNQSTVRLHLNLRP EDTAIYYCAK	240
L153R	QAPGKLEFVASIDKTGSR TWYGA AVKGRATISRDNQSTVRLHLNLRP EDTAIYYCAK	240
L153D	QAPGKLEFVASIDKTGSR TWYGA AVKGRATISRDNQSTVRLHLNLRP EDTAIYYCAK	240
2G1wt	QAPGKLEFVASIDKTGSR TWYGA AVKGRATISRDNQSTVRLHLNLRP EDTAIYYCAK	240
L124D	QAPGKLEFVASIDKTGSR TWYGA AVKGRATISRDNQSTVRLHLNLRP EDTAIYYCAK	240
L124R	QAPGKLEFVASIDKTGSR TWYGA AVKGRATISRDNQSTVRLHLNLRP EDTAIYYCAK	240

I255R	GNINIEEWGHGTEV RVSSSTSGQAGQH HHHHH	279
I255D	GNINIEEWGHGTEV DVSSSTSGQAGQH HHHHH-----	271
L153R	GNINIEEWGHGTEV IVSSSTSGQAGQH HHHHH-----	271
L153D	GNINIEEWGHGTEV IVSSSTSGQAGQH HHHHH-----	271
2G1wt	GNINIEEWGHGTEV IVSSSTSGQAGQH HHHHH-----	271
L124D	GNINIEEWGHGTEV IVSSSTSGQAGQH HHHHH-----	271
L124R	GNINIEEWGHGTEV IVSSSTSGQAGQH HHHHH-----	271
***** ** : . :		

Figure 4.9: Sequence alignment of 2G1 wild type and six stability mutant clones. The 2G1 wild type and each mutant were sequenced by Sanger Sequencing. Sequence alignment was performed using Clustal Omega (Sievers *et al.*, 2014). Note on nomenclature: the numbering of the AA sequence in this case is different than that of the Kabat numbering system. In this case, numbering begins from the methionine residue.

Table 4.4: Theoretical pI values for the 2G1 wild type, single Asp/Arg mutants and triple Asp/Arg mutants, for which all three sites, L124, L153 and I255, were theoretically substituted to aspartic acid or arginine. Theoretical pI values were calculated using the Protein-Sol online tool (Hebditch *et al.*, 2017).

Clone	Theoretical pI
2G1 wild type	8.09
L124D	7.20
L124R	9.01
L153D	7.20
L153R	9.01
I255D	7.20
I255R	9.01
Triple Asp Mutant	5.94
Triple Arg Mutant	9.93

The pI values calculated and presented in Table 4.4 indicate that the wild type scFv has a slightly basic pI. Each of the single aspartic acid mutants were calculated to have a relatively neutral pI value of 7.20 while it was predicted for each of the arginine mutants to have a higher pI value of 9.01. It was also calculated as to the pI values for triple aspartic acid mutants and triple arginine mutants; these were calculated as 5.94 and 9.93, respectively.

4.5.2 Determination of mutant binding response by indirect ELISA

The purpose of this experiment was to determine the binding response of each antibody mutant lysate and to determine a suitable dilution factor that would produce a response ≈ 1 absorbance unit. This dilution factor would then be subsequently used in a competitive ELISA. The binding response for the six generated mutants and the wild type scFv are presented in Figure 4.10. The titre values for each clone are presented in Table 4.5. In addition, the dilution factors that correlated with an absorbance value of 1 are presented in Table 4.5.

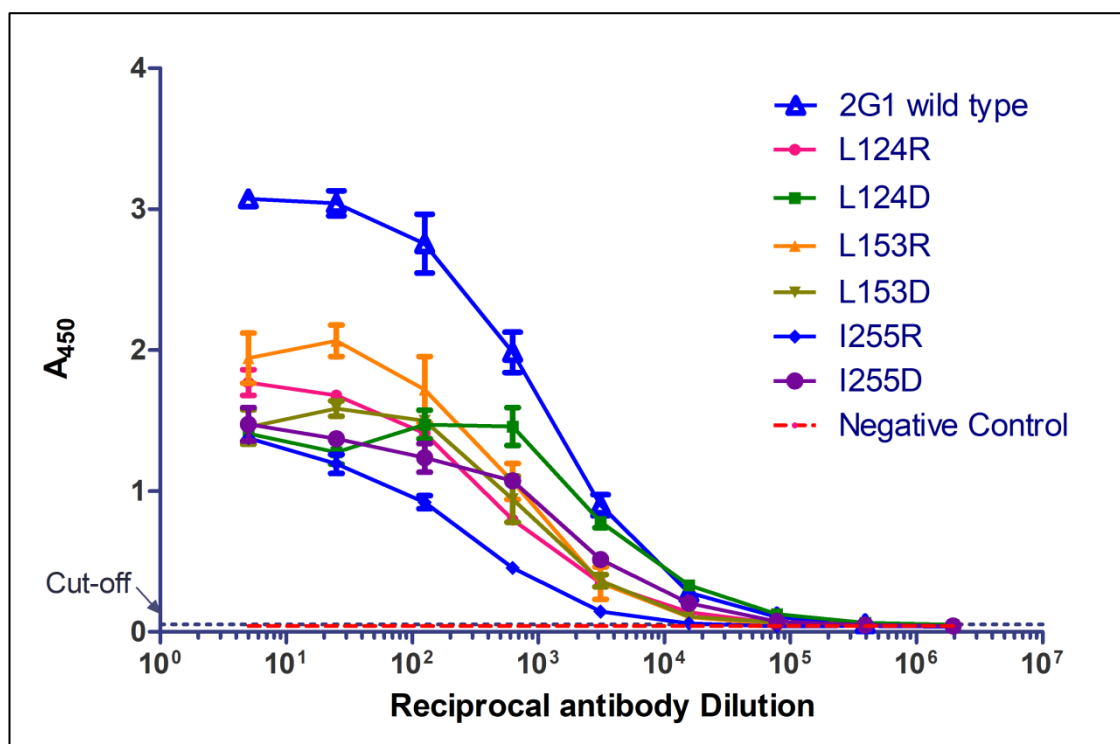


Figure 4.10: Indirect ELISA comparing the binding profiles of 2G1 wild type and stability mutant lysates. The wells of a multiwell plate were coated with 5 $\mu\text{g/mL}$ MC-LR-BSA. The lysate of each antibody clone was diluted from 1:5 to 1:1.95 $\times 10^6$ and applied to the multiwell plate in triplicate. The negative control included all test components but omitted the bacterial lysate. The ‘cut-off’ value was determined at three times the mean of the negative control. Error bars represent the standard error of the mean (SEM) ($n = 3$).

Table 4.5: Titre values of the 2G1 wild type and stability mutant lysates as determined by indirect ELISA. For each clone, the dilution factor that corresponds to an absorbance value = 1 is also shown.

Sample	Titre	Dilution factor ($A_{450} = 1$)
2G1	9.5×10^5	2,700
L124D	1.52×10^6	1,800
L124R	1.55×10^5	700
L153D	6.0×10^5	500
L153R	9.2×10^4	700
I255D	2.9×10^5	700
I255R	2.7×10^4	80

4.5.3 Determination of mutant binding response by competitive ELISA

The purpose of this experiment was to determine if any of the mutations carried out had any deleterious effects on the binding response of the antibody to MC-LR. It can be

seen from Figure 4.11 and Table 4.6 that the I255R mutation appeared to cause a 22-fold reduction in binding response versus the wild type. Therefore, this clone was omitted from further testing. The other changes in binding response were not considered large enough to disregard these clones from further testing; therefore, the remaining 5 mutant clones were kept for further analyses.

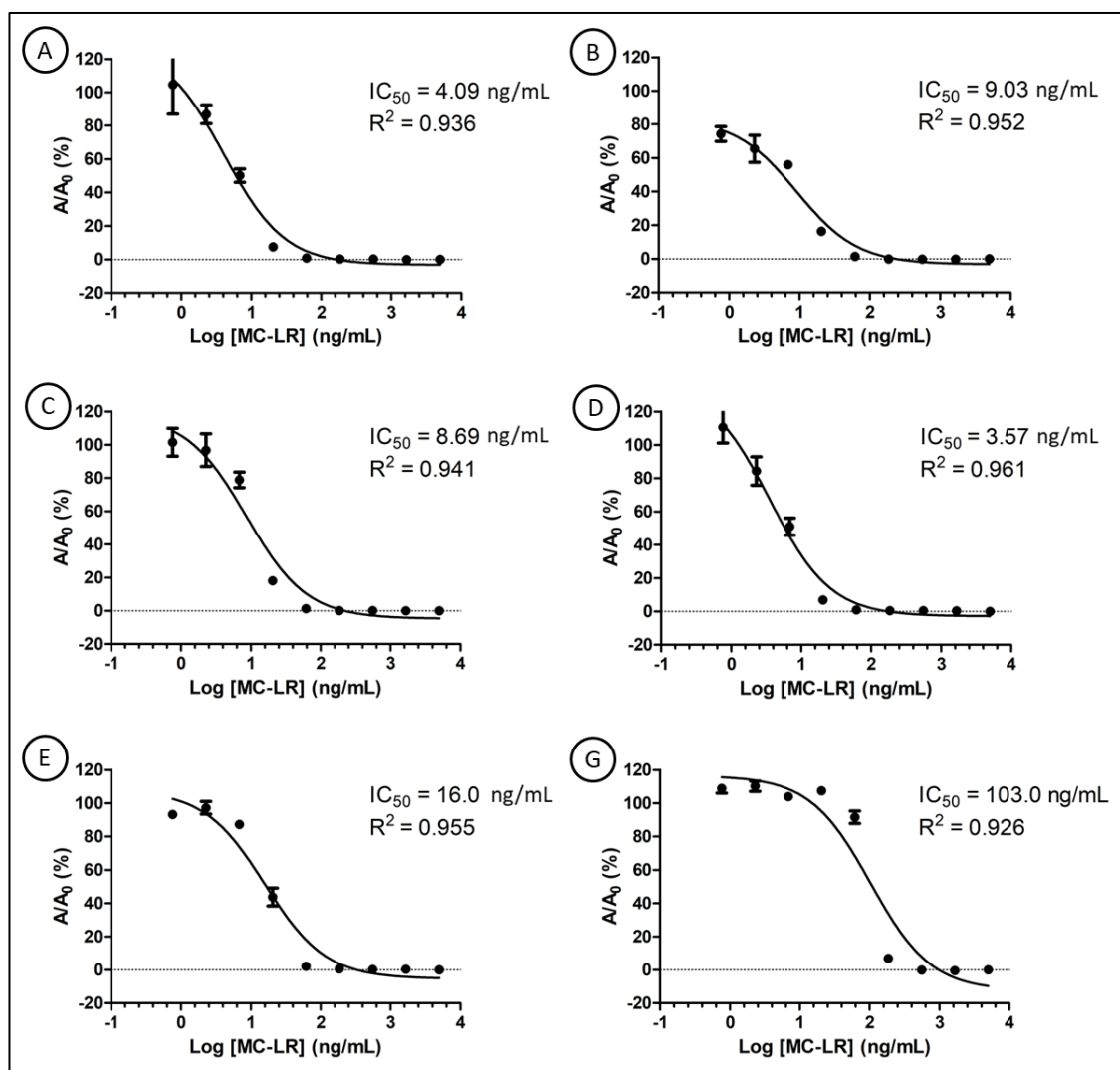


Figure 4.11: Competitive ELISAs of 2G1 wild type and stability mutants. The wells of a multiwell plate were coated with 5 $\mu\text{g/mL}$ MC-LR-BSA. The lysates of each antibody clone were diluted such that they should produce an absorbance value ≈ 1 . The diluted lysates were mixed 1:1 with free MC-LR that was diluted to concentrations ranging from 5,000 to 0.76 ng/mL. Following this, the lysate-free MC-LR mixtures were applied to the multiwell plate. Error bars represent the standard error of the mean (SEM) ($n = 3$). A = L124D, B = L124R, C = L153D, D = L153R, E = I255D, F = I255R.

Table 4.6: Comparison of IC₅₀ values for the 2G1 wild type and stability mutants. The relative affinity change was calculated as the IC₅₀ value of the wild type divided by that of the mutant clone.

Clone	IC ₅₀ (ng/mL)	Relative change
Wild type	4.68	1
L124D	4.09	0.88
L124R	9.03	1.93
L153D	8.69	1.86
L153R	3.57	0.77
I255D	16.01	3.42
I255R	103.0	22.0

4.5.4 Evaluation of the effect of mutations to surface-exposed hydrophilic residues on protein expression

The purpose of these experiments was to determine if the mutations to the surface-exposed hydrophilic residues would affect the expression characteristics of the scFv. This was investigated by culturing each clone in 200 mL SB and subsequently purifying the expressed scFv by IMAC. The levels of scFv were then analysed by SDS-PAGE, Western blotting and BCA assays. The SDS-PAGE and Western blotting analyses are shown in Figure 4.12 below. After imaging the SDS-PAGE gels, the concentrated elution lanes (lane 6) were analysed using ImageJ software. The bands at ~25 kDa and ~55 kDa (corresponding to the monomeric scFv and dimerised aggregated scFv, respectively) were analysed for pixel intensity. The ratio of band intensity was calculated as the mean pixel intensity of the ~25 kDa band divided by the mean pixel intensity of the ~55 kDa band. The results are presented in Table 4.7. The yields of each scFv, as determined by BCA assay, are shown in Figure 4.13 below.

From Figure 4.12(A)(i), lanes 5 and 6, it can be seen that the wild type 2G1 scFv (~27 kDa) was successfully purified. However, a number of additional bands can be observed at higher molecular weight values. These are likely aggregation products. These aggregation products were also quite prominent in the clones L124D (Figure 4.12(C)), L153D (Figure 4.12(E)), and L153R (Figure 4.12(F)). The aggregation bands do not appear to be as prominent in the elutions of clone I255D (Figure 4.12(B)) or L124R (Figure 4.12(D)). To quantitatively analyse the intensity of these bands, ImageJ software was used. The mean of the pixel intensities was calculated and a ratio of pixel

intensity between the 25 kDa band and the 55 kDa band was also calculated; this serves as a useful indication of the aggregation propensity of the expressed scFv. It can be seen from Table 4.7 that the 2G1 wild type scFv appeared to have 1.12 ratio of band intensity (25 kDa:55 kDa). This would indicate close to equal intensity of the monomeric scFv and aggregated scFv, which would indicate a high aggregation propensity. By comparison, each of the mutant clones appeared to reduce the aggregation propensity, as indicated by a higher intensity of the 25 kDa band versus the 55 kDa band. The largest improvement was observed for clone L153D, which exhibited a 19.6 ratio of band intensity. This can easily be observed in Figure 4.12(E)(i) in which the ~27 kDa scFv is very prominent.

The protein yields obtained from each clone were quite varied (Figure 4.13). The 2G1 wild type exhibited the highest yield of protein after expression and purification, with 2,940 μ g obtained. However, given the high aggregation propensity reported in Table 4.7, it is probable that only a small proportion of this protein yield accounts for monomeric, soluble scFv. Clone I255D exhibited the lowest yield of protein at 513 μ g. (Note: this expression and purification was carried out in triplicate due to the low yield and the high consumption of antibody stocks in later experiments. However, the small error bars (SEM) indicate good reproducibility of the expression and purification process). Despite the low yield and given that I255D exhibited the second highest reduction in terms of aggregation propensity, it is likely that this protein yield should contain a high proportion of I255D scFv. Clones L124R, L124D and L153R exhibited intermediate levels of protein yield and a reduction of aggregation propensity. However, clones L153D showed good protein yield (2,390 μ g) and the high ratio of 25 kDa:55 kDa band intensity would indicate the a very high proportion of this yield should be accounted for by monomeric soluble scFv.

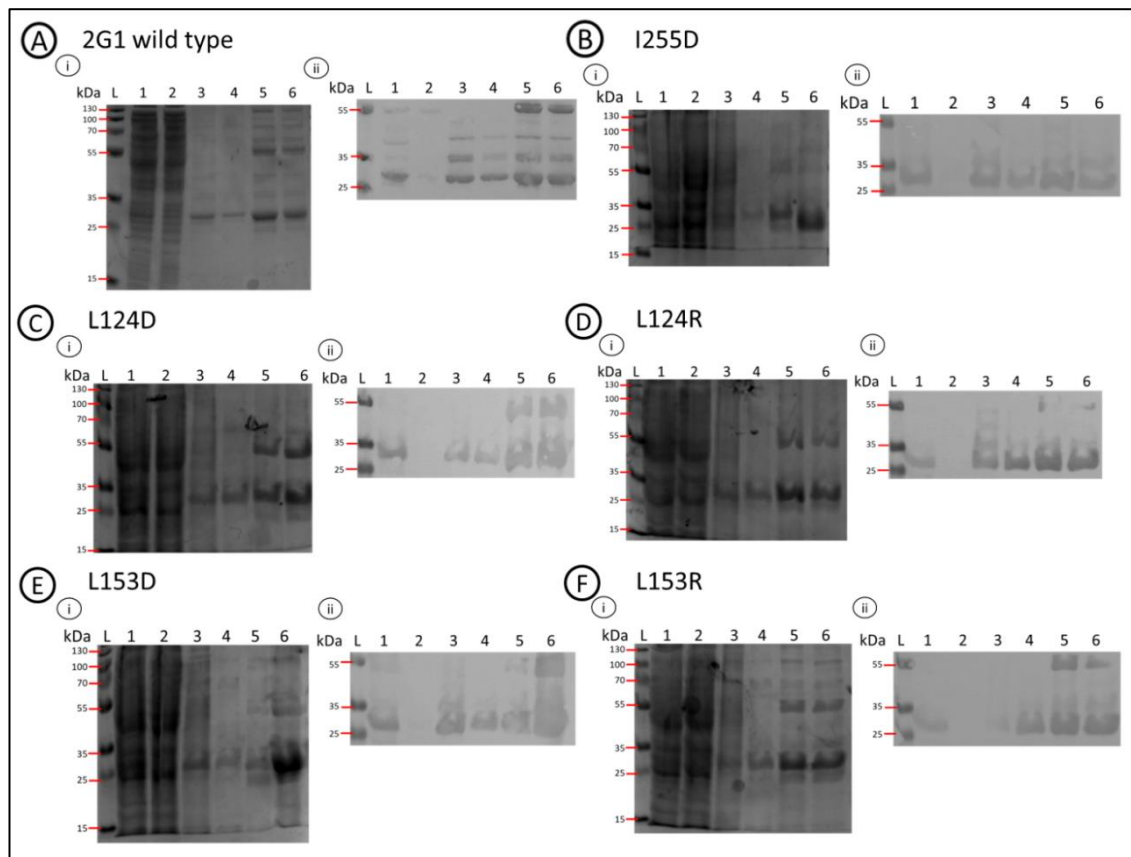


Figure 4.12: Analysis of 2G1 wild type and mutant clones by (i) SDS-PAGE and (ii) Western blotting. A = 2G1 wild type; B = I255D; C = L124D; D = L124R; E = L153D; F = L153R. Within each image, the lanes are numbered as follows; 1 = Lysate (diluted 1:5); 2 = Flow through (diluted 1:5); 3 = Wash A; 4 = Wash B; 5 = pooled elution fraction; 6 = concentrated elution (diluted 1:5).

Table 4.7: Image analysis results of 2G1 wild type and mutant SDS-PAGE images. For each of the six clones, the concentrated elution (lane 6) of each SDS-PAGE image was analysed by ImageJ software. The ~25 kDa and ~55 kDa bands were analysed for pixel intensity. The ratio of band intensity was calculated as the mean pixel intensity of the ~25 kDa band divided by the mean pixel intensity of the ~55 kDa band.

Clone	Ratio of band intensity (25 kDa:55 kDa)
2G1 wild type	1.12
I255D	2.80
L124D	1.39
L124R	2.19
L153D	19.6
L153R	2.65

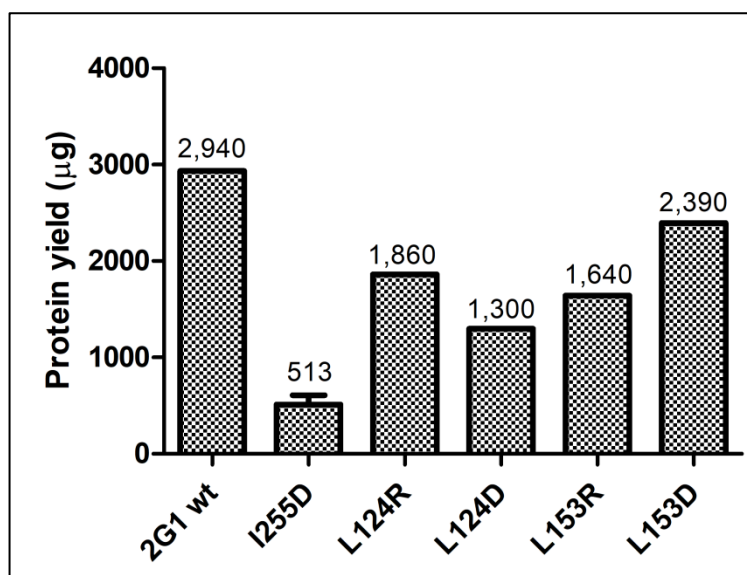


Figure 4.13: Protein yields of 2G1 wild type and hydrophobicity mutants. The numerical values are presented above each bar. The expression and purification of clone I255D was carried out in triplicate. Error bars = SEM (n = 3).

4.5.5 Analysis of the solubility of 2G1 wild type and hydrophobicity mutants

The purpose of these experiments was to determine if the mutations to the surface exposed hydrophobic residues affected the solubility of the antibody. It was hypothesized that a higher number of surface hydrophilic residues should improve the protein solubility. This was tested by incubating each antibody clone at the same concentration under different treatments; for native solubility, each clone was incubated at 25 °C for 0 – 6 d; for non-native solubility, each clone was incubated at temperatures ranging from 25 to 95 °C for 1 h. Following this, the protein that came out of solution was sedimented by centrifugation and the protein concentration of the supernatant was measured by BCA assay. The results of the native and non-native solubility measurements are presented in Figures 4.14 and 4.15 below. All data points represent the mean of triplicate independent measurements.

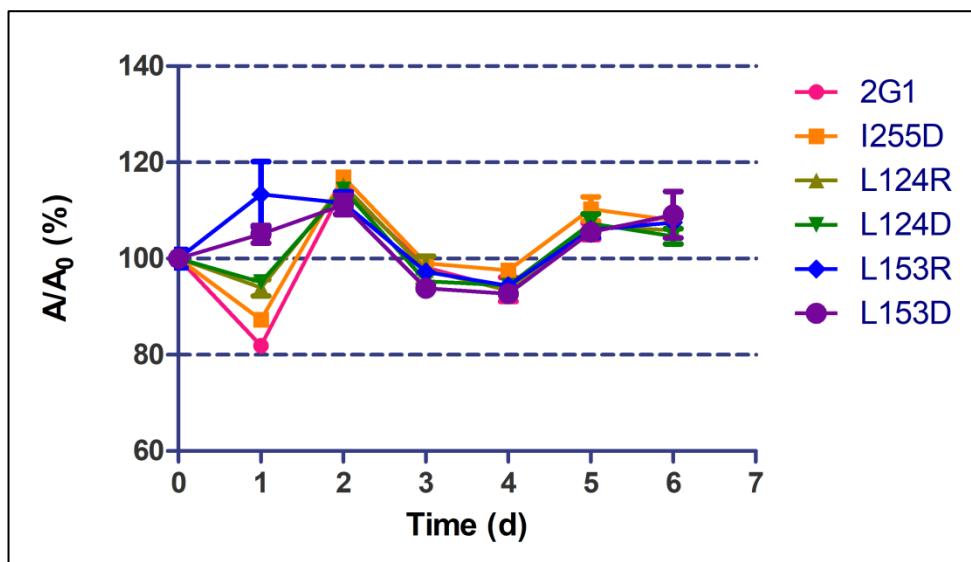


Figure 4.14: Native solubility of the 2G1 wild type compared to the stability mutants. Each antibody clone was prepared at 300 $\mu\text{g/mL}$ in PBS (150 mM, pH 7.2), supplemented with protease inhibitor. Each clone was incubated at 25 $^{\circ}\text{C}$ for several days. Each day three aliquots of each clone was tested for the concentrations of protein remaining in the supernatant. 0% defined as $A_{562} = 0.07$ (which is the absorbance observed for 0 mg/mL protein). 100% was defined as the absorbance of day 0 data point for each data set. Error bars = SEM (n = 3).

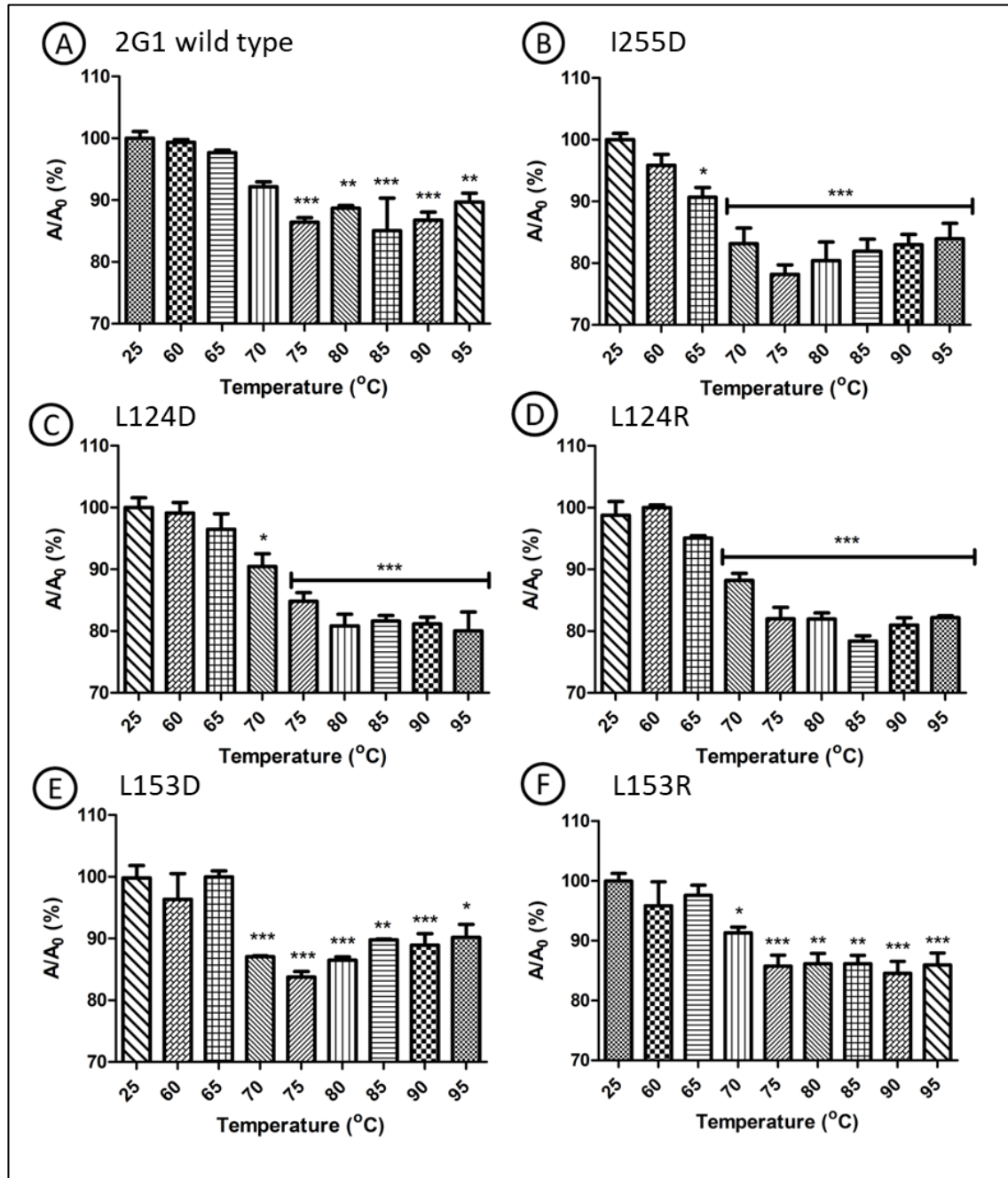


Figure 4.15: Non-native solubility of the wild type 2G1 scFv compared to the stability mutants. Each antibody clone was prepared at 300 $\mu\text{g}/\text{mL}$ in PBS (150 mM, pH 7.2), supplemented with protease inhibitor. Each clone was incubated at a variety of temperatures for 20 min. Each clone was tested in triplicate for the concentrations of protein remaining in the supernatant. A = 2G1; B = I255D; C = L124D; D = L124R; E = L153D; F = L153R. 0% defined as $A_{562} = 0.07$ (which is the absorbance observed for 0 mg/mL protein). 100% was defined as the absorbance of the 25 °C data point for each data set. Error bars = SEM (n = 3). Significance: $P < 0.05^*$; $P < 0.01^{**}$; $P < 0.001^{***}$ as illustrated, all relative to the 25 °C data point.

As can be seen from Figure 4.15, a statistically significant decrease in protein concentration ($P < 0.001$) was observed after 75 °C for the wild type 2G1 scFv. For the mutant clones L124D, L124R, L153D and L153R, a statistically significant decrease in protein concentration was observed after 70 °C ($P < 0.05$; $P < 0.001$, $P < 0.001$, $P < 0.05$, respectively). For the mutant clone I255D, a significant decrease was observed after 65 °C ($P < 0.05$).

4.5.6 Investigation into the temperature stability of the 2G1 wild type and hydrophobicity mutants

The purpose of this experiment was to determine if, after treating each scFv clone to a range of different temperatures (4 – 70 °C), the antibodies would retain the ability to bind to the MC-LR target. All scFv mutants were exposed to different conditions and then tested for binding by ELISA in triplicate. The result of this experiment is presented in Figure 4.16. In addition, the effective temperature that results in 50% reduction in binding response (ET_{50}) for each clone is presented in Table 4.8. Note: L153D was unable to be tested due to depletion of stocks of this scFv mutant.

As can be seen in Figure 4.16, a sharp decrease in response was observed for all clones as the temperature was increased. ANOVA statistical analysis showed that at 37 °C significant decreases in binding response were observed ($P < 0.05$ for L124D, $P < 0.01$ for L124R and I255D, and $P < 0.001$ for 2G1 and L153R). For all clones, highly significant decreases in binding response were observed at 50 – 70 °C ($P < 0.001$).

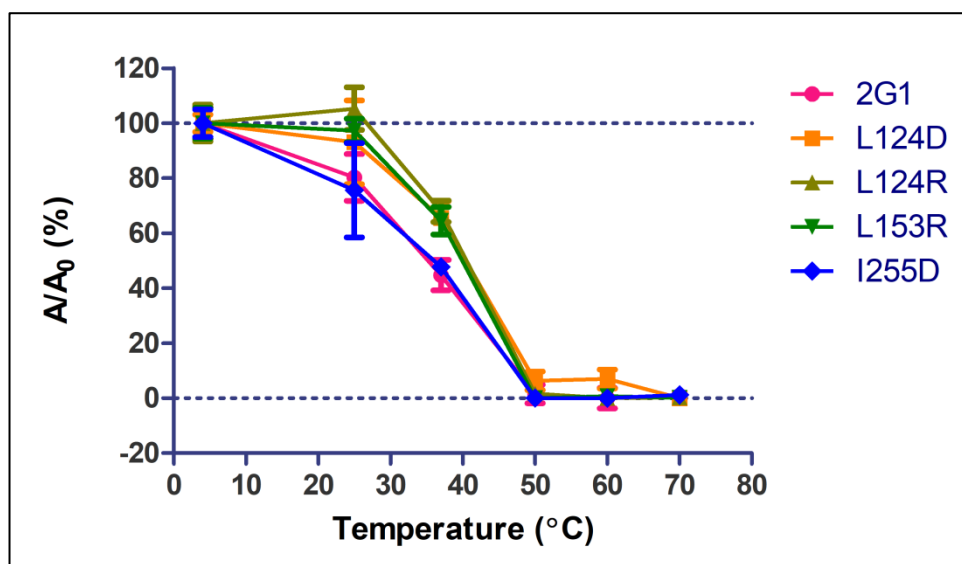


Figure 4.16: Functional temperature stability of wild type 2G1 and mutant clones. A multiwell plate was coated with MC-LR-BSA and blocked. Each antibody was diluted to 10 $\mu\text{g}/\text{mL}$ and treated at a range of temperatures (4 – 70 $^{\circ}\text{C}$) for 1 h and then cooled. The treated antibodies were placed onto the coated and blocked ELISA plate. A HRP-labelled anti-HA secondary antibody was used to probe any bound scFv on the surface. Error bars = SEM (n = 3).

Table 4.8: ET_{50} values of hydrophobicity mutants after temperature treatment. The ET_{50} is the effective temperature that results in 50% reduction in binding response.

Clone	ET_{50} value ($^{\circ}\text{C}$)
2G1	35.2
L124D	40.4
L124R	40.6
L153R	40.0
I255D	36.1

Table 4.9: Summary of findings in this section. AP = aggregation-propensity; NT = not tested. Due to the large reduction in binding affinity, clone I255R was omitted from further testing.

Mutant Clone	ELISA		AP	Non-Native		Thermal Stability
	IC ₅₀	Yield		Solubility	Solubility	
L124D	↑	↓	↓	-	↓	↑
L124R	↓	↓	↓	-	↓	↑
L153D	↓	↓	↓↓	-	↓	NT
L153R	↑	↓	↓	-	↓	↑
I255D	↓	↓	↓	-	↓	-
I255R	↓↓	N/A*	N/A*	N/A*	N/A*	N/A*

4.6 Discussion – stability optimisation

In this section, mutations were made in order to improve the stability, solubility and expression characteristics of the 2G1 scFv. It is reported in the literature that in comparison to large antibody molecules such as IgG and Fab, antibody fragments such as scFv tend to have poor biophysical properties such as high aggregation propensity even at relatively low concentrations (Jespers *et al.*, 2004a; Jespers *et al.*, 2004b; Dudgeon *et al.*, 2012). This is likely due to the lack of stabilising intermolecular bonds such as disulfide bonds between the variable heavy and light regions and exposure of hydrophobic areas between the variable regions to the bulk solvent (Gil and Schrum, 2013). Thus, after examining the 3D structural model of the 2G1 scFv, three surface exposed hydrophobic residues were identified and chosen for mutation: L124, L153 and I255. From the generated 2G1 model (Figure 4.8), it appeared that the three chosen AAs reside in β -strands and may fit the definition of aggregation prone sequence regions (APRs), i.e. surface-exposed AA regions that contain hydrophobic residues and assemble by intermolecular β -strand interactions (Ganesan *et al.*, 2016). It was reported that the most efficient strategy to suppress APRs was to mutate a central or flanking APR residue to a charged residue or Pro, which are so-called aggregation ‘gatekeepers’. It is suggested that these ‘gatekeepers’ disfavour the β -structure formed by hydrophobic sequences in aggregates (Rousseau and Serrano, 2006) and kinetically control aggregation sufficiently to favour folding (Ganesan *et al.*, 2016). A number of other studies have shown that the most successful mutations involve the introduction of

charged residues. It is suggested that this may be due to the increase of the colloidal stability by altering the net charge of the protein (Jespers *et al.*, 2004; Sahin *et al.*, 2011; Perchiacca *et al.*, 2011; Zhang *et al.*, 2012; Buck *et al.*, 2012; Perchiacca *et al.*, 2014; Rouet *et al.*, 2014). Therefore, based on much literature evidence, it was decided to mutate these residues with the hydrophilic charged residues arginine and aspartic acid. It was decided to investigate both positively and negatively charged mutations at each site because a charged mutation may inadvertently lead to charge repulsion, leading to destabilisation (Strub *et al.*, 2004). Thus, it is possible that introduction of a positive charge in a position may cause destabilisation, whereas a negative charge at that position may improve stability, or *vice versa*.

In this preliminary study, the strategy devised was to investigate each mutation individually to determine if any improvements in expression, solubility and functional stability were observed. Following this, any promising mutations would be combined to determine if any cumulative effects could be achieved as it was observed in a number of studies that multiple mutations can result in significant improvements in production, solubility and stability (Strub *et al.*, 2004).

Firstly, it was investigated if the mutations had an effect on the binding of the scFv to MC-LR, as it was desired in the utmost to preserve the antigen-binding ability of the wild type scFv. It can be seen from Table 4.6 that the mutations L124R, L153D and I255D caused a 1.93-, 1.86- and 3.42-fold changes (reductions) in binding, respectively. A slight improvement in antigen-binding was observed after L124D and L153R mutations, with 0.88- and 0.77-fold changes in IC_{50} versus the wild type, respectively. For these five mutants, the changes in binding were considered acceptably small and so these mutants were brought forward for further analysis. In contrast, however, the largest relative change in IC_{50} was observed for clone I255R, which exhibited a 22.03-fold reduction in binding versus the wild type. However, when looking at the sequence of this mutant, it was observed that an 8 AA insertion was made adjacent to the target mutation (Figure 4.9). It is shown by the I255D mutation (with a 3.424-fold relative change in IC_{50} versus the wild type), that this location appears to be quite sensitive to any mutations. Therefore, a significant structural change such as an 8 AA insertion would likely account for the large reduction in binding observed for I255R. Thus, it was decided to omit this clone from further testing.

After expressing and purifying the wild type 2G1 and five mutant clones, the IMAC purification products were analysed by SDS-PAGE and Western blotting. It was evident from the results that the 27 kDa scFv was successfully expressed and purified for all clones. However, with the exception of clones I225D and L124R, additional prominent bands were observed for all clones at molecular weights up to 55 kDa in the Western blotting results (Figure 4.12 (C, E and F)). Staining of these proteins on the Western blot indicates that these protein bands are positive for the hemagglutinin (HA) affinity tag. Thus, it is likely that these protein bands are aggregated forms of the expressed scFv molecule. Furthermore, additional bands were observed in some of the elutions at sizes lower than 25 kDa. However, these bands were not observed when subsequently analysed by Western blotting. This would indicate that these might correspond to truncated scFv which can occur from proteolytic digestion or incomplete translation by the ribosome (Dunnen and Van Ommon, 1999; Hauss and Muller, 2007; Whitaker *et al.*, 2015).

In order to determine the extent of aggregation present in the purified samples, the ~25 kDa and ~55 kDa bands in the concentrated elution lanes of each SDS-PAGE gel were analysed for mean pixel intensity using ImageJ software. This produced a ratio of pixel intensity, presented in Table 4.7, which is highly useful for determining the proportion of the intact scFv (27 kDa) to aggregated, dimerised scFv (~54 kDa) (which tended to be the most prominent protein bands observed in the elutions). This can serve as an overall indication of the aggregation-propensity of the scFv. For the 2G1 wild type, it appeared there was approximately equal intensity of the ~25 kDa and ~55 kDa bands (ratio 1.12:1). This would indicate a high aggregation-propensity for the wild type. The yield of the 2G1 wild type from the expression study was the highest of all the clones (2,940 µg), but the high aggregation-propensity would indicate that only a relatively small proportion of this yield accounted for the monomeric, native scFv product. The mutant clone L124D, exhibited a slight improvement in the ratio of 25 kDa to 55 kDa protein bands (1.39:1) versus the wild type. Nevertheless, the yield of protein product was also considerably reduced (1,300 µg). Further reductions in aggregation-propensity were observed for the mutant clones I255D, L124R and L153R, with 25 kDa to 55 kDa ratios of 2.80:1, 2.19:1 and 2.65:1, respectively. However, the yields of these clones varied considerably and were markedly reduced versus the wild type; the yields of I255D, L124R and L153R were 513 µg, 1,860 µg, and 1,640 µg, respectively. The

greatest changes in expression characteristics were observed for clone L153D (Figure 4.12(E)); the ratio of 25 kDa to 55 kDa protein bands improved to 19.6:1 versus the wild type. While the yield of L153D was slightly lower than the wild type (2,390 µg), given the high proportion of monomeric scFv present, it appears that this mutation greatly improved the scFv yield. Furthermore, the reduced aggregation-propensity would also greatly improve the efficiency of the bacterial expression and purification method, as less antibody product would be lost due to aggregation. It is possible that the mutation to this site may have suppressed the APR in this area; hydrophobic-to-charged mutations are reported to suppress APRs and can improve solubility and expression (Rousseau and Serrano, 2006; Ganesan *et al.*, 2016).

Indeed, the image analysis method applied here provides a useful estimation of the ratio of 25 kDa to 55 kDa protein bands. However, it was not estimated as to the ratio of the 25 kDa band to all of the other protein bands present in the elutions, which is prohibitively arduous. It is difficult at this stage, without further testing, to accurately and quantitatively determine the exact percentage purity of the 27 kDa scFv in each sample. The purification method used in this study was IMAC, and while it greatly reduced the amount non-specific proteins present compared to the unprocessed lysate (lane 1 for all images in Figure 4.12), the persistent presence in the elutions of proteins other than the target indicate that the purification process could be improved. A highly beneficial component that could compliment this process is the addition of size exclusion chromatography (SEC) after IMAC. This would allow for the IMAC elutions to be further polished to remove aggregated products and obtain pure scFv product. Quantification of this pure product would give a much better indication as to which mutations had a beneficial impact on protein expression. Furthermore, this method can be coupled with absorbance measurements and is highly sensitive to aggregation bodies. Using SEC, aggregated proteins will stick to the wall of the column, which can be interpreted as poor elution peaks on the chromatogram, and so SEC could also allow for the quantification of the extent of protein aggregation in the scFv samples (den Engelsman *et al.*, 2011; Perchiacca *et al.*, 2014).

Another aim of this study was to determine if the mutations to the scFv surface residues would enhance the protein solubility. Similar work in this area was carried out by Perchiacca *et al.* (2012, 2014) and their work was used as a guideline for this current

study. In order to estimate if the mutations induced changes in the scFv solubility, native solubility measurements were conducted. Native solubility is a measure of how well the protein stays in solution when it is in its native folded conformation. Estimating the native solubility involved exposing each protein to favourable conditions (i.e. ambient temperature, neutral pH, physiological salinity levels) that will encourage the retention of the native conformation. The exposure was carried out for an extended duration (several days) and the proteins were continuously monitored to determine the time when aggregation occurred and the extent of protein loss due aggregation. Such measurements are related to the observations that antibodies tend to unfold after prolonged storage (Perchiacca and Tessier, 2012; Gil and Schrum, 2013). It was expected that the proteins with poorer solubility would precipitate out of solution at an earlier time point than those with enhanced solubility, and this would be indicated by a decrease in protein concentration in the supernatant. However, from Figure 4.14, with the exception of slight fluctuations on Day 1, there was no apparent change in protein concentration after 6 days of treatment for any of the clones. A possible reason for this is that the protein concentration used at the beginning of the experiment may have been too low for changes in solubility to be observed using this technique; the scFv concentration for all samples was 300 µg/mL (11.1 µM). By comparison, the initial antibody concentration used by Perchiacca *et al.* (2014) was ~55 µM. In that report, it was observed that for native-solubility measurements, the minimum concentration for each antibody after aggregation had occurred was ~10 – 15 µM (see Figure 4.17 below). It is important to remember that protein solubility is a concentration-dependent parameter, and even unfolded protein can remain soluble, albeit at a much lower concentration than the folded protein. Thus, the range of 10 – 15 µM may represent the concentration at which the unfolded antibody will remain soluble. In the case of the present study, the use of starting concentrations of >50 µM of each scFv clone (as used by Perchiacca *et al.* (2012, 2014)) was not feasible, due to the very high protein-consumption. To illustrate this, the use of 300 µg/mL (11.1 µM) of each antibody equated to a consumption of ~360 µg in total for each antibody. By comparison, increasing this concentration to 55 µM would have led to a very high consumption of ~1800 µg of each antibody, which was simply not feasible given the yields of antibody achieved (Figure 4.13). In future experiments, if this method of analysis is to be used for native solubility determination, higher protein concentrations should be used, which in

turn will require larger scale of protein expression and purification to facilitate the inherent higher cost of protein. However, an alternative means to determine the native solubility, with a reduced cost in terms of scFv product, is the use of circular dichroism (CD). CD is a method that is frequently used for the analysis of protein solubility and folding. This technique has the distinct advantage of being non-destructive (i.e. the protein is not used up in the measurement), its high sensitivity means that it can also be used to analyse very small quantities of protein sample and has frequently been used for the analysis of protein solubility, as reported in the literature (Hawe *et al.*, 2009; Miklos *et al.*, 2009; den Engelsman *et al.*, 2011; Perchiacca *et al.*, 2014).

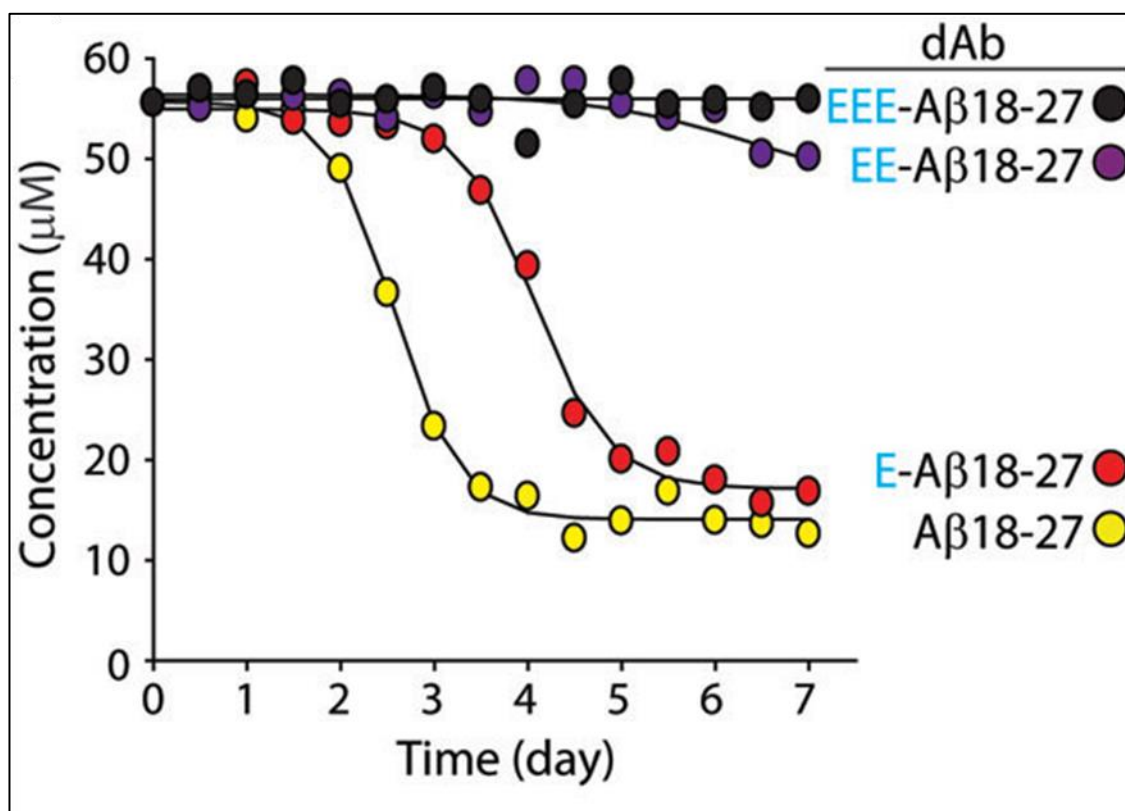


Figure 4.17: Native solubility measurements of antibody mutants reported by Perchiacca *et al.* (2014). For native solubility measurements, the starting concentration used in this study was $\sim 55 \mu\text{M}$, which was prohibitively high to be replicated in the present study. Furthermore, the starting concentrations used in the present study ($11.1 \mu\text{M}$) approximated the lowest concentrations observed by Perchiacca *et al.* (2014).

When it was observed that no significant changes in native solubility measurements could be determined, it was decided to evaluate if the mutations resulted in any changes in non-native solubility. Non-native solubility is a measure of how well the protein remains soluble when it is in its non-native, unfolded conformation. It is also a measure of how well a protein can both resist unfolding and how well it can refold back into its

native folded state (Gil and Schrum, 2013). The advantage of this analysis is that it is expected that exposure to unfavourable conditions (elevated temperatures of 60 – 95 °C) will induce aggregation at a lower concentration; thus, changes in protein concentration should be more observable using the current methodology (as it would be expected that the protein concentration in the supernatant would drop to ~4 – 8 µM (Perchiacca *et al.*, 2012, 2014). Indeed, the results presented in Figure 4.15 show that changes in protein concentration were observed, and slight variations were observed in the profiles of each clone. The results indicated that the wild type 2G1 scFv appeared to have the highest non-native solubility, as a significant decrease in protein concentration ($P < 0.001$) was observed only upon treatment at 75 °C. By comparison, for the clones L124D, L124R, L153D and L153R, significant reductions in protein concentration were observed after treatment at the lower temperature of 70 °C. Finally, clone I255D appeared to have the lowest non-native solubility, as a significant reduction in protein concentration was observed at 65 °C ($P < 0.05$). In general, these observations are in agreement with many studies in that antibody fragments tend to precipitate out of solution when exposed to temperatures greater than 70 °C (Wang *et al.*, 2007; Zhang *et al.*, 2012; Gil and Schrum, 2013). These results would indicate that none of the mutant clones improved upon the non-native solubility of the 2G1 wild type scFv.

It should also be noted that a potential benefit of carrying out multiple hydrophobic-to-charged mutations would be to shift the pI of the protein. It is well known that proteins are less stable when around their pI, where their net charge is zero (Cohn and Edsall, 1943; Lawrence *et al.*, 2007). It can be seen in Table 4.4 that the theoretical pI of the wild type was calculated as 8.09. While the arginine mutations shifted the pI of the respective mutants to 9.01, the aspartic acid mutations shifted the pI to 7.20, which is approximately the same pH of the PBS buffer used for suspending the antibody clones. Thus, it is possible that the near-neutral pI of the aspartic acid mutants may have led to unfavourable conditions in terms of net charge. In contrast to the individual mutants, the pI of the triple aspartic acid mutant and arginine mutants was predicted to be 5.94 and 9.93, respectively. Shifting the pI drastically in this way might help to improve the solubility and/or stability of the mutant clones when they are suspended in neutral pH buffers as was observed by Lawrence *et al.* (2007) who observed significant stability benefits in green fluorescent protein (GFP), streptavidin and glutathione-S-transferase

(GST) upon ‘supercharging’ the protein surfaces (see Section 1.5.2). This should be investigated in future studies.

However, returning to the current study, in order to gain greater insight into how the mutations caused changes in protein solubility and stability, further experiments were carried out to examine how each clone could retain antigen-binding ability after heat-induced unfolding, i.e. the functional stability of the clones was measured. The functional stability of each clone was determined by pre-heating each clone to a specified temperature for 1 h, returning the clones to room temperature and then measuring the binding response to a MC-LR-BSA-coated and blocked ELISA plate. This ELISA functional stability method is highly useful because it relies on the exquisite sensitivity of the 2G1 scFv for the MC-LR molecule. Any loss in protein conformation will have a pronounced effect on binding capacity and so was expected that this method would be quite indicative of changes in protein folding. It was expected that any clones with enhanced thermal stability and refolding ability would exhibit higher binding responses than clones with poorer stability. It was shown in Section 4.5.3 that there were slight variations in binding shown by each mutant that occurred as a result of the mutations. However, in the current method, each antibody clone was treated at the same protein concentration and the only differing factor between each treatment was the temperature of exposure; thus, any changes in binding response observed are due to the antibody’s ability to withstand heat denaturation and to refold, rather than due to changes in affinity. (Note: unfortunately, due to depletion of the stocks of clone L153D, this clone was not tested. This clone may be retested in future experiments). It can be seen from Table 4.8 that the wild type 2G1 exhibited an ET_{50} of 35.2 °C, i.e. at this temperature the response of the 2G1 antibody was reduced to 50%. A similar response was observed for clone I255D. By comparison, the L124D, L124R and L153R mutations appeared to improve the heat resistance of the antibody by approximately 5 °C, which is an indication of a slight improvement in stability. Given that only one site was mutated per clone, an improvement of 5 °C is considerable. Generally, it is rare that a single mutation alone would result in improvements in stability (Pedone *et al.*, 2001; Perchiacca *et al.*, 2011) and usually 2 or 3 mutations are required before significant improvements in stability are observed (Strub *et al.*, 2004). It is possible that the introduction of charged residues in these positions increased the electrostatic interactions with the surrounding water, which plays a key role in protein

stability (Boulet-Audet, 2014). It was noted elsewhere that the introduction of charged residues can help to finely modulate protein stability (Loladze and Makhatadza, 2002). The stabilising effect of these charged residues may be due to the kosmotropic nature of their side chain groups, which can form favourable interactions with water to improve hydration and thus enhance stability (Perchiacca *et al.*, 2014).

It is also important to comment on the apparent reduction in ELISA binding activity at 37 °C. At first glance, the result presented in Figure 4.16 may indicate that it is unfavourable to carry out ELISA incubations at 37 °C, as is generally the traditional method. However, in this circumstance, and in contrast to an ELISA, the antibodies were incubated in the absence of their antigen target. It was noted in a number of previous studies that the CDRs introduce considerable instability in the antibody molecule (Rothlisberger *et al.*, 2005; Perchiacca *et al.*, 2011; Gil and Schrum, 2013). For example, the presence of hydrophobic residues in the CDR could lead to instability. However, in ELISA, when an antibody binds to its antigen, the result is a lower entropy state which also conceals such hydrophobic residues. In the absence of the epitope, the flexible structure of the CDRs may compromise the folding of an isolated antibody fragment (Saerens *et al.*, 2005; Vincke *et al.*, 2009; Gil and Schrum, 2013). Furthermore, in ELISA, the use of a higher temperature improves the reaction rates of the antibody with its antigen (Bommarius and Paye, 2013; Magliery, 2015).

The work presented in this preliminary study indicates at the complexity surrounding antibody stability/solubility. Table 4.9 summarises the results of the various tests carried out on the different antibody clones. Clones L124D and L153R showed modest improvements in antigen binding and also showed improvements in terms of reduced aggregation-propensity and increased thermal stability. Clones L124R and I255D each exhibited a drop in antigen binding affinity (clone I255D more so) but also displayed reduced aggregation propensity versus the wild type. Further, L124R exhibited an improvement in thermal stability, whereas the thermal stability of I255D was largely unchanged versus the wild type. Generally, clone I255D exhibited the greatest reduction in binding affinity, protein yield and non-native solubility and exhibited no improvements in thermal stability. These observations may give credence to the observations of Perchiacca *et al.* (2014) and Ganesan *et al.* (2016) that the precise positioning of the mutations can have considerable effect on protein solubility and

stability. Furthermore, it is possible that residue I255 is important for the antibody structure as it has been observed that some hydrophobic residues may be beneficial for stability if they provide a shield from penetrating water molecules (Strub *et al.*, 2004). Thus, perhaps in future work, the I255D mutation should be omitted as it did not confer an acceptable balance of advantages to disadvantages. Meanwhile, clone L153D exhibited a considerable reduction in aggregation propensity. Unfortunately, due to depletion of stocks of this clone, it was unable to be tested for thermal stability. However, in future work, this gap will be addressed. No improvements were observed in terms of the native solubility for any of the clones. Furthermore, the analysis of protein yield and native solubility will require more refined techniques in order to more accurately measure changes in terms of these parameters (see below).

In general, with the exception of the reduced aggregation propensity of clone L153D, the single point mutations carried out in this work resulted in modest changes in terms of the measured parameters. This is mostly in line with the published literature that, generally, single point mutations do not greatly change a protein's solubility/stability (Reidhaar-Olson and Sauer, 1990, Rennell *et al.*, 1991, Perchiacca *et al.*, 2014). The aim of this early stage of the research was to carry out systematic analysis of how individual point mutations would affect the antibody's solubility and stability before combining multiple mutations together. The work presented here is still in the preliminary stages of the research, but lays a good groundwork for future experiments. It is expected that incorporating multiple mutations, such as L124D/R with L153D/R, could result in more drastic changes in protein stability and solubility than the individual mutations and could result in cumulative beneficial effects, as was reported previously (Strub *et al.*, 2004; Ganesan *et al.*, 2016).

4.7 Future work – stability optimisation

As was mentioned throughout the discussion, in general, the individual mutations were observed to result in only slight alterations in the antibody's stability and solubility, which is in line with the literature. The greatest gains were observed for the L153D mutation which considerably reduced the aggregation propensity. However, in future studies, multiple mutations may be combined to determine the possibility of cumulative benefits in stability, solubility and expression. Particular focus should be placed on

investigating the cumulative effects of mutations to positions L124 and L153 which generally appeared more amenable to mutations than position I255.

It was suggested in a number of studies that conformational stability of antibodies can be increased by replacing hydrophobic residues situated on the complementary surfaces between the light and heavy chains with charged AAs (Riechmann and Muyldermans, 1999; Muyldermans, 2001). This proposition follows the examples of shark and camelid domain antibodies (dAbs) which have excellent stability properties owing to the highly charged surfaces of their interfacial regions. This avenue could be investigated in future studies.

A promising means to screen mutant clones with favourable properties was developed by Dudgeon *et al.* (2009), and briefly discussed in Section 1.5.2. Mutant antibody libraries could be generated to incorporate substitutions at designated target locations with all 20 standard AAs. The antibody library could then be displayed on phage and screened by heat denaturation. Protein A is a highly conformation-specific protein with affinity for V_H domains (Jansson *et al.*, 1998) and so it could be used to retrieve antibody clones that can withstand denaturation and that remain stable. This method should also be easily facilitated in the research group as the technology required can be adapted from the phage display techniques currently in use.

As was also discussed above, a number of the analyses could benefit from more refined technologies or methodologies to observe the subtle improvements expected from single point mutations. For example, the use of CD in future experiments may allow for better resolution of the native solubility measurements. Furthermore, the incorporation of SEC into the antibody purification method would greatly enhance the purity of the end product and would aid in measuring the changes in protein yield.

4.8 Future work – integration of antibodies into a microfluidic detection system

It was discussed in earlier sections that it was the long-term aim of this project to incorporate the anti-MC-LR antibody fragments into a biosensor system to allow for sensitive detection of this toxin at the point-of-need (PON). The system developed by Murphy *et al.* (2015), which was already discussed in detail, allows for highly sensitive MC-LR-detection. However, a disadvantage of this system is the requirement of an

analyst to process the suspect sample for analysis. Thus, this system is not currently amenable to autonomous and continuous long-term monitoring. However, a project that was on-going during the time of the present research was on the development of such an autonomous biosensor system. The ToxiSense system was developed in the Water Institute in DCU and consists of a microfluidic, centrifugally-driven lab-on-a-disk (LOAD), a spin stand motor to generate the centrifugal force and a fluorescence reader to quantify the fluorescent signal. The design of the ToxiSense system is described in Figure 4.18. Work was carried out on the optimisation of the anti-MC-LR scFv and MC-LR-BSA coating concentrations on the disk, including the optimisation of the surface-activation and conjugation chemistry, as described by Maguire *et al.* (2018).

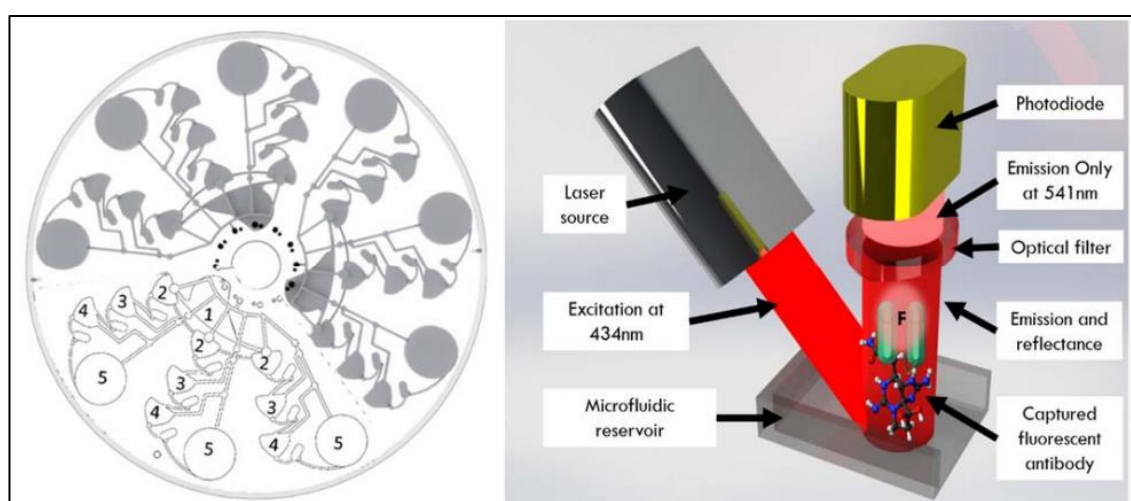


Figure 4.18: ToxiSense LOAD design. The ToxiSense disk allows for measurement of triplicate measurements of either three target molecules, MC-LR, Domoic acid and Saxitoxin, or three day analysis of the same target molecule. In zone 1, a test sample, such as a suspect freshwater sample, is added and this is separated and mixed with detection antibodies located in zone 2. In the case of MC-LR-detection, during fabrication of the disk, the anti-MC-LR scFv is fluorescently labelled with Alexa 430 and is adsorbed and dried onto the surface of zone 2. Upon mixing of the water sample in zone 2, the anti-MC-LR scFv is resuspended and interacts with any free MC-LR toxin in the sample. The sample is driven by the centrifugal force to zone 3 in which MC-LR-BSA is conjugated onto the surface. In this competitive assay, any anti-MC-LR scFv that did not bind to free MC-LR in solution will bind onto the surface-immobilised MC-LR, thus, there is an inverse relationship between the toxin concentration in the sample and the fluorescent signal. The sample further proceeds to zone 4, the control zone. In this chamber, any remaining anti-MC-LR scFv will be captured by polyclonal anti-IgY that is conjugated onto the surface. The amount of bound anti-MC-LR scFv in the detection and control zones can be quantified by fluorescence measurement, with excitation and emission wavelengths at 434 and 541 nm, respectively. Finally, the analysed sample will accumulate in zone 5, the waste reservoir. Image sourced from Maguire *et al.* (2017).

The ToxiSense system was designed as part of a larger EU Seventh Framework Program project called MariaBox (**M**arine environmental *in-situ* assessment and monitoring tool**box**). The aim of this consortium project was to incorporate the ToxiSense biosensor system into a custom-built marine monitoring buoy that could be

deployed for months at a time in fresh or brackish waters. The buoy would incorporate automated fluid handling to filter the water sample and deliver the sample to the ToxiSense LOADs for analysis. A stockpile of the ToxiSense disks would be stored on the buoy and automatic disk-changing would facilitate periodic measurements of the surrounding waters for a targeted deployment of six months. In addition, the fluorescent signal measured by the reader would be relayed to the laboratory via wireless network (Maguire, 2019).

The work described in this thesis chapter focused on the optimisation of the anti-MC-LR scFv such that it would achieve high-sensitivity detection of the MC-LR target molecule as well as the improvement of the antibody's stability such that it would remain stable for the expected six month deployment of the biosensor system. In future experiments, if such anti-MC-LR mutant scFv are to be incorporated into the ToxiSense system, optimisations of the antibody coating concentrations and analysis of the on-disk binding characteristics would be required. Furthermore, long-term stability studies would be required to determine the stability of the mutant clones over the required six month deployment period, during which time, wide temperature fluctuations would be expected. However, if such challenges can be met, this detection system may provide a revolutionary means to monitor algal toxins in real-time and may help to mitigate their harmful effects on humans and wildlife.

5 Generation of an avian anti-*B. cereus* scFv antibody fragment

5.1 Introduction

This chapter describes the development of recombinant antibody fragments for targeting *B. cereus* vegetative cells and spores. *B. cereus* is an endospore-forming, toxin-producing foodborne pathogen (Agata *et al.*, 1994; Ehling-Schulz *et al.*, 2004; Alonzo *et al.*, 2015). The current EC regulations on *B. cereus* states that *Bacillus* contamination should be “as low as possible” for dried infant formula and dried dietary food, with a limit of 500 cfu/g (European Commission, 2005). While there are no official EC regulations on *B. cereus* levels in milk, companies often impose a strict limit of 10 cfu/mL (International Dairy Federation, 2016). However, the approved culture-based detection methods have significant disadvantages such as a long turnaround time of days and are labour- and time-intensive (Izadi *et al.*, 2016). Another disadvantage of culture-based methods is the inability to enumerate viable but non-culturable (VBNC) or non-viable cells present (Cronin and Wilkinson, 2010). Therefore, there is a pressing need for a system that can rapidly and sensitively measure *B. cereus* contamination in food. A viable system to achieve this is the use of flow cytometry (FCM). FCM is an established method that can distinguish live cells from VBNC and non-viable cells with excellent sensitivity. FCM can be coupled with fluorescent dyes and species-specific antibodies to allow for species-level identification and quantification. However, *B. cereus* is a very difficult target to measure; many members of the *Bacillus* genus are very closely related and share a high number of similar genetic and morphological features. Thus, in order to facilitate accurate measurement of *B. cereus* using FCM, there is a requirement of species-specific antibodies.

Therefore, the aim of this chapter was to develop rAbs with high specificity to *B. cereus* vegetative cells and spores and that have low cross-reactivity to the closely related *Bacillus* species *B. subtilis* (vegetative cells and spores). This was carried out through the processes of host-immunisation, library construction and screening via phage display and whole-cell panning. It was intended then that these rAbs will then be incorporated into a FCM assay being developed in the University of Limerick that will quantify *B. cereus* cells and spores in dairy products with high sensitivity and specificity.

In this chapter, a White Leghorn chicken was immunised with inactivated *B. cereus* cells and a strong immune response was generated. Polyclonal IgY antibodies were

harvested and purified from eggs. This polyclonal IgY was shown to exhibit strong binding to *B. cereus* cells and spores but also showed cross reactivity to *B. subtilis*. This highlighted the requirement to screen the antibody repertoire for *B. cereus*-specific antibodies. Thus, following the completion of the immunisation regime, the host spleen was harvested and the RNA was extracted. The RNA was converted to cDNA by reverse transcription to allow for the amplification of the variable antibody genes. Following amplification, the variable genes were joined by SOE PCR to form a scFv-encoding gene that was subsequently restriction-digested and ligated into a phagemid vector. This vector was transformed into *E. coli* to form an antibody library of 2.8×10^7 clones. This scFv library was subsequently screened by phage display and whole-cell panning. Each round of this whole-cell panning approach utilised a negative selection step with *B. subtilis* followed by a positive selection step with *B. cereus*. Following two rounds of panning, 192 clones were isolated and tested by monoclonal ELISA, which allowed for the identification of 9 potential scFv clones. Despite exhibiting some degree of cross-reactivity, these appeared to show preferential binding towards *B. cereus*. Future work on this project would require further characterisation of the identified scFv clones. In addition, further work should focus on the identification of species-specific biomarkers for *B. cereus* and further rounds of screening to isolate more potential antibodies specific to *B. cereus*.

5.2 Results

5.2.1 Development of polyclonal anti-*B. cereus* IgY

5.2.1.1 Determination of avian immune response to *B. cereus* by indirect ELISA

During the immunisation regime, in order to determine the level of immune response exhibited by the immunised chicken towards *B. cereus*, a serum titre was performed according to Section 2.2.5.2. A high serum titre indicates a strong immune response towards the target. The serum titres of the pre-bleed and bleed 3 antisera are shown in Figure 5.1. It was observed that the titres of the pre-bleed and bleed 3 antisera were 1:7,300 and 1:86,000, respectively.

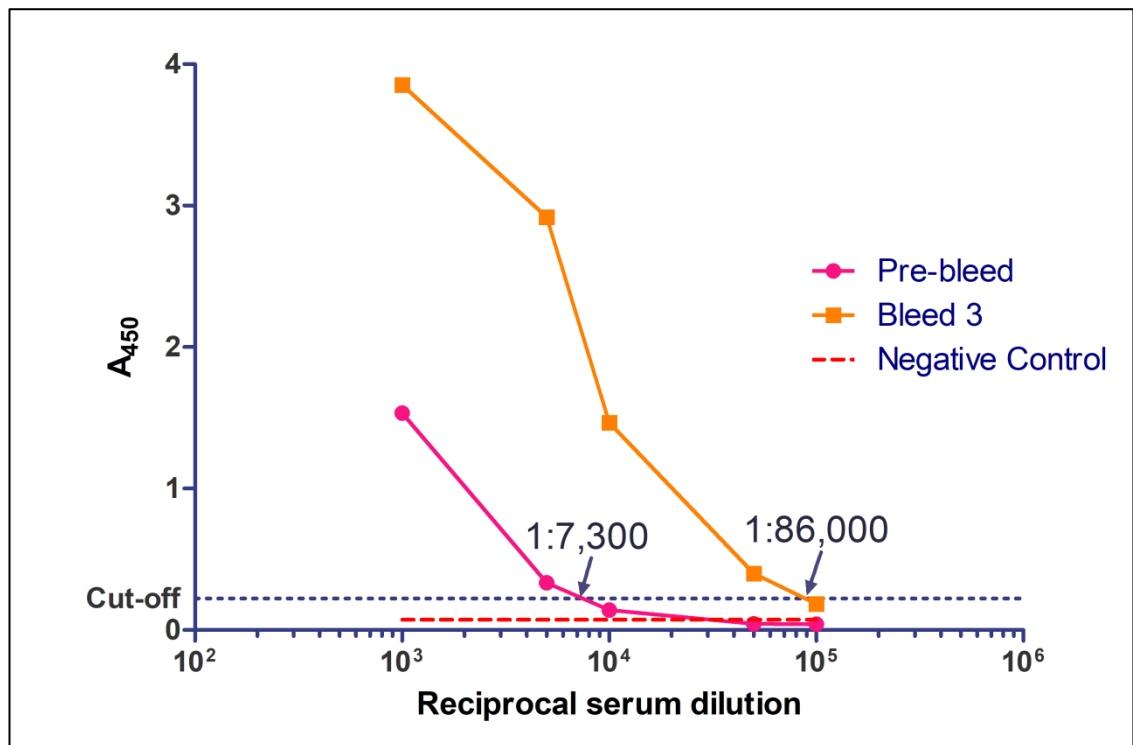


Figure 5.1: Serum titre of *B. cereus*-immunised chicken pre-bleed and bleed 3 antisera. The wells were coated with 8×10^7 cells/mL in PBS. In duplicate, the diluted serum was added to the plate. In the negative control wells, the same conditions as the test wells were used but the serum was omitted. The ‘cut-off’ was determined at three times the negative control (i.e. the lowest signal that can be distinguished from background).

5.2.1.2 Purification of polyclonal IgY from an egg of the *B. cereus*-immunised chicken

The purpose of this experiment was to isolate polyclonal IgY from an egg of the *B. cereus*-immunised chicken. Egg yolk is a rich and readily-available source of IgY and this polyclonal IgY is highly useful for assay development. The polyclonal IgY was purified using an IgY EggsPress Purification kit (Gallus Immunotech) according to Section 2.2.5.3. The IgY solution was quantified using a Pierce BCA Protein Assay kit according to Section 2.2.1.4. The standard curve for the BCA assay is presented in Figure 5.2. The polyclonal IgY protein concentration was determined as 5.97 mg/mL in a total volume of ~60 mL.

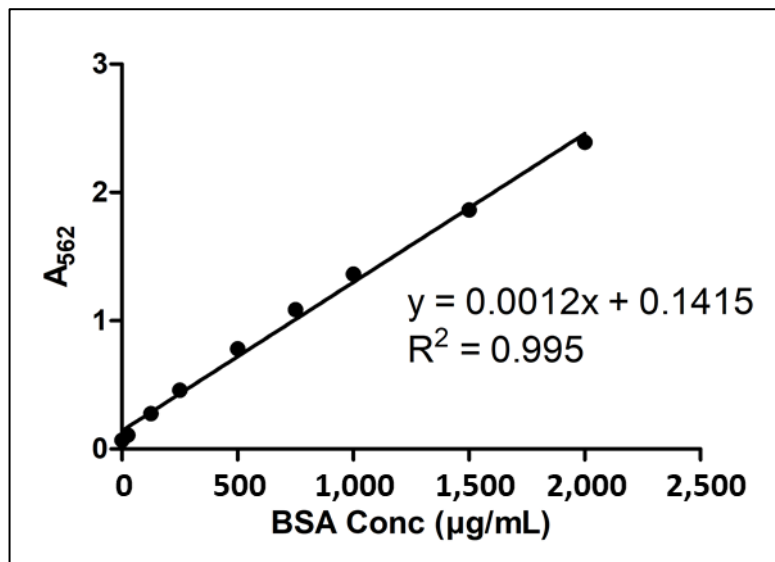


Figure 5.2: BCA assay standard curve. BSA protein standards were diluted from 25 to 2,000 µg/mL and measured in triplicate. Error bars = SEM (n = 3).

5.2.1.3 Measurement of specificity of purified IgY by ELISA

The purpose of this experiment was to determine the response of the purified polyclonal IgY to *B. cereus* and *B. subtilis* vegetative cells and spores. Due to how closely related *B. cereus* is to *B. subtilis*, and given that the antibody used was polyclonal in nature, it was expected that cross-reactivity would be observed. Due to limited stocks of *B. cereus* and *B. subtilis* vegetative cells and spores, each measurement was carried out singly. For the test wells, the polyclonal IgY from the *B. cereus*-immunised chicken was used, while for the control wells, polyclonal IgY from a non-immunised chicken was used. The ELISA absorbance readings are presented in Figure 5.3 while the titres of each antibody are presented in Table 5.1. It can be seen in Figure 5.3 that a similar response curve was observed from the *B. cereus*-immunised chicken IgY for the four targets, which shows high cross-reactivity of this antibody pool for both *B. cereus* and *B. subtilis* cells and spores. The control IgY also showed a response to the four targets, albeit at a lower level. However, it can be seen that the response from the *B. cereus*-immunised chicken IgY was in general higher for all four targets than the control IgY, which is likely due to the enrichment of the immune response after the immunisation regime.

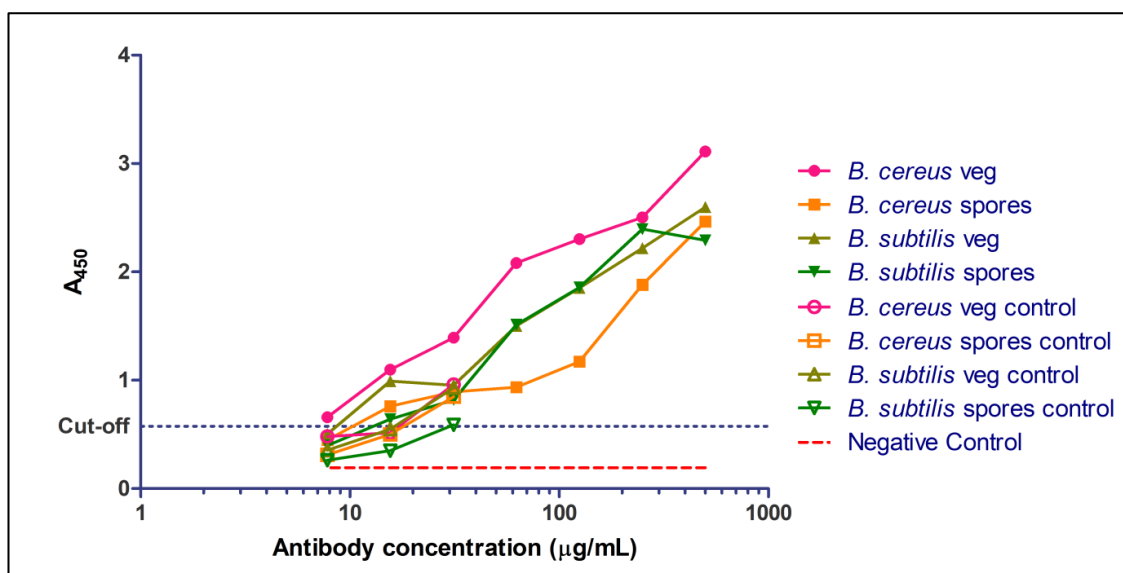


Figure 5.3: Response of polyclonal IgY from *B. cereus*-immunised (test) and non-immunised (control) chickens. The wells were coated with 1×10^7 cells or spores per mL. Singly, the diluted IgY from *B. cereus*-immunised chicken and non-immunised chicken (control) were added to the plate. A negative control was included, which omitted IgY from the test. The ‘cut-off’ was determined at three times the negative control.

Table 5.1: Titre values of *B. cereus*-immunised and control IgY samples for *B. cereus* and *B. subtilis* cells or spores.

Target	<i>B. cereus</i> -immunised IgY	Control IgY Titre
	Titre ($\mu\text{g/mL}$)	($\mu\text{g/mL}$)
<i>B. cereus</i> vegetative cells	<7.8	17
<i>B. cereus</i> spores	10.4	18
<i>B. subtilis</i> vegetative cells	8.6	16
<i>B. subtilis</i> spores	12.9	30

5.2.1.4 Measurement of the specificity of the affinity-matured polyclonal IgY by ELISA

The purpose of this experiment was to determine if it is possible to improve the cross-reactivity profile of the purified polyclonal IgY; it is desirable to improve the ratio of binding such that the IgY selectively binds to *B. cereus* and not *B. subtilis*. This was carried out by negatively depleting the IgY using *B. subtilis* cells (‘Negative selection’). Following this, the remaining IgY underwent positive selection using *B. cereus* cells (‘Positive selection’). The *B. cereus* cells will bound IgY were washed to remove non-specific antibodies and finally the bound IgY were eluted using a low pH elution (‘Positive elution’).

Following each stage of this process, antibody samples were kept for protein concentration analysis, as measured by BCA assay. This was carried out so as to facilitate analysis of equal quantities of antibody by ELISA. The protein concentrations of the samples obtained from the affinity preparation process are outlined in Figure 5.4.

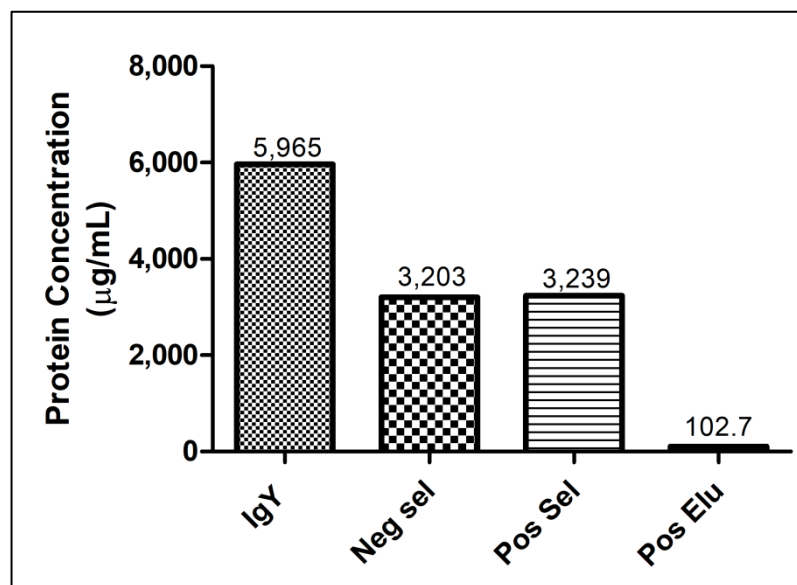


Figure 5.4: Protein concentration measurements after affinity preparation of IgY. The concentrations of stock the IgY, the negative selection (Neg sel), positive selection (Pos sel) and positive elution (Pos Elu) samples obtained after the affinity preparation of the IgY were determined by BCA assay. Each data point represents a single measurement for each sample. The protein concentration (µg/mL) in numerical format is presented above each bar.

In addition to measuring the protein concentrations of each sample, the binding response of the samples from the IgY affinity preparation process to *B. cereus* and *B. subtilis* vegetative cells and spores were determined by ELISA. So as to provide an equal estimation of the binding response of each sample, the antibody-containing samples were each normalised to 16.7 µg/mL. The results of this ELISA are shown in Figure 5.5.

Looking at the response to *B. cereus* cells, a slight drop was observed after the negative selection step. This might suggest that some of the IgY clones that were cross-reactive between *B. cereus* cells and *B. subtilis* cells were removed. For *B. cereus* spores, very little change was observed between the stock IgY, negative selection and positive selection. This might suggest that the *B. cereus* spore-specific IgY in the sample were retained. For *B. subtilis* cells and spores, there was no change observed between the stock IgY and the negative and positive selections. The result of the positive elution for all 4 targets shows a significant drop in binding response of this sample, with responses

close to the negative control. This would suggest that there was insufficient IgY in this sample to produce an observable response.

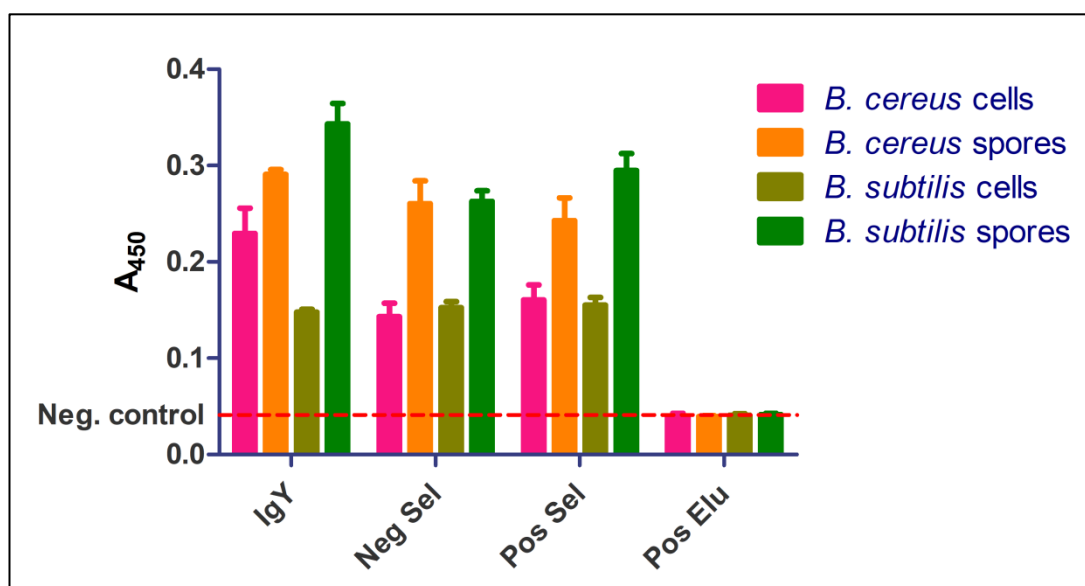


Figure 5.5: Binding response of the affinity preparation samples towards *B. cereus* and *B. subtilis* cells and spores. The stock IgY, the negative selection (Neg sel), positive selection (Pos sel) and positive elution (Pos Elu) samples were tested on wells coated with 1×10^7 cells or spores per mL. Each IgY-containing sample was diluted to 16.7 $\mu\text{g/mL}$. The negative control consisted of all test components but omitted the IgY. Error bars = SEM (n = 3).

5.2.2 Development of an anti-*B. cereus* recombinant scFv library

5.2.2.1 Spectrophotometric determination of extracted avian RNA and synthesized cDNA concentration

After the extraction of RNA from the *B. cereus*-immunised chicken spleen, the RNA was quantified by absorbance measurement at 260 nm. After cDNA-synthesis, the cDNA was also quantified by absorbance measurement at 260 nm (see Table 5.2).

Table 5.2: Measurement of extracted RNA and synthesized cDNA concentrations

Sample	Concentration (ng/ μL)
Extracted RNA	10,752
Synthesized cDNA	2,366

5.2.2.2 Amplification of antibody variable light and heavy genes

The purpose of these experiments was to amplify the variable light and heavy antibody genes from the synthesised cDNA template using sequence-specific primers (outlined in Table 2.31). The amplified variable light and heavy DNA was used in further experiments to produce a scFv-encoding gene by SOE PCR using SOE primers (Section 2.2.5.11). All PCR products were separated on 1% (w/v) agarose gels stained with SYBR® Safe. The gel image of the small-scale V_L and V_H amplifications is presented in Figure 5.6.

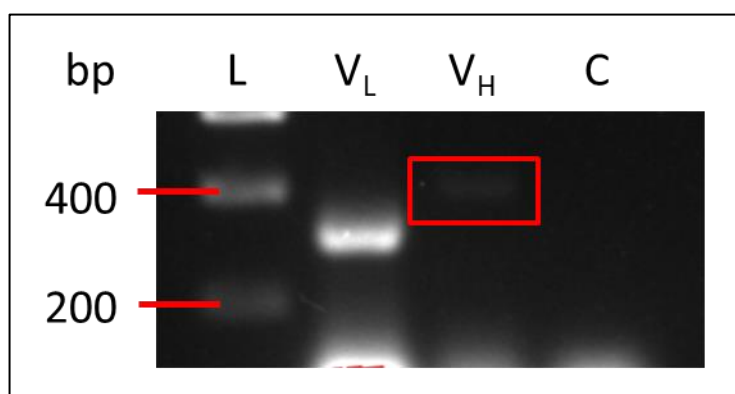


Figure 5.6: Small-scale V_L and V_H amplification. A faint band was observed at ~ 400 bp in the V_H lane, as indicated by the red box. L = Hyperladder 1 kb; C = control. (The control reaction included all reaction components except cDNA).

The V_L and V_H fragments were observed at ~ 350 and 400 bp, respectively. The intensity of the V_L reaction suggested that the conditions were well optimised. These conditions were utilised and a large-scale V_L PCR was carried out. The gel image from the large-scale V_L PCR is presented in Figure 5.7. The large-scale V_L product was purified and quantified by absorbance measurement at 260 nm (see Table 5.3). The V_H PCR band was not very intense, which suggested that further optimisation would be required. For the V_H PCR optimisation, the primer concentration was varied to 0.5 , 1 and 1.5 μM . The gel image of these amplification reactions can be observed in Figure 5.8. Each of the reactions appeared to have similar, albeit faint, intensity of bands. Therefore, a primer concentration of 0.5 μM was subsequently used.

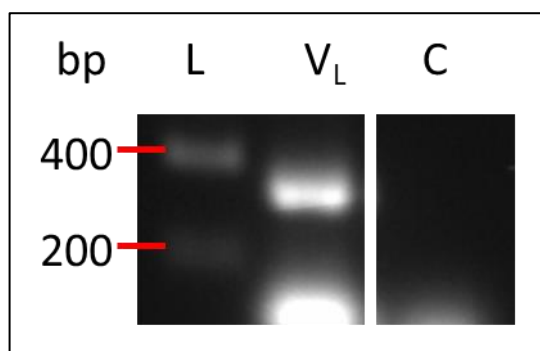


Figure 5.7: Large-scale V_L amplification. The V_L fragment was observed at ~350 bp. L = Hyperladder 1 kb; C = control. (The control reaction included all reaction components except cDNA).

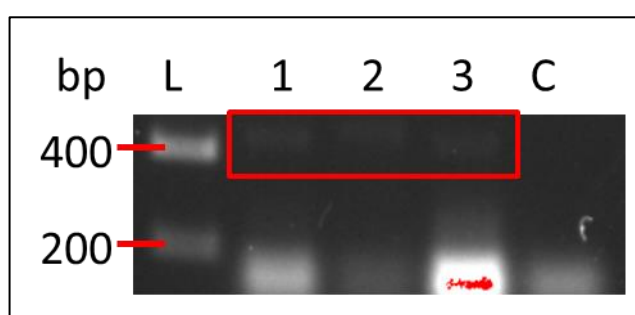


Figure 5.8: V_H PCR optimisation. The V_H fragment was observed in all test lanes at ~400 bp, as indicated by the red box. L = Hyperladder 1 kb; 1 – 3 = V_H amplification using 0.5, 1 and 1.5 μM primer concentration, respectively; C = control. (The control reaction included all reaction components except cDNA).

A large-scale V_H PCR was carried out using the optimised 0.5 μM primer concentration. A sample of the large-scale PCR was run on a 1% (w/v) agarose gel stained with SYBR® Safe. The gel image of the large-scale V_H PCR is presented in Figure 5.9. The large-scale V_H product was purified and quantified by absorbance measurement at 260 nm (see Table 5.3).

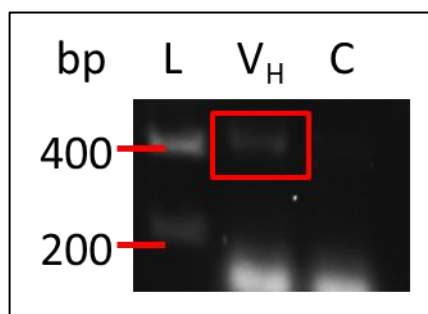


Figure 5.9: Large-scale V_H amplification. The V_H fragment was observed at 400 bp as indicated by the red box. L = Hyperladder 1 kb; C = control. (The control reaction included all reaction components except cDNA).

5.2.2.3 Generation of scFv-encoding gene by SOE PCR

As can be seen from Figure 5.9, the V_H band at ~400 bp is quite faint. It was decided to attempt to amplify the SOE PCR fragment using this V_H product and the V_L product. The purpose was to determine if the SOE PCR product could be amplified; if it could not be amplified, further optimisation of the V_H PCR would be carried out.

The purified V_L and V_H DNA samples were used for the amplification of the scFv DNA fragment by SOE PCR. A small-scale SOE PCR and subsequently a large-scale SOE PCR were carried out. The small-scale SOE PCR product and a sample of the pooled SOE PCR product were separated on a 1% (w/v) agarose gel stained with SYBR® Safe. The gel image of the SOE PCR products is presented in Figure 5.10. It can be seen in Figure 5.10 that strong bands were observed at ~800 bp, hence further optimisation of the V_H PCR was not required.

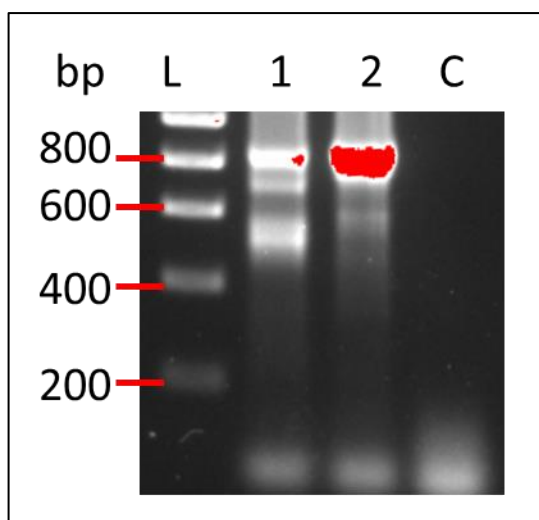


Figure 5.10: SOE PCR. The small-scale and large-scale SOE products can be observed in lanes 1 and 2, respectively, at ~800 bp. L = Hyperladder 1 kb; C = control. (The control reaction included all reaction components except V_L and V_H DNA).

Table 5.3: DNA concentration measurements of purified PCR products as determined by spectroscopic measurement at 260 nm.

Sample	Concentration (ng/ μ L)
V_L	128.9
V_H	15.7
SOE	207.6

5.2.2.4 Restriction enzyme digestion and ligation of scFv DNA and pComb3XSS plasmid

The purpose of this experiment was to digest the scFv DNA and pComb3XSS products using the *Sfi*I restriction enzyme in order to form complementary ‘sticky’ ends that would facilitate the insertion of the scFv DNA into the plasmid. The pComb3XSS was also digested with *Xba*I and *Xho*I, which act on restriction sites within the plasmid’s Stuffer fragment. This was carried out in order to reduce the chance of the Stuffer fragment being re-ligated back into the plasmid. Sufficient stocks of pComb3XSS plasmid were obtained in Chapter 3. The digested scFv DNA and pComb3XSS plasmid were separated on 1% (w/v) and 0.7% (w/v) agarose gels, respectively. They were each gel-purified and the DNA concentrations were measured by spectroscopic measurement as 332.8 and 312.4 ng/μL, respectively. These concentrations were needed in order to determine the volumes of scFv and pComb3XSS plasmid to be included in the ligation reaction. After the ligation was carried out, the ligated DNA was ethanol-precipitated in order to remove the ligase enzyme and buffer components. The DNA was then stored at -20 °C.

5.2.2.5 Electroporation of SOE-pComb3XSS into XL1 Blue *E. coli*

The purpose of this experiment was to transform *E. coli* with the scFv-encoding phagemid to allow for expression of scFv-displaying phage. The pComb3XSS plasmid containing the scFv gene insert was electroporated into XL1 Blue *E. coli* to allow for expression of the scFv-pIII fusion protein. A titre was carried out to determine the approximate library size. This titre was determined to be 2.8×10^7 clones. A colony pick PCR was carried out to determine the proportion of the transformed clones that contained the scFv insert (see Figure 5.11). Eleven out of twelve picked colonies (91.7%) contained the scFv insert, indicating that a high proportion of the transformed clones have potential of expressing scFv fragments.

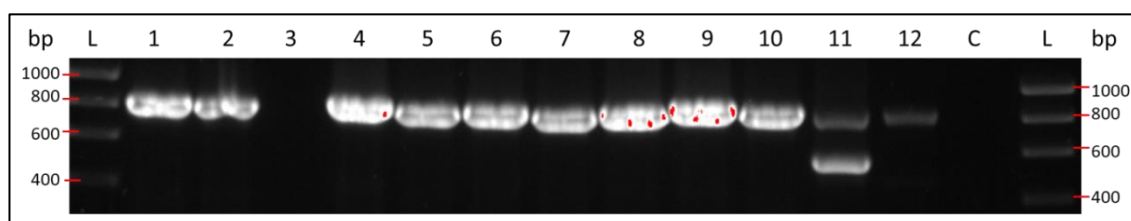


Figure 5.11: Colony pick PCR of transformed anti-*B. cereus* scFv library. The scFv gene was observed at ~800 bp in 11 out of 12 tested colonies. L = Hyperladder 1 kb; C = Control. (The control reaction included all reaction components except a picked colony).

5.2.2.6 Screening of anti-*B. cereus* recombinant scFv library by whole-cell panning

The purpose of the panning experiments was to screen and enrich the constructed antibody library for clones that preferentially bound to *B. cereus* and not to *B. subtilis*. In order to determine if the screening process was sequentially reducing the size of the antibody library, after each round, the input and output phage titres were determined by counting the colonies grown on titre plates (see Table 5.4).

Table 5.4: Input and output phage titres from each round of panning.

Round	Input titre (cfu/mL)	Output titre (cfu/mL)
1	4.61×10^{13}	1.06×10^8
2	2.10×10^{13}	3.57×10^7

5.2.2.7 Colony Pick PCR of screened scFv library

A colony pick PCR was carried out on a number of colonies in order to determine if the scFv gene insert was still present within the input and output phage library after each round of panning. Five colonies from the input and output titre plates from rounds 1 and 2 of panning were picked and PCRs were carried out to amplify the scFv-encoding gene present. The PCR products were separated on a 1% (w/v) agarose gel stained with SYBR® Safe. The gel image of the colony pick PCRs is presented in Figure 5.12. It can be seen from round 1 that the 800 bp scFv fragment was observed in 2 of the 5 tested input colonies and 2 of the 5 tested output colonies; this suggests that the scFv insert is present in ~40% of the colonies. From round 2, the 800 bp scFv fragment was observed in 4 of the 5 tested input colonies and 1 of the 5 tested output colonies; this would suggest that going into round 2, the insert was present in ~80% of clones, however, following round 2, this was reduced to ~20%.

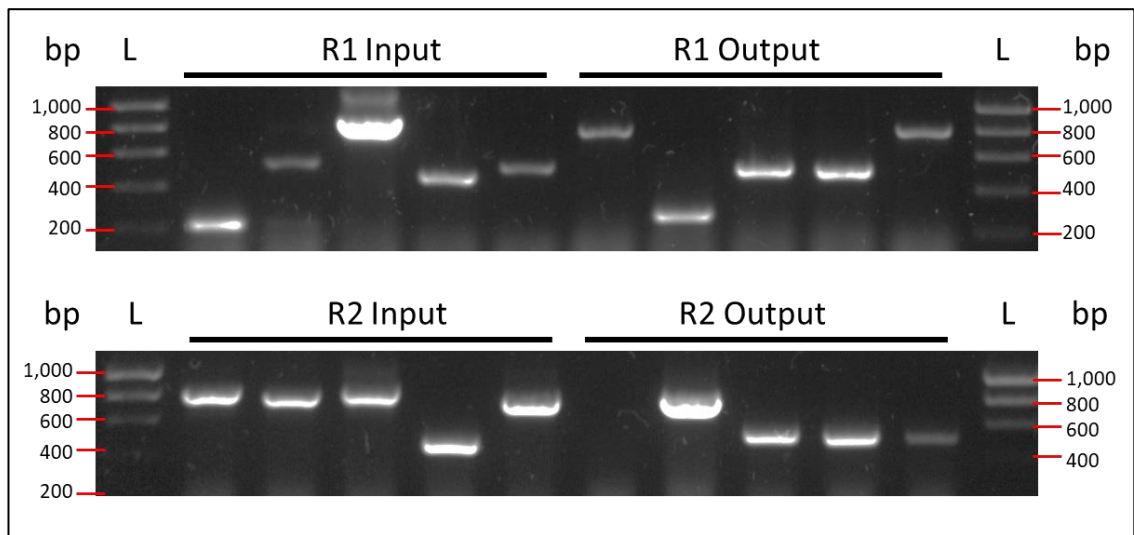


Figure 5.12: Colony pick PCR of panning input and output titres. The scFv gene insert was observed at ~800 bp. L = Hyperladder 1 kb.

5.2.2.8 Measurement of response of individual scFv clones for *B. cereus* and *B. subtilis* by monoclonal ELISA

The purpose of this experiment was to determine the response of individual scFv molecules for *B. cereus* and *B. subtilis* vegetative cells. After re-infection of the round 2 output phage into Top10F' *E. coli*, 192 colonies were picked and grown to express their encoded scFv molecules. Each scFv molecule was analysed for binding to *B. cereus* and *B. subtilis* vegetative cells adsorbed onto multiwell plates. The response of each clone is shown in Figures 5.13 and 5.14 below. An average background absorbance value of 0.041 was determined. A 'cut-off' value equal to 2x the background absorbance (0.082) was applied.

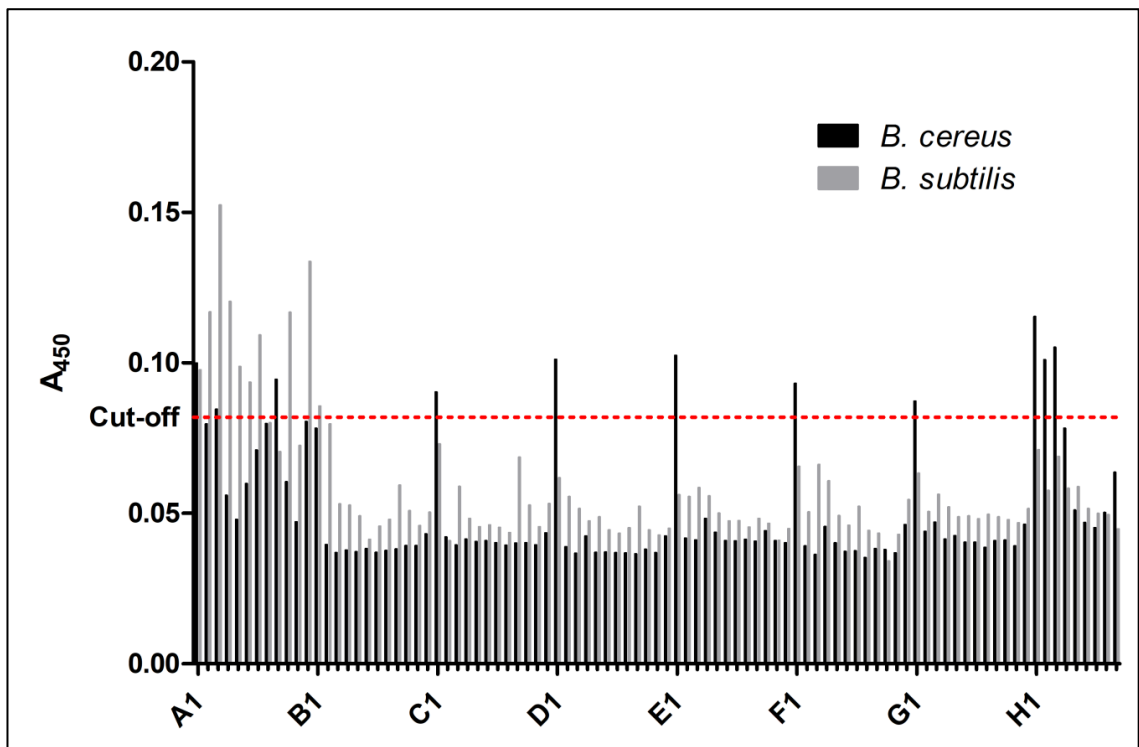


Figure 5.13: Monoclonal ELISA Plate 1. Response of 96 colonies from Round 2 to *B. cereus* (black bars) and *B. subtilis* (grey bars). The 'cut-off' was established as 2x the absorbance of the background response.

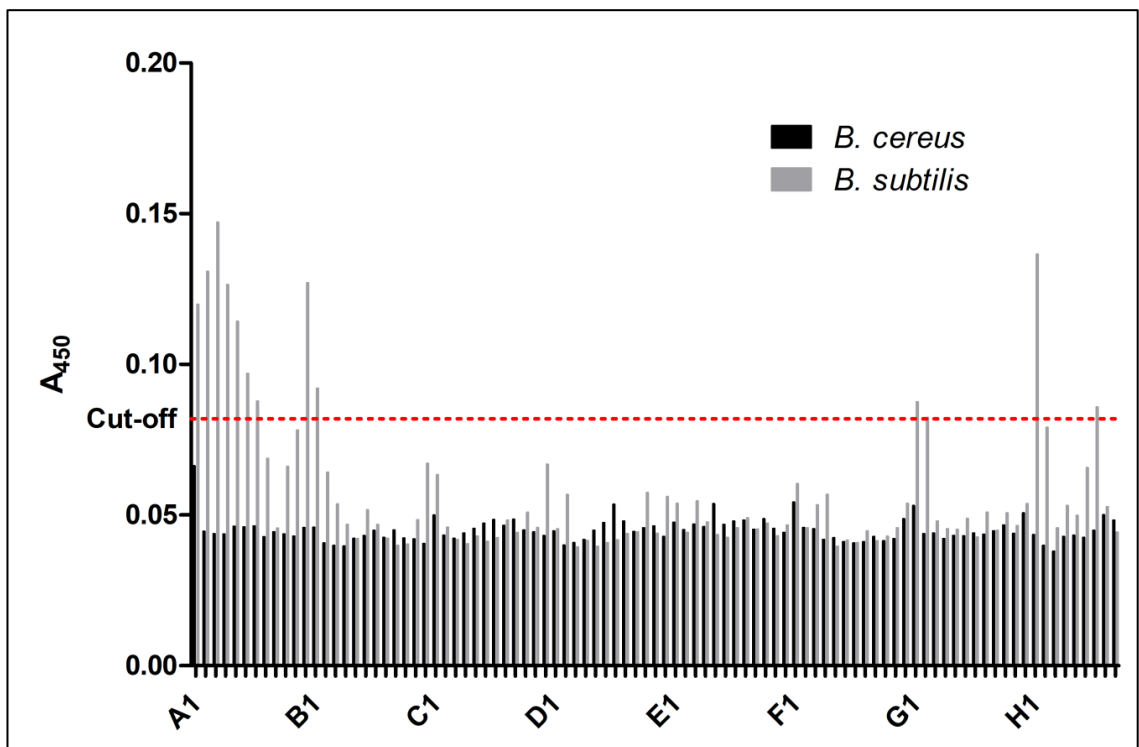


Figure 5.14: Monoclonal ELISA Plate 2. Response of 96 colonies from Round 2 to *B. cereus* (black bars) and *B. subtilis* (grey bars). The 'cut-off' was established as 2x the absorbance of the background response.

As can be seen from Figure 5.13, 11 clones appeared to display responses to *B. cereus* greater than the ‘cut-off’, while 10 clones showed responses to *B. subtilis* greater than the ‘cut-off’. Meanwhile, from Figure 5.14, it can be seen that 0 clones and 12 clones appeared to display responses to *B. cereus* and *B. subtilis* greater than the ‘cut-off’, respectively.

Due to how closely related *B. cereus* and *B. subtilis* are, it was assumed that cross-reactivity would be observed for many of the scFv molecules. Therefore, the responses of each clone to *B. cereus* was divided by the response to *B. subtilis*, to obtain a response ratio (*B. cereus*:*B. subtilis*). The response ratios for plates 1 and 2 are presented in Figures 5.15 and 5.16 below. It can be seen from Figure 5.15 that a number of colonies showed a response ratio >1, which indicates that these scFv molecules may show more favourable binding towards *B. cereus* than to *B. subtilis*. Of these clones, 9 clones were picked for further analysis; these clones with their respective responses are shown in Table 5.5 below. Only clones from Plate 1 were chosen, as none of the clones on plate 2 displayed responses towards *B. cereus* greater than the ‘cut-off’.

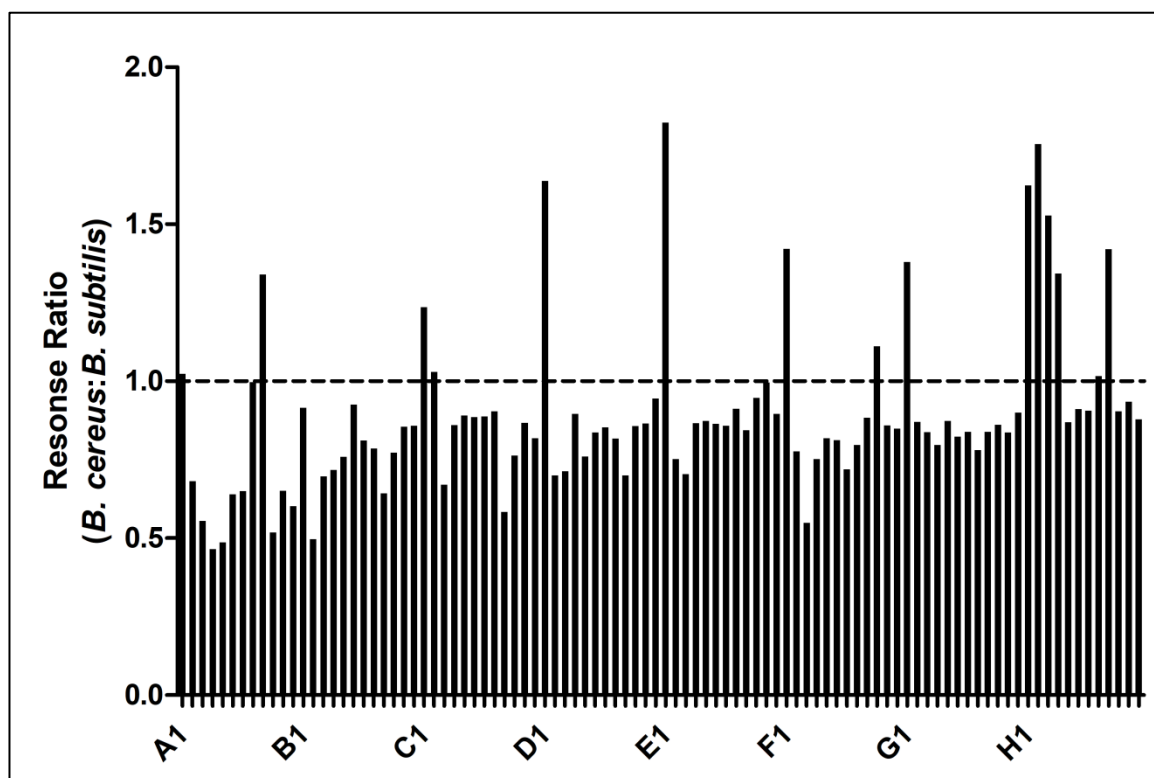


Figure 5.15: Monoclonal ELISA Plate 1 Response Ratio. The response ratio was calculated as the response of each clone to *B. cereus* was divided by the response to *B. subtilis*. Clones that show preferential binding to *B. cereus* should have a response ratio >1.

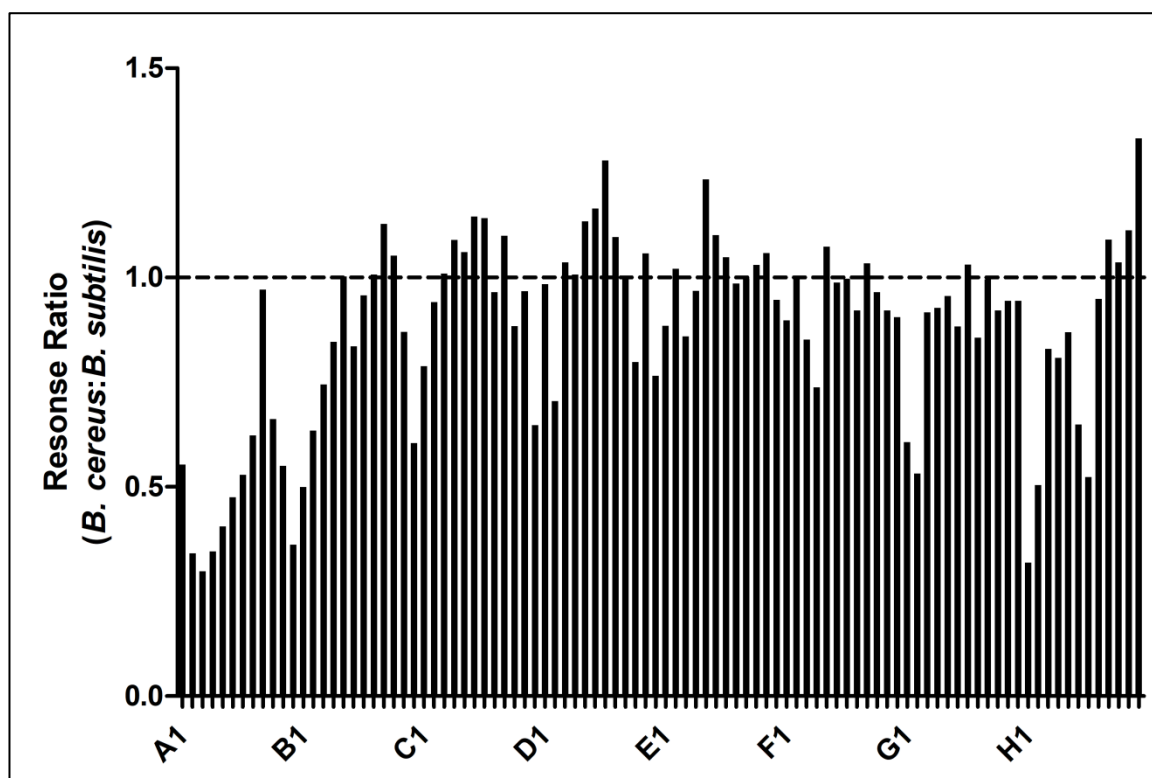


Figure 5.16: Monoclonal ELISA Plate 2 Response Ratio. The response ratio was calculated as the response of each clone to *B. cereus* was divided by the response to *B. subtilis*. Clones that show preferential binding to *B. cereus* should have a response ratio >1.

Table 5.5: Clones chosen from Monoclonal ELISA. Clones were chosen only from Plate 1, as no clones from Plate 2 showed response to *B. cereus* greater than the 'cut-off'.

Clone	Response to <i>B. cereus</i> (A ₄₅₀)	Response to <i>B. subtilis</i> (A ₄₅₀)	Response Ratio (<i>B. cereus</i> : <i>B. subtilis</i>)
E1	0.1025	0.0562	1.82
H2	0.1011	0.0576	1.76
D1	0.1012	0.0618	1.64
H1	0.1154	0.0711	1.62
H3	0.1052	0.0689	1.53
F1	0.0932	0.0656	1.42
G1	0.0873	0.0633	1.38
A9	0.0945	0.0705	1.34
C1	0.0903	0.0731	1.24

5.2.2.9 Colony pick PCR of the chosen scFv clones

The purpose of this experiment was to determine if the scFv-encoding gene could be identified in each of the nine clones chosen from the screened library. The PCR products were separated on a 1% (w/v) agarose gel stained with SYBR® Safe. The gel image of the colony pick PCRs is presented in Figure 5.17. It can be seen from Figure 5.17 that a band was observed at ~800 bp for clones A9, C1, D1, G1 and H3. A band was observed at ~500 bp for clones A9, E1, H1, H2 and H3.

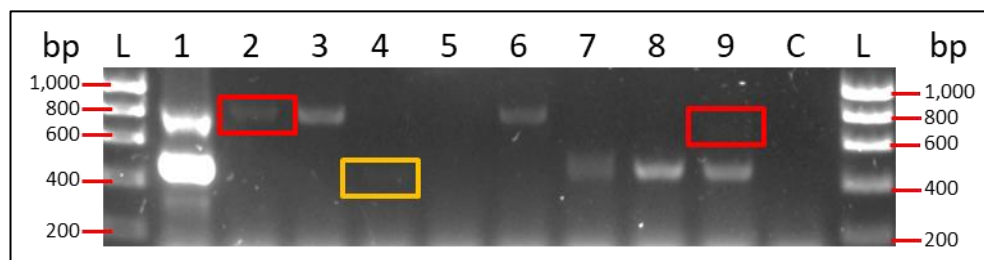


Figure 5.17: Colony pick PCR of nine clones from Monoclonal ELISA. L = Hyperladder 1 kb; 1 = A9; 2 = C1; 3 = D1; 4 = E1; 5 = F1; 6 = G1; 7 = H1; 8 = H2; 9 = H3; C = Control. (The control assay included all reaction components but included SB that contained no bacterial growth). A band was observed at ~800 bp in lanes 1, 2, 3, 6 and 9 (faint 800 bp bands in lanes 2 and 9 are indicated by red boxes). A band was observed at ~500 bp in lanes 1, 4, 7, 8 and 9 (a faint ~500 bp band in lane 4 is indicated by a yellow box).

5.3 Discussion

The development of a recombinant antibody library specific to *B. cereus* was initiated by the immunisation of a female White Leghorn chicken with formaldehyde-inactivated *B. cereus* vegetative cells. Whole cells were used for this purpose as, in the absence of a known *B. cereus*-specific biomarker, they present the most viable approach to displaying all *B. cereus* antigens to the host's immune system in their native state. After observing enrichment in the response of the host antiserum towards *B. cereus* following the third booster immunisation, the host was sacrificed and the RNA was extracted from the spleen. The RNA was successfully converted to cDNA and the antibody V genes were amplified. After joining the V_L and V_H genes by SOE PCR, the scFv-encoding genes were digested and ligated into the pComb3XSS phagemid vector. This vector was transformed into *E. coli*, creating a recombinant antibody of 2.8×10^7 clones. Finally, this library was screened by whole cell panning in order to enrich for clones showing specificity to *B. cereus*.

The use of chickens as a host for immunisations and generation of antibodies has a number of advantages over mammalian hosts; these include the ability to produce high yields of IgY from egg yolks, and easier construction of recombinant antibody libraries, which is due to the highly conserved framework regions of the IgY variable regions meaning that fewer primer combinations are required to amplify these V genes. It has also been observed that chickens can be used to generate immune responses towards targets that would be difficult to achieve with mice or rabbits (Barbas *et al.*, 2001).

In this current work, the immunisation regime consisted of the initial immunisation plus two subsequent booster immunisations. It was discussed in an earlier chapter that a serum titre is an effective means to determine the extent of the immune response in an immunised host. The serum titre is used to measure the level of antibodies present in the serum that are specific to the target of interest. The serum titre of 1:7,300 was observed for the pre-bleed antiserum. This is an interesting observation, as it would ordinarily be assumed that the host would not have prior exposure to the immunogen and so the pre-bleed antiserum would not be expected to show a response to the target. For example, the mice used for the generation of an anti-AZA antibody did not show any response in the pre-bleed antisera towards AZA (see Figure 3.2). However, as was discussed in Section 1.4, *B. cereus* is a ubiquitous organism in nature. Hence, it could reasonably be expected that a chicken may become exposed to *B. cereus* via food or water that is contaminated with *B. cereus* cells or spores. Therefore, perhaps it is not surprising that prior to immunisations the response of the host antiserum to whole *B. cereus* cells was relatively high. Despite this, enrichment in the host's immune response was observed, since following the second booster immunisation, a strong immune response towards *B. cereus* was observed, as indicated by a serum titre of 1:86,000 for the bleed 3 antiserum.

After a strong immune response was observed from the host, IgY was purified from egg yolk. The protein concentration of the purified IgY was 5.97 mg/mL in a volume of ~60 mL. Assuming 90% purity of IgY in the sample (based on the manufacturer's guidelines; Gallus Immunotech (2018)), this equates to 322 mg of IgY. It was discussed by Carlander *et al.*, (1999) that 2 g of IgY from egg yolk approximately corresponds to the IgY content of 600 mL of blood, which demonstrates the advantage of using chickens as a host for immunisations.

The specificity of the purified IgY was measured by indirect ELISA. Polyclonal IgY of the *B. cereus*-immunised and a non-immunised chicken were tested for binding to *B. cereus* and *B. subtilis* vegetative cells and spores. The IgY of the *B. cereus*-immunised chicken showed strong response to all four targets, with titre values of <7.8, 10.4, 8.6 and 12.9 µg/mL observed for *B. cereus* vegetative cells, *B. cereus* spores, *B. subtilis* vegetative cells and *B. subtilis* spores, respectively. The control IgY also showed a response to all four targets, with titre values of 17, 18, 16 and 30 µg/mL observed for *B. cereus* vegetative cells, *B. cereus* spores, *B. subtilis* vegetative cells and *B. subtilis* spores, respectively. The response from the control IgY is similar to the observation of the pre-bleed antiserum response to *B. cereus* (Figure 5.3). It was discussed previously that these bacteria are highly ubiquitous in nature, thus, it is possible that the control chicken was pre-exposed to these *Bacillus* species, and this immune response may have been passed from mother to embryo. Furthermore, these observations are similar to the results reported by the collaborating researchers in the University of Limerick (UL). The purified IgY from Section 5.2.1 were sent to UL to facilitate early development of a FCM method. Preliminary work showed that this polyclonal chicken IgY responded to three *B. cereus* strains and to one *B. subtilis* strain (see Section 9.1). In any case, the result presented in Figure 5.3 shows a strong albeit non-specific response to *B. cereus*. However, this result and the result of Section 9.1 also highlight the requirement of a stringent screening process to enrich for only *B. cereus*-specific antibodies.

Following on from this, given the abundant quantities of IgY available, enrichment of the polyclonal IgY pool for *B. cereus*-specific antibodies was attempted. If this relatively rapid method proved successful, it would indicate the high potential of the recombinant scFv library to produce *B. cereus*-specific clones. The theory posited was based on the whole-cell panning approach applied to the recombinant antibody-phage library in Section 5.2.2.6; by exposing the IgY pool to *B. subtilis* spores, allowing Abs specific for this species to bind, and by subsequently separating the spores, the remaining pool will be more depleted of *B. subtilis*-specific Abs. This pool could then be subjected to positive selection by exposing the Abs to *B. cereus* spores and allowed to bind. By separating the *B. cereus* spores and the bound Abs, and by subsequently eluting the Abs, the resultant pool should be enriched towards *B. cereus* antigens. The concept of this immunoaffinity-purification is illustrated in Figure 5.18 below.

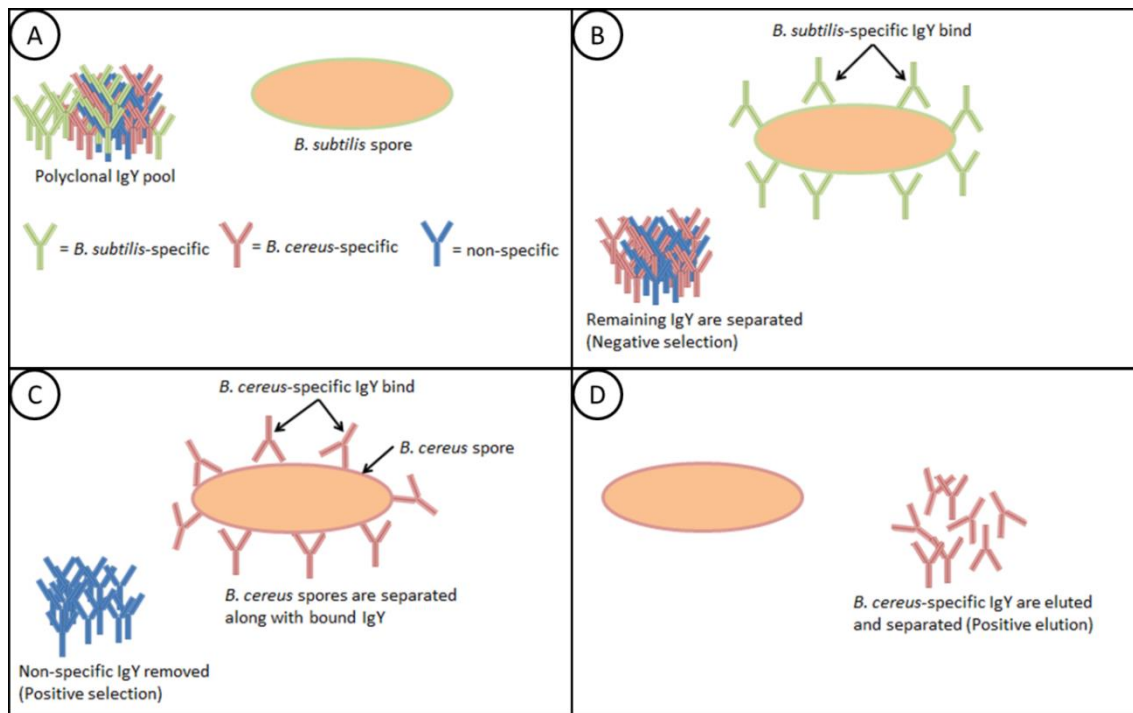


Figure 5.18: Concept for immunoaffinity-purification of IgY sample. (a) The polyclonal IgY pool consists of antibody clones specific to *B. subtilis* (green) and *B. cereus* (red) and also contains non-specific IgY (blue). (b) The IgY pool is presented with *B. subtilis* spores. The *B. subtilis*-specific IgY (green) bind to these spores. By applying a centrifugation step, the spores and the bound IgY are removed, while the remaining IgY are retained (these are designated ‘Negative Selection’). (c) The ‘Negative Selection’ IgY pool are presented with *B. cereus* spores. *B. cereus*-specific IgY (red) bind to the spores. A centrifugation step is carried out to separate the spores with bound IgY from the non-specific IgY (blue). These non-specific IgY are removed and designated ‘Positive Selection’. (d) The *B. cereus* spores are subjected to a wash step to remove any loosely bound IgY. The remaining *B. cereus*-specific IgY are eluted by low pH elution and are separated from the spores by centrifugation. These eluted *B. cereus* specific IgY are designated ‘Positive Elution’.

As can be seen from Figure 5.4, the treatment effectively reduced the protein concentration, with a successive drop in protein concentration with each step. The result shows that the negative selection resulted in a ~50% drop in protein concentration versus the stock IgY. There is negligible difference in protein concentration between the negative and positive selection samples. The negative selection step should effectively remove most *B. subtilis* spore-specific IgY in the pool. The remaining pool was then exposed to *B. cereus* spores and only those IgY molecules that remained bound after the wash step and that were eluted went into the positive elution sample. It can be seen from the Positive Elution sample that the concentration measured, 102.7 $\mu\text{g/mL}$, is a considerable reduction when compared to the starting stock IgY concentration of 5,965 $\mu\text{g/mL}$. The low concentration is due to the very small number of antibody molecules that would be permitted to bind to the *B. cereus* spore surface and that were subsequently eluted.

By normalising the protein concentration of each sample to 16.7 $\mu\text{g}/\text{mL}$ (which was chosen due to the limitation of the positive elution sample), it was expected that the cross-reactivity of the IgY pool towards *B. subtilis* would drop with each step of the process while the response specific to *B. cereus* was expected to increase. However, as can be seen from Figure 5.5, the stock IgY, negative selection and positive selection samples each showed similar binding responses to the four targets. Meanwhile, little or no response was observed from the positive elution for the four targets. It is likely that very little IgY was retained and subsequently eluted from the *B. cereus* spores used in the positive selection step. It was discussed in the BCA assay section that this was likely due to the low number of unique binding sites on *B. cereus* compared to *B. subtilis* that would allow for binding to the enriched IgY pool. It could be reasonably expected that the low number of binding sites and the small surface area of the *B. cereus* spores would have implications for the number of IgY molecules that would be pulled through this selection process. Whereas in phage display, the scFv-phage molecules brought through the selection can be subsequently amplified by re-infection and propagation in *E. coli*, in this case, the IgY brought through the selection cannot be amplified; hence, the number of IgY molecules available for ELISA was too low to allow for a signal to be observed. It is possible that the protein concentration for the positive elution sample in the BCA assay was close to the limit of detection of the assay and may have over-estimated the true concentration. It may be also possible that the pH elution process was not stringent enough to elute any high affinity binders on the *B. cereus* spore surface. It was subsequently attempted to develop a recombinant scFv library keeping these issues in mind.

Following the immunisation of the host and the development of a strong immune response to *B. cereus*, the host was sacrificed and the spleen tissue was harvested. The RNA of this tissue was successfully extracted and converted to cDNA, with RNA and DNA concentrations of 10,752 $\text{ng}/\mu\text{L}$ and 2,366 $\text{ng}/\mu\text{L}$ obtained, respectively. The V_L region was subsequently amplified by large-scale PCR (Figure 5.7) and was purified with a DNA concentration of 128.9 $\text{ng}/\mu\text{L}$ obtained. However, the V_H gene proved more difficult to amplify. It was attempted to optimise the primer concentration, but the resultant bands were of similar intensity (Figure 5.8). The 0.5 μM primer concentration was used for further experiments as this was the most economical use of the primers. Following this a large-scale V_H PCR was carried out and purified, with a DNA

concentration of 15.7 ng/ μ L obtained. The low concentration observed may have been due to this particular lot of the NucleoSpin kit being used, as it was observed by other users at this time that issues with this particular kit had arisen. The purified V_H DNA was kept and was used to carry out a single SOE PCR. It can be observed in Figure 5.10 lane 1 that a strong band at ~800 bp was observed. This suggests that the V_H region was successfully purified, as poor SOE amplification would be expected otherwise. It is possible that some of the NucleoSpin kit reagents were not thoroughly removed by the wash steps. Such reagents may have been co-eluted from the silica membrane with the V_H DNA. The presence of interfering substances in the DNA solution may have caused an error in the 260 nm absorbance reading, which in turn may have caused the V_H DNA concentration to be underestimated. It should be noted that the V_L, V_H and SOE PCRs were carried out over several months and different lots of the NucleoSpin kits were used for the purifications. It is possible that the kit used for V_H purification may have experienced degeneration of kit components.

A large-scale SOE PCR was carried out in order to have sufficient scFv gene product to transform into *E. coli*. The SOE PCR product was observed at ~800 bp (Figure 5.10 lane 2). A number of additional bands can also be observed at sizes between 500 – 700 bp in lanes 1 and 2. These are likely PCR products that did not undergo complete polymerisation or perhaps occurred from imperfect pairing of the V_L and V_H genes. However, the 800 bp band was carefully excised from the gel and was subsequently purified, with a concentration of 207.6 ng/ μ L obtained.

This scFv-encoding gene along with the phagemid vector pCOMB3XSS were subsequently restriction enzyme digested. The scFv gene was ligated into the pCOMB3XSS vector and this was transformed into *E. coli*. The resultant library size was 2.8×10^7 clones, which is considered a suitable size for a recombinant scFv library before screening (Barbas *et al.*, 2001). A colony pick PCR was also carried out which confirmed the presence of the scFv gene in eleven out of the twelve colonies, which indicates high transformation efficiency.

The *E. coli* scFv library was subsequently infected with helper phage to convert the library into a phage-displayed antibody library. Following this, it was attempted to screen the library by whole-cell panning. The theory behind the strategy employed is the same as that applied to the IgY immunoaffinity maturation; in each round the library

would be depleted for *B. subtilis*-specific clones by negative selection with *B. subtilis* vegetative cells; following this *B. cereus*-specific clones would be enriched by a positive selection step using *B. cereus* cells. The stringency of the screening was also increased by reducing the concentration of *B. cereus* cells and increasing the number of wash steps. In addition, the potential issue of poor elution of high affinity binders (as was alluded to in the IgY immunoaffinity section) was addressed through the use of a competitive elution strategy. By mixing the scFv-phage-bound *B. cereus* cells with the *E. coli* used for phage recovery, the number of F pili on the *E. coli* cells will far outnumber the binding sites on *B. cereus* cells, thereby out-competing these sites. After 2 rounds of panning, the number of clones was reduced, as presented in Table 5.4. Also, as shown in the colony pick PCR result (Figure 5.12), the scFv gene was retained after the 2 rounds of panning, albeit in a relatively low proportion of the tested colonies. The presence of empty-vector clones in a phage pool is often a cause for concern, as these clones will not have the burden of expressing the encoded protein, hence they will have a competitive growth advantage. However, it appears that in most of the tested clones, DNA bands with sizes ranging from 400 – 600 bp were observed. These may have occurred due to truncation of the DNA molecule, low specificity of binding with the amplification primers, or by incomplete polymerisation of the target DNA. In the case that clones containing an empty vector or truncated scFv gene, such clones would likely have a growth advantage over the clones that over-express a full length scFv gene; hence it is possible that the latter clones would be out-competed by those growing at a faster rate, which would have negative implications for the successful isolation of *B. cereus*-specific scFv molecules. Thus, it was decided to temporarily end the panning process in order to check for the presence of *B. cereus*-specific clones by monoclonal ELISA. If such clones could not be identified at this stage of panning, further rounds of screening could be subsequently carried out.

It was decided to test 192 individual clones after round 2 of panning, as it was hoped that by showing preferential enrichment for *B. cereus* rather than *B. subtilis*, it would show the potential of this library for producing scFv molecules that can distinguish these bacterial species. It was also anticipated that the identification of such clones would show the potential for this whole-cell panning approach for enriching such clones, even in the absence of a species-specific biomarker. The result of the monoclonal ELISA, plate (Figures 5.13 and 5.14) shows that 11 clones showed a

response to *B. cereus* greater than the 'cut-off' value, while and 10 clones showed a response to *B. subtilis* greater than the 'cut-off' value. When looking at the response ratio data for this plate (Figure 5.15), a number of clones had favourable binding for *B. cereus* over *B. subtilis*. Nine clones were chosen from the original 192 clones picked from Round 2 of panning. These clones were chosen on the basis that they showed a binding response towards *B. cereus* in a monoclonal ELISA greater than the 'cut-off' and they also showed a response ratio for *B. cereus*: *B. subtilis* of greater than 1.2. The scFv-encoding gene was observed in clones A9, C1, D1, G1 and H3. A band was observed at ~500 bp for clones A9, E1, H1, H2 and H3, which may indicate that the scFv gene was truncated or incompletely polymerised for these clones.

As can be seen from Table 5.5 that the nine clones picked were obtained from outermost wells of the 96 well plate. This phenomenon is frequently observed by colleagues in this research group; these wells will experience much more efficient heat exchange with the surrounding medium. This has important implications for the expression of the encoded scFv molecule as these *E. coli* clones will have a growth- and protein-expression-advantage as they will achieve the designated temperature more quickly, whereas those in the inner wells will experience a lag due to the slower rate of heat transfer. In addition, the location of the wells, and hence the heat-transfer characteristics, will also have implications for the freeze-thaw lysis method employed, as the outer wells will more quickly freeze and thaw than inner wells and, therefore, the lysis method will be less efficient for these inner wells. In future experiments, the lysis method could be adjusted to include a lysozyme treatment. Alternatively, if using the freeze-thaw method, which has proven to be effective, the inoculation of each clone into individual microtubes would allow for more efficient heat-transfer for each tube. Thus, this would allow for better representation of the entire array of clones being tested, rather than just the outermost wells of a 96 well plate.

Further work is also required to more fully determine the response of these clones for *B. cereus* and *B. subtilis*. A limitation of the monoclonal ELISA method is that the signal observed is proportional to not only the binding response of the antibody to the target but also the levels of the antibody present, which is in turn proportional to the expression characteristics of this protein. Therefore, future experiments would entail the expression and purification of each individual scFv. Following this, each scFv can be

assayed for binding to *B. cereus* cells and spores. A potential means to determine cross-reactivity for *B. subtilis* would be to carry out competitive assays, whereby each scFv would be mixed with varying concentrations of *B. subtilis* in solution and applied to a *B. cereus*-coated ELISA plate. Any clones that exhibit cross-reactivity to *B. subtilis* antigens will show a decrease in binding to the *B. cereus* surface when the *B. subtilis* concentration in solution is increased. On the reverse side of this, clones that exhibit no cross-reactivity to *B. subtilis* antigens will exhibit no change in binding to the *B. cereus* surface regardless of the *B. subtilis* concentration in solution.

As mentioned previously, by the end of the work carried out here, only two rounds of panning were carried out. Future work on this project would also entail carrying out further screening by panning. It is the author's belief that the results of the monoclonal ELISAs show the potential of this scFv library; after just two rounds of panning clones were isolated that, based on the results, appear to show preferential binding towards *B. cereus*. It must also be noted that the absence of a species-specific biomarker for distinguishing *B. cereus* is a significant impediment to the screening of this scFv library. Until such a time when a species-specific marker, ideally a surface protein or carbohydrate, is identified, it will be highly difficult to isolate a scFv that can perfectly distinguish *B. cereus* from *B. subtilis*.

6 Evaluation of the toxic effects of AZA1, MC-LR and *M. aeruginosa* on human hepatocellular carcinoma cells

6.1 Introduction

This chapter features toxicity work carried out to determine the toxic effects of exposure of HepG2 liver carcinoma cells to AZA1, MC-LR and *M. aeruginosa*. The effects of combinations of these harmful contaminants on HepG2 cells were also investigated.

Much *in vivo* and *in vitro* work was previously carried out on AZA1 to elucidate its mode of toxicity, as was discussed in Section 1.2.7. To date, it is well established that AZAs target the liver, pancreas, lung, spleen, thymus and small intestine (Ito *et al.*, 2000; Ito *et al.*, 2002) and they display toxicity in all cell lines tested (Twiner *et al.*, 2005; Ronzitti *et al.*, 2007). A number of previous studies aimed to identify the mode of cell death induced by AZA exposure and have demonstrated apoptosis-induced effects of AZAs in lymphocytes, intestinal, neuroblastoma and liver cell lines (Román *et al.*, 2001; Twiner *et al.*, 2012; Doerr *et al.*, 2016). However, there is a gap in the knowledge as to the apoptotic effects of AZA1 in HepG2 cells at 24 h and also the effects of higher AZA1 concentrations on HepG2 viability.

Since its discovery in the middle of the 20th century (Bishop *et al.*, 1959; Konst *et al.*, 1965), significant research was directed at understanding MC-LR hepatotoxicity e.g. the effects of microcystins on primary hepatocytes as well as on HepG2 cells (Ding *et al.*, 1998; Fladmark *et al.*, 1998; Ding *et al.*, 1999; Humpage and Falconer, 1999; Ding *et al.*, 2000; Ito *et al.*, 2000; Gehringer *et al.*, 2004; Gan *et al.*, 2010; Zhang *et al.*, 2013; Ma *et al.*, 2017). A number of *in vivo* models have been used to determine the toxic effects of *M. aeruginosa* cyanobacteria on live fish cultures (Rogers *et al.*, 2011; Abdel-Latif and Khashaba, 2017; Rodrigues Pires Júnior *et al.*, 2018; Xia *et al.*, 2018; Qian *et al.*, 2019). A small number of studies have investigated the effects of *M. aeruginosa* on mammalian cell lines but from these reports, it was indicated that *M. aeruginosa* has highly toxic effects, inducing cell changes associated with necrosis. Furthermore, it was indicated that exposure to *M. aeruginosa* had a higher potency than exposure to pure MC-LR (Rao *et al.*, 1998; Masango *et al.*, 2008). However, while the World Health Organisation's (WHO) guideline limit for MC-LR is 1 µg of MC-LR per litre of water for consumption (WHO, 2003), no guidelines are in place for acceptable levels of *M. aeruginosa*. In addition, it is expected that humans and other organisms would be exposed to combinations of waterborne contaminants rather than individual compounds. However, there appears to be a lack of information on the combined effects of *M.*

aeruginosa and MC-LR in the literature. In addition, there are no published studies on the combined effects of AZA1 and MC-LR in the literature.

Thus, the aim of this chapter was to identify the potential effects of individual and binary combinations of AZA1, MC-LR and *M. aeruginosa* on HepG2 cells using a number of metrics:

- a) the effects on cell proliferation measured by 3-(4,5-dimethylthiazol-2-yl)-2,5-diphenyltetrazolium bromide (MTT) assays;
- b) induction of apoptosis as measured by changes in caspase 3/7 activity using carboxyfluorescein-Fluorescent Labelled Inhibitors of Caspases (FAM-FLICA) assays; and
- c) the combined effects of MC-LR with *M. aeruginosa*, or with AZA1, investigated in great detail using next generation High Content Analysis (HCA).

In this study, using proliferation assays, it was found that MC-LR can modulate the toxic effects of lipopolysaccharide (LPS) on HepG2 cells. Whole and lysed *M. aeruginosa* cultures can induce highly significant reductions in cellular proliferation, with potential hormetic effects also observed. The cytotoxic effects of AZA1 were determined following 24 h and 48 h exposure, with the EC₅₀ values determined as 2.43 μ M and 0.92 μ M, respectively. Using HCA, it was found that AZA1-exposure induces apoptosis-associated cellular changes at sub-nanomolar concentrations. In addition, co-exposure of AZA1 with LPS increases the potency of the toxic effects of AZA1. It was also determined, using HCA, that exposure to 2.5 μ M MC-LR appeared to induce necrosis- and proliferation-associated cellular changes. When HepG2 cells were co-exposed to MC-LR and AZA1, antagonistic effects were observed, likely due to the induction of different cell death pathways. Further, it was observed that co-exposure of HepG2 cells to MC-LR and *M. aeruginosa* increased the necrotic and proliferative effects versus exposure to MC-LR alone. In addition to the necrotic and proliferative effects of MC-LR, it was indicated from FAM-FLICA assays that MC-LR also induced apoptosis at concentrations of 5 and 1 μ M, indicating a highly complex mode of toxicity. It was speculated that the occurrence of such opposing cellular processes may have been due to the heterogeneous morphology associated with the HepG2 cell line. Overall, the work presented in this chapter expands our understanding of the effects

AZA1-induced apoptosis, MC-LR-induced necrosis and proliferation, and the cytotoxic effects of *M. aeruginosa* cells on HepG2 cells.

6.2 Results

6.2.1 Determination of the effects of MC-LR, *M. aeruginosa* cells and AZA1 on HepG2 cell proliferation

The aim of this experiment was to determine the effect of MC-LR, whole and lysed *M. aeruginosa* cells, and AZA1 on HepG2 cell proliferation. HepG2 cells were cultured with 1×10^5 cells per well and were exposed to various treatments. For MC-LR exposures, HepG2 cells were treated with varying concentrations of MC-LR (5 – 0.008 μM) alone and in the presence of 100 ng/mL LPS for 24 h (Figure 6.1). For *M. aeruginosa* exposures, HepG2 cells were treated with whole and lysed *M. aeruginosa* cells (1×10^7 – 1.6×10^4 cells/mL) for 24 h (Figure 6.2). For AZA1 exposures, HepG2 cells were treated with AZA1 (10 – 0.0001 μM) alone for 24 h (Figure 6.3). MTT assays were carried out after each exposure to measure cell proliferation, the results of which are presented below.

6.2.1.1 Effect of MC-LR on HepG2 proliferation

Treatment of HepG2 cells with 5 μM – 0.008 μM MC-LR alone did not significantly affect cell proliferation. Treatment with 100 ng/mL LPS alone caused 92.5% reduction in cell proliferation ($P < 0.01$). However, exposures to 5, 0.4 and 0.008 μM MC-LR used in combination with 100 ng/mL LPS, resulted in 88.3 – 94.1% reduction in cell proliferation ($P < 0.01$), while 1 μM MC-LR with LPS resulted in 65.4% reduction in cell proliferation ($P < 0.05$).

6.2.1.2 Effect of *M. aeruginosa* cells on HepG2 proliferation

Treatment of HepG2 cells with whole *M. aeruginosa* cells caused a number of significant reductions in cell proliferation; 1×10^7 *M. aeruginosa* cells/mL resulted in 98.5% reduction in cell proliferation ($P < 0.001$), 1.6×10^4 cells/mL caused 83.5% reduction ($P < 0.01$) and 2×10^6 – 8×10^4 cells/mL caused 48.2 – 63.5% reduction ($P < 0.05$). Treatment with lysed *M. aeruginosa* appeared to increase the potency of the toxic effects; 1×10^7 and 2×10^6 lysed cells/mL caused 98.0% and 98.3% reduction, respectively ($P < 0.001$). Exposure to 4×10^5 lysed cells/mL caused 72.9% reduction in

cell proliferation ($P < 0.01$), while exposure to 8×10^4 and 8×10^4 cells/mL caused 46.4% and 59.9% reduction ($P < 0.05$).

6.2.1.3 Effect of AZA1 on HepG2 proliferation

Exposure of HepG2 cells to AZA1 for 24 h caused highly significant changes in cell proliferation, with 10 μM and 1 μM resulting in 91.9% and 26.8% reductions in proliferation, respectively ($P < 0.001$). The EC_{50} value of 24 h exposure to AZA1 was calculated as 2.43 μM . In addition, the EC_{50} value for 48 h exposure to AZA1 was also determined to be 0.92 μM .

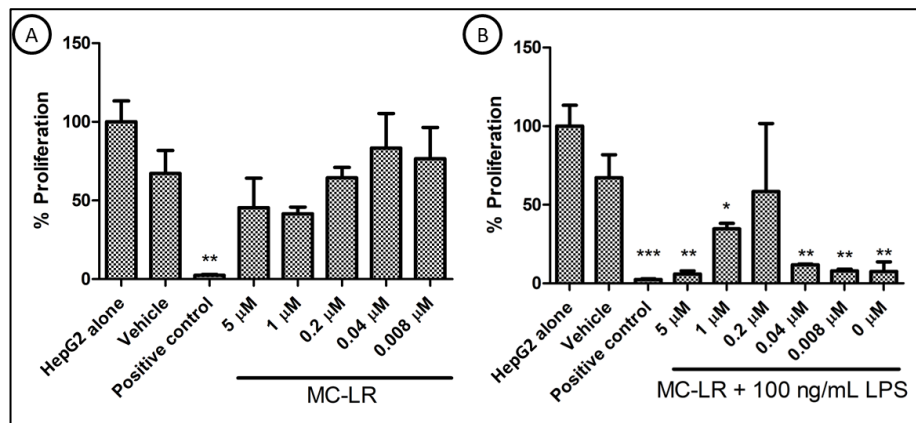


Figure 6.1: Proliferation of HepG2 cells after 24 h exposure to (A) MC-LR and (B) MC-LR + 100 ng/mL LPS. Results indicate a mean value from three independent replicates and error bars represent mean \pm SEM (standard error of mean). Significance: $P < 0.05^*$; $P < 0.01^{**}$; $P < 0.001^{***}$ as illustrated, all relative to the HepG2 cells alone control.

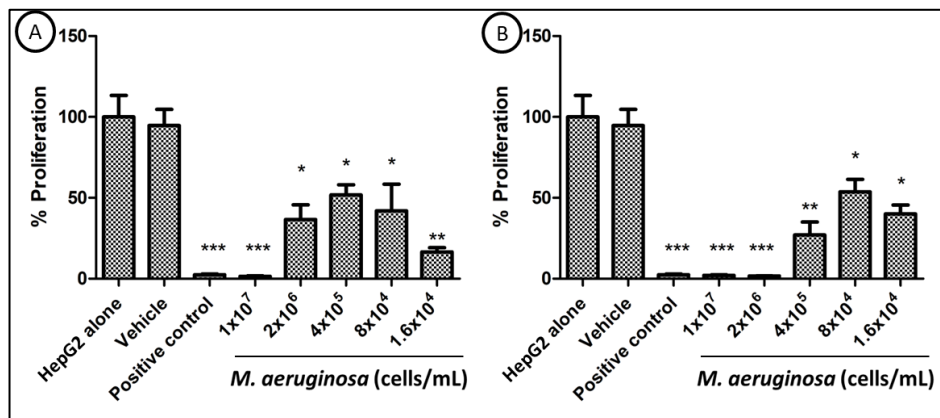


Figure 6.2: Proliferation of HepG2 cells after 24 h exposure to (A) whole and (B) lysed *M. aeruginosa* cells. Results indicate a mean value from three independent replicates and error bars represent mean \pm SEM. Significance: $P < 0.05^*$; $P < 0.01^{**}$; $P < 0.001^{***}$ as illustrated, all relative to the HepG2 cells alone control.

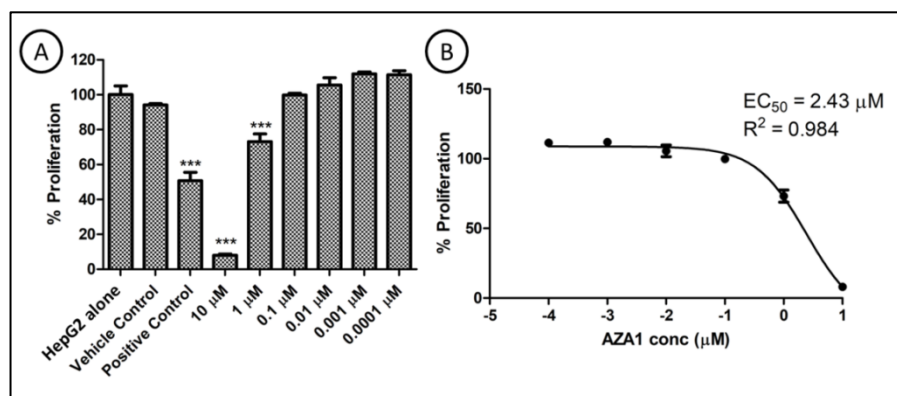


Figure 6.3: Effect of 24 h exposure to AZA1 on HepG2 cells. (A) Proliferation of HepG2 cells after 24 h exposure to AZA1. (B) Calculation of the half maximal effective concentration (EC_{50}) value of 24 h exposure of HepG2 cells to AZA1. Results indicate a mean value from three independent replicates and error bars represent mean \pm SEM. Significance: $P < 0.05^*$; $P < 0.01^{**}$; $P < 0.001^{***}$ as illustrated, all relative to the HepG2 cells alone control.

6.2.2 Analysis of the effects of AZA1 on HepG2 cell health using High Content Analysis (HCA)

The aim of this experiment was to gain greater insight into the effects of AZA1 on HepG2 by simultaneously measuring five indicators of cell health and this was achieved through use of next generation HCA.

6.2.2.1 Exposure of HepG2 cells to AZA1 indicates activation of apoptosis

For AZA1 exposures, HepG2 cells were exposed to AZA1 at concentrations ranging from 5 to 0.005 μM alone and in the presence of 100 ng/mL LPS for 18 h. HepG2 cells were stained with MitoTracker® Orange CMTMRos mitochondrial stain and Hoechst nuclear stain and analysed by HCA, which allows for the automated and rapid analysis of a number of cell parameters, including cell number (CN), nuclear area (NA), nuclear intensity (NI), mitochondrial mass (MM) and mitochondrial membrane potential (MMP). The results of the analyses are presented in Figure 6.4 below and are summarised in Table 6.1. It can be seen in Figure 6.4(A) that treatments with AZA1 alone and with LPS did not have any significant effect on HepG2 CN at any of the tested concentrations.

6.2.2.1.1 AZA1 exposure significantly reduced Nuclear Area and increased Nuclear Intensity

From Figure 6.4(B)(i) it can be observed that treatment with 5, 0.5 and 0.005 μM AZA1 alone resulted in a significant decrease in NA, ranging from 7.0 – 7.9% reduction ($P < 0.05$), and a highly significant decrease in NA was observed at lowest tested concentration of 0.0005 μM , with a 9.3% reduction ($P < 0.01$). No significant change was observed for 0.05 μM AZA1. In the presence of 100 ng/mL LPS alone (Figure 6.4(B)(ii); 0 μM AZA1), there was no significant change in NA. However, treatment with both AZA1 and LPS resulted in a more potent effect on HepG2 NA; treatment with 0.5 and 0.005 μM AZA1 plus 100 ng/mL LPS resulted in a significant decrease in NA (10.8% reduction; $P < 0.01$), while at 5, 0.05 and 0.0005 μM AZA1 plus 100 ng/mL LPS a greater decrease in NA was observed (12.7 – 13.5 % reduction; $P < 0.001$). For NI analysis (Figure 6.4 (C)(i)), treatment with AZA1 at all concentrations resulted in a highly significant increase in NI (35.0 – 38.9% increase; $P < 0.001$). When exposed to LPS alone (Figure 6.4 (C) (ii); 0 μM AZA1), no significant change was observed, whereas treatment with LPS plus all concentrations of AZA1 resulted in a highly

significant increase in NI (40.9 – 44.7% increase; $P < 0.001$). Thus, it appeared that the use of LPS in tandem with AZA1 increased the potency of the effect on NI.

6.2.2.1.2 AZA1 exposure significantly increased Mitochondrial Membrane Potential

The effects of AZA1 on the mitochondria were determined by MM and MMP measurements. For MM analysis (Figure 6.4(D)), treatment with AZA1 at all concentrations, with and without 100 ng/mL LPS, resulted in a highly significant decrease in MM (AZA1 alone: 26.9 – 28.4% reduction; AZA1 + LPS: 29.9 – 31.4% reduction; $P < 0.001$). Treatment with 100 ng/mL LPS alone (Figure 6.4(D)(ii)) resulted in a significant decrease in MM (7.0% reduction; $P < 0.05$). For MMP analysis (Figure 6.4(E)(i)), treatment with AZA1 alone resulted in changes in MMP ranging from 18.7% to 29.9%, but these changes were not statistically significant ($P > 0.05$). However, treatment with 0.5 μ M AZA1 + 100 ng/mL LPS (Figure 6.4(E)(ii)) resulted in 24.6% increase in MMP ($P < 0.05$).

Table 6.1: Summary of the effects of AZA1 alone and with 100 ng/mL LPS on five HepG2 cell health parameters. Arrows indicate a significant increase or decrease in each parameter, relative to the vehicle control. The number of arrows corresponds to the significance value; P < 0.05 *; P < 0.01 **; P < 0.001 ***. CN = cell number; NA = nuclear area; NI = nuclear intensity; MM = mitochondrial mass; MMP = mitochondrial membrane potential.

Cell Health Parameter	AZA1 (μM)					AZA1 (μM) + LPS				
	5	0.5	0.05	0.005	0.0005	5	0.5	0.05	0.005	0.0005
CN										
NA	↓	↓		↓	↓↓	↓↓↓	↓↓	↓↓↓	↓↓	↓↓↓
NI	↑↑↑	↑↑↑	↑↑↑	↑↑↑	↑↑↑	↑↑↑	↑↑↑	↑↑↑	↑↑↑	↑↑↑
MM	↓↓↓	↓↓↓	↓↓↓	↓↓↓	↓↓↓	↓↓↓	↓↓↓	↓↓↓	↓↓↓	↓↓↓
MMP							↑			

6.2.3 Investigation of the combined effects of MC-LR with *M. aeruginosa* and MC-LR with AZA1 on HepG2 proliferation

The purpose of these experiments was to determine the effects of MC-LR in combination with either lysed *M. aeruginosa* cells or with AZA1. It was shown in Section 6.2.1 that different concentrations of each toxin/cyanobacteria exhibited different degrees of toxicity, as shown by changes in HepG2 cell proliferation. In this section, an attempt was made to determine if concentrations of these toxins/cyanobacteria that did not have a highly significant effect on their own would have an effect of higher significance when used in combination. HepG2 cells were exposed to multiple combinations of MC-LR (1, 0.2 and 0 μM), lysed *M. aeruginosa* cells (8×10^4 , 1.6×10^4 and 0 cells/mL) and AZA1 (1, 0.1 and 0 μM). The effects on HepG2 cell proliferation were tested by MTT assay. The results of the combination exposures with MC-LR and AZA1, and with MC-LR and *M. aeruginosa* were normalised to the HepG2 'Cells Alone' control and are shown in Figures 6.5 and 6.6 below.

It was observed Figure 6.6 that only the combination of 0.2 μM MC-LR plus 8×10^4 *M. aeruginosa* cells/mL resulted in a significant effect on HepG2 proliferation (31.1% reduction; $P < 0.05$). No significant changes in HepG2 proliferation were observed for any of the other MC-LR and *M. aeruginosa* combinations. Furthermore, no significant changes in proliferation were observed for any of the tested MC-LR and AZA1 combinations (Figure 6.5).

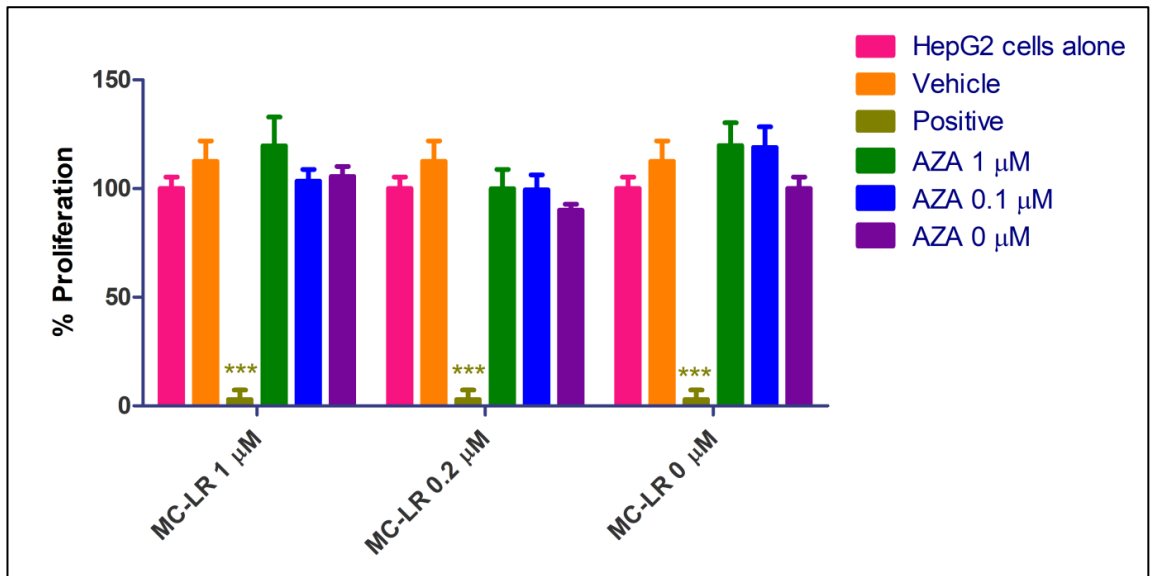


Figure 6.5: Proliferation of HepG2 cells after 24 h exposure to MC-LR and AZA1. Results indicate a mean value from at least three independent experiments and error bars represent mean \pm SEM (standard error of mean). Significance: $P < 0.05^*$; $P < 0.01^{**}$; $P < 0.001^{***}$ as illustrated, all relative to the HepG2 cells alone control.

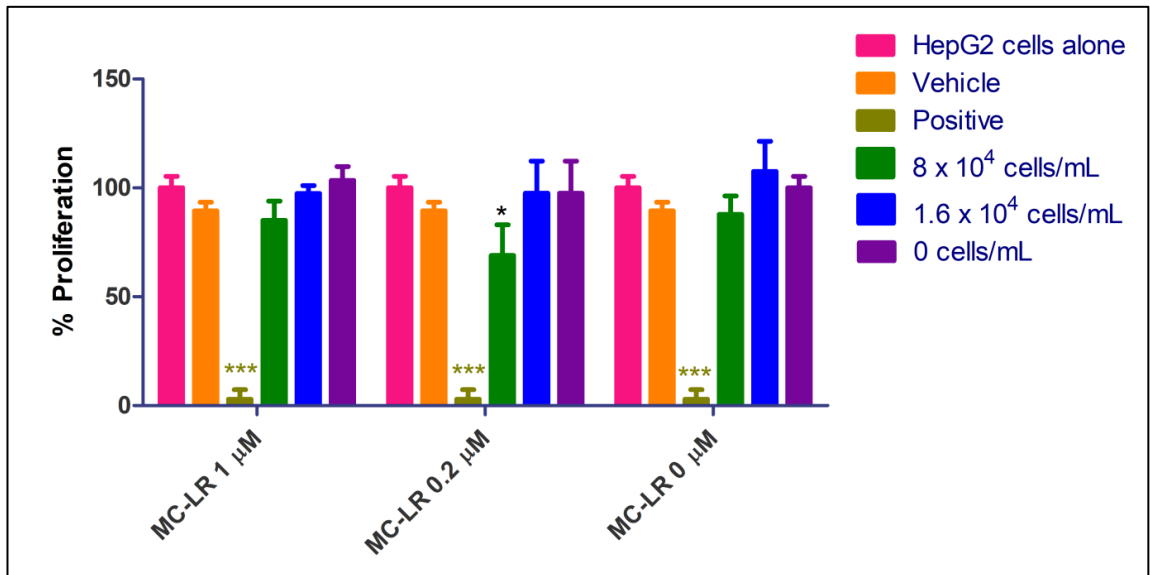


Figure 6.6: Proliferation of HepG2 cells after 24 h exposure to MC-LR and *M. aeruginosa*. Results indicate a mean value from at least three independent experiments and error bars represent mean \pm SEM (standard error of mean). Significance: $P < 0.05^*$; $P < 0.01^{**}$; $P < 0.001^{***}$ as illustrated, all relative to the HepG2 cells alone control.

6.2.4 Determination of the combined effects of MC-LR-, AZA1- and *M. aeruginosa*-exposure on HepG2 using HCA

The aim of this experiment was to use HCA to gain greater insight into the combined effects of MC-LR, AZA1 and *M. aeruginosa*. It was shown previously in the Section 6.2.4 that the combined effects of MC-LR with AZA1 and/or *M. aeruginosa* could not be fully elucidated using MTT assays. The advantage of HCA versus MTT assays for investigating combinations of different compounds is its excellent sensitivity. In addition, analysis of changes in CN, NA, NI MM and MMP can provide insights into apoptosis and/or necrosis and, thus, HCA has an ability to better demonstrate the risk of human exposure to mixtures of environmental toxins (Wilson *et al.*, 2016). HepG2 cells were exposed to MC-LR at 2.5, 0.5 and 0 μM in combination with AZA1 at 0.5 0.05 and 0 μM for 18 h. Additionally, exposures were carried out using MC-LR at concentrations of 2.5, 0.5 and 0 μM in combination with lysed *M. aeruginosa* cells at 2×10^5 , 4×10^4 and 0 cells/mL for 18 h. Treated HepG2 cells were subsequently stained with MitoTracker® Orange CMTMRos mitochondrial stain and Hoechst nuclear stain and analysed by HCA to measure changes in CN, NA, NI MM and MMP. The results from each measurement were normalised to the vehicle control. The results of the analyses are presented in Figures 6.7 and 6.9 and are summarised in Tables 6.2 and 6.3 below.

6.2.4.1 MC-LR-exposure appeared to activate necrosis while AZA1-exposure appeared to activate apoptosis

It can be seen from Figure 6.7(A) that treatment with 2.5 μM MC-LR alone resulted in an 18.7% increase ($P < 0.05$) in CN. No significant changes were observed for exposures to AZA1 alone or for any of the tested combinations of the two toxins. From Figure 6.7(B), it can be observed that exposure to 2.5 μM and 0.5 μM MC-LR resulted in 13.0% increase ($P < 0.001$) and 8.6% increase ($P < 0.05$) in NA, respectively, which is an indicator of necrosis. Treatment with AZA1 alone at 0.5 μM and 0.05 μM did not cause any significant changes in NA (3.0% and 5.2% reduction, respectively). A combination of 2.5 μM MC-LR and 0.5 μM AZA1 resulted in 11.1% increase ($P < 0.01$) in NA. The result of the combination of 2.5 μM MC-LR plus 0.05 μM AZA1 would suggest that this concentration of AZA1 is antagonistic to the effect of 2.5 μM MC-LR. NA and NI are parameters that are intrinsically linked, and usually an increase in one results in a decrease in the other, or vice versa. It can be seen in Figure 6.7(C)

that at 2.5 μM and 0.5 μM MC-LR alone, a decrease of 9.8% and 5.0% in NI was observed, however, these data were not statistically significant. However, treatment with 0.5 and 0.05 μM AZA1 alone resulted in 26.0% and 26.2% increases in NI, respectively ($P < 0.001$), which is an indicator of apoptosis. A combination of 0.5 μM MC-LR plus 0.5 μM and 0.05 μM AZA1 resulted in 18.4% ($P < 0.05$) and 25.6% ($P < 0.001$) increase in NI, respectively. A combination of 2.5 μM MC-LR plus 0.05 μM AZA1 resulted in 17.5% ($P < 0.05$) increase in NI.

To observe the effect of the toxins on the mitochondria, changes in MM and MMP were measured. It can be observed in Figure 6.7(D) that treatment with MC-LR alone did not cause any significant changes in MM, whereas exposure to 0.5 and 0.05 μM AZA1 alone resulted in 26.5% ($P < 0.05$) and 29.1% ($P < 0.01$) decrease in MM, respectively. A combination of 2.5 μM MC-LR with 0.5 and 0.05 μM AZA1 caused 25.0% and 25.2% reduction in MM ($P < 0.05$), respectively. This can be clearly visualised from the microscopy images presented in Figure 6.8. A combination of 0.5 μM MC-LR with 0.5 and 0.05 μM AZA1 caused 35.2% ($P < 0.01$) and 27.3% ($P < 0.05$) reduction in MM, respectively. From Figure 6.7(E), it can be observed that treatment with MC-LR alone did not significantly affect MMP. However, treatment with AZA1 alone at 0.5 μM and 0.05 μM resulted in 44.8% and 51.4% increase in MMP, respectively ($P < 0.001$). A combination of 0.5 μM MC-LR with 0.05 μM resulted in 85.4% increase in MMP ($P < 0.001$), while the remaining combinations of MC-LR with AZA1 resulted in increases in MMP ranging from 36.9% to 57.2% ($P < 0.001$) relative to the vehicle control.

6.2.4.2 Co-exposure with lysed *M. aeruginosa* cells appeared to enhance the necrotic effect of MC-LR

The results of the HepG2 exposure to MC-LR and *M. aeruginosa* cells are presented in Figure 6.9 below. It can be observed in Figure 6.9(A) that treatment with MC-LR alone at 2.5 μM and 0.5 μM caused 18.7% and 16.6% increase in CN, respectively ($P < 0.05$). Treatment with 2×10^5 and 4×10^4 *M. aeruginosa* cells/mL alone caused 17.3% and 17.1% increase in CN, but this change was not statistically significant. A combination of 2.5 μM MC-LR with 2×10^5 and 4×10^4 *M. aeruginosa* cells/mL caused 19.0% and 21.2% increase in CN, respectively ($P < 0.05$). A combination of 0.5 μM MC-LR with 2×10^5 *M. aeruginosa* cells/mL caused 22.7% increase in CN ($P < 0.05$). From Figure 6.9(B), it can be observed that treatment with MC-LR alone at 2.5 μM resulted in 13.0%

increase in NA ($P < 0.01$), while treatments with *M. aeruginosa* cells alone at either concentration did not cause any significant changes in NA. A combination of 2×10^5 *M. aeruginosa* cells/mL with 2.5 μM and 0.5 μM MC-LR resulted in 18.8% ($P < 0.001$) and 12.2% increase in NA, respectively ($P < 0.05$). This suggests that the presence of 2×10^5 *M. aeruginosa* cells/mL had a synergistic effect on MC-LR toxicity. No significant changes were observed for the remaining parameters (NI, MM and MMP).

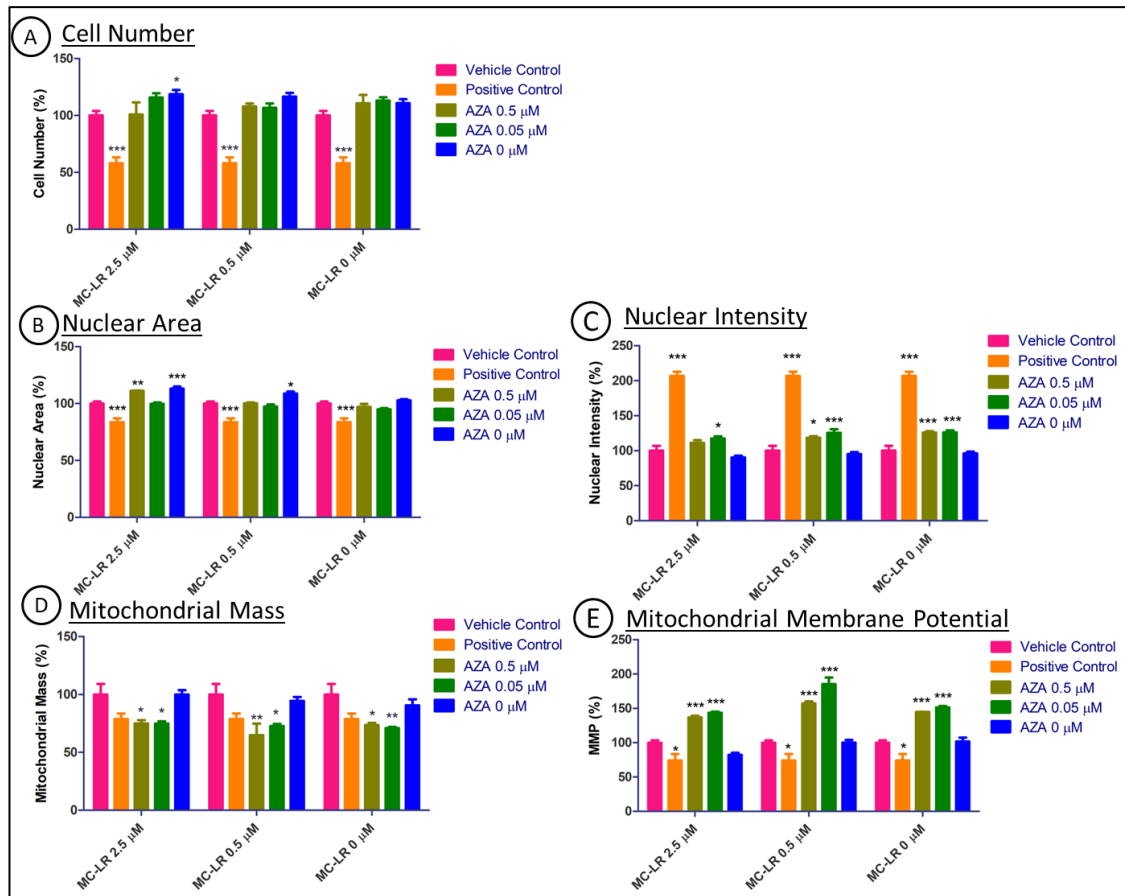


Figure 6.7: Effects of combined exposure of HepG2 cells to MC-LR and AZA1 for 18 h. A = Cell Number Analysis; B = Nuclear Area Analysis; C = Nuclear Intensity Analysis; D = Mitochondrial Mass Analysis; E = Mitochondrial Membrane Potential Analysis. Results indicate a mean value from at least three independent experiments and error bars represent mean \pm SEM (standard error of mean). Significance: $P < 0.05$ *; $P < 0.01$ **; $P < 0.001$ *** as illustrated, all relative to the vehicle control.

Table 6.2: Summary of the effects of combinations of MC-LR and AZA1 on five HepG2 cell health parameters. Arrows indicate a significant increase or decrease in each parameter, relative to the vehicle control. The number of arrows corresponds to the significance value; P < 0.05 *; P < 0.01 **; P < 0.001 ***. CN = cell number; NA = nuclear area; NI = nuclear intensity; MM = mitochondrial mass; MMP = mitochondrial membrane potential.

	MC-LR concentration 2.5 μ M			MC-LR concentration 0.5 μ M			MC-LR concentration 0 μ M			
	AZA1 (μ M)	0.5	0.05	0	0.5	0.05	0	0.5	0.05	0
Cell Health Component										
CN										
NA		↑↑					↑			
NI			↑		↑	↑↑		↑↑↑	↑↑↑	
MM		↓	↓		↓↓	↓		↓	↓↓	
MMP		↑↑↑	↑↑↑		↑↑↑	↑↑↑		↑↑↑	↑↑↑	

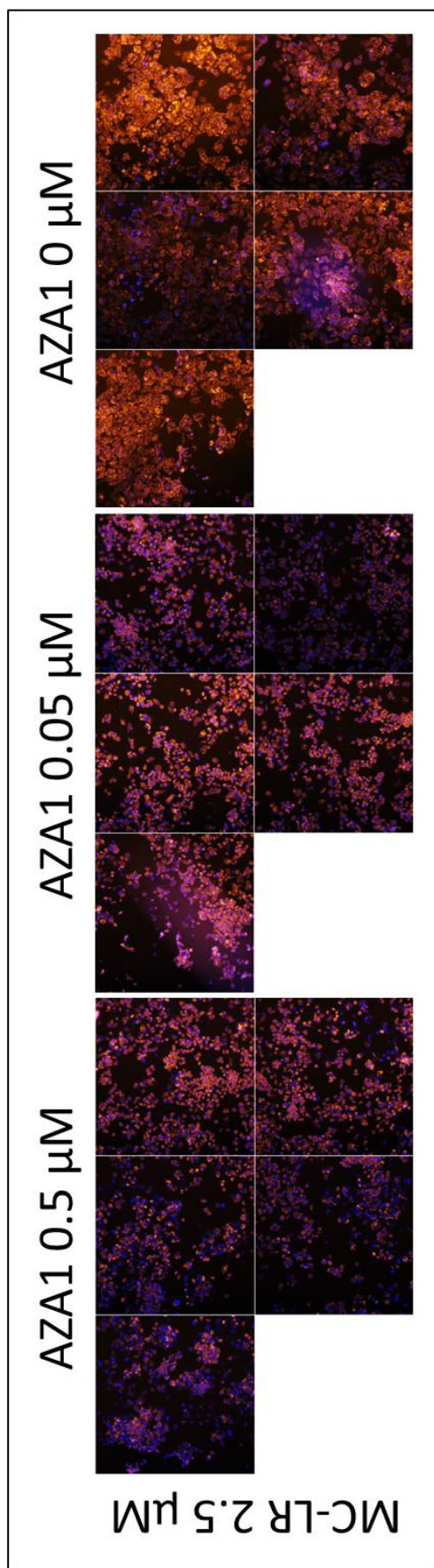


Figure 6.8: Microscopy images of HepG2 cells exposed to combinations of 2.5 μM MC-LR with 0 – 0.05 μM AZA1. Each image is a composite of five examined fields per well. In each image, the cell nuclei are stained with Hoechst nuclear stain (blue) and the mitochondria are stained with MitoTracker® Orange CMTMRos (orange). At 2.5 μM MC-LR and 0 μM AZA1, it can be clearly seen that the mitochondria are much more prominent than after treatment with 0.05 or 0.5 μM AZA1, after which the mitochondrial mass has significantly decreased. Using the naked eye it is very difficult to discern changes in the nuclear area or intensity.

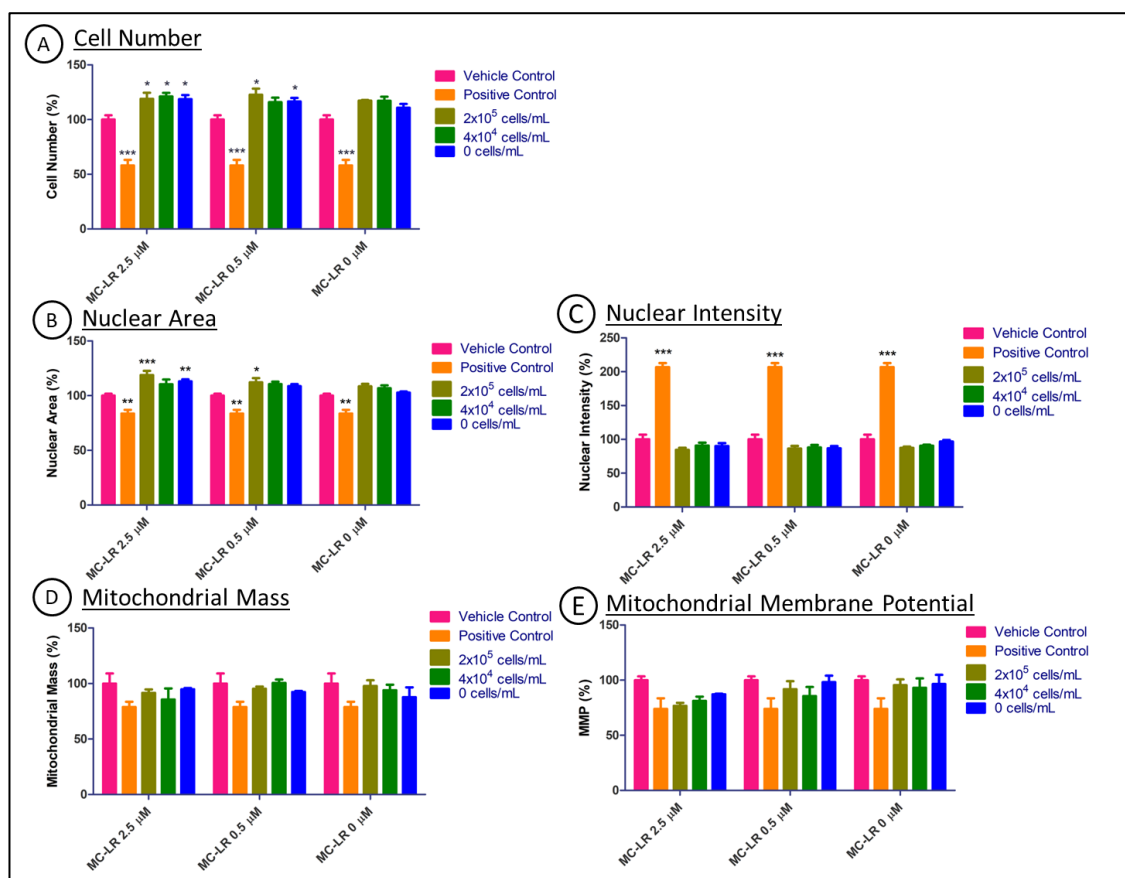


Figure 6.9: Effects of combined exposure of HepG2 cells to MC-LR and *M. aeruginosa* cells for 18 h. A = Cell Number Analysis; B = Nuclear Area Analysis; C = Nuclear Intensity Analysis; D = Mitochondrial Mass Analysis; E = Mitochondrial Membrane Potential Analysis. Results indicate a mean value from at least three independent experiments and error bars represent mean ±SEM (standard error of mean). Significance: P < 0.05*; P < 0.01**; P < 0.001*** as illustrated, all relative to the vehicle control.

Table 6.3: Summary of the effects of combinations of MC-LR and lysed *M. aeruginosa* cells on five HepG2 cell health parameters. Arrows indicate a significant increase or decrease in each parameter, relative to the vehicle control. The number of arrows corresponds to the significance value; P < 0.05*; P < 0.01**; P < 0.001***. CN = cell number; NA = nuclear area; NI = nuclear intensity; MM = mitochondrial mass; MMP = mitochondrial membrane potential.

	MC-LR concentration 2.5 μM			MC-LR concentration 0.5 μM			MC-LR concentration 0 μM		
	2x10 ⁵	4x10 ⁴	0	2x10 ⁵	4x10 ⁴	0	2x10 ⁵	4x10 ⁴	0
<i>M. aeruginosa</i> (Cells/mL)									
Cell Health Component									
CN	↑	↑	↑	↑	↑				
NA	↑↑↑		↑↑	↑					
NI									
MM									
MMP									

6.2.5 Determination of the effect of MC-LR- and AZA1-exposure on caspase-dependent apoptosis in HepG2 cells

In order to delve deeper into the interactions at play between HepG2 cells and the toxins, FAM-FLICA assays were carried out to determine if the caspases 3 and 7 were activated, which are indicators of apoptosis. In the previous sections, the HepG2 cell concentration required ranged from 10^4 to 10^5 cells/well. For analysis of apoptosis using FAM-FLICA and measurement using a fluorescent plate reader, a higher cell concentration of 10^6 cells/well was required. Therefore, the HepG2 cells were grown in 6 well plates and treated at a cell concentration of 10^6 cells/mL in a 1 mL volume. This larger volume (1 mL/well for FAM-FLICA assay versus 100 μ L/well for MTT assay) inherently required larger volumes of toxin stocks for the exposures. Therefore, the number of toxin concentrations to be tested was reduced. This higher consumption of toxins meant that each experiment was carried out once. It was shown previously that peak activities of caspase 3/7 correspond to the AZA1 concentration and time points associated with cytotoxicity (Twiner *et al.*, 2012). Thus, AZA1 was tested at 5 and 1 μ M (i.e. concentrations similar to the EC_{50} value of 2.43 μ M), with and without 100 ng/mL LPS. For the sake of comparison, MC-LR was also used at these concentrations with and without LPS. When measuring the fluorescence output by the fluorescence plate reader, measurements were carried out in triplicate. In order to account for differing cell numbers per well, cell counts were performed on each sample prior to fluorescence measurement. The fluorescent output was then divided by the corresponding cell number and these values were normalised against the Vehicle control to obtain a 'fold change' value. The results of the FAM-FLICA assays are presented in Figure 6.10 below.

It can be seen from Figure 6.10 that treatment with 5 μ M and 1 μ M MC-LR caused ~2.45-fold and ~1.77-fold increases in caspase 3/7 activity ($P < 0.001$), while in the presence of 100 ng/mL LPS, co-exposure with 5 μ M and 1 μ M MC-LR caused 1.81-fold increase ($P < 0.001$) and 0.66-fold decrease ($P < 0.05$) in caspase 3/7 activity. When treated with AZA1, highly significant decreases in caspase activity were observed for both concentrations of AZA1, with and without LPS, ranging from 0.33- to 0.56-fold decreases in caspase 3/7 activity ($P < 0.001$).

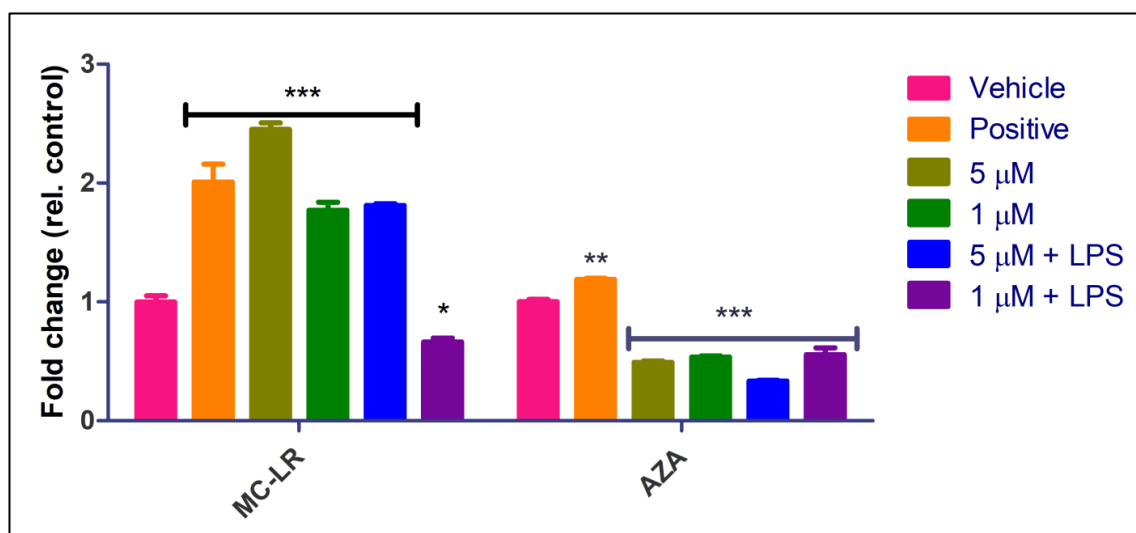


Figure 6.10: Effect of 24 h exposure to MC-LR and AZA1, with and without 100 ng/mL LPS, on activation of Caspase 3/7 in HepG2 cells. Results indicate a mean value from three fluorescence measurements and error bars represent the mean \pm SEM (standard error of mean). Significance: $P < 0.05^*$; $P < 0.01^{**}$; $P < 0.001^{***}$ as illustrated, all relative to the vehicle control.

6.2.6 IL1 β and TNF α ELISAs

The aim of these experiments was to determine if the exposures of HepG2 cells to MC-LR, *M. aeruginosa* and AZA1 lead the production of the cytokines IL-1 β and TNF- α , which are indicators of cell stress. The supernatants from Sections 6.2.3 and 6.2.5 were retained for testing for the presence of these cytokines using commercial DuoSet™ ELISA kits (Bio-Techne). It was expected that low levels of these cytokines would be present in the cell supernatants, therefore these supernatants were tested neat by ELISA. However, no statistically significant changes in IL-1 β or TNF- α levels were observed after any of the toxin treatments.

6.3 Discussion

AZAs, MCs and *M. aeruginosa* are significant environmental hazards to humans and other terrestrial and aquatic animals with highly toxic effects being observed in numerous animal models and cell lines. However, to date the combined effects of these toxins/pathogen have not been investigated. Furthermore, there are gaps in the published research on the effects of AZAs on liver cell lines. Thus, in this chapter, the effects of MC-LR, *M. aeruginosa* cells and AZA1 on HepG2 cells were investigated. In addition, the effects of MC-LR and AZA1 in combination with LPS were also investigated. The rationale behind the combination of MC-LR or AZA1 with LPS stemmed from discussions with Prof. Geoffrey Codd of the University of Dundee (G.

Codd, personal communication). It was proposed that the true toxic potential of marine and/or freshwater toxins is due to co-exposure of toxins with microbial agents. This proposition is based on *in vivo* studies showing that the co-exposure of LPS can enhance the potency of toxins present (Best *et al.*, 2003; Stewart *et al.*, 2006). It was shown through a number of different tests that the effects of these harmful contaminants are greatly varied. It was shown that different combinations of these can even further vary the potency. In this section, the results of these exposures will be discussed in detail and the observations made in this study will be equated to those published in the literature.

6.3.1 The effects of individual exposure to MC-LR, *M. aeruginosa* cells and AZA1 on HepG2 cell proliferation

Firstly, the effects of MC-LR alone and in combination with LPS were investigated by means of cell proliferation assays. It can be seen in the MC-LR treatment results (Figure 6.1) that exposure to MC-LR alone did not have a significant effect on HepG2 proliferation at the concentrations tested (Figure 6.1(A)). This is in agreement with the published literature. For example, it was shown that treatment of HepG2 cells with 10 μM MC-LR for 24 h resulted in ~40% reduction in cell survival ($P < 0.01$), whereas treatment with 5 μM MC-LR did not significantly affect cell survival. The IC_{50} was calculated as 21.9 μM (Gan *et al.*, 2010). Meanwhile, Zhang *et al.* (2013) exposed HepG2 cells and primary mouse hepatocytes (PMHs) to 0.001 – 1 μM MC-LR showed no significant changes in HepG2 proliferation but significant changes were observed in PMHs as low as 0.05 μM . It was also shown elsewhere that HepG2 cells are not as sensitive to MC-LR as primary liver cells (Fladmark *et al.*, 1998). Thus, the observations in the present study further verify the observations of a number of other sources.

However, treatments with MC-LR in combination with LPS (which may simulate co-infection with Gram negative bacteria), significant effects on proliferation were observed (Figure 6.1(B)). The results suggested that LPS was playing the dominant role in affecting HepG2 proliferation. Exposure to 100 ng/mL LPS alone (i.e. 0 μM MC-LR) resulted in a significant reduction in HepG2 proliferation ($P < 0.01$). However, the combination of 100 ng/mL LPS and MC-LR at 5, 0.04 and 0.008 μM showed similar reductions in cell proliferation. In addition, co-exposure of 1 μM MC-LR with 100 ng/mL LPS significantly reduced HepG2 proliferation, albeit at a lower significance

level ($P < 0.05$). While $0.2 \mu\text{M}$ MC-LR did not have an observable significant effect on HepG2 proliferation, it should be noted that the error bars on this data point are very large, indicating high variability. Testing at this concentration, therefore, would require further investigation. Interestingly, the result of exposure to $1 \mu\text{M}$ MC-LR with LPS suggested that the toxin appeared to have an almost protective effect on the cells or may be having an antagonistic effect on LPS toxicity. This indicated a complex relationship between toxin and LPS concentrations. Such complex interactions have been reported in the literature. For example, Best *et al.* (2002) exposed zebra fish to *Microcystis* and *E. coli* LPS with MC-LR and measured the effect on detoxification activity of glutathione-S-transferase (GST). Exposure to *E. coli* LPS alone resulted in a significant reduction in GST activity. However, co-exposure of *E. coli* LPS and MC-LR did not change GST activity and it was speculated that this could have been due to a potential interaction, such as non-specific binding, between *E. coli* LPS and MC-LR in the medium, making the LPS unavailable. In contrast, treatment with *Microcystis* LPS with and without MC-LR caused significant reductions in GST activity. The combined effects of MC-LR ($0.001 - 1 \mu\text{M}$) with LPS was also tested in macrophages, but no significant changes in cell viability were observed (Adamovsky *et al.*, 2015).

Following on from the findings of HepG2 exposure to MC-LR, from the result of the exposure to whole *M. aeruginosa* cells (Figure 6.2(A)) indicated a ‘bell-shaped curve’ effect on HepG2 proliferation; 1×10^7 and 1.6×10^4 cells/mL of whole *M. aeruginosa* cells each had a significant effect, with $P < 0.001$ and $P < 0.01$, respectively; however, the intermediate concentrations had an effect of a lower significance ($P < 0.05$). Such a ‘bell-shaped curve’ is suggestive of complex biological effects, such as multiple targets or more than one mechanism of action (Owen *et al.*, 2014). A ‘bell-shaped curve’ is characteristic of the phenomenon known as ‘hormesis’, which can be defined as an adaptive response characterised by a biphasic dose response (Calabrese and Baldwin, 2002). Such hormetic responses are frequently reported in the literature using many different cell lines and treatments (Sonnenschein *et al.*, 1989; Moriguchi *et al.*, 1997; Wetherill *et al.*, 2002; Vandenberg *et al.*, 2012; Wang *et al.*, 2012; Jiao *et al.*, 2014), and are highly indicative of the plasticity associated with biological responses (Calabrese and Mattson, 2011). This suggests a complex relationship about how living *M. aeruginosa* cells interact at different cells concentrations. Different cyanobacterial concentrations may affect quorum sensing and, therefore, may change how the

cyanobacteria interact with their environment. It is well known that both Gram-positive and Gram-negative bacteria use quorum sensing communication to regulate a diverse range of physiological activities, including virulence (Miller and Bassler, 2001; Hibbing *et al.*, 2010). Changes in quorum sensing may change the expression of bioactive peptide products of *M. aeruginosa* other than microcystins, such as microginins, cyanopeptolins and aeruginosins, which have been shown to exert cytotoxic effects (Le Manach *et al.*, 2018). It was also reported in the literature that changes in the toxic potential of drug molecules can be observed due to the formation of drug aggregates (Owen *et al.*, 2014). It is known that *M. aeruginosa* can undergo morphological changes and form cell aggregates depending on cell concentration (Shen *et al.*, 2011). Thus, *M. aeruginosa* cell-aggregation may have also played a role in the ‘bell-shaped’ dose response observed in this study. In any case, further work is required to more fully elucidate such cell aggregation and the toxic effects of living *M. aeruginosa* cells on liver toxicity.

That being said, it is likely that ingestion of *M. aeruginosa*-contaminated water or food will result in the breaking-down of the cyanobacteria by the digestive system. Hence, it is more likely that *in vivo* the liver will be presented with lysed *M. aeruginosa* cell components rather than whole living cells. Therefore, Figure 6.2(B) may illustrate a more telling result; as can be seen from Figure 6.2(B), there is a concentration-dependent effect on HepG2 proliferation and significant decreases in cell proliferation were observed; at 1×10^7 and 2×10^6 cells/mL, at 4×10^5 cells/mL, and at 8×10^4 and 1.6×10^4 cells/mL, decreases of ~98% ($P < 0.001$), ~73% ($P < 0.01$), and 46 – 60% ($P < 0.05$) were observed, respectively. It appears that exposure to lysed *M. aeruginosa* cells was more potent than whole cells. The higher potency of lysed *M. aeruginosa* cells was also observed by Best *et al.* (2003). After 24 h exposure of rainbow trout to lysed *M. aeruginosa* cells, significant increases in gut water content were observed, but this effect was not observed using whole *M. aeruginosa*. It was suggested that this greater volume of water entering the gut would increase the exposure to heterotrophic bacteria and cyanobacteria as well as toxins, which could cause subsequent toxicity to internal organs such as the liver. It is likely that the cytotoxic effect on HepG2 proliferation observed in this study is due to the toxic effect of the cyanobacteria’s own LPS structure, as cyanobacterial LPS has been shown to be highly toxic and inflammatory, causing stimulation of a number of cytokines such as TNF- α and IL-1 (Hewett and

Roth, 1993). However, cyanobacterial LPS has approximately one tenth of the toxic potential as *Salmonella* LPS (Raziuddin *et al.*, 1983), while *M. aeruginosa* LPS had a potency ~12 times lower than *E. coli* O113:10 (Bláhová *et al.*, 2013). It is possible that the toxic effect of *M. aeruginosa* cells may be due to LPS toxicity as well as the release of intracellular digestive enzymes or other bioactive peptides. Such effects have been reported in the literature; it was observed that both non-MC-producing and MC-producing strains of *M. aeruginosa* induced significant hepatocellular damages along with disruption to cell death and survival pathways. It was speculated that this was due to bioactive peptide products of *M. aeruginosa* other than microcystins, such as microginins, cyanopeptolins and aeruginosins (Le Manach *et al.*, 2018).

It is apparent from the results of the exposures to MC-LR and *M. aeruginosa* cells that the cyanobacterial cells exhibited much higher potency than pure MC-LR. Such observations were also reported by Masango *et al.* (2008), who observed that after 72 h treatment of primary hepatocytes, *M. aeruginosa*-containing extracts had 6.5-fold high potency than exposure to purified MC-LR (however, it should be noted that the concentrations of other toxins and/or toxic algae were not measured, and so the higher potency of the *M. aeruginosa*-containing extracts cannot be attributed to *M. aeruginosa* cells alone). In addition, it was noted that exposure of medaka fish to *M. aeruginosa* cells induced a more acute effect than treatment with MC-LR extract (Le Manach *et al.*, 2018). Considering the highly toxic effects of lysed *M. aeruginosa* cells observed in the proliferation assays, the effects of these lysed cyanobacteria were further explored by HCA, as discussed below.

In addition to treatments with MC-LR and *M. aeruginosa*, HepG2 cells were also exposed to a range of AZA1 concentrations and changes in cell proliferation were measured. To the best of the author's knowledge, this is the first reported exposure of HepG2 cells to this wide range of AZA1 concentrations and the first elucidation of EC₅₀ values for AZA1 exposure in this cell line. It can be seen in Figure 6.3 that after 24 h exposure, a concentration-dependent effect was observed on HepG2 proliferation, with the highest concentrations of 10 and 1 µM AZA1 causing a significant reduction in cell proliferation (91.92% and 26.81%, respectively; $P < 0.001$). The EC₅₀ values of 24 and 48 h exposure to AZA1 were calculated from this data as 2.43 µM and 0.92 µM, respectively. In the current study, the toxicity of AZA1 towards HepG2 cells appears to

be more acute than MC-LR, however, it does not appear to have near the same level of toxicity as in other cell lines. The cytotoxicity of AZA1 has been reported in a number of other cell lines and the EC₅₀ values differ greatly depending on the cell type used, but the EC₅₀ values generally range from low nanomolar to hundreds of nanomolar (Twiner *et al.*, 2005; Vilarino *et al.*, 2006; Vilarino *et al.*, 2007; Twiner *et al.*, 2008; Cao *et al.*, 2010; Vale *et al.*, 2010; Twiner *et al.*, 2012). For example, the 48 h EC₅₀ of AZA1 in Jurkat T lymphocytes, Caco-2 intestinal and BE(2)-M17 neuroblastoma cell lines was reported by Twiner *et al.* (2012) as 1.5, 2.6 and 7.5 nM, respectively. It is well documented that AZAs have been shown to be open stage blockers of hERG potassium channels (Twiner *et al.*, 2012). The lower potency of AZA1 towards HepG2 observed in the current study may be explained by the expression levels of hERG potassium channels, which were shown to be upregulated in liver cells, and especially for HepG2 cells (Zhang *et al.*, 2012; Babcock and Li, 2013; Xia *et al.*, 2016). Thus, in order to effectively block hERG channels and exert a toxic effect on HepG2 cells, a higher concentration of AZA1 would be required. The toxic effects of AZA1 on HepG2 were further investigated through the use of HCA.

6.3.2 HCA indicates that AZA1 induces apoptosis

Following on from the cell proliferation assays, it was decided to attempt to delve deeper into the effects of AZA1 on HepG2, using HCA. One of the key advantages of HCA is the retrieval of vast amounts of data for each test (see Section 1.2.10). In this work, HCA data was gathered in the form of CN, NA, NI, MM and MMP data. These parameters provide in-depth information on the effects of a compound on cytotoxicity, cell count and cell morphology, which can in turn be re-interpreted to determine modes of cell death, such as apoptosis and/or necrosis (Mattiuzzi Usaj *et al.*, 2016; Meneely *et al.*, 2018).

The treatments of HepG2 cells with AZA1 revealed that the toxin can have significant effects on cell health at concentrations several orders of magnitude lower than the EC₅₀ established above. Treatments with AZA1 at concentrations as low as 0.5 nM (0.0005 µM) had significant effects on NA and NI (P < 0.01 and P < 0.001, respectively). After 18 h exposure to 0.5 nM AZA1, it was observed that NA reduced by 9.3% while NI increased by 36.9%. Nuclear shrinkage is morphological trait characteristic of apoptosis (Raffray and Cohen, 1997). Hence, the reduction in NA and increase in NI would

indicate nuclear shrinkage is occurring, which would indicate that the cells are likely undergoing apoptosis as a result of AZA1 exposure.

As was reported in the literature, mitochondria are very sensitive to toxins and effects on this organelle are observed more rapidly than other cell parameters (O'Brien *et al.*, 2006), hence, MM and MMP serve as valuable indicators of cell health (Meneely *et al.*, 2018). The results of exposure to AZA1 alone showed significant reductions in MM at concentrations as low as 0.5 nM, with 28.0% reduction in MM observed after 18 h exposure to 0.5 nM ($P < 0.001$). This reduction in MM may suggest a reduction in mitochondrial biogenesis has occurred (Addabbo *et al.*, 2009; Lohr *et al.*, 2016). No significant changes in MMP were observed for the exposures tested in this assay, however, it was observed in Section 6.2.5 that treatment with AZA1 alone caused significant increases in MMP ($P < 0.001$). Disruption of MMP is considered a 'point-of-no-return' in apoptotic signalling (Susin *et al.*, 1997). Mitochondrial dysfunction is known to be central to the apoptotic pathway and is more classically associated to a decrease in MMP rather than an increase (Ly *et al.*, 2003). However, an increase in MMP, also known as mitochondrial hyperpolarisation (MHP), has been reported as occurring in several cell death pathways. For example, MHP is an early event in apoptosis that occurs before activation of caspases or phosphatidylserine externalisation in Jurkat T lymphocytes and normal human peripheral blood lymphocytes (PBLs) (Banki *et al.*, 1999). It was also reported that MHP was observed in TNF-induced necrosis (Goossens *et al.*, 1999). In any case, it is clear from the HCA results that exposure to AZA1 resulted in cell death pathway activation, and most signs indicated that apoptosis was the likely pathway.

Next, the effects of co-exposure of HepG2 cells to AZA1 and LPS were investigated. It is well established that each microbial species has different structures of LPS (Milner *et al.*, 1971; Best *et al.*, 2002). Indeed, the LPS structure of *Azadinium spinosum* would be an ideal compound to use for co-exposure with AZA1, as it could be reasonably expected that the two compounds would be present together in contaminated food or water. However, unfortunately, *A. spinosum* cultures were not available when these experiments were being conducted, nor were any putative *A. spinosum* LPS structures. Despite this, the LPS structure used was that of *E. coli*, which is highly ubiquitous in nature. Thus, it was proposed that for the lack of availability of *A. spinosum* LPS, the *E.*

coli LPS would serve as a proxy for the effect of co-exposure to AZA1 and Gram negative bacterial agents.

As can be seen from the results of exposure to AZA1 and LPS, the presence of LPS greatly increased the potency of AZA1 on HepG2 cells. Relative to treatments with AZA1 alone, treatments with AZA1 and LPS resulted in changes to NA of much higher significance, while such treatments also further increased and decreased the effects on NI and MM, respectively. It was also observed that exposure to LPS alone resulted in significant reduction in MM (7.0% reduction; $P < 0.05$). Previously, it was shown that exposure to LPS alone resulted in significant reduction in HepG2 proliferation (92.5% reduction; $P < 0.01$) (Section 6.2.1). The MTT assay is a measure of mitochondrial activity/health (Meneely *et al.*, 2018), thus, these results suggest treatment with LPS alone had a significant detrimental effect on the mitochondria. In addition, treatment with 0.5 μM AZA1 with LPS showed a significant increase in MMP. Overall the results together further verify the apoptotic effect of AZA1 on HepG2 cells discussed above and indicate that co-exposure of AZA1 with microbial agents may have a synergistic effect, resulting in greater toxicity.

6.3.3 Investigations into the combined effects of MC-LR with *M. aeruginosa* and MC-LR with AZA1 on HepG2 proliferation

Exposure to single toxic compounds is widely reported in the literature in numerous human or animal *in vitro* and *in vivo* models. However, there is limited evidence on the effects of co-exposure of multiple toxic compounds. It is generally considered that animals and humans are most likely to be exposed to multiple water pollutants rather than individual compounds, likely as a result of inadvertent consumption of contaminated water or during swimming (Ma *et al.*, 2017). It was shown in Section 6.2.1 that exposure to individual toxins and cyanobacteria can result in a range of toxic effects on HepG2 cells, with concentration-dependent effects being observed (e.g. for AZA1), and concentration-independent effects also occurring (as was the case for whole *M. aeruginosa* cells). In general, it was observed that the highest concentrations of toxin/cyanobacteria resulted in the greatest reductions in cell proliferation. Thus, it was proposed to investigate the effects of combinations of these toxins and cyanobacteria at concentrations did not have highly significant effects when used individually to

determine if co-exposure to these contaminants could result in synergistic effects on cellular proliferation.

From the results (Figure 6.6), it can be observed that with the exception of treatment with 0.2 μM MC-LR and 8×10^4 *M. aeruginosa* cells/mL, there was no significant change for any of the other tested combinations of MC-LR and *M. aeruginosa* and no significant effects were observed for any combinations of MC-LR and AZA1 on HepG2 proliferation. It was expected that exposure to 1 μM AZA1 alone should cause a significant decrease in HepG2 proliferation, as was shown to occur in Figure 6.3. In a similar way, treatments with *M. aeruginosa* alone did not significantly affect cell proliferation as was shown to occur previously in Figure 6.2. It was noted that during these experiments that the HepG2 morphology was different to that of the earlier MTT assays; the HepG2 cells were noticeably more clumped together. It is possible that the occurrence of such clumping may have allowed the cells to better tolerate the tested concentrations in this experiment. It has been reported in the literature that the susceptibility of cells to drug treatment can vary greatly due to variations in morphology such cell size and local cell density (Slack *et al.*, 2008, Snijder *et al.*, 2009). The higher tolerance of the HepG2 cells in this experiment is apparent when comparing the results of this proliferation assay to those of the previous proliferation assays (Section 6.2.1). In the current experiment, it can be observed in Figure 6.6 that treatment with 0.2 μM MC-LR and 8×10^4 *M. aeruginosa* cells/mL resulted in a 31.10% reduction in cell proliferation ($P < 0.05$). By comparison, it was observed in Figure 6.2 that treatment with 8×10^4 cells/mL of *M. aeruginosa* resulted in 46.38% reduction in proliferation ($P < 0.05$). In addition, treatment with 0.2 μM MC-LR resulted in 35.58% reduction in proliferation, though this was not statistically significant in this assay (Figure 6.1). Thus, there appeared to be a less potent effect on the HepG2 cells used in this experiment. The occurrence of clumping is a well-known feature of HepG2 cells in culture and is dependent on the cell confluency before subculturing. In these experiments, typically, the HepG2 cells were cultured to ~80% confluency before seeding or subculturing, but differences in culturing technique may have caused slight changes in inter-assay variability. In future experiments, the cells should be seeded at lower confluency level to reduce the occurrence of cell clumping and experiments will be replicated in greater number to reduce inter-assay variability.

6.3.4 High Content Analysis – Combination of MC-LR and AZA1

In order to address the issues that occurred in the previous experiment, in collaboration with researchers at Queen's University Belfast, fresh cultures of HepG2 cells were prepared. It was then attempted to determine the effects of combinations of MC-LR with AZA1 and MC-LR with *M. aeruginosa* on HepG2 cells using HCA analysis, as it was expected that the excellent sensitivity of HCA should allow for the elucidation of the complex effects of these toxins/cyanobacteria, such as synergistic or antagonistic effects. In addition to this, the concentrations of MC-LR and *M. aeruginosa* were increased so as to induce a greater and more measureable effect on the HepG2 cells. In contrast, it was shown in Section 6.2.2 that AZA1 produced significant effects at a range of concentrations in NA, NI and MM analysis. In addition, when AZA1 was used in combination with LPS, a significant increase in MMP was observed after exposure to 0.5 μM AZA1. Therefore, the concentrations of AZA1 used for HCA combination analysis were 0.5 and 0.05 μM .

Firstly, evaluating the results of exposures to MC-LR with AZA1 (Figure 6.7), it is interesting that exposure to 2.5 μM MC-LR significantly increased cell numbers ($P < 0.05$), which would indicate a proliferative effect on the cells. A proliferative effect of MC-LR was observed in HepG2 cells previously, with increases in cell viability observed for treatments with MC-LR at 0.01 – 5 μM (Zhang *et al.*, 2013). It was also previously observed that, depending on the MC-LR concentration, hepatocytes can undergo apoptosis or increased cellular proliferation (Humpage and Falconer, 1999). However, in other reports, the proliferative effect of MC-LR was observed at MC-LR concentrations several orders of magnitude lower than used in this study. For example, it was observed by Ma *et al.* (2017) that treatment of HepG2 with MC-LR alone at 1 pM to 1 nM induced proliferation whereas treatment at 1 – 0.001 μM decreased viability. Treatments with AZA1 alone did not have any significant effect on cell number. When used in combination with 2.5 μM MC-LR, AZA1 treatment appeared to negate the proliferative effect of MC-LR.

Treatments with 2.5 μM and 0.5 μM MC-LR alone significantly increased NA ($P < 0.001$ and $P < 0.05$, respectively) but had no significant effect on NI. However, treatment with a combination of 2.5 μM MC-LR and 0.5 μM AZA1 resulted in a significant increase in NA ($P < 0.01$), albeit a lower increase than 2.5 μM MC-LR

alone. In addition, combinations of 2.5 μM MC-LR with 0.05 μM AZA1, and 0.5 μM MC-LR with 0.05 μM AZA1 did not have significant effects on NA. This would suggest AZA1 and MC-LR are having antagonistic effects on NA. Further evidence of antagonism may be observed in the NI data. Exposure to 0.5 μM and 0.05 μM AZA1 alone causes highly significant increase in NI ($P < 0.001$). However, with increasing concentration of MC-LR, the significance level drops, and a combination of 2.5 μM MC-LR with 0.5 μM AZA1 did not significantly affect NI ($P > 0.05$). It is also interesting that the lower concentration of AZA1 rather than the higher is having more of an effect on NI. This would suggest a complicated relationship between toxin concentration and co-exposure of toxins with different modes of action. The apparent antagonism observed in these results may be explained by the effects of the treatments with toxins alone; as was mentioned above, nuclear shrinkage is associated with apoptosis. Therefore, the significant increases in NI would suggest nuclear shrinkage is occurring, which would further suggest that AZA1 alone at 0.5 μM and 0.05 μM has induced apoptosis. Meanwhile, the result of the NA analysis showed that MC-LR alone significantly increased NA, which is an indicator of necrosis (Berghe *et al.*, 2010). Clearly, further work is required to fully evaluate these findings but it is possible that the apparent antagonistic relationship between AZA1 and MC-LR is due to the induction of different cell death pathways.

Meanwhile, analysing the effects of co-exposure of the toxins on HepG2 mitochondrial health, AZA1 appears to have much more of a significant impact than MC-LR. Treatments with MC-LR alone at 2.5 μM and 0.5 μM MC-LR had no effect on MM or MMP, whereas exposure to AZA1 caused significant decrease in MM and increase in MMP, regardless of the concentration of MC-LR co-exposure. This might suggest that the tested concentrations of MC-LR do not affect mitochondrial health. Further evidence of this can be observed in the co-exposure of MC-LR with *M. aeruginosa* (Figure 6.9); MM and MMP were not significantly affected by any of tested concentrations of MC-LR or *M. aeruginosa*. This reflects the observation by Zhang *et al.* (2013) that treatment of HepG2 with up to 5 μM MC-LR induced only slight MMP loss. In contrast, it was indicated in other reports (Ding *et al.*, 2000; Gehringer, 2004) that in hepatocytes, MC-LR treatment is associated with onset of mitochondrial permeability transition (MPT). However, as was discussed earlier, HepG2 cells appear to be less susceptible to MC-LR-induced damage than primary hepatocytes (Fladmark

et al., 1998; Zhang *et al.*, 2013) and so changes to HepG2 mitochondrial health may not occur at the concentrations and duration tested in this study.

Analysing of the results of co-exposure of MC-LR and *M. aeruginosa*, it appears that MC-LR significantly increased CN, which may indicate that this toxin has proliferative effects on HepG2 cells, similar to the previous observations described above. Further, the co-exposure of MC-LR with *M. aeruginosa* cells also caused similar increases in CN, which might indicate that *M. aeruginosa* cells did not have any significant effect on CN. However, more interesting is the observation that co-exposure of 2.5 μM MC-LR and 2×10^5 *M. aeruginosa* cells/mL caused an increase in NA with a higher significance than the two components alone (Figure 6.9(B)). This would suggest that the presence of *M. aeruginosa* cells increases the effect of MC-LR on NA, which may indicate a synergistic interaction. No significant changes were observed for NI, MM or MMP, which is in agreement with the previous observations MC-LR alone (HCA MC-LR+AZA). However, given the highly significant reductions in cell proliferation observed in Section 6.2.1.2, it was expected the exposure to *M. aeruginosa* cell would result in significant changes in cell health as measured by HCA. It is possible that the differences observed between these two experiments may have been due to the different stocks of *M. aeruginosa* cells used; for proliferation assays (Sections 6.2.1.2 and 6.2.3), the lysed cells used were prepared from active cultures that were readily growing at 25 °C with 16 h/8 h light/dark cycles. However, due to the unavailability of live *M. aeruginosa* cultures at the time of the HCA assays, the cells used were prepared from frozen starter culture stocks. The difference in growth conditions may have affected the *M. aeruginosa* physiology and hence may have had implications on the toxic effect on HepG2 cells. Therefore, further work is required to investigate the effects of lysed *M. aeruginosa* cells on HepG2 cells.

Treatments with MC-LR appeared to induce both cellular proliferation and necrosis (Figure 6.7), which intuitively would be considered opposing cellular processes. However, in previous work, it was shown that MC-LR exposure leads to the generation of ROS (Zegura *et al.*, 2004; Nong *et al.*, 2007), which has major implications on a number of cellular activities. Oxidative stress can stimulate mitogen-activated protein kinase (MAPK) and H_2O_2 and can result in the induction of c-Jun N-terminal kinase (JNK) (Jones and Czaja, 1998). These mechanisms have further implications, inducing

hepatic damage leading to apoptosis or necrosis, and/or increasing cellular proliferation (Toivola and Eriksson, 1999; Ding and Nam Ong, 2003).

Furthermore, it has been observed that cell populations exist as mixtures of a limited number of phenotypically distinct subpopulations. It was briefly discussed early that it has been reported that susceptibility to drug treatment can vary greatly from cell to cell, which can occur due to cellular heterogeneity, such as variations in gene expression, cell size, local cell density, and position on a cell islet edge (Slack *et al.*, 2008, Snijder *et al.*, 2009). Such factors may be quite relevant in the current work which focuses on exposures with HepG2, a cell line known to have a varied morphology (such as single cells or large cellular clumps). For example, the effects of cell-cell variability in HCA results was assessed by Snijder *et al.* (2009), who ascertained that 60-80% of variability in treatments was due to differences in local microenvironment, which can occur due to subtle variations in local cell density, cell size and mitotic state. It was found that different cell states within a population can arise from adaptation of individual cells to the 'population context' that they find themselves in. Thus, the occurrence of the opposing cellular processes of necrosis and proliferation may be due to the heterogeneity of the HepG2 cultures. Clearly further work is required to culture more homogeneous HepG2 cells and to more clearly establish the dominant cellular processes induced by MC-LR. These effects of heterogeneity may also be addressed with the inclusion of more inter-day and intra-day replicates of these experiments.

In summary, the investigations into the combined effects of AZA1 and MC-LR on HepG2 using HCA revealed a number of antagonistic interactions between these toxins:

- a) Treatment with 2.5 μ M MC-LR alone exhibited proliferative effects on HepG2, but this effect was negated by the co-exposure to AZA1.
- b) Treatment with AZA1 alone caused nuclear shrinkage, as indicated by significant increases in NI, which is indicative of apoptosis. In contrast, treatment with MC-LR caused nuclear de-condensation, as indicated by significant increases in NA, which is an indicator of necrosis. Co-exposure of these toxins resulted reduced effects on both NA and NI, which would indicate antagonistic effects.
- c) Exposure of HepG2 cells to AZA1 alone caused significant effects on MM and MMP. However, exposure to MC-LR alone did not cause any significant

changes in mitochondrial health. The effects of co-exposure to AZA1 and MC-LR were the same as the effects of exposure to AZA1 alone, indicating the MC-LR did not act antagonistically or synergistically in effecting mitochondrial health.

Meanwhile, the combination of MC-LR with *M. aeruginosa* appeared to have a synergistic effect on nuclear de-condensation, as the exposure to both of these components resulted in a greater increase in NA than the effect of the individual components. No other synergistic or any antagonistic effects were observed for MC-LR and *M. aeruginosa*.

6.3.5 FAM-FLICA experiments indicated MC-LR induced apoptosis in HepG2

As it was indicated in HCA experiments that AZA1 exposure may induce apoptosis, while MC-LR exposure may cause necrosis, it was decided to further investigate apoptosis pathways by means of FAM-FLICA assays to measure caspase 3/7 activity. Due to restrictions in terms of equipment available at the time of testing, such FAM-FLICA assays were carried out using fluorescence plate reader measurements. It was predicted that use of such a measurement system may not be as sensitive to changes in caspase activity as a system like flow cytometry, for example. Therefore, the concentrations of both toxins were increased to 5 μM and 1 μM . In addition, it was shown in Section 6.2.2 that the presence of LPS increases the potency of AZA1, whereas in Section 6.2.1.1, it was suggested that the co-exposure of MC-LR and LPS may have inhibitive effects. Thus, HepG2 cells were treated with each toxin alone and in the presence of 100 ng/mL LPS.

It was shown in Figure 6.10 that a range of changes in caspase 3/7 activity were observed. Treatment with 5 μM MC-LR caused the largest increase in caspase 3/7 activity, which is in agreement with the literature (Ding *et al.*, 2000; Gan *et al.*, 2010; Zhang *et al.*, 2013). However, when combined with LPS, 5 μM MC-LR had a significant effect, albeit with lower fold-change than without LPS. The increase in caspase 3/7 activity would indicate that the cells are undergoing apoptosis. Interestingly, a combination of 1 μM MC-LR with LPS resulted in a reduction in caspase 3/7 activity.

In a similar way, all tested concentration of AZA1 with and without LPS resulted in an apparent reduction or absence of in caspase 3/7 activity. Such observations may be

explained by published literature in the area. A previous report on exposure of neuroblastoma cells to AZAs indicated cell death occurred via a non-apoptotic pathway (Roman *et al.*, 2002), which may have been explained by simultaneous induction of apoptosis and necrosis (Cao *et al.*, 2010). However, it was observed by Twiner *et al.* (2012) that 24 h treatment with 1 – 95 nM AZA1 did not significantly increase caspase 3/7 activity, whereas caspase 3/7 activity was significantly increased only after 48 h exposure. Thus, the exposure duration in the present study may not have been sufficient in order to observe increased caspase 3/7 activity with AZA1 treatment. This observation might be corroborated by the observed increase in MMP during HCA analysis, which is associated with the early stages of apoptosis that precede caspase-activation (Banki *et al.*, 1999). However, the results of the NA and NI parameters in HCA analysis would indicate successful induction of apoptosis using lower AZA1 concentrations and shorter duration of exposure; thus, the lack of caspase 3/7 activation may indicate early-stage apoptosis or a non-classical induction of apoptosis. Such effects were observed previously in other reports. For example, it was shown that T lymphocytes exposed to AZA1 showed late stage DNA laddering but in the absence of cell shrinkage and membrane blebbing (Twiner *et al.*, 2012). Clearly, further testing is required to more fully elucidate the cell death pathway involved, whether early-stage apoptosis or a non-classical apoptosis induction, perhaps by investigating other markers of apoptosis. Other potential markers of apoptosis include cytoplasmic levels of cytochrome c (McConkey, 1998), or an alternative mean to measure cell stress would be to measure levels of reactive oxygen intermediates (ROI) (Banki *et al.*, 1999; Wilson *et al.*, 2016; Meneely *et al.*, 2018).

It was shown in the current study and in the literature that MC-LR alone is not highly potent when treating HepG2 cells *in vitro* (Gan *et al.*, 2010) whereas, by comparison, AZA1 shows much greater toxicity. It is possible that the concentrations of the AZA1 used in these instances were of such a toxicity level that, by the time of testing, the HepG2 cells had proceeded past apoptosis and were necrotic or already dead. It should also be noted that carrying out these FAM-FLICA assays using fluorescence plate reader measurements required much higher numbers of cells and involved a considerable number of processing steps. This inevitably limited the ability to scale up the number of replicates available per assay. Thus, it is also possible that due to the lack of biological replicates, the inherent variability in cell-based assays was not fully

accounted for, and the number of processing steps may have introduced unwanted cell stress. Therefore, it is difficult to draw definitive conclusions from these apoptosis results without further replicates of these experiments. Ideally, in future experiments FAM-FLICA assays should be carried out in experimental triplicates using flow cytometry as a measurement.

6.3.6 Cytokine ELISAs

In addition to investigating the effects of MC-LR, *M. aeruginosa* and AZA1 on HepG2 proliferation and cell health, it was attempted to use ELISA to determine the levels of the cytokines IL-1 β and TNF- α produced during exposure to these contaminants. A number of previous studies have shown the exposure to MC-LR can result in changes in cytokine expression (Chen *et al.*, 2004; Chen *et al.*, 2005; Adamovsky *et al.*, 2015). Only a small number of studies reported the effects of *M. aeruginosa* cells on cytokine expression (Mayer *et al.*, 2011; Bláhová *et al.*, 2013) and no studies feature the HepG2 cell line. Furthermore, to the best of the author's knowledge, there are no reports on the effect of AZA1 exposure on cytokine expression. However, in this present study no significant increases in IL-1 β or TNF- α levels observed for the MC-LR-, *M. aeruginosa*- or AZA1-exposed HepG2 cells in these experiments. It is possible that exposure to these contaminants does not cause a change in expression of these cytokines. However, it is also possible that the levels of these expressed cytokines were below the limit of quantification of the ELISA assays, as it is known that hepatocyte cells express IL-1 β , TNF- α and other cytokines, albeit in low levels (Humpage and Falconer, 1999; Stonans *et al.*, 1999; Gallucci *et al.*, 2000; Gutierrez-Ruiz *et al.*, 2001). It is also possible that the lack of observed cytokine expression in this study may have been due to the toxin concentration and exposure duration. For example, it was observed that treatment of primary mouse hepatocytes with MC-LR induced IL-6 production for exposures with up to 0.02 μ M MC-LR, with maximal production after 12 h exposure. However, higher concentrations and longer duration of exposure did not significantly increase cytokine levels (Zhang *et al.*, 2013). Hence, in future experiments, concentrations of toxins should be reduced and the cytokine levels should be measured at earlier time points.

7 Outcomes and Conclusions

HABs and their toxic secondary metabolites are a major global health hazard, with the effects of these toxins exhibited as gastrointestinal disorders, liver disease, cancer promotion and death. Two specific toxins were investigated. Microcystins (MCs) are the most common cyanotoxins and are found globally (Harke *et al.*, 2016), while, azaspiracids (AZAs) are a widely distributed group of marine toxins associated with shellfish contamination and gastrointestinal disorders. In addition to these algal toxins, a focus of the research was the pathogenic food-poisoning bacterium, *Bacillus cereus*. The monitoring of waterborne and foodborne toxins and bacterial contaminants is highly important for reducing and preventing their entry into the food chain and for ensuring consumer safety. The aim of this thesis was the development and optimisation of recombinant antibody fragments specific to AZA1, MC-LR and *B. cereus*. Ideally the anti-AZA1 and anti-MC-LR antibodies would be incorporated into novel autonomous biosensor systems that would improve the monitoring and detection of these toxins at the point-of-need. It was desirable that the anti-*B. cereus* antibody would allow for species-level identification and could be incorporated into a flow cytometry-based platform to enhance food safety monitoring.

The development of a novel recombinant anti-AZA1 scFv was described in Chapter 3 of the thesis. This was undertaken by the immunisation of BALB/c mice with an AZA1-KLH conjugate. After a moderate immune response of 1:20,000 was observed, the recombinant scFv library was constructed. Initial attempts to screen this scFv library were unsuccessful and it was determined that this was due to non-specific binding of the M13 phage to the AZA1-BSA conjugate used for screening. A new AZA1-OVA toxin-conjugate was subsequently developed which overcame this non-specific interaction. The anti-AZA1 scFv library was re-constructed and screened using the new AZA1-OVA conjugate. Unfortunately, this second screening did not successfully isolate AZA1-specific scFv clones. While the aim of this chapter was to generate novel AZA1-specific rAbs, it was speculated that the moderate immune response generated in the immunised mice was not sufficiently strong for AZA1-specific clones to be highly represented in the recombinant scFv library; this in turn meant that the whole-library screening approach was not sensitive enough to isolate these rare AZA1-specific clones.

Thus, in order to develop an assay to measure AZA1 in solution, a competitive assay was developed using mouse polyclonal antiserum. This assay could detect free AZA1, with the lowest IC_{50} determined as 1.19 ng/mL. However, the assay suffered from inter-assay variability due to the heterogeneous nature of the polyclonal antibody used. Future experiments should aim to utilise single cell analysis systems to simultaneously screen high numbers of individual clones for antibodies with desirable binding properties. Such systems have been reported to improve the outcomes of screening experiments and could improve the retrieval of rare AZA1-specific scFv present in the libraries developed. Isolation of high affinity scFv from the library would allow for high sensitivity detection of AZA1 and would have great potential to improve the monitoring and detection of AZA1 in the environment and in food.

Chapter 4 of this thesis described the optimisation of the anti-MC-LR scFv, 2G1, through the use of modern computational modelling and docking, as well as through the use of targeted mutagenesis. The aim of the first section was to identify key amino acid (AA) residues involved in scFv-MC-LR binding and to improve the binding interaction. The combination of homology modelling, putative binding pocket identification by 'CASTp' and ligand docking by 'AutoDock Vina' provided an easily accessible route to gain valuable information into an antibody-antigen interaction and facilitated rational mutagenesis. The use of molecular modelling and antigen docking allowed for the identification of 8 putative AA residues in the scFv's binding pocket. These AA residues were each investigated using alanine scanning targeted mutagenesis. It was observed that 5 of the putative AAs were involved in binding to MC-LR, as indicated by reductions in antigen-binding upon substitution with alanine. In particular, the residue H-E102 was identified as having a key role in MC-LR-binding, as indicated by a reduction in relative affinity to 1.2% upon alanine substitution. The model for the lowest energy docking pose indicated that it is likely that the negatively charged side chain of H-E102 was directly interacting with the guanidinium group of the MC-LR arginine residue.

In addition to identifying key residues essential for MC-LR-binding, mutations at 2 AA sites resulted in improvements in antigen-binding. The residues L-S56 and L-D57 were identified as being poorly optimised in these positions in the wild type antibody as upon substitution with alanine the antigen-binding improved to 347% and 219%, respectively.

Furthermore, this was confirmed by the substitution of residue L-D57 with asparagine which retained 99.6% antigen binding ability; this indicated that the L-D57 side chain was likely not protonated and was interacting only via van der Waals interactions. Furthermore, it is possible that the side chains of residues L-S56 and L-D57 were sterically hindering a closer interaction between 2G1 and MC-LR. Thus, the aims of identifying key AA residues involved in antigen-binding and of improving the binding properties of the scFv were achieved. The results indicated that further work on the mutant clones L-S56A and L-D57A is warranted. The effect of combining these two mutations should be investigated and the binding affinity of the mutant clones should be further investigated by techniques such as surface plasmon resonance. The improvement in binding response may allow for higher sensitivity of MC-LR-detection and/or an improved dynamic range for the assay.

In the second part of Chapter 4, the focus was on using 3D modelling and targeted mutagenesis to identify surface exposed hydrophobic residues that could be mutated, as it is extensively reported in the literature that such mutations may improve the protein stability, solubility and expression. Three AA residues, i.e. L124, L153 and I255, were identified, and each mutated to aspartic acid and arginine. It was observed that the L124D/R and L153D/R mutants did not greatly affect antigen-binding. However, mutant I255R considerably reduced antigen-binding and was omitted from further work. None of the mutations appeared to improve the net yield of protein after expression and IMAC purification. However, all of the mutants reduced the aggregation propensity versus the wild type; in particular, the L153D mutation considerably reduced aggregation propensity. No changes in native solubility were observed following any of the mutations, which was possibly due to the lack of sensitivity of the assay. In addition, none of the mutant clones exhibited improved non-native solubility versus the wild type. It was observed that the mutations L124D, L124R and L153R improved the thermal stability of the antibody by ~5 °C. With regard to the overall aims of this section, no individual mutations resulted in improvements in solubility or expression, but improvements in terms of aggregation propensity and thermal stability were observed. Based on much literature evidence, it can be reasonably expected that such individual mutations may not greatly affect protein solubility and/or expression, but combinations of multiple mutations may give rise to more observable improvements. Thus, in future studies, multiple mutations should be combined to determine cumulative

benefits in terms of antibody solubility, stability and expression. Taken together, the work presented in this Chapter furthers our understanding of the interactions between antibodies and small molecule antigens and sheds more light onto the complex effects of AA mutations on antibody structure and function. The work presented should help with future investigations into the rational design of antibodies for specific targets.

Next, the aim of Chapter 5 was the development of *B. cereus*-specific recombinant antibodies that can distinguish between *B. cereus* and non-pathogenic *B. subtilis*. This was undertaken by the immunisation of an avian host with inactivated *B. cereus* vegetative cells, so as to present all available epitopes to the host's immune system. A strong immune response was generated, as evident by the serum titre of 1:86,000. A high yield of polyclonal IgY was obtained from an egg of the immunised chicken. It was shown in this work, and in work carried out by collaborators in the University of Limerick, that this polyclonal IgY exhibited high cross reactivity to the non-pathogenic *B. subtilis*. This highlighted the requirement to stringently screen the antibody repertoire for *B. cereus*-specific antibodies. Thus, a recombinant antibody library was developed, with the library size estimated at 2.8×10^7 clones. In order to screen this library, a whole-cell panning approach with negative depletion steps was utilised. This approach was used as it appeared to be the most viable means to isolate *B. cereus*-specific antibodies, due to the lack of species-specific biomarkers. After two rounds of screening, 192 clones were picked and their encoded scFv were tested by monoclonal ELISA against *B. cereus* and *B. subtilis*. It was observed that 9 clones exhibited preferential binding towards *B. cereus* versus *B. subtilis*. Due to time constraints, these clones were unable to be tested further, but future work should investigate the binding response of these antibodies towards selected bacterial targets. The work presented shows the promise of the generated scFv library to contain antibodies that can distinguish *B. cereus* from *B. subtilis* and also shows the potential of the whole-cell panning approach to effectively enrich the library for such antibodies.

In addition to the generation and optimisation of antibodies for toxin- and pathogen-detection, the aim of Chapter 6 of this thesis was to further extend our understanding of the toxic effects of individual and combined exposure of MC-LR, *M. aeruginosa* and AZA1 on HepG2 cells. Initial proliferation assays showed that whole *M. aeruginosa* cells exhibited a hormetic response on HepG2 proliferation, while lysed *M. aeruginosa*

cells exhibited cytotoxicity with as few as 1.6×10^4 cells/mL present. It was shown that AZA1 induced dose- and time-dependent cytotoxic effects on HepG2 cells, with EC_{50} values for 24 h and 48 h exposure determined as 2.43 μ M and 0.92 μ M, respectively. To the best of the author's knowledge, this is the first study to report the EC_{50} values of AZA1 in the HepG2 cell line. Using High Content Analysis (HCA) it was further shown that exposure to AZA1 alone induced apoptosis and that co-exposure to AZA1 with LPS increased the potency of AZA1 toxicity, potentially due to synergistic effects. The effects of co-exposure to MC-LR with *M. aeruginosa* and MC-LR with AZA1 were also investigated. Initial attempts involved the use of MTT assays and it was observed that only the combination of 8×10^4 *M. aeruginosa* cells/mL with 0.2 μ M MC-LR resulted in significant reductions in HepG2 proliferation. The clumping effects observed with HepG2 cells introduced variability between the individual- and combined-exposure experiments and was a considerable impediment to obtaining meaningful results from these experiments. However, HCA was used to determine the effects of individual- and combined- exposure to MC-LR, *M. aeruginosa* and AZA1. The apoptotic effect of AZA1 alone was further verified, while exposure to MC-LR alone resulted in necrotic and proliferative effects. Co-exposure to AZA1 and MC-LR appeared to cause antagonistic effects, whereas co-exposure to MC-LR with *M. aeruginosa* had synergistic effects, resulting in enhanced proliferation and necrosis. In future experiments, the HCA assays should be replicated to obtain inter-day replicates and improve statistical power. The investigations into the toxic effects of *M. aeruginosa* should also be replicated as it is possible that the cyanobacteria's cell state and physiology may affect its toxic potential. Thus, the work in this chapter highlights the complexity of co-exposure to multiple toxic contaminants but sheds some light onto possible antagonistic and synergistic relationships between toxins and cyanobacteria.

8 Bibliography

- 3M** (2018). *3M Tecra info*. Available at: <https://multimedia.3m.com/mws/media/7681880/3m-tecra-pathogen-and-toxin-visual-immunoassay-via-tests.pdf> (Accessed: 18 December 2018).
- Abdel-Latif**, H.M.R., Khashaba, A.M.A. (2017). Subchronic toxicity of *Nile tilapia* with different exposure routes to *Microcystis aeruginosa*: Histopathology, liver functions, and oxidative stress biomarkers. *Veterinary World*, **10**, 955–963.
- Adamovsky**, O., Moosova, Z., Pekarova, M., Basu, A., Babica, P., Svihalkova, Sindlerova, L., Kubala, L., Blaha, L. (2015). Immunomodulatory Potency of Microcystin, an Important Water-Polluting Cyanobacterial Toxin. *Environmental Science & Technology*, **49**, 12457–12464.
- Addabbo**, F., Ratliff, B., Park, H.C., Kuo, M.C., Ungvari, Z., Ciszar, A., Krasnikof, B., Sodhi, K., Zhang, F., Nasjletti, A., Goligorsky, M.S. (2009). The Krebs Cycle and Mitochondrial Mass Are Early Victims of Endothelial Dysfunction: Proteomic Approach. *The American Journal of Pathology*, **174**, 34–43.
- Adib-Conquy**, M., Gilbert, M., Avrameas, S. (1998). Effect of amino acid substitutions in the heavy chain CDR3 of an autoantibody on its reactivity. *International Immunology*, **10**, 341–346.
- Afanasieva**, T., Wittmer, M., Vitaliti, A., Ajmo, M., Neri, D., Klemenz, R. (2003). Single-chain antibody and its derivatives directed against vascular endothelial growth factor: application for antiangiogenic gene therapy. *Gene Therapy*, **10**, 1850–1859.
- Agata**, N., Mori, M., Ohta, M., Suwan, S., Ohtani, I., Isobe, M. (1994). A novel dodecadepsipeptide, cereulide, isolated from *Bacillus cereus* causes vacuole formation in HEP-2 cells. *FEMS Microbiology Letters*, **121**, 31–34.
- Agata**, N., Ohta, M., Mori, M., Isobe, M. (1995). A novel dodecadepsipeptide, cereulide, is an emetic toxin of *Bacillus cereus*. *FEMS Microbiology Letters*, **129**, 17–20.
- Ahern**, T.J., Manning, M.C. (1992). *Stability of Protein Pharmaceuticals: Chemical and Physical Pathways of Protein Degradation*. New York: Plenum Press.
- Alfaleh**, M., Jones, M., Howard, C., Mahler, S., Alfaleh, M.A., Jones, M.L., Howard, C.B., Mahler, S.M. (2017). Strategies for Selecting Membrane Protein-Specific Antibodies using Phage Display with Cell-Based Panning. *Antibodies*, **6**, 10.

- Almagro**, J.C., Hernández, I., Ramírez, M.C., Vargas-Madrazo, E. (1998). Structural differences between the repertoires of mouse and human germline genes and their evolutionary implications. *Immunogenetics*, **47**, 355–363.
- Almeida**, V.P.S., Cogo, K., Tsai, S.M., Moon, D.H. (2006). Colorimetric test for the monitoring of microcystins in cyanobacterial culture and environmental samples from southeast Brazil. *Brazilian Journal of Microbiology*, **37**, 192–198.
- Alonzo**, D.A., Magarvey, N.A., Schmeing, T.M. (2015). Characterization of Cereulide Synthetase, a Toxin-Producing Macromolecular Machine. *PLoS ONE*, **10**, e0128569.
- Altenburger**, R., Backhaus, T., Boedeker, W., Faust, M., Scholze, M. (2013). Simplifying complexity: Mixture toxicity assessment in the last 20 years. *Environmental Toxicology and Chemistry*, **32**, 1685–1687.
- Altshuler**, E.P., Serebryanaya, D.V., Katrukha, A.G. (2010). Generation of recombinant antibodies and means for increasing their affinity. *Biochemistry (Moscow)*, **75**, 1584–1605.
- Anderson**, D., Gilbert, P., Burkholder, J. (2002). Harmful algal blooms and eutrophication: Nutrient sources, composition, and consequences. *Estuaries*, **25**, 704–726.
- Anderson**, D.M., Cembella, A.D., Hallegraeff, G.M. (2012). Progress in Understanding Harmful Algal Blooms: Paradigm Shifts and New Technologies for Research, Monitoring, and Management. *Annual Review of Marine Science*, **4**, 143–176.
- Anderson**, I., Sorokin, A., Kapatral, V., Reznik, G., Bhattacharya, A., Mikhailova, N., Burd, H., Joukov, V., Kaznadzey, D., Walunas, T., D'souza, M., Larsen, N., Pusch, G., Liolios, K., Grechkin, Y., Lapidus, A., Goltsman, E., Chu, L., Fonstein, M., Ehrlich, S.D., Overbeek, R., Kyrpides, N., Ivanova, N. (2005). Comparative genome analysis of *Bacillus cereus* group genomes with *Bacillus subtilis*. *FEMS Microbiology Letters*, **250**, 175–184.
- Andersson**, A., Granum, P.E., Rønner, U. (1998). The adhesion of *Bacillus cereus* spores to epithelial cells might be an additional virulence mechanism. *International Journal of Food Microbiology*, **39**, 93–99.
- Ankolekar**, C., Rahmati, T., Labbé, R.G. (2009). Detection of toxigenic *Bacillus cereus* and *Bacillus thuringiensis* spores in U.S. rice. *International Journal of Food Microbiology*, **128**, 460–466.

- Arakawa**, T., Timasheff, S.N. (1985). Theory of protein solubility. *Methods in Enzymology*, **114**, 49–77.
- Argos**, P., Rossmann, M.G., Grau, U.M., Zuber, H., Frank, G., Tratschin, J.D., (1979). Thermal stability and protein structure. *Biochemistry*, **18**, 5698–5703.
- Aronson**, A.I., Shai, Y. (2001). Why *Bacillus thuringiensis* insecticidal toxins are so effective: unique features of their mode of action. *FEMS Microbiology Letters*, **195**, 1–8.
- Asano**, S.I., Nukumizu, Y., Bando, H., Iizuka, T., Yamamoto, T. (1997). Cloning of novel enterotoxin genes from *Bacillus cereus* and *Bacillus thuringiensis*. *Applied and Environmental Microbiology*, **63**, 1054–1057.
- Ash**, C., Farrow, J.A., Dorsch, M., Stackebrandt, E., Collins, M.D. (1991). Comparative analysis of *Bacillus anthracis*, *Bacillus cereus*, and related species on the basis of reverse transcriptase sequencing of 16S rRNA. *International Journal of Systematic and Evolutionary Microbiology*, **41**, 343–346.
- Auerbach**, G., Ostendorp, R., Prade, L., Korndörfer, I., Dams, T., Huber, R., Jaenicke, R. (1998). Lactate dehydrogenase from the hyperthermophilic bacterium *Thermotoga maritima*: the crystal structure at 2.1 Å resolution reveals strategies for intrinsic protein stabilization. *Structure*, **6**, 769–781.
- Augustine**, J.G., de la Calle, A., Knarr, G., Buchner, J., Frederick, C.A. (2001). The crystal structure of the Fab fragment of the monoclonal antibody MAK33: Implications for folding and interaction with the chaperone BiP. *Journal of Biological Chemistry*, **276**, 3287–3294.
- Azevedo**, S.M.F.O., Carmichael, W.W., Jochimsen, E.M., Rinehart, K.L., Lau, S., Shaw, G.R., Eaglesham, G.K. (2002). Human intoxication by microcystins during renal dialysis treatment in Caruaru, Brazil. *Toxicology*, **181**, 441–446.
- Babcock**, J.J., Li, M. (2013). hERG channel function: beyond long QT. *Acta Pharmacologica Sinica*, **34**, 329–335.
- Bacchiocchi**, S., Siracusa, M., Ruzzi, A., Gorbi, S., Ercolessi, M., Cosentino, M.A., Ammazzalorso, P., Orletti, R. (2015). Two-year study of lipophilic marine toxin profile in mussels of the North-central Adriatic Sea: First report of azaspiracids in Mediterranean seafood. *Toxicon*, **108**, 115–125.

- Backer**, L.C., Landsberg, J.H., Miller, M., Keel, K., Taylor, T.K. (2013). Canine Cyanotoxin Poisonings in the United States (1920s–2012): Review of Suspected and Confirmed Cases from Three Data Sources. *Toxins*, **5**, 1597–1628.
- Bais**, H.P., Fall, R., Vivanco, J.M. (2004). Biocontrol of *Bacillus subtilis* against infection of *Arabidopsis* roots by *Pseudomonas syringae* is facilitated by biofilm formation and surfactin production. *Plant Physiology*, **134**, 307–319.
- Baltrusch**, S., Lenzen, S., Okar, D., Lange, A., Tiedge, M. (2001). Characterization of glucokinase-binding protein epitopes by a phage-displayed peptide library - Identification of 6-phosphofructo-2-kinase/fructose-2,6-bisphosphatase as a novel interaction partner. *Journal of Biological Chemistry*, **276**, 43915–43923.
- Banki**, K., Hutter, E., Gonchoroff, N.J., Perl, A. (1999). Elevation of mitochondrial transmembrane potential and reactive oxygen intermediate levels are early events and occur independently from activation of caspases in Fas signaling. *Journal of Immunology*, **162**, 1466–1479.
- Barbas**, C.F., Burton, D.R., Scott, J.K. (2001). Phage Display: A Laboratory Manual. Cold Spring Harbour Press, Cold Spring Harbour, NY.
- Barthelemy**, P.A., Raab, H., Appleton, B.A., Bond, C.J., Wu, P., Wiesmann, C., Sidhu, S.S. (2008). Comprehensive analysis of the factors contributing to the stability and solubility of autonomous human VH domains. *Journal of Biological Chemistry*, **283**, 3639–3654.
- Bashford**, D., Chothia, C., Lesk, A.M. (1987). Determinants of a protein fold. Unique features of the globin amino acid sequences. *Journal of Molecular Biology*, **196**, 199–216.
- Beecher**, D.J., Macmillan, J.D. (1991). Characterization of the components of hemolysin BL from *Bacillus cereus*. *Infection and Immunity*, **59**, 1778–1784.
- Berg**, J.M., Tymoczko, J.L., Stryer, L. (2002). ‘Diversity Is Generated by Gene Rearrangements’, *Biochemistry*. 5th edn. New York: W.H. Freeman.
- Berger**, V., Richter, F., Zettlitz, K., Unverdorben, F., Scheurich, P., Herrmann, A., Pfizenmaier, K., Kontermann, R.E. (2013). An anti-TNFR1 scFv-HSA fusion protein as selective antagonist of TNF action. *Protein Engineering Design & Selection*, **26**, 581–587.
- Berghe**, T.V., Vanlangenakker, N., Parthoens, E., Deckers, W., Devos, M., Festjens, N., Guerin, C.J., Brunk, U.T., Declercq, W., Vandenabeele, P. (2010). Necroptosis, necrosis

and secondary necrosis converge on similar cellular disintegration features. *Cell Death and Differentiation*, **17**, 922–930.

Best, J.H., Eddy, F.B., Codd, G.A. (2003). Effects of *Microcystis* cells, cell extracts and lipopolysaccharide on drinking and liver function in rainbow trout *Oncorhynchus mykiss* Walbaum. *Aquatic Toxicology*, **64**, 419–426.

Best, J.H., Pflugmacher, S., Wiegand, C., Eddy, F.B., Metcalf, J.S., Codd, G.A. (2002). Effects of enteric bacterial and cyanobacterial lipopolysaccharides, and of microcystin-LR, on glutathione S-transferase activities in zebra fish (*Danio rerio*). *Aquatic Toxicology*, **60**, 223–231.

Biasini, M., Bienert, S., Waterhouse, A., Arnold, K., Studer, G., Schmidt, T., Kiefer, F., Cassarino, T.G., Bertoni, M., Bordoli, L., Schwede, T. (2014). SWISS-MODEL: modelling protein tertiary and quaternary structure using evolutionary information. *Nucleic Acids Research*, **42**, W252–W258.

Bishop, C.T., Anet, E.F.L.J., Gorham, P.R., (1959). Isolation and identification of the fast-death factor in *Microcystis aeruginosa* nrc-1. *Canadian Journal of Biochemistry and Physiology*, **37**, 453–471.

Black, K., Yilmaz, M., Phlips, E.J. (2011). Growth and Toxin Production by *Microcystis aeruginosa* PCC 7806 (Kutzing) Lemmerman at Elevated Salt Concentrations. *Journal of Environmental Protection*, **2**, 669–674.

Bláhová, L., Adamovský, O., Kubala, L., Švihálková Šindlerová, L., Zounková, R., Bláha, L. (2013). The isolation and characterization of lipopolysaccharides from *Microcystis aeruginosa*, a prominent toxic water bloom forming cyanobacteria. *Toxicon*, **76**, 187–196.

Bogan, A.A., Thorn, K.S. (1998). Anatomy of hot spots in protein interfaces. *Journal of Molecular Biology*, **280**, 1–9.

Bommarius, A.S., Paye, M.F. (2013). Stabilizing biocatalysts. *Chemical Society Reviews*, **42**, 6534–6565.

Botha, N., van de Venter, M., Downing, T.G., Shephard, E.G., Gehringer, M.M. (2004). The effect of intraperitoneally administered microcystin-LR on the gastrointestinal tract of BALB/c mice. *Toxicon*, **43**, 251–254.

Bouaïcha, N., Maatouk, I., Plessis, M.J., Périn, F. (2005). Genotoxic potential of Microcystin-LR and nodularin *in vitro* in primary cultured rat hepatocytes and *in vivo* in rat liver. *Environmental Toxicology*, **20**, 341–347.

- Bouchard, H.,** Viskov, C., Garcia-Echeverria, C. (2014). Antibody–drug conjugates—A new wave of cancer drugs. *Bioorganic and Medicinal Chemistry Letters*, **24**, 5357–5363.
- Boulet-Audet, M.,** Byrne, B., Kazarian, S.G. (2014). High-Throughput Thermal Stability Analysis of a Monoclonal Antibody by Attenuated Total Reflection FT-IR Spectroscopic Imaging. *Analytical Chemistry*, **86**, 9786–9793.
- Bradley, W.G.,** Mash, D.C. (2009). Beyond Guam: The cyanobacteria/BMAA hypothesis of the cause of ALS and other neurodegenerative diseases. *Amyotrophic Lateral Sclerosis*, **10**, 7–20.
- Broom, A.,** Jacobi, Z., Trainor, K., Meiering, E.M. (2017). Computational tools help improve protein stability but with a solubility tradeoff. *Journal of Biological Chemistry*, **292**, 14349–14361.
- Buck, P.M.,** Kumar, S., Wang, X., Agrawal, N.J., Trout, B.L., Singh, S.K. (2012). ‘Computational Methods to Predict Therapeutic Protein Aggregation’, in: Voynov, V., Caravella, J.A. (Eds.), *Therapeutic Proteins: Methods and Protocols, Methods in Molecular Biology*. Totowa, NJ: Humana Press, pp. 425–451.
- Bunde, R.,** Jarvi, E., Rosentreter, J. (1998). Piezoelectric quartz crystal biosensors. *Talanta*, **46**, 1223–1236.
- Byrne, B.,** Stack, E., Gilmartin, N., O’Kennedy, R. (2009). Antibody-Based Sensors: Principles, Problems and Potential for Detection of Pathogens and Associated Toxins. *Sensors*, **9**, 4407–4445.
- Cacace, M.G.,** Santin, M., Sada, A. (1990). Behaviour of amino acids in gel permeation chromatography: Correlation with the effect of Hofmeister solutes on the conformational stability of macromolecules. *Journal of Chromatography A*, **510**, 41–46.
- Cai, J.,** Yang, J., Jones, D. (1998). Mitochondrial control of apoptosis: the role of cytochrome c. *Biochimica et Biophysica Acta – Bioenergetics*, **1366**, 139–149.
- Calabrese, E.J.,** Baldwin, L.A. (2002). Defining hormesis. *Human and Experimental Toxicology*, **21**, 91–97.
- Calabrese, E.J.,** Mattson, M.P. (2011). Hormesis provides a generalized quantitative estimate of biological plasticity. *Journal of Cell Communication and Signalling*, **5**, 25–38.
- Campos, A.,** Vasconcelos, V. (2010). Molecular Mechanisms of Microcystin Toxicity in Animal Cells. *International Journal of Molecular Sciences*, **11**, 268–287.

- Cao, Z., LePage, K.T., Frederick, M.O., Nicolaou, K.C., Murray, T.F.** (2010). Involvement of caspase activation in azaspiracid-induced neurotoxicity in neocortical neurons. *Toxicological Sciences*, **114**, 323–334.
- Carlander, D., Stålberg, J., Larsson, A.** (1999). Chicken Antibodies: A Clinical Chemistry Perspective. *Upsala Journal of Medical Sciences*, **104**, 179–189.
- Carter, P.H., Shimizu, M., Luck, M.D., Gardella, T.J.** (1999). The Hydrophobic Residues Phenylalanine 184 and Leucine 187 in the Type-1 Parathyroid Hormone (PTH) Receptor Functionally Interact with the Amino-terminal Portion of PTH-(1–34). *Journal of Biological Chemistry*, **274**, 31955–31960.
- Castillo, V., Graña-Montes, R., Ventura, S.** (2011). The aggregation properties of *Escherichia coli* proteins associated with their cellular abundance. *Biotechnology Journal*, **6**, 752–760.
- Ceuppens, S., Boon, N., Uyttendaele, M.** (2013). Diversity of *Bacillus cereus* group strains is reflected in their broad range of pathogenicity and diverse ecological lifestyles. *FEMS Microbiology Ecology*, **84**, 433–450.
- Ceuppens, S., Rajkovic, A., Hamelink, S., Van de Wiele, T., Boon, N., Uyttendaele, M.** (2012). Enterotoxin Production by *Bacillus cereus* under gastrointestinal conditions and their immunological detection by commercially available kits. *Foodborne Pathogens and Disease*, **9**, 1130–1136.
- Chames, P., Van Regenmortel, M., Weiss, E., Baty, D.** (2009). Therapeutic antibodies: successes, limitations and hopes for the future. *British Journal of Pharmacology*, **157**, 220–233.
- Chan, L.L., Sit, W.H., Lam, P.K.S., Hsieh, D.P.H., Hodgkiss, I.J., Wan, J.M.F., Ho, A.Y.T., Choi, N.M.C., Wang, D.Z., Dudgeon, D.** (2006). Identification and characterization of a “biomarker of toxicity” from the proteome of the paralytic shellfish toxin-producing dinoflagellate *Alexandrium tamarense* (*Dinophyceae*). *Proteomics*, **6**, 654–666.
- Charni, N., Perissol, C., Petit, J.L., Rugani, N.** (2000). Production and characterization of monoclonal antibodies against vegetative cells of *Bacillus cereus*. *Applied and Environmental Microbiology*, **66**, 2278–2281.
- Chen, T., Shen, P., Zhang, J., Hua, Z.** (2005). Effects of microcystin-LR on patterns of iNOS and cytokine mRNA expression in macrophages *in vitro*. *Environmental Toxicology*, **20**, 85–91.

- Chen**, T., Zhao, X., Liu, Y., Shi, Q., Hua, Z., Shen, P. (2004). Analysis of immunomodulating nitric oxide, iNOS and cytokines mRNA in mouse macrophages induced by microcystin-LR. *Toxicology*, **197**, 67–77.
- Chiti**, F., Dobson, C.M. (2006). Protein misfolding, functional amyloid, and human disease. *Annual Review of Biochemistry*, **75**, 333–366.
- Cho**, U.S., Xu, W. (2007). Crystal structure of a protein phosphatase 2A heterotrimeric holoenzyme. *Nature*, **445**, 53–57.
- Chorus**, I., Falconer, I.R., Salas, H.J., Bartram, J. (2000). Health risks caused by freshwater cyanobacteria in recreational waters. *Journal of Toxicology and Environmental Health - Part B: Critical Reviews*, **3**, 323–347.
- Cirés**, S., Ballot, A. (2016). A review of the phylogeny, ecology and toxin production of bloom-forming *Aphanizomenon* spp. and related species within the Nostocales (cyanobacteria). *Harmful Algae*, **54**, 21–43.
- Cirés**, S., Casero, M.C., Quesada, A. (2017). Toxicity at the Edge of Life: A Review on Cyanobacterial Toxins from Extreme Environments. *Marine Drugs*, **15**, 233.
- Clarke**, R., Connolly, L., Frizzell, C., Elliott, C.T. (2015). High content analysis: A sensitive tool to detect and quantify the cytotoxic, synergistic and antagonistic effects of chemical contaminants in foods. *Toxicology Letters*, **233**, 278–286.
- Clavel**, T., Carlin, F., Lairon, D., Nguyen-The, C., Schmitt, P. (2004). Survival of *Bacillus cereus* spores and vegetative cells in acid media simulating human stomach. *Journal of Applied Microbiology*, **97**, 214–219.
- Cohen**, F.E., Kelly, J.W. (2003). Therapeutic approaches to protein-misfolding diseases. *Nature*, **426**, 905–909.
- Cohn**, E.J., Edsall, J.T., (1943). Proteins, amino acids, and peptides as polar and non-polar ions. *The Journal of Physical Chemistry*, **47**, 713–714.
- Colman**, J.R., Twiner, M.J., Hess, P., McMahan, T., Satake, M., Yasumoto, T., Doucette, G.J., Ramsdell, J.S. (2005). Teratogenic effects of azaspiracid-1 identified by microinjection of Japanese medaka (*Oryzias latipes*) embryos. *Toxicon*, **45**, 881–890.
- Conroy**, P.J., Hearty, S., Leonard, P., O’Kennedy, R.J. (2009). Antibody production, design and use for biosensor-based applications. *Seminars in Cell and Developmental Biology*, **20**, 10–26.

- Conroy**, P.J., Law, R.H.P., Gilgunn, S., Hearty, S., Caradoc-Davies, T.T., Lloyd, G., O’Kennedy, R.J., Whisstock, J.C. (2014). Reconciling the Structural Attributes of Avian Antibodies. *Journal of Biological Chemistry*, **289**, 15384–15392.
- Consler**, T.G., Tsolas, O., Kaback, H.R. (1991). Role of proline residues in the structure and function of a membrane transport protein. *Biochemistry*, **30**, 1291–1298.
- Cote**, C.K., Rossi, C.A., Kang, A.S., Morrow, P.R., Lee, J.S., Welkos, S.L. (2005). The detection of protective antigen (PA) associated with spores of *Bacillus anthracis* and the effects of anti-PA antibodies on spore germination and macrophage interactions. *Microbial Pathogenesis*, **38**, 209–225.
- Cox**, P.A., Banack, S.A., Murch, S.J., Rasmussen, U., Tien, G., Bidigare, R.R., Metcalf, J.S., Morrison, L.F., Codd, G.A., Bergman, B. (2005). Diverse taxa of cyanobacteria produce β -N-methylamino-l-alanine, a neurotoxic amino acid. *Proceedings of the National Academy of Sciences (USA)*, **102**, 5074–5078.
- Cox**, P.A., Sacks, O.W. (2018). Cycad neurotoxins, consumption of flying foxes, and ALS-PDC disease in Guam. *Neurology*, **58**, 956–959.
- Cronin**, U.P., Wilkinson, M.G. (2010). The potential of flow cytometry in the study of *Bacillus cereus*. *Journal of Applied Microbiology*, **108**, 1–16.
- Cusack**, C., Dabrowski, T., Lyons, K., Berry, A., Westbrook, G., Salas, R., Duffy, C., Nolan, G., Silke, J. (2016). Harmful algal bloom forecast system for SW Ireland. Part II: Are operational oceanographic models useful in a HAB warning system. *Harmful Algae*, **53**, 86–101.
- Dale**, B., Murphy, M. (2014). A retrospective appraisal of the importance of high-resolution sampling for harmful algal blooms: Lessons from long-term phytoplankton monitoring at Sherkin Island, S.W. Ireland. *Harmful Algae*, **40**, 23–33.
- Danchin**, A. (2001). ‘*Bacillus subtilis*’, in: Brenner, S., Miller, J.H. (Eds.), *Encyclopaedia of Genetics*. New York: Academic Press, pp. 135–144.
- Daubenspeck**, J.M., Zeng, H., Chen, P., Dong, S., Steichen, C.T., Krishna, N.R., Pritchard, D.G., Turnbough, C.L. (2004). Novel oligosaccharide side chains of the collagen-like region of BclA, the major glycoprotein of the *Bacillus anthracis* exosporium. *Journal of Biological Chemistry*, **279**, 30945–30953.
- Demarest**, S.J., Chen, G., Kimmel, B.E., Gustafson, D., Wu, J., Salbato, J., Poland, J., Elia, M., Tan, X., Wong, K., Short, J., Hansen, G. (2006). Engineering stability into

Escherichia coli secreted Fabs leads to increased functional expression. *Protein Engineering, Design and Selection* **19**, 325–336.

den Engelsman, J., Garidel, P., Smulders, R., Koll, H., Smith, B., Bassarab, S., Seidl, A., Hainzl, O., Jiskoot, W. (2011). Strategies for the assessment of protein aggregates in pharmaceutical biotech product development. *Pharmaceutical Research*, **28**, 920–933.

Derda, R., Tang, K.S., Li, S.C., Ng, S., Matochko, W., Jafari, R.M. (2011). Diversity of Phage-Displayed Libraries of Peptides during Panning and Amplification. *Molecules*, **16**, 1776–803.

Derda, R., Tang, S., Whitesides, G.M. (2010). Uniform amplification of phage with different growth characteristics in individual compartments consisting of monodisperse droplets. *Angewandte Chemie International Edition*, **49**, 5301–5304.

Desrochers, G., Cappadocia, L., Lussier-Price, M., Ton, A.T., Ayoubi, R., Serohijos, A., Omichinski, J.G., Angers, A. (2017). Molecular basis of interactions between SH3 domain-containing proteins and the proline-rich region of the ubiquitin ligase Itch. *Journal of Biological Chemistry*, **292**, 6325–6338.

Dierick, K., Van Coillie, E., Swiecicka, I., Meyfroidt, G., Devlieger, H., Meulemans, A., Hoedemaekers, G., Fourie, L., Heyndrickx, M., Mahillon, J. (2005). Fatal family outbreak of *Bacillus cereus*-associated food poisoning. *Journal of Clinical Microbiology*, **43**, 4277–4279.

Dietrich, R., Moravek, M., Bürk, C., Granum, P.E., Märtlbauer, E. (2005). Production and characterization of antibodies against each of the three subunits of the *Bacillus cereus* nonhemolytic enterotoxin complex. *Applied and Environmental Microbiology*, **71**, 8214–8220.

Ding, W.X., Nam Ong, C. (2003). Role of oxidative stress and mitochondrial changes in cyanobacteria-induced apoptosis and hepatotoxicity. *FEMS Microbiology Letters*, **220**, 1–7.

Ding, W.X., Shen, H.M., Ong, C.N. (2000). Critical role of reactive oxygen species and mitochondrial permeability transition in microcystin-induced rapid apoptosis in rat hepatocytes. *Hepatology*, **32**, 547–555.

Ding, W.X., Shen, H.M., Zhu, H.G., Ong, C.N. (1998). Studies on oxidative damage induced by cyanobacteria extract in primary cultured rat hepatocytes. *Environmental Research*, **78**, 12–18.

- Ding**, X.S., Li, X.Y., Duan, H.Y., Chung, I.K., Lee, J.A. (2006). Toxic effects of *Microcystis* cell extracts on the reproductive system of male mice. *Toxicol*, **48**, 973–979.
- Ding**, Y., Liu, M., Han, W., Yang, S., Liu, H., Gong, Y. (2005). Application of phage-displayed single chain antibodies in western blot. *Acta Biochimica et Biophysica Sinica*, **37**, 205–209.
- Diskin**, R., Scheid, J.F., Marcovecchio, P.M., West, A.P., Klein, F., Gao, H., Gnanapragasam, P.N.P., Abadir, A., Seaman, M.S., Nussenzweig, M.C., Bjorkman, P.J. (2011). Increasing the potency and breadth of an HIV antibody by using structure-based rational design. *Science*, **334**, 1289–1293.
- Doerner**, A., Rhiel, L., Zielonka, S., Kolmar, H. (2014). Therapeutic antibody engineering by high efficiency cell screening. *FEBS Letters, Protein Engineering*, **588**, 278–287.
- Doerr**, B., O’Halloran, J., O’Brien, N., van Pelt, F. (2016). Investigation of the genotoxic potential of the marine biotoxins azaspiracid 1–3. *Toxicol*, **121**, 61–69.
- Doi**, H., Chang, K.H., Ando, T., Imai, H., Nakano, S., Kajimoto, A., Katano, I. (2008). Drifting plankton from a reservoir subsidize downstream food webs and alter community structure. *Oecologia*, **156**, 363–371.
- Dolman**, A.M., Rücker, J., Pick, F.R., Fastner, J., Rohrlack, T., Mischke, U., Wiedner, C. (2012). Cyanobacteria and cyanotoxins: The influence of nitrogen versus phosphorus. *PLoS ONE*, **7**, e38757.
- Douglas**, P., Moorhead, G.B., Ye, R., Lees-Miller, S.P. (2001). Protein phosphatases regulate DNA-dependent protein kinase activity. *Journal of Biological Chemistry*, **276**, 18992–18998.
- Dr. Oleg Trott** (2014). *AutoDock Vina Video Tutorial*. Available at: <https://www.youtube.com/watch?v=-GVZP0X0Tg8> (Accessed: 5 January 2019).
- Ducruix**, A.F., Ries-Kautt, M.M. (1990). Solubility diagram analysis and the relative effectiveness of different ions on protein crystal growth. *Methods*, **1**, 25–30.
- Dudgeon**, K., Famm, K., Christ, D. (2009). Sequence determinants of protein aggregation in human VH domains. *Protein Engineering, Design and Selection*, **22**, 217–220.

- Dundas, J., Ouyang, Z., Tseng, J., Binkowski, A., Turpaz, Y., Liang, J.** (2006). CASTp: computed atlas of surface topography of proteins with structural and topographical mapping of functionally annotated residues. *Nucleic Acids Research*, **34**, W116–W118.
- Earl, A.M., Losick, R., Kolter, R.** (2008). Ecology and genomics of *Bacillus subtilis*. *Trends in Microbiology*, **16**, 269–275.
- Ehling-Schulz, M., Fricker, M., Scherer, S.** (2004). Identification of emetic toxin producing *Bacillus cereus* strains by a novel molecular assay. *FEMS Microbiology Letters*, **232**, 189–195.
- Elshal, M.F., McCoy, J.P.** (2006). Multiplex bead array assays: performance evaluation and comparison of sensitivity to ELISA. *Methods*, **38**, 317–323.
- Environment Protection Agency** (2007). *Report on cumulative effects of combined presence of pesticides in foodstuffs*. Available at: <http://www.epa.gov/pesticides/cumulative/> (Accessed: 5 January 2019)
- European Commission** (2011). *Commission Regulation (EU) No 15/2011*. Available at: <https://eur-lex.europa.eu/LexUriServ/LexUriServ.do?uri=OJ:L:2011:006:0003:0006:EN:PDF> (Accessed: 5 January 2019)
- European Commission** (2004). *Commission Regulation (EC) No 853/2004*. Available at: [https://www.fsai.ie/uploadedFiles/Reg853_2004\(1\).pdf](https://www.fsai.ie/uploadedFiles/Reg853_2004(1).pdf) (Accessed: 4 January 2019).
- European Food Safety Authority** (2008). Marine biotoxins in shellfish - okadaic acid and analogues - Scientific Opinion of the Panel on Contaminants in the Food chain: Marine biotoxins in shellfish - okadaic acid and analogues - Scientific Opinion of the Panel on Contaminants in the Food chain. *EFSA Journal*, **589**, 1–62.
- Ewert, S., Cambillau, C., Conrath, K., Plückthun, A.** (2002). Biophysical properties of camelid V(HH) domains compared to those of human V(H)3 domains. *Biochemistry*, **41**, 3628–3636.
- Falco, M., Romeo, E., Marcenaro, S., Martini, S., Vitale, M., Bottino, C., Mingari, M.C., Moretta, L., Moretta, A., Pende, D.** (2010). Combined Genotypic and Phenotypic Killer Cell Ig-Like Receptor Analyses Reveal KIR2DL3 Alleles Displaying Unexpected Monoclonal Antibody Reactivity: Identification of the Amino Acid Residues Critical for Staining. *The Journal of Immunology*, **185**, 433–441.
- Falconer, I.R., Yeung, D.S.** (1992). Cytoskeletal changes in hepatocytes induced by *Microcystis* toxins and their relation to hyperphosphorylation of cell proteins. *Chemico-Biological Interactions*, **81**, 181–196.

- Fan, D., Li, Q., Korando, L., Jerome, W.G., Wang, J. (2004).** A Monomeric Human Apolipoprotein E Carboxyl-Terminal Domain. *Biochemistry*, **43**, 5055–5064.
- Farrell, H., Gentien, P., Fernand, L., Lunven, M., Reguera, B., González-Gil, S., Raine, R. (2012).** Scales characterising a high density thin layer of *Dinophysis acuta* Ehrenberg and its transport within a coastal jet. *Harmful Algae*, **15**, 36–46.
- Fellouse, F.A., Wiesmann, C., Sidhu, S.S. (2004).** Synthetic antibodies from a four-amino-acid code: A dominant role for tyrosine in antigen recognition. *Proceedings of the National Academy of Sciences (USA)*, **101**, 12467–12472.
- Ferreiro, Sara F., Vilariño, N., Carrera, C., Louzao, M.C., Santamarina, G., Cantalapiedra, A.G., Rodríguez, L.P., Cifuentes, J.M., Vieira, A.C., Nicolaou, K.C., Frederick, M.O., Botana, L.M. (2014).** *In vivo* arrhythmogenicity of the marine biotoxin azaspiracid-2 in rats. *Archives of Toxicology*, **88**, 425–434.
- Ferreiro, S. F., Vilarino, N., Louzao, M.C., Nicolaou, K.C., Frederick, M.O., Botana, L.M. (2014).** *In vitro* chronic effects on hERG channel caused by the marine biotoxin azaspiracid-2. *Toxicol*, **91**, 69–75.
- Fitzgerald, V., Leonard, P. (2017).** Single cell screening approaches for antibody discovery. *Antibodies –Analytical Masterpieces Production and Applications*, **116**, 34–42.
- Fitzgerald, V., Manning, B., O'Donnell, B., O'Reilly, B., O'Sullivan, D., O'Kennedy, R., Leonard, P. (2015).** Exploiting highly ordered subnanoliter volume microcapillaries as microtools for the analysis of antibody producing cells. *Analytical Chemistry*, **87**, 997–1003.
- Forsyth, C.J., Xu, J., Nguyen, S.T., Samdal, I.A., Briggs, L.R., Rundberget, T., Sandvik, M., Miles, C.O. (2006).** Antibodies with broad specificity to azaspiracids by use of synthetic haptens. *Journal of the American Chemical Society*, **128**, 15114–15116.
- Frederick, M.O., De Lamo Marin, S., Janda, K.D., Nicolaou, K.C., Dickerson, T.J. (2009).** Monoclonal antibodies with orthogonal azaspiracid epitopes. *ChemBioChem.*, **10**, 1625–1629.
- Frenzel, A., Hust, M., Schirrmann, T. (2013).** Expression of Recombinant Antibodies. *Frontiers in Immunology*, **4**, 217.
- Fricker, M., Messelhäuser, U., Busch, U., Scherer, S., Ehling-Schulz, M. (2007).** Diagnostic real-time pcr assays for the detection of emetic *Bacillus cereus* strains in

foods and recent food-borne outbreaks. *Applied and Environmental Microbiology*, **73**, 1892–1898.

FSAI (2016). *Best Practice for Testing Foods when Assessing Compliance with the Microbiological Criteria*. Available at: <https://www.fsai.ie/WorkArea/DownloadAsset.aspx?id=10484>. (Accessed: 4 January 2019).

Fu, W., Chen, J., Wang, X., Xu, L. (2005). Altered expression of p53, Bcl-2 and Bax induced by microcystin-LR *in vivo* and *in vitro*. *Toxicol*, **46**, 171–177.

Fujiki, H., Suganuma, M. (2009). Carcinogenic aspects of protein phosphatase 1 and 2A inhibitors. *Progress in Molecular and Subcellular Biology*, **46**, 221–254.

Gallucci, R.M., Simeonova, P.P., Toriumi, W., Luster, M.I. (2000). TNF- α regulates transforming growth factor- α expression in regenerating murine liver and isolated hepatocytes. *The Journal of Immunology*, **164**, 872–878.

Gallus Immunotech (2018). EggsPress Purification Kit instructions Available at: <http://gallusimmunotech.com/yolk-igy-purification-kit/instructions> (Accessed: 24 October 2018).

Gan, N., Mi, L., Sun, X., Dai, G., Chung, F.L., Song, L. (2010). Sulforaphane protects Microcystin-LR-induced toxicity through activation of the Nrf2-mediated defensive response. *Toxicology and Applied Pharmacology*, **247**, 129–137.

Ganesan, A., Siekierska, A., Beerten, J., Brams, M., Van Durme, J., De Baets, G., Van der Kant, R., Gallardo, R., Ramakers, M., Langenberg, T., Wilkinson, H., De Smet, F., Ulens, C., Rousseau, F., Schymkowitz, J. (2016). Structural hot spots for the solubility of globular proteins. *Nature Communications*, **7**, 10816.

Gaudin, J., Huet, S., Jarry, G., Fessard, V. (2008). *In vivo* DNA damage induced by the cyanotoxin microcystin-LR: comparison of intra-peritoneal and oral administrations by use of the comet assay. *Mutation Research*, **652**, 65–71.

Gehring, M.M. (2004). Microcystin-LR and okadaic acid-induced cellular effects: a dualistic response. *FEBS Letters*, **557**, 1–8.

Gerber, H.P., Sapra, P., Loganzo, F., May, C. (2016). Combining antibody-drug conjugates and immune-mediated cancer therapy: What to expect? *Biochemical Pharmacology*, **102**, 1–6.

GESAMP (2001). Protecting the oceans from land-based activities: land-based sources and activities affecting the quality and uses of the marine, coastal and associated freshwater environment. *GESAMP reports and studies*. UNEP, Nairobi.

- Gil, D., Schrum, A.G.** (2013). Strategies to stabilize compact folding and minimize aggregation of antibody-based fragments. *Advances in Bioscience and Biotechnology*, **4**, 73–84.
- Glasset, B., Herbin, S., Guillier, L., Cadel-Six, S., Vignaud, M.L., Grout, J., Pairaud, S., Michel, V., Hennekinne, J.A., Ramarao, N., Brisabois, A.** (2016). *Bacillus cereus*-induced food-borne outbreaks in France (2007) to (2014): epidemiology and genetic characterisation. *Eurosurveillance*, **21**.
- Glockshuber, R., Malia, M., Pfitzinger, I., Plueckthun, A.** (1990). A comparison of strategies to stabilize immunoglobulin Fv-fragments. *Biochemistry (N.Y.)*, **29**, 1362–1367.
- Goldberg, J., Huang, H., Kwon, Y., Greengard, P., Nairn, A.C., Kuriyan, J.** (1995). Three-dimensional structure of the catalytic subunit of protein serine/threonine phosphatase-1. *Nature*, **376**, 745–753.
- Granum, P.E.** (1994). *Bacillus cereus* and its toxins. *Journal of Applied Bacteriology*, **76**, 61S-66S.
- Granum, P.E., Brynestad, S., O’Sullivan, K., Nissen, H.** (1993). Enterotoxin from *Bacillus cereus*: production and biochemical characterization. *Netherlands Milk and Dairy Journal (Netherlands)*, **47**, 63–70.
- Gromiha, M.M.** (2010). ‘Protein Stability’, in: Gromiha, M.M. (Ed.), *Protein Bioinformatics*. Singapore: Academic Press, pp. 209–245.
- Grosse, Y., Baan, R., Straif, K., Secretan, B., El Ghissassi, F., Coglianò, V.** (2006). Carcinogenicity of nitrate, nitrite, and cyanobacterial peptide toxins. *The Lancet Oncology*, **7**, 628–629.
- Gu, H., Luo, Z., Krock, B., Witt, M., Tillmann, U.** (2013). Morphology, phylogeny and azaspiracid profile of *Azadinium poporum* (*Dinophyceae*) from the China Sea. *Harmful Algae*, **21**, 64–75.
- Guex, N., Peitsch, M.C., Schwede, T.** (2009). Automated comparative protein structure modeling with SWISS-MODEL and Swiss-PdbViewer: A historical perspective. *Electrophoresis*, **30**, S162–S173.
- Gulledgea, B.M., Aggena, J.B., Huangb, H.B., Nairnc, A.C., Chamberlin, A.R.** (2002). The microcystins and nodularins: cyclic polypeptide inhibitors of PP1 and PP2A. *Current Medicinal Chemistry*, **9**, 1991–2003.

- Gupta**, N., Pant, S.C., Vijayaraghavan, R., Rao, P.V.L. (2003). Comparative toxicity evaluation of cyanobacterial cyclic peptide toxin microcystin variants (LR, RR, YR) in mice. *Toxicology*, **188**, 285–296.
- Gutiérrez-Ruiz**, M.C., Gomez-Quiroz, L.E., Hernandez, E., Bucio, L., Souza, V., LLorente, L., Kershenobich, D. (2001). Cytokine response and oxidative stress produced by ethanol, acetaldehyde and endotoxin treatment in HepG2 cells. *The Israel Medical Association Journal*, **3**, 131–136.
- Hakami**, A.R., Ball, J.K., Tarr, A.W. (2015). Non-ionic detergents facilitate non-specific binding of M13 bacteriophage to polystyrene surfaces. *Journal of Virological Methods*, **221**, 1–8.
- Hamers-Casterman**, C., Atarhouch, T., Muyldermans, S., Robinson, G., Hammers, C., Songa, E.B., Bendahman, N., Hammers, R. (1993). Naturally occurring antibodies devoid of light chains. *Nature*, **363**, 446–448.
- Hansel**, T.T., Kropshofer, H., Singer, T., Mitchell, J.A., George, A.J.T. (2010). The safety and side effects of monoclonal antibodies. *Nature Reviews Drug Discovery*, **9**, 325–338.
- Harke**, M.J., Steffen, M.M., Gobler, C.J., Otten, T.G., Wilhelm, S.W., Wood, S.A., Paerl, H.W. (2016). A review of the global ecology, genomics, and biogeography of the toxic cyanobacterium, *Microcystis* spp. *Harmful Algae*, **54**, 4–20.
- Hauss**, O., Müller, O. (2007). The protein truncation test in mutation detection and molecular diagnosis. *Methods in Molecular Biology*, **375**, 151–164.
- Hawe**, A., Kasper, J.C., Friess, W., Jiskoot, W. (2009). Structural properties of monoclonal antibody aggregates induced by freeze-thawing and thermal stress. *European Journal of Pharmaceutical Sciences*, **38**, 79–87.
- Healy**, D.A., Hayes, C.J., Leonard, P., McKenna, L., O’Kennedy, R. (2007). Biosensor developments: application to prostate-specific antigen detection. *Trends Biotechnology*, **25**, 125–131.
- Hebditch**, M., Carballo-Amador, M.A., Charonis, S., Curtis, R., Warwicker, J. (2017). Protein–Sol: a web tool for predicting protein solubility from sequence. *Bioinformatics*, **33**, 3098–3100.
- Hermanson**, G.T. (2013). *Bioconjugate Techniques*. Cambridge, MA: Academic Press.
- Hibbing**, M.E., Fuqua, C., Parsek, M.R., Peterson, S.B. (2010). Bacterial competition: surviving and thriving in the microbial jungle. *Nature Reviews Microbiology*, **8**, 15–25.

- Hilborn**, E.D., Roberts, V.A., Backer, L., Deconno, E., Egan, J.S., Hyde, J.B., Nicholas, D.C., Wiegert, E.J., Billing, L.M., Diorio, M., Mohr, M.C., Joan Hardy, F., Wade, T.J., Yoder, J.S., Hlavsa, M.C. (2014). Algal bloom-associated disease outbreaks among users of freshwater lakes - United States 2009-2010. *Morbidity and Mortality Weekly Report*, **63**, 11–15.
- Hong**, H.A., Duc, L.H., Cutting, S.M. (2005). The use of bacterial spore formers as probiotics. *FEMS Microbiology Reviews*, **29**, 813–835.
- Hoogenboom**, H.R. (2005). Selecting and screening recombinant antibody libraries. *Nature Biotechnology*, **23**, 1105–1116.
- Horecka**, H.M., Thomas, A.C., Weatherbee, R.A. (2014). Environmental links to interannual variability in shellfish toxicity in Cobscook Bay and eastern Maine, a strongly tidally mixed coastal region. *Deep Sea Research Part II: Topical Studies in Oceanography*, **103**, 318–328.
- Huey**, W.R., Morris, G.M., Forli, S. *Using AutoDock 4 and AutoDock Vina with AutoDockTools: A Tutorial*. Available at: http://autodock.scripps.edu/faqs-help/tutorial/using-autodock-4-with-autodocktools/2012_ADTtut.pdf. (Accessed: 05 January 2019).
- Hughes**, S., Bartholomew, B., Hardy, J.C., Kramer, J.M. (1988). Potential application of a HEp-2 cell assay in the investigation of *Bacillus cereus* emetic-syndrome food poisoning. *FEMS Microbiology Letters*, **52**, 7–11.
- Humpage**, A.R., Falconer, I.R. (1999). Microcystin-LR and liver tumor promotion: effects on cytokinesis, ploidy, and apoptosis in cultured hepatocytes. *Environmental Toxicology*, **14**, 61–75.
- Humpage**, A.R., Hardy, S.J., Moore, E.J., Froschio, S.M., Falconer, I.R. (2000). Microcystins (cyanobacterial toxins) in drinking water enhance the growth of aberrant crypt foci in the mouse colon. *Journal of Toxicology and Environmental Health Part A*, **61**, 155–165.
- IARC** (2010). *IARC monographs on the evaluation of carcinogenic risks to humans. Ingested nitrate and nitrite, and cyanobacterial peptide toxins*. Available at: <https://monographs.iarc.fr/wp-content/uploads/2018/06/mono94.pdf>. (Accessed: 5 January 2019).
- in't Veld**, P.H., Ritmeester, W.S., Delfgou-van Asch, E.H., Dufrenne, J.B., Wernars, K., Smit, E., van Leusden, F.M. (2001). Detection of genes encoding for enterotoxins

and determination of the production of enterotoxins by HBL blood plates and immunoassays of psychrotrophic strains of *Bacillus cereus* isolated from pasteurised milk. *International Journal of Food Microbiology*, **64**, 63–70.

International Dairy Federation (2016). *Bacillus cereus in Milk and Dairy Products*. Available at: <https://www.fil-idf.org/wp-content/uploads/2016/12/Bacillus-cereus-in-Milk-and-Dairy-Products.pdf>. (Accessed: 5 January 2019).

Ito, E., Kondo, F., Terao, K., Harada, K. (1997). Neoplastic nodular formation in mouse liver induced by repeated intraperitoneal injections of microcystin-LR. *Toxicon*, **35**, 1453–1457.

Ito, E., Satake, M., Ofuji, K., Higashi, M., Harigaya, K., McMahon, T., Yasumoto, T. (2002). Chronic effects in mice caused by oral administration of sublethal doses of azaspiracid, a new marine toxin isolated from mussels. *Toxicon*, **40**, 193–203.

Ito, E., Satake, M., Ofuji, K., Kurita, N., McMahon, T., James, K., Yasumoto, T. (2000). Multiple organ damage caused by a new toxin azaspiracid, isolated from mussels produced in Ireland. *Toxicon*, **38**, 917–930.

Izadi, Z., Sheikh-Zeinoddin, M., Ensafi, A.A., Soleimanian-Zad, S. (2016). Fabrication of an electrochemical DNA-based biosensor for *Bacillus cereus* detection in milk and infant formula. *Biosensors and Bioelectronics*, **80**, 582–589.

Jacoby, J.M., Collier, D.C., Welch, E.B., Hardy, F.J., Crayton, M. (2000). Environmental factors associated with a toxic bloom of *Microcystis aeruginosa*. *Canadian Journal of Fisheries and Aquatic Sciences*, **57**, 231–240.

Jaenicke, R. (1998). What ultrastable globular proteins teach us about protein stabilization. *Biochemistry Moscow*, **63**, 312–321.

Jäger, M., Plückthun, A. (1999). Domain interactions in antibody Fv and scFv fragments: effects on unfolding kinetics and equilibria. *FEBS Letters*, **462**, 307–312.

James, K.J., Fidalgo Sáez, M.J., Furey, A., Lehane, M. (2004). Azaspiracid poisoning, the food-borne illness associated with shellfish consumption. *Food Additives and Contaminants*, **21**, 879–892.

Jeffrey, G.A. (1997). *An Introduction to Hydrogen Bonding*. Oxford University Press.

Jespers, L., Schon, O., Famm, K., Winter, G. (2004a). Aggregation-resistant domain antibodies selected on phage by heat denaturation. *Nature Biotechnology*, **22**, 1161–1165.

- Jespers**, L., Schon, O., James, L.C., Veprintsev, D., Winter, G. (2004b). Crystal Structure of HEL4, a Soluble, Refoldable Human VH Single Domain with a Germ-line Scaffold. *Journal of Molecular Biology*, **337**, 893–903.
- Jiao**, Z.H., Li, M., Feng, Y.X., Shi, J.C., Zhang, J., Shao, B. (2014). Hormesis Effects of Silver Nanoparticles at Non-Cytotoxic Doses to Human Hepatoma Cells. *PLoS ONE*, **9**, e102564.
- Jones**, B.E., Czaja, M.J. (1998). Intracellular signaling in response to toxic liver injury. *American Journal of Physiology-Gastrointestinal and Liver Physiology*, **275**, G874–G878.
- Jonsson**, P.R., Pavia, H., Toth, G. (2009). Formation of harmful algal blooms cannot be explained by allelopathic interactions. *Proceedings of the National Academy of Sciences (USA)*, **106**, 11177–11182.
- Kaneko**, T., Nakajima, N., Okamoto, S., Suzuki, I., Tanabe, Y., Tamaoki, M., Nakamura, Y., Kasai, F., Watanabe, A., Kawashima, K., Kishida, Y., Ono, A., Shimizu, Y., Takahashi, C., Minami, C., Fujishiro, T., Kohara, M., Katoh, M., Nakazaki, N., Nakayama, S., Yamada, M., Tabata, S., Watanabe, M.M. (2007). Complete Genomic Structure of the Bloom-forming Toxic Cyanobacterium *Microcystis aeruginosa* NIES-843. *DNA Research*, **14**, 247–256.
- Kim**, S., Davis, M., Sinn, E., Patten, P., Hood, L., (1981). *Antibody diversity: somatic hypermutation of rearranged VH genes*. Available at: <https://www.ncbi.nlm.nih.gov/pmc/articles/PMC6101208/> (Accessed: 1 January 2019).
- Kim**, W.T., Shin, S., Hwang, H.J., Kim, M.K., Jung, H.S., Park, H., Ryu, C.J. (2016). Molecular Characterization of Two Monoclonal Antibodies against the Same Epitope on B-Cell Receptor Associated Protein 31. *PLoS ONE*, **11**, e0167527.
- Kliman**, R., M. (2016). *Encyclopedia of Evolutionary Biology*. Cambridge, MA: Academic Press.
- Koide**, S., Sidhu, S.S. (2009). The Importance of Being Tyrosine: Lessons in Molecular Recognition from Minimalist Synthetic Binding Proteins. *ACS Chemistry Biology*, **4**, 325–334.
- Komárek**, J., Komárková, J. (2002). Review of the European *Microcystis* morphospecies (Cyanoprokaryotes) from nature. *Czech Phycology, Olomouc*, **2**, 1–24.

- Kong, M., Sim, J., Kang, T., Nguyen, H.H., Park, H.K., Chung, B.H., Ryu, S. (2015).** A novel and highly specific phage endolysin cell wall binding domain for detection of *Bacillus cereus*. *European Biophysics Journal*, **44**, 437–446.
- Konst, H., McKercher, P.D., Gorham, P.R., Robertson, A., Howell, J., (1965).** Symptoms and pathology produced by toxic *Microcystis aeruginosa* NRC-1 in laboratory and domestic animals. *Canadian Journal of Comparative Medicine and Veterinary Science*, **29**, 221–228.
- Kontermann, R.E. (2005).** Recombinant bispecific antibodies for cancer therapy. *Acta Pharmacologica Sinica*, **26**, 1–9.
- Kontermann, R.E., Brinkmann, U. (2015).** Bispecific antibodies. *Drug Discovery Today*, **20**, 838–847.
- Kotiranta, A., Lounatmaa, K., Haapasalo, M. (2000).** Epidemiology and pathogenesis of *Bacillus cereus* infections. *Microbes and Infection*, **2**, 189–198.
- Kramer, J.M., Gilbert, R.J. (1989).** ‘*Bacillus cereus* and other *Bacillus* species’, in: Doyle, M.P. (Ed.), *Foodborne Bacterial Pathogens*. New York: Marcel Dekker, Inc., pp. 21–50.
- Kramer, R.M., Shende, V.R., Motl, N., Pace, C.N., Scholtz, J.M. (2012).** Toward a Molecular Understanding of Protein Solubility: Increased Negative Surface Charge Correlates with Increased Solubility. *Biophysical Journal*, **102**, 1907–1915.
- Kretzschmar, T., Geiser, M. (1995).** Evaluation of antibodies fused to minor coat protein III and major coat protein VIII of bacteriophage M13. *Gene*, **155**, 61–65.
- Kusharyoto, W., Pleiss, J., Bachmann, T.T., Schmid, R.D. (2002).** Mapping of a hapten-binding site: molecular modeling and site-directed mutagenesis study of an anti-atrazine antibody. *Protein Engineering, Design and Selection*, **15**, 233–241.
- Kwon, W.S., Da Silva, N.A., Kellis, J.T. (1996).** Relationship between thermal stability, degradation rate and expression yield of barnase variants in the periplasm of *Escherichia coli*. *Protein Engineering, Design and Selection* **9**, 1197–1202.
- Lamminmaki, U., Pauperio, S., Westerlund-Karlsson, A., Karvinen, J., Virtanen, P., Lovgren, T., Saviranta, P. (1999).** Expanding the conformational diversity by random insertions to CDRH2 results in improved anti-estradiol antibodies. *Journal of Molecular Biology*, **291**, 589–602.

- Lankoff, A., Bialczyk, J., Dziga, D., Carmichael, W.W., Lisowska, H., Wojcik, A.** (2006). Inhibition of nucleotide excision repair (NER) by microcystin-LR in CHO-K1 cells. *Toxicon*, **48**, 957–965.
- Lankoff, A., Sochacki, J., Spoo, L., Meriluoto, J., Wojcik, A., Wegierek, A., Verschaeve, L.** (2008). Nucleotide excision repair impairment by nodularin in CHO cell lines due to ERCC1/XPF inactivation. *Toxicology Letters*, **179**, 101–107.
- Larsen, H.D., Jørgensen, K.** (1999). Growth of *Bacillus cereus* in pasteurized milk products. *International Journal of Food Microbiology*, **46**, 173–176.
- Lawrence, M.S., Phillips, K.J., Liu, D.R.** (2007). Supercharging Proteins Can Impart Unusual Resilience. *Journal of the American Chemical Society*, **129**, 10110–10112.
- Le Manach, S., Sotton, B., Huet, H., Duval, C., Paris, A., Marie, A., Yépreman, C., Catherine, A., Mathéron, L., Vinh, J., Edery, M., Marie, B.** (2018). Physiological effects caused by microcystin-producing and non-microcystin producing *Microcystis aeruginosa* on medaka fish: A proteomic and metabolomic study on liver. *Environmental Pollution*, **234**, 523–537.
- Lechner, S., Mayr, R., Francis, K.P., Prüss, B.M., Kaplan, T., Wiessner-Gunkel, E., Stewart, G.S., Scherer, S.** (1998). *Bacillus weihenstephanensis* sp. nov. is a new psychrotolerant species of the *Bacillus cereus* group. *International Journal of Systematic and Evolutionary Microbiology*, **48**, 1373–1382.
- Lee, H.R., Seo, J.W., Kim, M.J., Song, S.H., Park, K.U., Song, J., Han, K.S.** (2012). Rapid detection of bacterial contamination of platelet-rich plasma-derived platelet concentrates using flow cytometry. *Annals of Clinical and Laboratory Science*, **42**, 174–181.
- Lee, S.K., Bridges, S.L., Koopman, W.J., Schroeder, H.W.** (1992). The immunoglobulin kappa light chain repertoire expressed in the synovium of a patient with rheumatoid arthritis. *Arthritis and Rheumatism*, **35**, 905–913.
- Lehman, P.W., Boyer, G., Hall, C., Waller, S., Gehrts, K.** (2005). Distribution and toxicity of a new colonial *Microcystis aeruginosa* bloom in the San Francisco Bay Estuary, California. *Hydrobiologia*, **541**, 87–99.
- Leoff, C., Saile, E., Rauvolfova, J., Quinn, C.P., Hoffmaster, A.R., Zhong, W., Mehta, A.S., Boons, G.J., Carlson, R.W., Kannenberg, E.L.** (2009). Secondary cell wall polysaccharides of *Bacillus anthracis* are antigens that contain specific epitopes which cross-react with three pathogenic *Bacillus cereus* strains that caused severe disease, and

other epitopes common to all the *Bacillus cereus* strains tested. *Glycobiology*, **19**, 665–673.

Leonard, P., Hearty, S., O’Kennedy, R. (2011). ‘Measuring Protein-Protein Interactions Using Biacore’, in: Walls, D., Loughran, T.S. (Eds.), *Protein Chromatography: Methods and Protocols*. Totowa, NJ: Humana Press, pp. 403–418.

Leonis, G., Steinbrecher, T., Papadopoulos, M.G. (2013). A Contribution to the Drug Resistance Mechanism of Darunavir, Amprenavir, Indinavir, and Saquinavir Complexes with HIV-1 Protease Due to Flap Mutation I50V: A Systematic MM–PBSA and Thermodynamic Integration Study. *Journal of Chemical Information and Modeling*, **53**, 2141–2153.

Leser, T.D., Knarreborg, A., Worm, J. (2008). Germination and outgrowth of *Bacillus subtilis* and *Bacillus licheniformis* spores in the gastrointestinal tract of pigs. *Journal of Applied Microbiology*, **104**, 1025–1033.

Li, H., Xie, P., Li, G., Hao, L., Xiong, Q. (2009). *In vivo* study on the effects of microcystin extracts on the expression profiles of proto-oncogenes (c-fos, c-jun and c-myc) in liver, kidney and testis of male Wistar rats injected i.v. with toxins. *Toxicol*, **53**, 169–175.

Li, H.H., Cai, X., Shouse, G.P., Piluso, L.G., Liu, X. (2007). A specific PP2A regulatory subunit, B56 γ , mediates DNA damage-induced dephosphorylation of p53 at Thr55. *EMBO Journal*, **26**, 402–411.

Li Y., Chen J., Zhao Q., Pu C., Qiu Z., Zhang R., Shu W. (2011). A Cross-Sectional Investigation of Chronic Exposure to Microcystin in Relationship to Childhood Liver Damage in the Three Gorges Reservoir Region, China. *Environmental Health Perspectives*, **119**, 1483–1488.

Li, Z., Woo, C.J., Iglesias-Ussel, M.D., Ronai, D., Scharff, M.D. (2004). The generation of antibody diversity through somatic hypermutation and class switch recombination. *Genes and Development*, **18**, 1–11.

Lin, S.S., Bassik, M.C., Suh, H., Nishino, M., Arroyo, J.D., Hahn, W.C., Korsmeyer, S.J., Roberts, T.M. (2006). PP2A regulates BCL-2 phosphorylation and proteasome-mediated degradation at the endoplasmic reticulum. *Journal of Biological Chemistry*, **281**, 23003–23012.

Lohr, K., Pahl, F., Moghaddas Gholami, A., Geillinger, K.E., Daniel, H., Kuster, B., Klingenspor, M. (2016). Reduced mitochondrial mass and function add to age-related

susceptibility toward diet-induced fatty liver in C57BL/6J mice. *Physiological Reports*, **4**, e12988.

Loladze, V.V., Makhatadze, G.I. (2002). Removal of surface charge-charge interactions from ubiquitin leaves the protein folded and very stable. *Protein Science*, **11**, 174–177.

Lone, Y., Koiri, R.K., Bhide, M. (2015). An overview of the toxic effect of potential human carcinogen Microcystin-LR on testis. *Toxicology Reports*, **2**, 289–296.

Lund, T., De Buyser, M.L., Granum, P.E. (2000). A new cytotoxin from *Bacillus cereus* that may cause necrotic enteritis. *Molecular Microbiology*, **38**, 254–261.

Lund, T., Granum, P.E. (1996). Characterisation of a non-haemolytic enterotoxin complex from *Bacillus cereus* isolated after a foodborne outbreak. *FEMS Microbiology Letters*, **141**, 151–156.

Ly, J.D., Grubb, D.R., Lawen, A. (2003). The mitochondrial membrane potential ($\Delta\psi_m$) in apoptosis; an update. *Apoptosis*, **8**, 115–128.

Ma, J., Li, Y., Wu, M., Li, X. (2018). Oxidative stress-mediated p53/p21WAF1/CIP1 pathway may be involved in microcystin-LR-induced cytotoxicity in HepG2 cells. *Chemosphere*, **194**, 773–783.

Ma, M., Pi, F., Wang, J., Ji, J., Sun, X. (2017). New insights into cytotoxicity induced by microcystin-LR, estradiol, and ractopamine with mathematical models: Individual and combined effects. *Chemosphere*, **168**, 223–233.

MacKintosh, C., Beattie, K.A., Klumpp, S., Cohen, P., Codd, G.A. (1990). Cyanobacterial microcystin-LR is a potent and specific inhibitor of protein phosphatases 1 and 2A from both mammals and higher plants. *FEBS Letters*, **264**, 187–192.

Maffini, M.V., Neltner, T.G. (2015). Brain drain: the cost of neglected responsibilities in evaluating cumulative effects of environmental chemicals. *Journal of Epidemiology and Community Health*, **69**, 496–499.

Magliery, T.J. (2015). Protein stability: computation, sequence statistics, and new experimental methods. *Current Opinion in Structural Biology*, **33**, 161–168.

Maguire, I. (2019). The development of microfluidic platforms for environmental analysis. Ph.D. Thesis, Dublin City University.

Maguire, I., Fitzgerald, J., Heery, B., Nwankire, C., O’Kennedy, R., Ducreé, J., Regan, F., (2018). Novel Microfluidic Analytical Sensing Platform for the Simultaneous Detection of Three Algal Toxins in Water. *ACS Omega*, **3**, 6624–6634.

- Maguire**, I., Fitzgerald, J., McPartlin, D., Heery, B., Murphy, C., Nwankire, C., O’Kennedy, R., Ducrée, J., Regan, F., (2017). A centrifugal microfluidic-based approach for multi-toxin detection for real-time marine water-quality monitoring. Presented at the OCEANS 2017 - Aberdeen, pp. 1–8.
- Mahler**, H., Pasi, A., Kramer, J.M., Schulte, P., Scoging, A.C., Bär, W., Krähenbühl, S. (1997). Fulminant liver failure in association with the emetic toxin of *Bacillus cereus*. *The New England Journal of Medicine*, **336**, 1142–1148.
- Maidana**, M., Carlis, V., Galhardi, F.G., Yunes, J.S., Geracitano, L.A., Monserrat, J.M., Barros, D.M. (2006). Effects of microcystins over short- and long-term memory and oxidative stress generation in hippocampus of rats. *Chemico-Biological Interactions*, **159**, 223–234.
- Manning**, M.C., Chou, D.K., Murphy, B.M., Payne, R.W., Katayama, D.S. (2010). Stability of Protein Pharmaceuticals: An Update. *Pharmaceutical Research*, **27**, 544–575.
- Martín-Luna**, B., Sevilla, E., Bes, M.T., Fillat, M.F., Peleato, M.L. (2015). Variation in the synthesis of microcystin in response to saline and osmotic stress in *Microcystis aeruginosa* PCC7806. *Limnetica*, **34**, 205–214.
- Marvin**, D.A., Symmons, M.F., Straus, S.K. (2014). Structure and assembly of filamentous bacteriophages. *Progress in Biophysics & Molecular Biology*, **114**, 80–122.
- Masango**, M., Myburgh, J., Botha, C., Labuschagne, L., Naicker, D. (2008). A comparison of *in vivo* and *in vitro* assays to assess the toxicity of algal blooms. *Water Research*, **42**, 3241–3248.
- Mattiazzi Usaj**, M., Styles, E.B., Verster, A.J., Friesen, H., Boone, C., Andrews, B.J. (2016). High-Content Screening for Quantitative Cell Biology. *Trends in Cell Biology*, **26**, 598–611.
- Mayer**, A.M.S., Clifford, J.A., Aldulescu, M., Frenkel, J.A., Holland, M.A., Hall, M.L., Glaser, K.B., Berry, J. (2011). Cyanobacterial *Microcystis aeruginosa* lipopolysaccharide elicits release of superoxide anion, thromboxane B₂, cytokines, chemokines, and matrix metalloproteinase-9 by rat microglia. *Toxicological Sciences*, **121**, 63–72.
- Maynes**, J.T., Luu, H.A., Cherney, M.M., Andersen, R.J., Williams, D., Holmes, C.F.B., James, M.N.G. (2006). Crystal Structures of Protein Phosphatase-1 Bound to

- Motuporin and Dihydromicrocystin-LA: Elucidation of the Mechanism of Enzyme Inhibition by Cyanobacterial Toxins. *Journal of Molecular Biology*, **356**, 111–120.
- McConkey**, D.J. (1998). Biochemical determinants of apoptosis and necrosis. *Toxicology Letters*, **99**, 157–168.
- McCoy**, G.R., Touzet, N., Fleming, G.T.A., Raine, R. (2015). Evolution of the MIDTAL microarray: the adaption and testing of oligonucleotide 18S and 28S rDNA probes and evaluation of subsequent microarray generations with *Prymnesium* spp. cultures and field samples. *Environmental Science and Pollution Research*, **22**, 9704–9716.
- McCullough**, K.C., Summerfield, A. (2005). Basic Concepts of Immune Response and Defence Development. *Institute for Laboratory Animal Research Journal*, **46**, 230–240.
- McIntyre**, L., Bernard, K., Beniac, D., Isaac-Renton, J.L., Naseby, D.C. (2008). Identification of *Bacillus cereus* Group Species Associated with Food Poisoning Outbreaks in British Columbia, Canada. *Applied and Environmental Microbiology*, **74**, 7451–7453.
- McLendon**, G., Radany, E., (1978). Is protein turnover thermodynamically controlled? *Journal of Biological Chemistry*, **253**, 6335–6337.
- McMahon**, T., Silke, J. (1996). Winter toxicity of unknown aetiology in mussels. *Harmful Algae News*, **14**, 2.
- McPartlin**, D.A., Lochhead, M.J., Connell, L.B., Doucette, G.J., O’Kennedy, R.J. (2016). Use of biosensors for the detection of marine toxins. *Essays in Biochemistry*, **60**, 49–58.
- McPartlin**, D.A., Loftus, J.H., Crawley, A.S., Silke, J., Murphy, C.S., O’Kennedy, R.J. (2017). Biosensors for the monitoring of harmful algal blooms. *Current Opinion in Biotechnology*, **45**, 164–169.
- Mechaly**, A., Zahavy, E., Fisher, M. (2008). Development and Implementation of a Single-Chain Fv Antibody for Specific Detection of *Bacillus anthracis* Spores. *Applied and Environmental Microbiology*, **74**, 818–822.
- Meehl**, M.A., Stadheim, T.A. (2014). Biopharmaceutical discovery and production in yeast. *Current Opinion in Biotechnology*, **30**, 120–127.
- Mehta**, A.S., Saile, E., Zhong, W., Buskas, T., Carlson, R., Kannenberg, E., Reed, Y., Quinn, C.P., Boons, G.J. (2006). Synthesis and antigenic analysis of the BclA

glycoprotein oligosaccharide from the *Bacillus anthracis* exosporium. *Chemistry*, **12**, 9136–9149.

Meneely, J.P., Hajšlová, J., Krska, R., Elliott, C.T. (2018). Assessing the combined toxicity of the natural toxins, aflatoxin B1, fumonisin B1 and microcystin-LR by high content analysis. *Food and Chemical Toxicology*, **121**, 527–540.

Merck (2018). *Duopath® Cereus Enterotoxins*. Available at: http://www.merckmillipore.com/IE/en/product/Duopath-Cereus-Enterotoxins,MDA_CHEM-104146#documentation (Accessed: 12 December 2018).

Merel, S., Walker, D., Chicana, R., Snyder, S., Baurès, E., Thomas, O. (2013). State of knowledge and concerns on cyanobacterial blooms and cyanotoxins. *Environment International*, **59**, 303–327.

Meriluoto, J., Codd, G.A. (Eds.) (2005). *Toxic cyanobacterial monitoring and cyanotoxin analysis*. Available at: <http://www.doria.fi/bitstream/handle/10024/76837/toxic.pdf?sequence=1> (Accessed: 5 January 2019).

Mian, I.S., Bradwell, A.R., Olson, A.J. (1991). Structure, function and properties of antibody binding sites. *Journal of Molecular Biology*, **217**, 133–151.

Michalak, A.M., Anderson, E.J., Beletsky, D., Boland, S., Bosch, N.S., Bridgeman, T.B., Chaffin, J.D., Cho, K., Confesor, R., Daloğlu, I., DePinto, J.V., Evans, M.A., Fahnenstiel, G.L., He, L., Ho, J.C., Jenkins, L., Johengen, T.H., Kuo, K.C., LaPorte, E., Liu, X., McWilliams, M.R., Moore, M.R., Posselt, D.J., Richards, R.P., Scavia, D., Steiner, A.L., Verhamme, E., Wright, D.M., Zagorski, M.A. (2013). Record-setting algal bloom in Lake Erie caused by agricultural and meteorological trends consistent with expected future conditions. *Proceedings of the National Academy of Sciences (USA)*, **110**, 6448–6452.

Miersch, S., Li, Z., Hanna, R., McLaughlin, M.E., Hornsby, M., Matsuguchi, T., Paduch, M., Sääf, A., Wells, J., Koide, S., Kossiakoff, A., Sidhu, S.S. (2015). Scalable High Throughput Selection From Phage-displayed Synthetic Antibody Libraries. *Journal of Visualized Experiments*, **17**, 51492.

Mikkola, R., Saris, N.E., Grigoriev, P.A., Andersson, M.A., Salkinoja-Salonen, M.S. (1999). Ionophoretic properties and mitochondrial effects of cereulide: the emetic toxin of *B. cereus*. *European Journal of Biochemistry*, **263**, 112–117.

Miklos, A.C., Li, C., Pielak, G.J. (2009). ‘Using NMR-Detected Backbone Amide 1H Exchange to Assess Macromolecular Crowding Effects on Globular-Protein Stability’,

in: *Methods in Enzymology, Biothermodynamics, Part B*. Cambridge, MA: Academic Press, pp. 1–18.

Miller, M.A., Kudela, R.M., Mekebri, A., Crane, D., Oates, S.C., Tinker, M.T., Staedler, M., Miller, W.A., Toy-Choutka, S., Dominik, C., Hardin, D., Langlois, G., Murray, M., Ward, K., Jessup, D.A. (2010). Evidence for a Novel Marine Harmful Algal Bloom: Cyanotoxin (Microcystin) Transfer from Land to Sea Otters. *PLoS ONE* **5**, e12576.

Miller, M.B., Bassler, B.L. (2001). Quorum Sensing in Bacteria. *Annual Review of Microbiology*, **55**, 165–199.

Mols, M., de Been, M., Zwietering, M.H., Moezelaar, R., Abee, T. (2007). Metabolic capacity of *Bacillus cereus* strains ATCC 14579 and ATCC 10987 interlinked with comparative genomics. *Environmental Microbiology*, **9**, 2933–2944.

Moore, S.K., Trainer, V.L., Mantua, N.J., Parker, M.S., Laws, E.A., Backer, L.C., Fleming, L.E. (2008). Impacts of climate variability and future climate change on harmful algal blooms and human health. *Environmental Health*, **7**, S4–S4.

Moriguchi, T., Matsuura, H., Itakura, Y., Katsuki, H., Saito, H., Nishiyama, N. (1997). Allixin, a phytoalexin produced by garlic, and its analogues as novel exogenous substances with neurotrophic activity. *Life Science*, **61**, 1413–1420.

Mostofa, K.M.G., Liu, C.Q., Vione, D., Gao, K., Ogawa, H. (2013). Sources, factors, mechanisms and possible solutions to pollutants in marine ecosystems. *Environmental Pollution*, **182**, 461–478.

Mulvenna, V., Dale, K., Priestly, B., Mueller, U., Humpage, A., Shaw, G., Allinson, G., Falconer, I. (2012). Health Risk Assessment for Cyanobacterial Toxins in Seafood. *International Journal of Environmental Research and Public Health*, **9**, 807–820.

Murphy, C., Stack, E., Krivelo, S., McPartlin, D.A., Byrne, B., Greef, C., Lochhead, M.J., Husar, G., Devlin, S., Elliott, C.T., O’Kennedy, R.J. (2015). Detection of the cyanobacterial toxin, microcystin-LR, using a novel recombinant antibody-based optical-planar waveguide platform. *Biosensors and Bioelectronics*, **67**, 708–714.

Muyldermans, S., Atarhouch, T., Saldanha, J., Barbosa, J.A., Hamers, R. (1994). Sequence and structure of VH domain from naturally occurring camel heavy chain immunoglobulins lacking light chains. *Protein Engineering*, **7**, 1129–1135.

- Muyldermans, S., Cambillau, C., Wyns, L. (2001).** Recognition of antigens by single-domain antibody fragments: the superfluous luxury of paired domains. *Trends in Biochemical Science*, **26**, 230–235.
- Nair, A., Thomas, A.C., Borsuk, M.E. (2013).** Interannual variability in the timing of New England shellfish toxicity and relationships to environmental forcing. *Science of the Total Environment*, **447**, 255–266.
- Nakamura, L.K. (1998).** *Bacillus pseudomycooides* sp. nov. *International Journal of Systematic and Evolutionary Microbiology*, **48**, 1031–1035.
- Neilan, B.A., Pearson, L.A., Muenchhoff, J., Moffitt, M.C., Dittmann, E. (2013).** Environmental conditions that influence toxin biosynthesis in cyanobacteria. *Environmental Microbiology*, **15**, 1239–1253.
- Nejatollahi, F., Malek-Hosseini, Z., Mehrabani, D. (2008).** Development of Single Chain Antibodies to P185 Tumor Antigen. *Iranian Red Crescent Medical Journal*, **10**, 298–302.
- Ní Rathaille, A., Raine, R. (2011).** Seasonality in the excystment of *Alexandrium minutum* and *Alexandrium tamarense* in Irish coastal waters. *Harmful Algae*, **10**, 629–635.
- Ni, Z., Bikadi, Z., Shuster, D.L., Zhao, C., Rosenberg, M.F., Mao, Q. (2011).** Identification of proline residues in or near the transmembrane helices of the human breast cancer resistance protein (BCRP/ABCG2) important for transport activity and substrate specificity. *Biochemistry*, **50**, 8057–8066.
- Nishiwaki-Matsushima, R., Ohta, T., Nishiwaki, S., Suganuma, M., Kohyama, K., Ishikawa, T., Carmichael, W.W., Fujiki, H. (1992).** Liver tumor promotion by the cyanobacterial cyclic peptide toxin microcystin-LR. *Journal of Cancer Research and Clinical Oncology*, **118**, 420–424.
- Nong, Q., Komatsu, M., Izumo, K., Indo, H.P., Xu, B., Aoyama, K., Majima, H.J., Horiuchi, M., Morimoto, K., Takeuchi, T. (2007).** Involvement of reactive oxygen species in Microcystin-LR-induced cytogenotoxicity. *Free Radical Research*, **41**, 1326–1337.
- Ohta, T., Nishiwaki, R., Yatsunami, J., Komori, A., Suganuma, M., Fujiki, H. (1992).** Hyperphosphorylation of cytokeratins 8 and 18 by microcystin-LR, a new liver tumor promoter, in primary cultured rat hepatocytes. *Carcinogenesis*, **13**, 2443–2447.

- O'Neil**, J.M., Davis, T.W., Burford, M.A., Gobler, C.J. (2012). The rise of harmful cyanobacteria blooms: The potential roles of eutrophication and climate change. *Harmful Algae*, **14**, 313–334.
- Ongley**, S.E., Pengelly, J.J.L., Neilan, B.A. (2016). Elevated Na(+) and pH influence the production and transport of saxitoxin in the cyanobacteria *Anabaena circinalis* AWQC131C and *Cylindrospermopsis raciborskii* T3. *Environmental Microbiology*, **18**, 427–438.
- Orr**, P.T., Jones, G.J., Douglas, G.B. (2004). Response of cultured *Microcystis aeruginosa* from the Swan River, Australia, to elevated salt concentration and consequences for bloom and toxin management in estuaries. *Marine and Freshwater Research*, **55**, 277–283.
- Ortea**, P.M., Allis, O., Healy, B.M., Lehane, M., Ní Shuilleabháin, A., Furey, A., James, K.J. (2004). Determination of toxic cyclic heptapeptides by liquid chromatography with detection using ultra-violet, protein phosphatase assay and tandem mass spectrometry. *Chemosphere*, **55**, 1395–1402.
- Osajima**, T., Suzuki, M., Neya, S., Hoshino, T. (2014). Computational and statistical study on the molecular interaction between antigen and antibody. *Journal of Molecular Graphics and Modelling*, **53**, 128–139.
- Ott**, M., Robertson, J.D., Gogvadze, V., Zhivotovsky, B., Orrenius, S. (2002). Cytochrome c release from mitochondria proceeds by a two-step process. *Proceedings of the National Academy of Sciences (USA)*, **99**, 1259–1263.
- Otten**, T.G., Crosswell, J.R., Mackey, S., Dreher, T.W. (2015). Application of molecular tools for microbial source tracking and public health risk assessment of a *Microcystis* bloom traversing 300km of the Klamath River. *Harmful Algae*, **46**, 71–81.
- Owen**, S.C., Doak, A.K., Ganesh, A.N., Nedyalkova, L., McLaughlin, C.K., Shoichet, B.K., Shoichet, M.S. (2014). Colloidal Drug Formulations Can Explain “Bell-Shaped” Concentration–Response Curves. *ACS Chemical Biology*, **9**, 777–784.
- Oxoid** (2018). *BCET-RPLA Toxin Detection Kit*. Available at: http://www.oxid.com/uk/blue/prod_detail/prod_detail.asp?pr=TD0950&org=9&c=uk&lang=EN (Accessed: 12 December 2018).
- Pace**, C.N., Scholtz, J.M. (1998). A helix propensity scale based on experimental studies of peptides and proteins. *Biophysical Journal*, **75**, 422–427.

- Paerl**, H.W. (2014). Mitigating Harmful Cyanobacterial Blooms in a Human- and Climatically-Impacted World. *Life*, **4**, 988–1012.
- Paerl**, H.W., Huisman, J. (2009). Climate change: a catalyst for global expansion of harmful cyanobacterial blooms. *Environmental Microbiology Reports*, **1**, 27–37.
- Paerl**, H.W., Valdes, L.M., Joyner, A.R., Peierls, B.L., Piehler, M.F., Riggs, S.R., Christian, R.R., Eby, L.A., Crowder, L.B., Ramus, J.S., Clesceri, E.J., Buzzelli, C.P., Luettich, R.A. (2006). Ecological response to hurricane events in the Pamlico Sound system, North Carolina, and implications for assessment and management in a regime of increased frequency. *Estuaries and Coasts*, **29**, 1033–1045.
- Pan**, K., Wang, H., Zhang, H., Liu, H., Lei, H., Huang, L., Sun, Y. (2006). Production and characterization of single chain Fv directed against beta(2)-agonist clenbuterol. *Journal of Agricultural and Food Chemistry*, **54**, 6654–6659.
- Paoli**, G.C., Chen, C.Y., Brewster, J.D. (2004). Single-chain Fv antibody with specificity for *Listeria monocytogenes*. *Journal of Immunological Methods*, **289**, 147–155.
- Paul**, W.E. (2016). Bridging Innate and Adaptive Immunity. *Cell*, **147**, 1212–1215.
- Paulik**, M., Grieco, P., Kim, C., Maxeiner, H.G., Grunert, H.P., Zeichhardt, H., Morr , D.M., Morr , D.J. (1999). Drug–antibody conjugates with anti-HIV activity. *Biochemical Pharmacology*, **58**, 1781–1790.
- Pedone**, E., Saviano, M., Rossi, M., Bartolucci, S. (2001). A single point mutation (Glu85Arg) increases the stability of the thioredoxin from *Escherichia coli*. *Protein Engineering, Design and Selection* **14**, 255–260.
- Perchiacca**, J.M., Bhattacharya, M., Tessier, P.M. (2011). Mutational analysis of domain antibodies reveals aggregation hotspots within and near the complementarity determining regions. *Proteins: Structure, Function, and Bioinformatics*, **79**, 2637–2647.
- Perchiacca**, J.M., Ladiwala, A.R.A., Bhattacharya, M., Tessier, P.M. (2012). Aggregation-resistant domain antibodies engineered with charged mutations near the edges of the complementarity-determining regions. *Protein Engineering, Design and Selection* **25**, 591–602.
- Perchiacca**, J.M., Lee, C.C., Tessier, P.M. (2014). Optimal charged mutations in the complementarity-determining regions that prevent domain antibody aggregation are dependent on the antibody scaffold. *Protein Engineering, Design and Selection* **27**, 29–39.

- Perchiacca, J.M., Tessier, P.M. (2012).** Engineering Aggregation-Resistant Antibodies. *Annual Review of Chemical and Biomolecular Engineering*, **3**, 263–286.
- Perl, D., Mueller, U., Heinemann, U., Schmid, F.X. (2000).** Two exposed amino acid residues confer thermostability on a cold shock protein. *Nature Structural and Molecular Biology*, **7**, 380–383.
- Perovich, G., Dortch, Q., Goodrich, J., Berger, P.S., Brooks, J., Evens, T.J., Gobler, C.J., Graham, J., Hyde, J., Karner, D., O’Shea, D. (Kevin), Paul, V., Paerl, H., Piehler, M., Rosen, B.H., Santelmann, M., Tester, P., Westrick, J. (2008).** ‘Causes, Prevention, and Mitigation Workgroup Report’, in: Hudnell, H.K. (Ed.), *Cyanobacterial Harmful Algal Blooms: State of the Science and Research Needs, Advances in Experimental Medicine and Biology*. New York, NY: Springer New York, pp. 185–215.
- Pettersen, E.F., Goddard, T.D., Huang, C.C., Couch, G.S., Greenblatt, D.M., Meng, E.C., Ferrin, T.E. (2004).** UCSF Chimera—A visualization system for exploratory research and analysis. *Journal of Computational Chemistry*, **25**, 1605–1612.
- Popovic, B., Gibson, S., Senussi, T., Carmen, S., Kidd, S., Slidel, T., Strickland, I., Jianqing, X., Spooner, J., Lewis, A., Hudson, N., Mackenzie, L., Keen, J., Kemp, B., Hardman, C., Hatton, D., Wilkinson, T., Vaughan, T., Lowe, D. (2017).** Engineering the expression of an anti-interleukin-13 antibody through rational design and mutagenesis. *Protein Engineering, Design and Selection*. **30**, 303–311.
- Poste, A.E., Hecky, R.E., Guildford, S.J. (2011).** Evaluating Microcystin Exposure Risk through Fish Consumption. *Environmental Science and Technology*, **45**, 5806–5811.
- Preece, E.P., Hardy, F.J., Moore, B.C., Bryan, M. (2017).** A review of microcystin detections in Estuarine and Marine waters: Environmental implications and human health risk. *Harmful Algae*, **61**, 31–45.
- Quinlan, J.J., Foegeding, P.M. (1997).** Monoclonal antibodies for use in detection of *Bacillus* and *Clostridium* spores. *Applied and Environmental Microbiology*, **63**, 482–487.
- Raffray, M., Cohen, G.M. (1997).** Apoptosis and necrosis in toxicology: A continuum or distinct modes of cell death? *Pharmacology & Therapeutics*, **75**, 153–177.
- Rajkovic, A., Uyttendaele, M., Ombregt, S.A., Jaaskelainen, E., Salkinoja-Salonen, M., Debevere, J. (2006).** Influence of type of food on the kinetics and overall production of *Bacillus cereus* emetic toxin. *Journal of Food Protection*, **69**, 847–852.

- Rao**, P.V.L., Bhattacharya, R., Parida, M.M., Jana, A.M., Bhaskar, A.S.B. (1998). Freshwater cyanobacterium *Microcystis aeruginosa* (UTEX 2385) induced DNA damage *in vivo* and *in vitro*. *Environmental Toxicology and Pharmacology*, **5**, 1–6.
- Reidhaar-Olson**, J.F., Sauer, R.T. (1990). Functionally acceptable substitutions in two alpha-helical regions of lambda repressor. *Proteins*, **7**, 306–316.
- Rennell**, D., Bouvier, S.E., Hardy, L.W., Poteete, A.R. (1991). Systematic mutation of bacteriophage T4 lysozyme. *Journal of Molecular Biology*, **222**, 67–88.
- Ressom**, R., San Soong, F., Fitzgerald, J., Turczynowicz, L., El Saadi, O., Roder, D., Maynard, T., Falconer, I. (2004). Health effects of toxic cyanobacteria (blue-green algae). *National Health and Research Council, Canberra*, **108**, 1–92.
- Reynolds**, C.S., Jaworski, G.H.M., Cmiech, H.A., Leedale, G.F., (1981). On the annual cycle of the blue-green alga *Microcystis aeruginosa* Kütz. *Philosophical Transactions of the Royal Society*. **293**, 419–477.
- Riechmann**, L., Muyldermans, S. (1999). Single domain antibodies: comparison of camel VH and camelised human VH domains. *Journal of Immunological Methods*, **231**, 25–38.
- Riès-kautt**, M., Ducruix, A. (1997). ‘Inferences drawn from physicochemical studies of crystallogenes and precrystalline state’, in: *Methods in Enzymology, Macromolecular Crystallography Part A*. Cambridge, MA: Academic Press, pp. 23–59.
- Rinehart**, K.L., Namikoshi, M., Choi, B.W. (1994). Structure and biosynthesis of toxins from blue-green algae (cyanobacteria). *Journal of Applied Phycology*, **6**, 159–176.
- Rita**, D.P., Valeria, V., Silvia, B.M., Pasquale, G., Milena, B. (2014). Microcystin Contamination in Sea Mussel Farms from the Italian Southern Adriatic Coast following Cyanobacterial Blooms in an Artificial Reservoir. *Journal of Ecosystems*, **2014**, 1–11.
- Robson**, B.J., Hamilton, D.P. (2003). Summer flow event induces a cyanobacterial bloom in a seasonal Western Australian estuary. *Marine and Freshwater Research*, **54**, 139–151.
- Rodrigues Pires Júnior**, O., de Oliveira, N.B., Bosque, R.J., Nice Ferreira, M.F., Morais Aurélio da Silva, V., Martins Magalhães, A.C., Correia de Santana, C.J., de Souza Castro, M. (2018). Histopathological Evaluation of the Exposure by Cyanobacteria Cultive Containing [d-Leu¹]Microcystin-LR on *Lithobates catesbeianus* Tadpoles. *Toxins (Basel)*, **10**, 318.

- Rogers**, E.D., Henry, T.B., Twiner, M.J., Gouffon, J.S., McPherson, J.T., Boyer, G.L., Sayler, G.S., Wilhelm, S.W. (2011). Global Gene Expression Profiling in Larval Zebrafish Exposed to Microcystin-LR and *Microcystis* Reveals Endocrine Disrupting Effects of Cyanobacteria. *Environmental Science & Technology*, **45**, 1962–1969.
- Román**, Y., Alfonso, A., Louzao, M.C., de la Rosa, L.A., Leira, F., Vieites, J.M., Vieytes, M.R., Ofuji, K., Satake, M., Yasumoto, T., Botana, L.M. (2002). Azaspiracid-1, a potent, nonapoptotic new phycotoxin with several cell targets. *Cell Signalling Technology*, **14**, 703–716.
- Roopenian**, D.C., Akilesh, S. (2007). FcRn: the neonatal Fc receptor comes of age. *Nature Reviews Immunology*, **7**, 715–725.
- Ross**, C., Santiago-Vázquez, L., Paul, V. (2006). Toxin release in response to oxidative stress and programmed cell death in the cyanobacterium *Microcystis aeruginosa*. *Aquatic Toxicology*, **78**, 66–73.
- Röthlisberger**, D., Honegger, A., Plückthun, A. (2005). Domain interactions in the Fab fragment: a comparative evaluation of the single-chain Fv and Fab format engineered with variable domains of different stability. *Journal of Molecular Biology*, **347**, 773–789.
- Rouet**, R., Lowe, D., Christ, D. (2014). Stability engineering of the human antibody repertoire. *FEBS Letters*, **588**, 269–277.
- Rousseau**, F., Serrano, L., Schymkowitz, J.W.H. (2006). How evolutionary pressure against protein aggregation shaped chaperone specificity. *Journal of Molecular Biology*, **355**, 1037–1047.
- Roy**, A., Nair, S., Sen, N., Soni, N., Madhusudhan, M.S. (2017). *In silico* methods for design of biological therapeutics. *Methods*, **131**, 33–65.
- Rudrappa**, T., Quinn, W.J., Stanley-Wall, N.R., Bais, H.P. (2007). A degradation product of the salicylic acid pathway triggers oxidative stress resulting in down-regulation of *Bacillus subtilis* biofilm formation on *Arabidopsis thaliana* roots. *Planta*, **226**, 283–297.
- Ryu**, J.H., Beuchat, L.R. (2005). Biofilm formation and sporulation by *Bacillus cereus* on a stainless steel surface and subsequent resistance of vegetative cells and spores to chlorine, chlorine dioxide, and a peroxyacetic acid-based sanitizer. *Journal of Food Protection*, **68**, 2614–2622.

- Saerens**, D., Pellis, M., Loris, R., Pardon, E., Dumoulin, M., Matagne, A., Wyns, L., Muyldermans, S., Conrath, K. (2005). Identification of a universal VHH framework to graft non-canonical antigen-binding loops of camel single-domain antibodies. *Journal of Molecular Biology*, **352**, 597–607.
- Sahin**, E., Jordan, J.L., Spataro, M.L., Naranjo, A., Costanzo, J.A., Weiss, W.F., Robinson, A.S., Fernandez, E.J., Roberts, C.J. (2011). Computational Design and Biophysical Characterization of Aggregation-Resistant Point Mutations for γ D Crystallin Illustrate a Balance of Conformational Stability and Intrinsic Aggregation Propensity. *Biochemistry*, **50**, 628–639.
- Samdal**, I.A., LÅyberg, K.E., Briggs, L.R., Kilcoyne, J., Xu, J., Forsyth, C.J., Miles, C.O. (2015). Development of an ELISA for the Detection of Azaspiracids. *Journal of Agricultural and Food Chemistry*, **63**, 7855–7861.
- San Francisco Estuary Institute** (2015). *University of California Santa Cruz assessing SPATT in San Francisco Bay*. Available at: [http://sfbaynutrients.sfei.org/sites/default/files/SPATT%20Final%20Report%20May\(2015\).pdf](http://sfbaynutrients.sfei.org/sites/default/files/SPATT%20Final%20Report%20May(2015).pdf) (Accessed: 4 December 2018).
- Sangolkar**, L.N., Maske, S.S., Chakrabarti, T. (2006). Methods for determining microcystins (peptide hepatotoxins) and microcystin-producing cyanobacteria. *Water Research*, **40**, 3485–3496.
- Sanjeev**, A., Mattaparthi, V.S.K. (2017). Effect of Tyrosine to Alanine Mutation on the Dimerization Process of α -Synuclein: A Potential of Mean Force study. *Biological Forum*.
- Sanseverino**, I., Loos, R., Lettieri, T., Conduto António, D., European Commission, Joint Research Centre (2017). *Cyanotoxins methods and approaches for their analysis and detection*. Available at: <http://publications.jrc.ec.europa.eu/repository/bitstream/JRC106478/kjna28624enn.pdf> (Accessed: 5 January 2019).
- Satake**, M., Ofuji, K., James, K.J., Furey, A., Yasumoto, T., James, K.J., Furey, C.G. (1998). ‘New toxic event caused by Irish mussels’. In: Reguera, B., Blanco, J., Fernandez, M.J., Watts, T. (Eds.) *Harmful algae. Santiago de Compostela: Xunta de Galicia and Intergovernmental Oceanographic Commission of UNESCO*, pp. 468–469.
- Sauerborn**, M., Brinks, V., Jiskoot, W., Schellekens, H. (2010). Immunological mechanism underlying the immune response to recombinant human protein therapeutics. *Trends in Pharmacological Sciences*, **31**, 53–59.

- Schade**, R., Calzado, E.G., Sarmiento, R., Chacana, P.A., Porankiewicz-Asplund, J., Terzolo, H.R. (2005). Chicken Egg Yolk Antibodies (IgY-technology): A Review of Progress in Production and Use in Research and Human and Veterinary Medicine. *Altern. Laboratory Animals*, **33**, 1–26.
- Schein**, C.H. (1990). Solubility as a Function of Protein Structure and Solvent Components. *Nature Biotechnology*, **8**, 308–317.
- Schindelin**, J., Arganda-Carreras, I., Frise, E., Kaynig, V., Longair, M., Pietzsch, T., Preibisch, S., Rueden, C., Saalfeld, S., Schmid, B., Tinevez, J.Y., White, D.J., Hartenstein, V., Eliceiri, K., Tomancak, P., Cardona, A. (2012). Fiji: an open-source platform for biological-image analysis. *Nature Methods*, **9**, 676–682.
- Schroeder**, H.W., Cavacini, L. (2010). Structure and Function of Immunoglobulins. *Journal of Allergy and Clinical Immunology*, **125**, S41–S52.
- Schumacher**, W.C., Storozuk, C.A., Dutta, P.K., Phipps, A.J. (2008). Identification and Characterization of *Bacillus anthracis* Spores by Multiparameter Flow Cytometry. *Applied and Environmental Microbiology*, **74**, 5220–5223.
- Schwehm**, J.M., Kristyenne, E.S., Biggers, C.C., Stites, W.E. (1998). Stability effects of increasing the hydrophobicity of solvent-exposed side chains in staphylococcal nuclease. *Biochemistry*, **37**, 6939–6948.
- Sedda**, T., Baralla, E., Varoni, M.V., Pasciu, V., Lorenzoni, G., Demontis, M.P. (2016). Determination of microcystin-LR in clams (*Tapes decussatus*) of two Sardinian coastal ponds (Italy). *Marine Pollutants Bulletin*, **108**, 317–320.
- Sekijima**, M., Tsutsumi, T., Yoshida, T., Harada, T., Tashiro, F., Chen, G., Yu, S.Z., Ueno, Y. (1999). Enhancement of glutathione S-transferase placental-form positive liver cell foci development by microcystin-LR in aflatoxin B1-initiated rats. *Carcinogenesis*, **20**, 161–165.
- Selvaraj**, P., Fifadara, N., Nagarajan, S., Cimino, A., Wang, G. (2004). Functional regulation of human neutrophil Fc γ receptors. *Immunologic Research*, **29**, 219–229.
- Shamsollahi**, H.R., Alimohammadi, M., Nabizadeh, R., Nazmara, S., Mahvi, A.H. (2015). Measurement of Microcystin-LR in Water Samples Using Improved HPLC Method. *Global Journal of Health and Science*, **7**, 66–70.
- Shen**, H., Niu, Y., Xie, P., Tao, M., Yang, X. (2011). Morphological and physiological changes in *Microcystis aeruginosa* as a result of interactions with heterotrophic bacteria. *Freshwater Biology*, **56**, 1065–1080.

- Shimba** (1995). Comparative thermodynamic analyses of the Fv, Fab* and Fab and Fab fragments of anti-dansyl mouse monoclonal antibody. *FEBS Letters*, **360**, 247–250.
- Shiota**, M., Saitou, K., Mizumoto, H., Matsusaka, M., Agata, N., Nakayama, M., Kage, M., Tatsumi, S., Okamoto, A., Yamaguchi, S., Ohta, M., Hata, D. (2010). Rapid detoxification of cereulide in *Bacillus cereus* food poisoning. *Pediatrics*, **125**, e951-955.
- Shire**, S.J. (2009). Formulation and manufacturability of biologics. *Current Opinion in Biotechnology*, **20**, 708–714.
- Shityakov**, S., Förster, C. (2014). *In silico* predictive model to determine vector-mediated transport properties for the blood–brain barrier choline transporter. *Advances and Applications in Bioinformatics and Chemistry*, **7**, 23–36.
- Sievers**, F., Wilm, A., Dineen, D., Gibson, T.J., Karplus, K., Li, W., Lopez, R., McWilliam, H., Remmert, M., Soding, J., Thompson, J.D., Higgins, D.G. (2014). Fast, scalable generation of high-quality protein multiple sequence alignments using Clustal Omega. *Molecular Systems Biology*, **7**, 539–539.
- Silke**, J., Duffy, C., Clarke, D. (2016a). *HABs inshore shellfish monitoring data*. Available at: <http://data.marine.ie/Dataset/Details/20935> (Accessed: 12 December 2016).
- Silke**, J., Duffy, C., Clarke, D. (2016b). *HABs inshore shellfish monitoring data*. Available at: <http://data.marine.ie/Dataset/Details/20944> (Accessed: 12 December 2016).
- Slack**, M.D., Martinez, E.D., Wu, L.F., Altschuler, S.J. (2008). Characterizing heterogeneous cellular responses to perturbations. *Proceedings of the National Academy of Sciences (USA)*, **105**, 19306–19311.
- Snijder**, B., Sacher, R., Rämö, P., Damm, E.M., Liberali, P., Pelkmans, L. (2009). Population context determines cell-to-cell variability in endocytosis and virus infection. *Nature*, **461**, 520–523.
- Soares**, R.M., Cagido, V.R., Ferraro, R.B., Meyer-Fernandes, J.R., Rocco, P.R.M., Zin, W.A., Azevedo, S.M.F.O. (2007). Effects of microcystin-LR on mouse lungs. *Toxicon*, **50**, 330–338.
- Song**, W., de la Cruz, A.A., Rein, K., O’Shea, K.E. (2006). Ultrasonically Induced Degradation of Microcystin-LR and -RR: Identification of Products, Effect of pH, Formation and Destruction of Peroxides. *Environmental Science and Technology*, **40**, 3941–3946.

- Sonnenschein**, C., Olea, N., Pasanen, M.E., Soto, A.M. (1989). Negative controls of cell proliferation: human prostate cancer cells and androgens. *Cancer Research*, **49**, 3474–3481.
- Spiess**, C., Zhai, Q., Carter, P.J. (2015). Alternative molecular formats and therapeutic applications for bispecific antibodies. *Molecular Immunology*, **67**, 95–106.
- Spoof**, L., Vesterkvist, P., Lindholm, T., Meriluoto, J. (2003). Screening for cyanobacterial hepatotoxins, microcystins and nodularin in environmental water samples by reversed-phase liquid chromatography-electrospray ionisation mass spectrometry. *Journal of Chromatography A*, **1020**, 105–119.
- Stack**, E. (2011). Studies on the immunosuppressive effects and detection of naturally-occurring toxins. Ph.D. Thesis, Dublin City University.
- Staelens**, S., Desmet, J., Ngo, T., Vauterin, S., Pareyn, I., Barbeaux, P., Van Rompaey, I., Stassen, J., Deckmyn, H., Vanhoorelbeke, K. (2006). Humanization by variable domain resurfacing and grafting on a human IgG(4), using a new approach for determination of non-human like surface accessible framework residues based on homology modelling of variable domains. *Molecular Immunology*, **43**, 1243–1257.
- Steele**, E.J., Rotheneluh, H.S., Blanden, R.V. (1997). Mechanism of antigen-driven somatic hypermutation of rearranged immunoglobulin V(D)J genes in the mouse. *Immunology and Cell Biology*, **75**, 82–95.
- Steinwand**, M., Droste, P., Frenzel, A., Hust, M., Duebel, S., Schirrmann, T. (2014). The influence of antibody fragment format on phage display based affinity maturation of IgG. *mAbs*, **6**, 204–218.
- Stenfors Arnesen**, L.P., Fagerlund, A., Granum, P.E. (2008). From soil to gut: *Bacillus cereus* and its food poisoning toxins. *FEMS Microbiology Reviews*, **32**, 579–606.
- Stephenson**, A.E., Fives-Taylor, P., Melamede, R.J. (1998). Cell-based panning as a means to isolate phage display Fabs specific for a bacterial surface protein. *Methods in Cell Science*, **20**, 241–249.
- Stewart**, I., Schluter, P.J., Shaw, G.R. (2006). Cyanobacterial lipopolysaccharides and human health – a review. *Environmental Health*, **5**.
- Stonans**, I., Stonane, E., Rußwurm, S., Deigner, H.-P., Böhm, K.J., Wiederhold, M., Jäger, L., Reinhart, K. (1999). HepG2 human hepatoma cells express multiple cytokine genes. *Cytokine*, **11**, 151–156.

- Strub**, C., Alies, C., Lougarre, A., Ladurantie, C., Czaplicki, J., Fournier, D. (2004). Mutation of exposed hydrophobic amino acids to arginine to increase protein stability. *BMC Biochemistry*, **5**, 9.
- Sun**, Y., Ban, B., Bradbury, A., Ansari, G. A. Shakeel, Blake, D.A. (2016). Combining Yeast Display and Competitive FACS to Select Rare Hapten-Specific Clones from Recombinant Antibody Libraries. *Analytical Chemistry*, **88**, 9181–9189.
- Sundberg**, E.J. (2009). ‘Structural Basis of Antibody-Antigen Interactions’, in: Schutkowski, M., Reineke, U. (Eds.), *Epitope Mapping Protocols: Second Edition*. Totowa, NJ: Humana Press, pp. 23–36.
- Susin**, S.A., Zamzami, N., Castedo, M., Daugas, E., Wang, H.G., Geley, S., Fassy, F., Reed, J.C., Kroemer, G. (1997). The Central Executioner of Apoptosis: Multiple Connections between Protease Activation and Mitochondria in Fas/APO-1/CD95- and Ceramide-induced Apoptosis. *Journal of Experimental Medicine*, **186**, 25–37.
- Szabo**, R.A., Speirs, J.I., Akhtar, M. (1991). Cell Culture Detection and Conditions for Production of a *Bacillus cereus* Heat-Stable Toxin. *Journal of Food Protection*, **54**, 272–276.
- Tagawa**, Y. (2014). Isolation and characterization of flagellar filaments from *Bacillus cereus* ATCC 14579. *Antonie van Leeuwenhoek*, **106**, 1157–1165.
- Tam**, N.K.M., Uyen, N.Q., Hong, H.A., Duc, L.H., Hoa, T.T., Serra, C.R., Henriques, A.O., Cutting, S.M. (2006). The intestinal life cycle of *Bacillus subtilis* and close relatives. *Journal of Bacteriology*, **188**, 2692–2700.
- Tanaka**, T., Kokuryu, Y., Matsunaga, T. (2008). Novel Method for Selection of Antimicrobial Peptides from a Phage Display Library by Use of Bacterial Magnetic Particles. *Applied and Environmental Microbiology* **74**, 7600–7606.
- Tartaglia**, G.G., Pechmann, S., Dobson, C.M., Vendruscolo, M. (2009). A relationship between mRNA expression levels and protein solubility in *E. coli*. *Journal of Molecular Biology*, **388**, 381–389.
- Tartaglia**, G.G., Vendruscolo, M. (2010). Proteome-level interplay between folding and aggregation propensities of proteins. *Journal of Molecular Biology*, **402**, 919–928.
- Tartaglia**, G.G., Vendruscolo, M. (2009). Correlation between mRNA expression levels and protein aggregation propensities in subcellular localisations. *Molecular Biosystems*, **5**, 1873–1876.

- Tasumi**, S., Velikovsky, C.A., Xu, G., Gai, S.A., Wittrup, K.D., Flajnik, M.F., Mariuzza, R.A., Pancer, Z. (2009). High-affinity lamprey VLRA and VLRB monoclonal antibodies. *Proceedings of the National Academy of Sciences (USA)*, **106**, 12891–12896.
- Te Giffel**, M.C., Beumer, R.R., Granum, P.E., Rombouts, F.M. (1997). Isolation and characterisation of *Bacillus cereus* from pasteurised milk in household refrigerators in The Netherlands. *International Journal of Food Microbiology*, **34**, 307–318.
- Tian**, B., Wong, W.Y., Hegmann, E., Gaspar, K., Kumar, P., Chao, H. (2015). Production and Characterization of a Camelid Single Domain Antibody-Urease Enzyme Conjugate for the Treatment of Cancer. *Bioconjugate Chemistry*, **26**, 1144–1155.
- Tillett**, D., Dittmann, E., Erhard, M., von Döhren, H., Börner, T., Neilan, B.A. (2000). Structural organization of microcystin biosynthesis in *Microcystis aeruginosa* PCC7806: an integrated peptide–polyketide synthetase system. *Chemistry & Biology*, **7**, 753–764.
- Tillmann**, U., Elbrächter, M., Krock, B., John, U., Cembella, A. (2009). *Azadinium spinosum* gen. et sp. nov. (*Dinophyceae*) identified as a primary producer of azaspiracid toxins. *European Journal of Phycology*, **44**, 63–79.
- Tillmanns**, A.R., Pick, F.R., Aranda-Rodriguez, R. (2007). Sampling and analysis of microcystins: Implications for the development of standardized methods. *Environmental Toxicology*, **22**, 132–143.
- Toivola**, D.M., Eriksson, J.E. (1999). Toxins affecting cell signalling and alteration of cytoskeletal structure. *Toxicology In vitro*, **13**, 521–530.
- Tonk**, L., Bosch, K., Visser, P.M., Huisman, J. (2007). Salt tolerance of the harmful cyanobacterium *Microcystis aeruginosa*. *Aquatic Microbial Ecology*, **46**, 117–123.
- Trainer**, V.L., Moore, L., Bill, B.D., Adams, N.G., Harrington, N., Borchert, J., Da Silva, D.A.M., Eberhart, B.T.L. (2013). Diarrhetic shellfish toxins and other lipophilic toxins of human health concern in Washington State. *Marine Drugs*, **11**, 1815–1835.
- Tran**, S.L., Guillemet, E., Gohar, M., Lereclus, D., Ramarao, N. (2010). CwpFM (EntFM) Is a *Bacillus cereus* Potential Cell Wall Peptidase Implicated in Adhesion, Biofilm Formation, and Virulence. *Journal of Bacteriology*, **192**, 2638–2642.
- Triantis**, T., Tsimeli, K., Kaloudis, T., Thanassoulas, N., Lytras, E., Hiskia, A. (2010). Development of an integrated laboratory system for the monitoring of cyanotoxins in surface and drinking waters. *Toxicon*, **55**, 979–989.

- Trogen**, G.B., Annila, A., Eriksson, J., Kontteli, M., Meriluoto, J., Sethson, I., Zdunek, J., Edlund, U. (1996). Conformational Studies of Microcystin-LR Using NMR Spectroscopy and Molecular Dynamics Calculations. *Biochemistry*, **35**, 3197–3205.
- Twiner**, M.J., Doucette, G.J., Rasky, A., Huang, X.P., Roth, B.L., Sanguinetti, M.C. (2012a). The marine algal toxin azaspiracid is an open state blocker of hERG potassium channels. *Chemical Research in Toxicology*, **25**, 1975–1984.
- Twiner**, M.J., El-Ladki, R., Kilcoyne, J., Doucette, G.J. (2012b). Comparative Effects of the Marine Algal Toxins Azaspiracid-1, -2, and -3 on Jurkat T Lymphocyte Cells. *Chemical Research in Toxicology*, **25**, 747–754.
- Twiner**, M.J., Hess, P., Bottein Dechraoui, M.Y., McMahon, T., Samons, M.S., Satake, M., Yasumoto, T., Ramsdell, J.S., Doucette, G.J. (2005a). Cytotoxic and cytoskeletal effects of azaspiracid-1 on mammalian cell lines. *Toxicon*, **45**, 891–900.
- Twiner**, M.J., Hess, P., Dechraoui, M.Y.B., McMahon, T., Samons, M.S., Satake, M., Yasumoto, T., Ramsdell, J.S., Doucette, G.J. (2005b). Cytotoxic and cytoskeletal effects of azaspiracid-1 on mammalian cell lines. *Toxicon*, **45**, 891–900.
- Twiner**, M.J., Rehmann, N., Hess, P., Doucette, G.J. (2008a). Azaspiracid Shellfish Poisoning: A Review on the Chemistry, Ecology, and Toxicology with an Emphasis on Human Health Impacts. *Marine Drugs*, **6**, 39–72.
- Twiner**, M.J., Ryan, J.C., Morey, J.S., Smith, K.J., Hammad, S.M., Van Dolah, F.M., Hess, P., McMahon, T., Satake, M., Yasumoto, T., Doucette, G.J. (2008b). Transcriptional profiling and inhibition of cholesterol biosynthesis in human T lymphocyte cells by the marine toxin azaspiracid. *Genomics*, **91**, 289–300.
- Vale**, C., Nicolaou, K.C., Frederick, M.O., Vieytes, M.R., Botana, L.M. (2010). Cell Volume Decrease as a Link between Azaspiracid-Induced Cytotoxicity and c-Jun-N-Terminal Kinase Activation in Cultured Neurons. *Toxicological Sciences*, **113**, 158–168.
- Vale**, P., Bire, R., Hess, P. (2008). Confirmation by LC–MS/MS of azaspiracids in shellfish from the Portuguese north-western coast. *Toxicon*, **51**, 1449–1456.
- Van Blarcom**, T., Rossi, A., Foletti, D., Sundar, P., Pitts, S., Bee, C., Melton Witt, J., Melton, Z., Hasa-Moreno, A., Shaughnessy, L., Telman, D., Zhao, L., Cheung, W.L., Berka, J., Zhai, W., Strop, P., Chaparro-Riggers, J., Shelton, D.L., Pons, J., Rajpal, A. (2015). Precise and Efficient Antibody Epitope Determination through Library Design,

- Yeast Display and Next-Generation Sequencing. *Journal of Molecular Biology*, **427**, 1513–1534.
- van Netten**, P., van De Moosdijk, A., van Hoensel, P., Mossel, D.A., Perales, I. (1990). Psychrotrophic strains of *Bacillus cereus* producing enterotoxin. *Journal of Applied Bacteriology*, **69**, 73–79.
- Vandenberg**, L.N., Wadia, P.R., Schaeberle, C.M., Rubin, B.S., Sonnenschein, C., Soto, A.M. (2006). The mammary gland response to estradiol: monotonic at the cellular level, non-monotonic at the tissue-level of organization? *The Journal of Steroid Biochemistry and Molecular Biology*, **101**, 263–274.
- Verspagen**, J.M.H., Passarge, J., Jöhnk, K.D., Visser, P.M., Peperzak, L., Boers, P., Laanbroek, H.J., Huisman, J. (2006). Water Management Strategies Against Toxic *Microcystis* Blooms In The Dutch Delta. *Ecological Applications*, **16**, 313–327.
- Vesterkvist**, P.S.M., Misiorek, J.O., Spoof, L.E.M., Toivola, D.M., Meriluoto, J.A.O. (2012). Comparative Cellular Toxicity of Hydrophilic and Hydrophobic Microcystins on Caco-2 Cells. *Toxins*, **4**, 1008–1023.
- Vilariño**, N., Nicolaou, K.C., Frederick, M.O., Cagide, E., Ares, I.R., Louzao, M.C., Vieytes, M.R., Botana, L.M. (2006). Cell growth inhibition and actin cytoskeleton disorganization induced by azaspiracid-1 structure-activity studies. *Chemical Research in Toxicology*, **19**, 1459–1466.
- Vilariño**, N., Nicolaou, K.C., Frederick, M.O., Vieytes, M.R., Botana, L.M. (2007). Irreversible cytoskeletal disarrangement is independent of caspase activation during *in vitro* azaspiracid toxicity in human neuroblastoma cells. *Biochemical Pharmacology*, **74**, 327–335.
- Vincke**, C., Loris, R., Saerens, D., Martinez-Rodriguez, S., Muyltermans, S., Conrath, K. (2009). General strategy to humanize a camelid single-domain antibody and identification of a universal humanized nanobody scaffold. *Journal of Biological Chemistry*, **284**, 3273–3284.
- Visser**, P.M., Verspagen, J.M.H., Sandrini, G., Stal, L.J., Matthijs, H.C.P., Davis, T.W., Paerl, H.W., Huisman, J. (2016). How rising CO₂ and global warming may stimulate harmful cyanobacterial blooms. *Harmful Algae*, **4**, 145–159.
- Vogt**, G., Woell, S., Argos, P. (1997). Protein thermal stability, hydrogen bonds, and ion pairs. *Journal of Molecular Biology*, **269**, 631–643.

- von Stetten**, F., Mayr, R., Scherer, S. (1999). Climatic influence on mesophilic *Bacillus cereus* and psychrotolerant *Bacillus weihenstephanensis* populations in tropical, temperate and alpine soil. *Environmental Microbiology*, **1**, 503–515.
- Wang**, L., Zou, W., Zhong, Y., An, J., Zhang, X., Wu, M., Yu, Z. (2012). The hormesis effect of BDE-47 in HepG2 cells and the potential molecular mechanism. *Toxicology Letters*, **209**, 193–201.
- Wang**, S., Tian, D., Zheng, W., Jiang, S., Wang, X., Andersen, M.E., Zheng, Y., He, G., Qu, W. (2013). Combined Exposure to 3-Chloro-4-dichloromethyl-5-hydroxy-2(5H)-furanone and Microcystin-LR Increases Genotoxicity in Chinese Hamster Ovary Cells through Oxidative Stress. *Environmental Science and Technology*, **47**, 1678–1687.
- Ward**, R., Clark, M., Lees, J., Hawkins, N. (1996). Retrieval of human antibodies from phage-display libraries using enzymatic cleavage. *Journal of Immunological Methods*, **189**, 73–82.
- Watson**, S.B., Miller, C., Arhonditsis, G., Boyer, G.L., Carmichael, W., Charlton, M.N., Confesor, R., Depew, D.C., Höök, T.O., Ludsin, S.A., Matisoff, G., McElmurry, S.P., Murray, M.W., Peter Richards, R., Rao, Y.R., Steffen, M.M., Wilhelm, S.W. (2016). The re-eutrophication of Lake Erie: Harmful algal blooms and hypoxia. *Harmful Algae*, **56**, 44–66.
- Wehrle**, E., Didier, A., Moravek, M., Dietrich, R., Märtlbauer, E. (2010). Detection of *Bacillus cereus* with enteropathogenic potential by multiplex real-time PCR based on SYBR green I. *Molecular and Cellular Probes*, **24**, 124–130.
- Weidenmaier**, C., Peschel, A. (2008). Teichoic acids and related cell-wall glycopolymers in Gram-positive physiology and host interactions. *Nature Reviews Microbiology*, **6**, 276–287.
- Welkos**, S., Little, S., Friedlander, A., Fritz, D., Fellows, P. (2001). The role of antibodies to *Bacillus anthracis* and anthrax toxin components in inhibiting the early stages of infection by anthrax spores. *Microbiology (Reading, Engl.)*, **147**, 1677–1685.
- Weng**, D., Lu, Y., Wei, Y., Liu, Y., Shen, P. (2007). The role of ROS in microcystin-LR-induced hepatocyte apoptosis and liver injury in mice. *Toxicology*, **232**, 15–23.
- Weng**, Z., Rickles, R.J., Feng, S., Richard, S., Shaw, A.S., Schreiber, S.L., Brugge, J.S. (1995). Structure-function analysis of SH3 domains: SH3 binding specificity altered by single amino acid substitutions. *Molecular Cell Biology*, **15**, 5627–5634.

- Wetherill**, Y.B., Petre, C.E., Monk, K.R., Puga, A., Knudsen, K.E. (2002). The xenoestrogen bisphenol A induces inappropriate androgen receptor activation and mitogenesis in prostatic adenocarcinoma cells. *Molecular Cancer Therapeutics*, **1**, 515–524.
- Whitaker**, W.R., Lee, H., Arkin, A.P., Dueber, J.E. (2015). Avoidance of truncated proteins from unintended ribosome binding sites within heterologous protein coding sequences. *ACS Synthetic Biology*, **4**, 249–257.
- Wigley**, D.B., Clarke, A.R., Dunn, C.R., Barstow, D.A., Atkinson, T., Chia, W.N., Muirhead, H., Holbrook, J.J. (1987). The engineering of a more thermally stable lactate dehydrogenase by reduction of the area of a water-accessible hydrophobic surface. *Biochimica et Biophysica Acta*, **916**, 145–148.
- Wilkins**, A.L., Rehmann, N., Torgersen, T., Rundberget, T., Keogh, M., Petersen, D., Hess, P., Rise, F., Miles, C.O. (2006). Identification of fatty acid esters of pectenotoxin-2 seco acid in blue mussels (*Mytilus edulis*) from Ireland. *Journal of Agricultural and Food Chemistry*, **54**, 5672–5678.
- Wilkinson**, D.L., Harrison, R.G. (1991). Predicting the solubility of recombinant proteins in *Escherichia coli*. *Biotechnology (N.Y.)*, **9**, 443–448.
- Williams**, D.D., Benedek, O., Turnbough, C.L. (2003). Species-specific peptide ligands for the detection of *Bacillus anthracis* spores. *Applied and Environmental Microbiology*, **69**, 6288–6293.
- Wilson**, J., Berntsen, H.F., Zimmer, K.E., Frizzell, C., Verhaegen, S., Ropstad, E., Connolly, L. (2016). Effects of defined mixtures of persistent organic pollutants (POPs) on multiple cellular responses in the human hepatocarcinoma cell line, HepG2, using high content analysis screening. *Toxicology and Applied Pharmacology*, **294**, 21–31.
- Wong**, H.C., Chang, M.H., Fan, J.Y. (1988). Incidence and characterization of *Bacillus cereus* isolates contaminating dairy products. *Applied and Environmental Microbiology*, **54**, 699–702.
- Wood**, S.A., Dietrich, D.R. (2011). Quantitative assessment of aerosolized cyanobacterial toxins at two New Zealand lakes. *J. Environ. Monit.*, **13**, 1617–1624.
- Wörn**, A., Plückthun, A. (2001). Stability engineering of antibody single-chain Fv fragments. *Journal of Molecular Biology*, **305**, 989–1010.
- Xia**, H., Song, T., Wang, L., Jiang, L., Zhou, Q., Wang, W., Liu, L., Yang, P., Zhang, X. (2018). Effects of dietary toxic cyanobacteria and ammonia exposure on immune

function of blunt snout bream (*Megalabrama amblycephala*). *Fish and Shellfish Immunology*, **78**, 383–391.

Xia, Z., Huang, X., Chen, K., Wang, H., Xiao, J., He, K., Huang, R., Duan, X., Liu, H., Zhang, J., Xiang, G. (2016). Proapoptotic Role of Potassium Ions in Liver Cells. *BioMedical Research International*, **2016**.

Xu, Y., Lee, J., Cuong Tran, Heibeck, T.H., Wang, W.D., Yang, J., Stafford, R.L., Steiner, A.R., Sato, A.K., Hallam, T.J., Yin, G. (2015). Production of bispecific antibodies in “knobs-into-holes” using a cell-free expression system. *mAbs*, **7**, 231–242.

Yamaguchi, M., Kawai, T., Kitagawa, M., Kumeda, Y. (2013). A new method for rapid and quantitative detection of the *Bacillus cereus* emetic toxin cereulide in food products by liquid chromatography-tandem mass spectrometry analysis. *Food Microbiology*, **34**, 29–37.

Yamahara, K.M., Demir-Hilton, E., Preston, C.M., Marin, R., Pargett, D., Roman, B., Jensen, S., Birch, J.M., Boehm, A.B., Scholin, C.A. (2015). Simultaneous monitoring of faecal indicators and harmful algae using an in-situ autonomous sensor. *Letters Applied Microbiology*, **61**, 130–138.

Yatim, K.M., Lakkis, F.G. (2015). A brief journey through the immune system. *Clinical Journal of the American Society of Nephrology*, **10**, 1274–1281.

Yoshizawa, S., Matsushima, R., Watanabe, M.F., Harada, K., Ichihara, A., Carmichael, W.W., Fujiki, H. (1990). Inhibition of protein phosphatases by microcystins and nodularin associated with hepatotoxicity. *Journal of Cancer Research and Clinical Oncology*, **116**, 609–614.

Zare, H., Rajabibazl, M., Rasooli, I., Ebrahimizadeh, W., Bakherad, H., Ardakani, L.S., Gargari, S.L.M. (2014). Production of nanobodies against prostate-specific membrane antigen (PSMA) recognizing LnCaP cells. *The International Journal of Biological Markers*, **29**, 169–179.

Zegura, B. (2016). An Overview of the Mechanisms of Microcystin-LR Genotoxicity and Potential Carcinogenicity. *Mini-Reviews in Medicinal Chemistry*, **16**, 1042–1062.

Zegura, B., Gajski, G., Straser, A., Garaj-Vrhovac, V., Filipič, M. (2011). Microcystin-LR induced DNA damage in human peripheral blood lymphocytes. *Mutation Research*, **726**, 116–122.

Zegura, B., Lah, T.T., Filipic, M. (2004). The role of reactive oxygen species in microcystin-LR-induced DNA damage. *Toxicology*, **200**, 59–68.

- Zegura, B.,** Volcic, M., Lah, T.T., Filipic, M. (2008). Different sensitivities of human colon adenocarcinoma (CaCo-2), astrocytoma (IPDDC-A2) and lymphoblastoid (NCNC) cell lines to microcystin-LR induced reactive oxygen species and DNA damage. *Toxicon*, **52**, 518–525.
- Zhang, J.,** Chen, J., Xia, Z. (2013). Microcystin-LR Exhibits Immunomodulatory Role in Mouse Primary Hepatocytes Through Activation of the NF- κ B and MAPK Signaling Pathways. *Toxicological Science*, **136**, 86–96.
- Zhang, X.,** Xie, P., Zhang, Xuezheng, Zhou, W., Zhao, S., Zhao, Y., Cai, Y. (2013). Toxic effects of microcystin-LR on the HepG2 cell line under hypoxic and normoxic conditions: Toxic effects of MC-LR on the HepG2 cell line in hypoxia and normoxia. *Journal of Applied Toxicology*, **33**, 1180–1186.
- Zhou, Z.X.,** Yu, R.C., Zhou, M.J. (2017). Resolving the complex relationship between harmful algal blooms and environmental factors in the coastal waters adjacent to the Changjiang River estuary. *Harmful Algae*, **62**, 60–72.
- Zurawell, R.W.,** Chen, H., Burke, J.M., Prepas, E.E. (2005). Hepatotoxic Cyanobacteria: A Review of the Biological Importance of Microcystins in Freshwater Environments. *Journal of Toxicology and Environmental Health, Part B*, **8**, 1–37.

9 Appendix A

9.1 Testing the anti-*B. cereus* polyclonal antibody using flow cytometry

The polyclonal chicken antibodies isolated from the *B. cereus*-immunised chicken that were developed in Section 5.2.1 were sent to collaborating researchers in the University of Limerick (UL). This facilitated the preliminary development of a flow cytometry (FCM)-based assay to measure *B. cereus* levels in milk samples. The following is an assay performed in UL using the anti-*B. cereus* polyclonal antibodies developed in DCU.

Bacillus cereus strains DSM 4312, DSM 31 (DSMZ, Braunschweig, Germany), NCTC 7464 (Public Health England, Salisbury, UK) and *B. subtilis* strain DSM 10 (DSMZ) were grown for 18 hours in nutrient broth at 30 °C. Cells were harvested and incubated with the anti-*B. cereus* polyclonal antibody at a concentration of 10 µg/100 µL cell suspension. Following this the anti-*B. cereus* antibody was probed with an Alexa-Fluor 647-conjugated anti-chicken IgY antibody. The cells were stained with a universal DNA-binding dye to label all cells to ensure detection. Control cells were stained with fluorescence-labelled secondary antibody and the cell stain only (“- antibody” samples).

The stained *B. cereus* and *B. subtilis* cells were analysed by FCM. The results of these assays are presented in Figure 9.1 below. The cytograms display the DNA stain on the x-axis and Alexa-Fluor 647 on the y-axis. Events occurring in the upper right quadrant of the plots represent cells binding to the anti-*B. cereus* antibody. It was observed that the anti-*B. cereus* polyclonal antibody binds to the three live and unfixed *B. cereus* strains tested, and to the *B. subtilis* strain. This cross-reactivity for both the pathogenic *B. cereus* strains and the non-pathogenic *B. subtilis* highlights the need to stringently screen for antibodies with high specificity for only *B. cereus*.

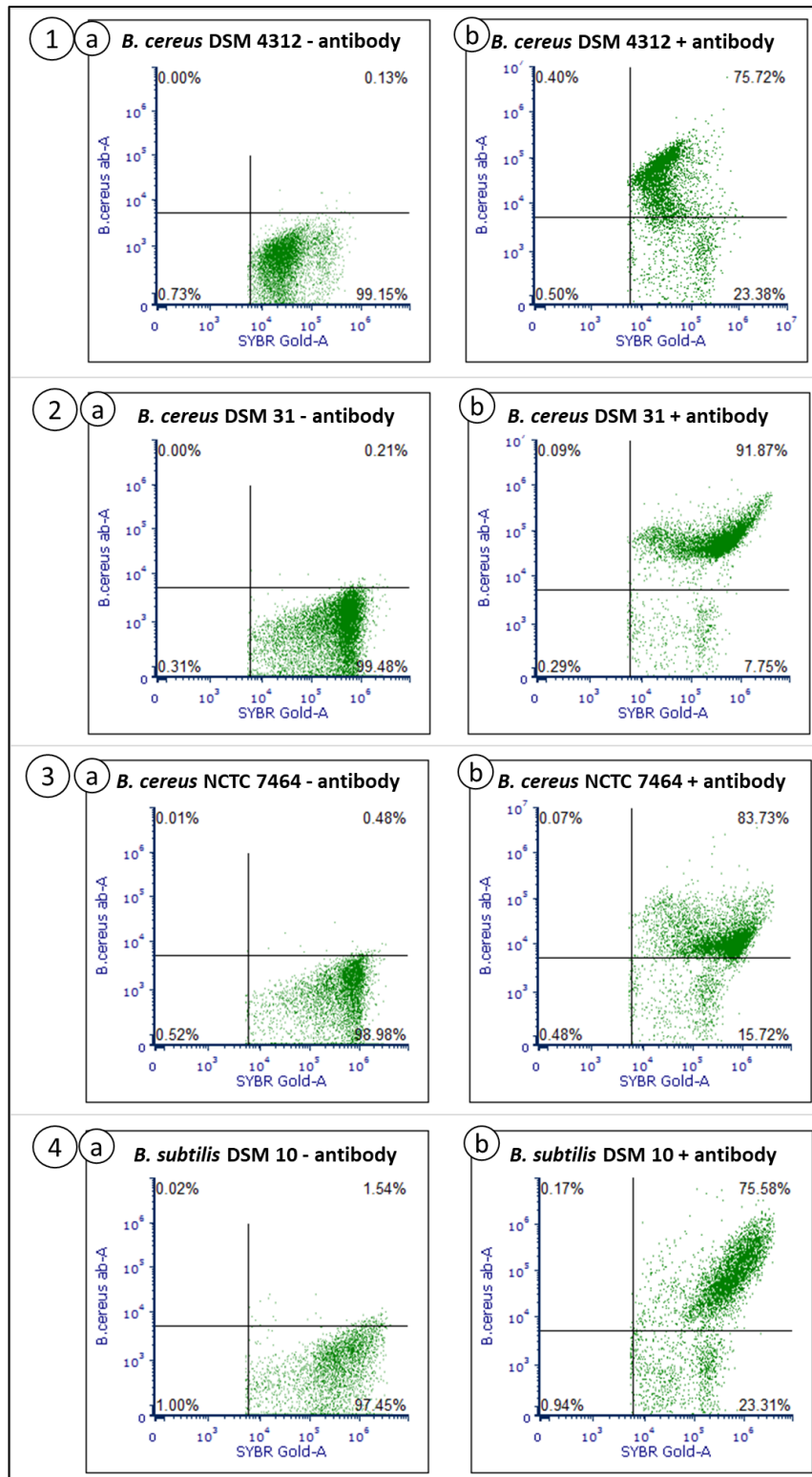


Figure 9.1: Response of anti-*B. cereus* chicken polyclonal antibody to *B. cereus* and *B. subtilis* strains. The anti-*B. cereus* polyclonal antibody was tested by FCM against the *B. cereus* strains DSM 4312 (1), DSM31 (2) and NCTC 7464 (3) and *B. subtilis* strain DSM 10 (4). For the analysis of each species and strain, the control cells were not treated with the anti-*B. cereus* polyclonal antibody (a), while the test cells were treated with the anti-*B. cereus* polyclonal antibody (b).